HAL
open science

New insights in vascular tissue engineering based on a functional scaffold, a natural coating of extracellular matrix and a intraluminal cellularization technique : from in vitro characterization to in vivo validation

Pan Dan

To cite this version:

Pan Dan. New insights in vascular tissue engineering based on a functional scaffold, a natural coating of extracellular matrix and a intraluminal cellularization technique : from in vitro characterization to in vivo validation. Bioengineering. Université de Lorraine, 2016. English. NNT : 2016LORR0304 . tel-02000743

HAL Id: tel-02000743

https://hal.univ-lorraine.fr/tel-02000743

Submitted on 25 Nov 2019

HAL is a multi-disciplinary open access archive for the deposit and dissemination of scientific research documents, whether they are published or not. The documents may come from teaching and research institutions in France or abroad, or from public or private research centers.

L'archive ouverte pluridisciplinaire **HAL**, est destinée au dépôt et à la diffusion de documents scientifiques de niveau recherche, publiés ou non, émanant des établissements d'enseignement et de recherche français ou étrangers, des laboratoires publics ou privés.

UNIVERSITÉ DE LORRAINE

AVERTISSEMENT

Ce document est le fruit d'un long travail approuvé par le jury de soutenance et mis à disposition de l'ensemble de la communauté universitaire élargie.

Il est soumis à la propriété intellectuelle de l'auteur. Ceci implique une obligation de citation et de référencement lors de l'utilisation de ce document.

D'autre part, toute contrefaçon, plagiat, reproduction illicite encourt une poursuite pénale.

Contact : ddoc-theses-contact@univ-lorraine.fr

LIENS

Code de la Propriété Intellectuelle. articles L 122. 4
Code de la Propriété Intellectuelle. articles L 335.2- L 335.10
http://www.cfcopies.com/V2/leg/leg_droi.php
http://www.culture.gouv.fr/culture/infos-pratiques/droits/protection.htm

UNIVERSITÉ DE LORRAINE

École Doctorale BioSE (Biologie-Santé-Environnement)

Thèse

Présentée et soutenue publiquement pour l'obtention du titre de

DOCTEUR DE L'UNIVERSITÉ DE LORRAINE

Mention: « Science de la vie et de la santé »

par : Pan DAN

Nouvelles approches en ingénierie vasculaire basées sur un scaffold fonctionnalisé, une matrice extra-cellulaire naturelle et une cellularisation intraluminale : de la caractérisation à la validation chez l'animal

Le 24 Novembre 2016

Directeur de thèse: Pr. Patrick MENU

Co-directrice de thèse: Dr. Véronique DECOT

Membres du jury:

Rapporteurs :	Mme. Dominique MAQUIN	PU-PH, EA-4691 BIOS, Reims
	M. Simon RINCKENBACH	PU-PH, CHRU Besançon
Examinateurs :	M. Juan-Pablo MAUREIRA	PU-PH, CHRU Nancy
	Mme. Halima KERDJOUDJ	MCU, EA-4691 BIOS, Reims
	Mme. Véronique DECOT	MCU-PH, UMR-CNRS 7365
	M. Patrick MENU	PR, UMR-CNRS 7365
Membre invité:	M. Bertrand LEHALLE	DR, Pôle Vaisseaux Nancy

UMR 7365-CNRS-Université de Lorraine. Laboratoire d'Ingénierie Moléculaire et Physiopathologie Articulaire (IMoPA)

Abréviations

AC	Angioplastie coronaire
Ac-LDL	Lipoprotéines acétylées
AO	artère ombilicale
CARS	Coherent Anti-Strokes Raman Scattering
CD31	Cluster of differentiation 31
CE	Cellules endothéliales
CML	Cellules musculaire lisse
CSM	Cellules souches mésenchymateuses
HUVEC	Human umbilical cord vein endothelial cells
ITV	Ingénierie tissulaire vasculaire
MEC	Matrice extra-cellulaire
PAC	Pontage aorto-coronaire
PO_2	Partial pressure of oxygen
P(VDF-TrFE)	Poly(vinylidene fluoride-trifluoroethylene)
SVF	Sérum de veau fœtal
TGF-beta1	Transforming growth factor beta 1
Tie-2	Endothelium-specific receptor tyrosine kinase
VEGFR2	Vascular endothelial growth factor receptor -2
VE-Cadherin	Vascular endothelial Cadherin
vWF	Von Willebrand factor
WJ-ECM	Extracellular matri derived from Wharton's jelly
ZnO	Zinc oxidex

Remerciements

A ma famille

A mes parents et beaux parents

A ma femme Mengmeng que j'aime…

Pour votre soutien et vos encouragements

Je remercie Madame **Dominique LAURENT-MAQUIN** et Monsieur **Simon RINCKENBACH** pour avoir accepté d'être les rapporteurs de cette thèse.

Je tiens à exprimer à Monsieur le professeur **Patrick MENU**, directeur de ma thèse, ma profonde gratitude pour m'avoir accueilli au sein de son équipe. Il m'a donné l'opportunité de d'étendre mes recherches sur différents axes, de collaborer avec différentes équipes interuniversitaires et internationales pour élargir mes connaissances scientifiques. Sa grande disponibilité a permis un suivi permanent du déroulement des travaux. Les discussions constantes entre nous m'ont beaucoup inspiré au niveau de la recherche scientifique et de la vie au cours de ces années de thèse. J'apprécie également son investissement dans la rédaction des articles et celle de ma thèse. Je lui suis profondément reconnaissant pour ses démarches et son dévouement aussi bien pour ma thèse que pour ma carrière.

J'exprime ma gratitude à Madame **Véronique DECOT**, Maître de conférences et praticien hospitalier, pour son rôle majeur au cours de ces années de thèse. Je la remercie plus spécialement pour les nombreuses discussions et suggestions précieuses concernant ma thèse et pour ses encouragements pour rédiger mes articles. Sa gentillesse et son soutien m'ont aidé à pallier les difficultés pendant ces années.

J'exprime également ma reconnaissance à Monsieur le professeur **Jean François STOLTZ**, qui m'a proposé de réaliser ma thèse dans cette unité. Sa disponibilité a permis un suivi au cours de mes travaux. Je le remercie pour toutes les opportunités de conférences et ses conseils pour ma carrière.

Je remercie vivement Madame **Emilie VELOT**, Maître de conférences de l'Université de Lorraine, qui m'a suivi dans la première période de ce travail. Elle a bien souvent trouvé une réponse à mes questions et a beaucoup participé aux activités scientifiques durant ces années.

Je remercie très sincèrement Madame **Monique GENTILS**, Madame **Ghislaine CAUCHOIS**, Monsieur **Naceur CHARIF** et Madame **Brigitte GUERBER** pour leurs aides essentielles dans différents niveaux d'expérimentations, merci pour leur gentillesse à mon égard et leur soutien constant. Je les remercie plus spécialement pour leur aide au niveau du français.

Je souhaiterais aussi remercier Monsieur **Dominique DUMAS**, pour son amitié depuis notre première rencontre en Chine. Sa disponibilité et ses connaissances en l'imagerie ont largement amélioré la qualité de cette thèse.

Monsieur **Nguyen TRAN**, directeur de l'école de chirurgie où toutes les expérimentations animales ont lieu. Je le remercie de m'avoir accueilli dans son laboratoire et pour sa participation dans mes expériences. Je remercie également toutes les personnes de son équipe pour leur gentillesse et l'ambiance qui m'ont permis de travailler confortablement.

J'exprime ma reconnaissance à Monsieur le professeur **Didier ROUXEL**. La collaboration entre nos deux équipes a été productible et efficace. Sa bonne humeur et sa rigueur m'ont beaucoup touché.

Un grand merci à Monsieur le professeur **Xiong WANG**, pour son soutien et sa participation aux expérimentations mécaniques.

Je souhaiterais également remercier **Jacqueline BEROUD**, qui m'a traité comme un frère. Sa gentillesse et son soutien constant m'ont permis de me familiariser à la vie et à la science en France. Je n'oublierai jamais tous les moments que nous avons passés ensemble pendant notre thèse. Un grand merci à **Hassan RAMMAL**, pour ses aides constantes et désintéressées depuis le début de mon arrivé au Biopôle. Tu es un vrai ami que j'apprécie pour toujours. Je remercie aussi **Reine El OMAR** pour sa gentillesse et son soutien. Les blagues et les éclats de rires sont des souvenirs précieux au cours de la thèse.

A tout le personnel du laboratoire ainsi qu'à mes collègues **Gabriel, Anne-Sophie, Benjamin,** Je leur souhaite évidemment beaucoup de réussite et beaucoup de bonheur dans leur vie. Je remercie **Léonore, Julie, Caroline, Paul, Matilde, David, Meriem, Vanessa, Jean-Marc et Karine** pour m'avoir encouragé et supporté durant ces années. Vous allez me manquer.

Un grand merci à la grande famille chinoise à Nancy **Xiaomeng, Peng lu, Xie zhe, Zhang lin, Xie yu, Luo yun, Liang Shiheng, Yang Xu, Wu Xianglei, Deng Chaohua, Zhang huiyi, Qian Chongsheng, Wei Chaojie, Zhang Ganggang, Hu Yong, Liu Xing** pour leur soutien et les rires aux éclats durant ces années.

La meilleure pour la fin, **Mengmeng** tu es toujours là pour moi. Merci pour ton soutien, tes encouragements, ton aide. Avec toi la vie est plus belle !!!

SOMMAIRE

INTRODUCTION GENERALE 1
PARTIE I : ETAT DE L'ART 3
1. La maladie coronarienne 4
1.1. L'histoire de la maladie coronarienne 4
1.2. Traitement de l'insuffisance coronarienne 6
1.2.1 Angioplastie coronaire (AC) 6
1.2.2 Pontage aorto-coronaire (PAC) 7
2. Ingénierie tissulaire vasculaire (ITV) 9
2.1. Les cellules 10
Publication N°1 12
2.2. Les biomatériaux 22
2.3. Ensemencement cellulaire en 3D 24
OBJECTIFS DE TRAVAIL 26
Partie II : Matériels, méthodes et résultats 28
Chapitre 1. Biomatériaux – Scaffold synthétique 29
Publication N° 2 29
Chapitre 2. Biomatériaux – coating naturel (1) 67
Publication N° 3 70
Chapitre 2. Biomatériaux – coating naturel (2) 86
Publication N° 4 88
Chapitre 3. Nouvelle stratégie 97
Publication N° 5 100
Chapitre 4. Expérimentation animale 115
DISCUSSION 123

INTRODUCTION GENERALE

Selon les dernières études statistiques de 2016, plus de 17,3 millions de personnes sont mortes de maladies cardiovasculaires en 2013, ce qui représente 1 décès sur 4 dans le monde [1]. Depuis 1990, la mortalité des personnes atteintes de maladies cardiovasculaires a augmenté de 40,8%. Et parmi ces maladies, la cardiopathie ischémique a été le plus grand contributeur à l'augmentation du nombre de décès cardiovasculaires (2,4 millions sur 5 millions de décès cardiovasculaires)[2]. Par conséquent, le développement de traitements pour soigner la maladie coronarienne à l'origine d'une cardiopathie ischémique, est une priorité.

A ce jour, les traitements de la maladie coronarienne comprennent l'approche thérapeutique en inhibant la progression de l'athérosclérose, la pose d'endoprothèses et/ou le pontage coronarien. Malgré l'augmentation de la pose d'endoprothèses, le pontage coronarien reste le traitement le plus durable au niveau de la revascularisation. Pourtant, l'indisponibilité des vaisseaux autologues est souvent rencontrée en clinique chez les patients atteints de diabète ou maladies vasculaires périphériques. Dans ce cas, l'ingénierie tissulaire vasculaire (ITV) représente une alternative thérapeutique potentielle.

L'ITV rassemble différents procédés ayant pour objectif de créer un substitut cellularisé qui présente des caractéristiques biologiques et mécaniques similaires à celles des vaisseaux natifs. Cependant, les cellules, les biomatériaux utilisés pour la construction des matrices (scaffolds), le coating ainsi que les techniques pour les combiner restent des enjeux majeurs.

Ce manuscrit rassemble les différents résultats obtenus au cours de notre travail de thèse. Il s'articule en une présentation de l'état de l'art, des résultats donnés au travers de quatre publications et d'une discussion-conclusion. Les mots clés sont l'élaboration d'un scaffold fonctionnalisé, la valorisation de la gelée de Wharton en tant que surface de recouvrement, et la proposition d'une approche originale pour permettre d'endothélialiser la lumière vasculaire. Ces différentes techniques permettent de lever des verrous et proposer de nouvelles alternatives dans le domaine de l'ITV.

PARTIE I
ETAT DE L’ART

1. La maladie coronarienne

1.1. Histoire de la maladie coronarienne

Il y a plus d'un siècle, le Dr. Alexis Carrel comprenait l'association entre l'angine de poitrine et la sténose coronarienne. Dans un modèle canin, Carrel a anastomosé un segment de carotide entre l'aorte descendante et la coronaire gauche dans le but de restaurer la circulation de la coronaire. Carrel a reçu le prix Nobel de physiologie et de médecine pour ce travail en 1912[3]. Dès lors, les traitements chirurgicaux pour les maladies cardiovasculaires, pontages aorto-coronariens en particulier, ont beaucoup progressé. Nul doute qu'aucune autre opération a prolongé plus de vies, a amené plus de soulagement des symptômes, et a été étudiée aussi minutieusement[4]. La raison de tous ces phénomènes est la morbidité et la mortalité la plus élevée des maladies cardiovasculaires, surtout la maladie coronarienne. En effet, les maladies cardiovasculaires restent la première cause de mortalité dans le monde [1], [5], et bien que la maladie coronarienne ait décliné significativement pendant la dernière décennie, elle représente encore environ la moitié des maladies cardiovasculaires[2], [6].

Les artères coronaires sont des artères qui vascularisent le cœur, elles recouvrent la surface du cœur, et par conséquent nourrissent le muscle cardiaque. Les artères coronaires ont un diamètre d'environ 5 mm. Une artère de petit diamètre comprend trois couches : l'intima (une couche monocellulaire de cellules endothéliales tapissant la lumière vasculaire qui reste en contact directement avec le sang), la média (couche musculaire lisse qui supporte l'élasticité de l'artère en réponse de contrainte cardiaque) et l'adventice (couche se composant de fibroblastes et de tissu connectif) (**Figure 1 A**).

L'athérome (athérosclérose) est le principal facteur qui endommage les artères. La formation d'athérosclérose est une accumulation segmentaire dans l'intima de l'artère, ces segments sont constitués de cellules spumeuses (macrophages chargés de cholestérol) ou débris tels que

des lipides, des glucides complexes, du sang et des produits sanguins, du tissus adipeux, des dépôts calcaires et autres minéraux (**Figure 2**) [7].

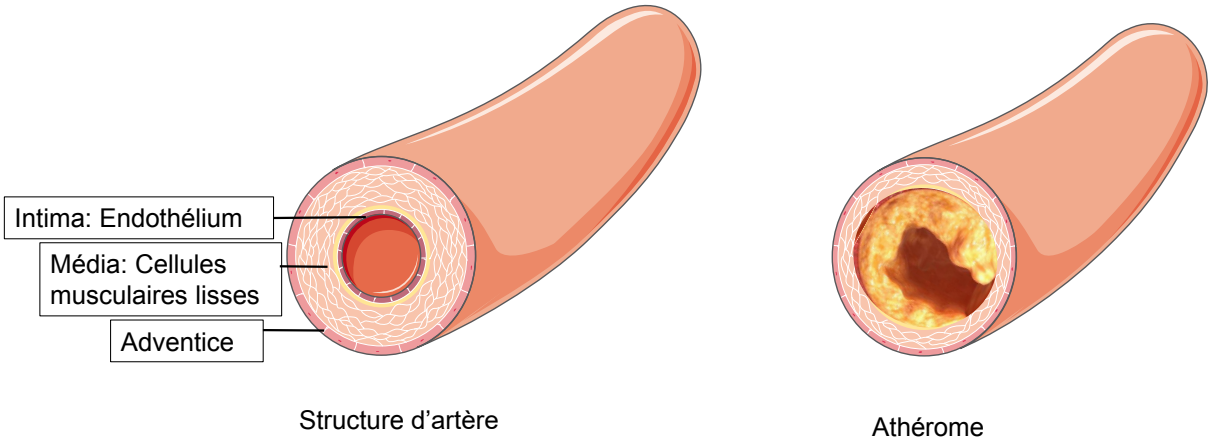

Figure 1. La structure d'une artère normale et d'une artère avec une plaque d'athérome

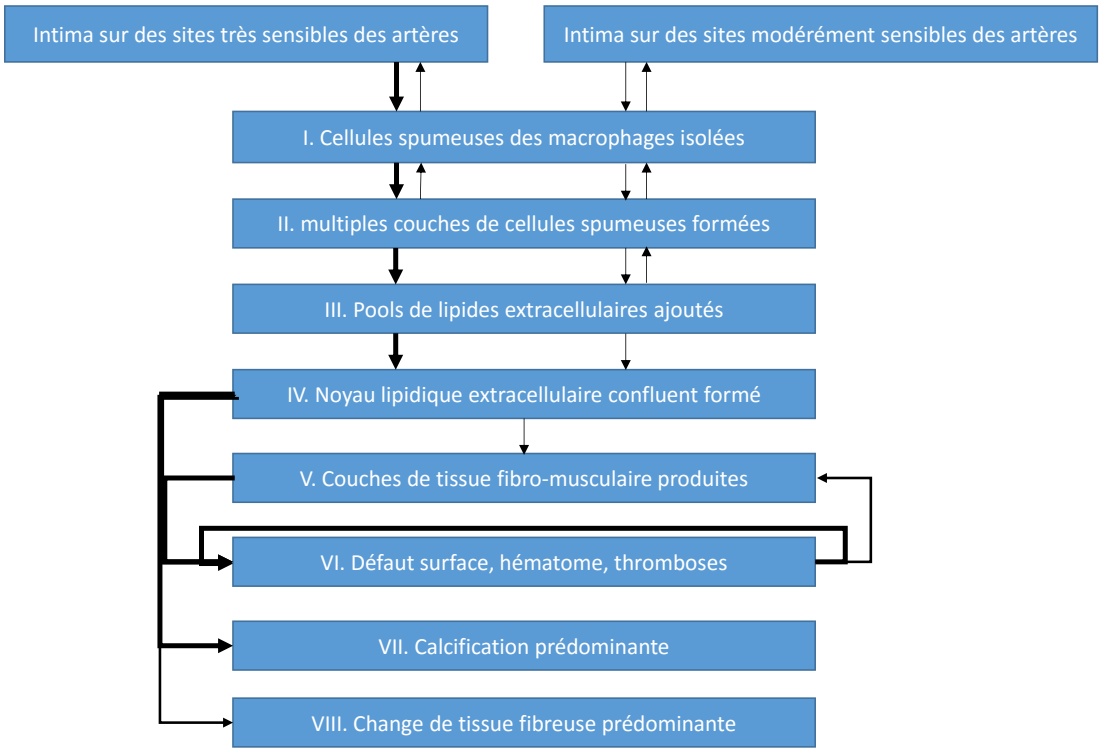

Figure 2. Schéma de la séquence dans l'évolution de la lésion athérosclérotique. Il montre les caractéristiques principales de chaque étape (type de lésion). Les flèches épaisses ou fines indiquent la fréquence et l'importance d'une voie de section[7].

Avec la formation de l'athérosclérose et sa progression, la lumière de l'artère réduit progressivement, en conséquence, l'athérome gêne le passage du sang (Figure 1B). Au cours du temps, les athéromes progressent en taille et en épaisseur, ce qui réduit la lumière de l'artère. Pour permettre le flux sanguin, une dilatation du vaisseau par l'étirement de la région centrale musculaire (la média) permet de compenser la taille d'ouverture de la lumière. Ce remodelage peut atteindre jusqu'à 50% de la surface en coupe transversale de l'artère[8]. Le rétrécissement de la lumière de l'artère continue à se prolonger dans certains sites, jusqu'à l'obstruction totale. Les cellules cardiaques ne sont alors plus suffisamment perfusées, et une ischémie myocardique se développe responsable, à terme, de événements fatals.

1.2. Traitement de l'insuffisance coronarienne

Il existe à ce jour deux types de traitement pour l'insuffisance coronarienne. Les traitements médicamenteux sont capables de normaliser la pression artérielle, d'abaisser la glycémie, de prévenir la formation de thrombus et l'inflammation. Les traitements chirurgicaux concernent les athérosclérose sévères, comme l'intervention coronarienne percutanée (angioplastie coronaire) et le pontage aorto-coronarien.

1.2.1 Angioplastie coronaire (AC)

L'angioplastie coronaire consiste à traiter une artère coronaire athéromateuse, en la dilatant au moyen d'une sonde munie d'un ballon gonflable à son extrémité. Pour renforcer l'effet de l'angioplastie coronaire, un stent peut être placé depuis une artère périphérique, à l'aide d'un guide métallique qui est glissé depuis l'artère brachiale en direction de la coronaire d'intérêt, pour maintenir ouverte la lumière de l'artère. Ainsi, la circulation sanguine est rétablie (**Figure 3**).

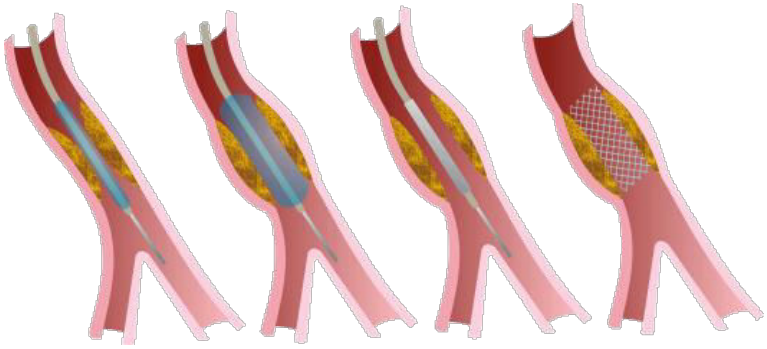

Figure 3. Schématique illustration de l'angioplastie. http://www.fedecardio.org/je-suis-cardiaque/examens/langioplastie

Depuis 1977 où le premier stent fut implanté chez l'homme[9], l'angioplastie coronaire s'est beaucoup développée, et devient une stratégie aussi importante que le pontage aorto-coronarien[10]. Pourtant, une des plus importantes complications de l'angioplastie coronaire est la re-sténose[11]. Pour pallier ce problème, les stents à élution de médicaments de deuxième génération se sont développés avec un grand succès[12]. Avec des prétraitements de molécules qui préviennent la formation de nouvelles plaques, ou des coating de polymères qui modifient leur surface, les nouveaux stents assurent une perméabilité plus durable[13][14]. Pour le développement de stents de la prochaine génération, de nombreuses études se concentrent sur la construction de nouveaux stents avec des matériaux anti-thrombogènes, incorporés de nanoparticules en améliorant leur perméabilité.

1.2.2 Pontage aorto-coronaire (PAC)

Le principe de pontage aorto-coronaire est le rétablissement de la circulation sanguine coronaire en anastomosant un greffon vasculaire entre l'aorte et le coronaire atteinte.

Bien que les stents à élution de médicaments favorisent davantage la perméabilité, le pontage aorto-coronaire donne de meilleurs résultats sur le long terme. Des études multicentriques ont clairement démontré la supériorité de PAC chez des patients atteints de diabète[15][16][17]. Une étude comparant 1800 patients atteints maladies coronariennes sévères traitées soit par PAC soit par Ac a montréque 3 ans après l'intervention, les patients traités par PAC ont un

taux d'événements cardiaques et cérébrovasculaires indésirables majeurs moins important que ceux traités par AC[18]. Avec les progrès au niveau du PAC tels que des interventions invasives à minima ou des opérations hybrides, et un meilleur traitement médical post-opératoire, le PAC demeure la procédure de prédilection pour traiter la maladie coronarienne.

Pour réaliser le pontage, il faut tout d'abord choisir le greffon adapté. Typiquement, il y a les veines (essentiellement la saphène) et les artères (mammaire, thoracique interne, …). Néanmoins, les veines saphènes sont les plus souvent utilisées et restent utiles dans plusieurs situations. Elles sont les plus facilement disponibles, elles fournissent un débit coronaire immédiat et fiable. Elles permettent une revascularisation coronaire rapide au cours des procédures d'urgence ou chez les patients sévèrement atteints pour lesquels la simplicité procédurale, la rapidité et la fiabilité sont les plus souhaitables. Cependant, en raison de la perméabilité inférieure à celle du greffon artériel à court et long termes, les veines saphènes ne sont plus le conduit de choix pour le PAC depuis une vingtaine d'années[19].

En effet, l'artère thoracique interne est le conduit préféré pour le PAC. Elle permet une meilleure survie à court et à long terme dans tous les sous-groupes de patients, y compris ceux de 75 ans et plus. En raison d'une meilleure compliance, les greffons artériels (artère thoracique interne, artère radiale, artère gastro-épiploïque) présentent toujours une meilleure perméabilité[20][21][22]. Cette observation est à la base de l'orientation de la recherche en ingénierie tissulaire vasculaire. On pourrait ainsi résumer le cahier des charges du greffon vasculaire idéal :

- une durabilité supérieure à l'espérance de vie du patient
- une bonne tolérance par l'organisme
- étanche au sang
- facile à suturer
- non thrombogénique
- souple mais ne s'oblitérant pas lorsqu'elle est fléchie
- résistante aux infections
- stérile et disponible en plusieurs dimensions

2. Ingénierie tissulaire vasculaire (ITV)

Même s'il existe déjà des greffons synthétiques commerciaux (Dacron®, par exemple) pour remplacer une artère malade de gros diamètre comme l'aorte, il n'y a pas encore de greffons hétérologues pour remplacer des artères de petit diamètre (<6mm). En effet, les thromboses se forment plus facilement dans les greffons exogènes lorsque le flux sanguin est réduit. Par conséquent, pour fournir des greffons hétérologues à des patients qui n'ont pas de vaisseaux autologues disponibles, l'ingénierie tissulaire vasculaire représente une alternative potentielle.

La conception d'ITV consiste à construire un vaisseau artériel en combinant des cellules et des biomatériaux afin d'obtenir un greffon qui présente les caractéristiques structurelles et bio-fonctionnelles proches du vaisseau natif. Pour l'usage clinique, le vaisseau issu de l'ingénierie doit posséder trois couches cellulaires, dont l'endothélium qui est nécessaire pour prévenir la thrombose. Les biomatériaux doivent être biocompatibles et biodégradables. Ainsi, les cellules utilisées et les biomatériaux restent deux enjeux majeurs dans l'ITV.

2.1. Les cellules

Un vaisseau cellularisé présente une perméabilité plus importante [23]. Le vaisseau idéal est celui qui contient trois couches : l'intima constituée de cellules endothéliales, la média avec des cellules musculaires lisses et l' adventice, avec des fibroblastes [24]. Les cellules endothéliales forment une couche monocellulaire dans la lumière de l'artère. Elles sont en contact directement avec le flux sanguin, forment une surface lisse pour laisser passer le sang, séparent la matrice sous-jacente des éléments thrombogènes, et secrètent des cytokines qui éliminent les plaquettes adhérentes à la paroi. Les cellules endothéliales matures sont souvent utilisées en ingénierie cellulaire pour mimer l'intima[25], mais ces CEs se dédifférencient rapidement *in vitro* en modifiant leur phénotype et perdant ainsi leurs fonctions.

Lors d'une lésion de la lumière artérielle, les progéniteurs endothéliaux circulantes se mobilisent et se localisent sur le site de la lésion pour se différencier en cellules endothéliales. D'autres cellules souches sont également capables de se différencier en cellules endothéliales et représentent une alternative utilisable en ingénierie tissulaire, plus particulièrement les cellules souches mésenchymateuses (CSM) (ref imm cell biol 2016). La différenciation de CSM en CE est caractérisée par l'expression de marqueurs spécifiques, dont les principaux sont :

- **CD 31** (Cluster of differentiation 31) ou appelé PECAM-1 (molécule d'adhésion des plaquettes aux cellules endothéliales -1)
- **VEGFR-2** (vascular endothelial growth factor receptor -2) encore appelé KDR (kinase domain containing receptor)
- **VE-Cadhérine** (Vascular endothelial Cadherin)
- **Tie-2** (Endothelium-specific receptor tyrosine kinase)
- **vWF** (Von Willebrand factor)

Les CSMs sont actuellement la source cellulaire la plus utilisée dans l'ITV[26], en raison de leur grande disponibilité, leur capacité à se différencier vers des CEs et des CMLs, et de leurs propriétés immunosuppressives[27]. La source classique de CSMs est la moelle osseuse. A ce jour, les CSMs peuvent être isolées à partir de plusieurs tissus tels que le tissu adipeux, la pulpe dentaire, le tissu périnatal comme la gelée de Wharton du cordon ombilical, etc. Cette dernière est considérée comme la source de préférences dans notre étude [28].

La différenciation des CSMs en cellules vasculaires (CEs et CMLs) in vitro peut être influencée par l'environnement dans lesquelles elles sont cultivées. Celui-ci est influencé par plusieurs facteurs: le milieu de culture contenant de multiples facteurs de croissance, surtout VEGF (vascular endothelial growth factor)[29][30], la stimulation par des contraintes de

cisaillement (shear stress)[31], la quantité ambiante d'oxygène et aussi la rigidité (stiffness) de la surface sur lesquelles les CSMs sont cultivées[32][33]. Bien que la différenciation induite par des facteurs de croissance soit bien étudiée, l'influence de contraintes mécaniques reste peu claire. Au cours de notre travail de thèse, nous nous sommes particulièrement intéressés, au regard de la littérature, à l'influence de celles-ci sur différentes sources cellulaires. Cela nous a donné l'occasion d'écrire une revue, qui constitue un chapitre de ce manuscrit.

Publication N°1
Manuscrit résumé en français

Rôle des stimulations mécaniques sur la différenciation vasculaire des cellules souches mésenchymateuses

Pan DAN, Emilie VELOT, Véronique DECOT et Patrick MENU

Les cellules souches, en particulier les cellules souches mésenchymateuses (CSM) sont souvent étudiées dans l'ingénierie vasculaire pour leur capacité de se différencier vers les lignées vasculaires (cellules endothéliales (CE) et cellules musculaires lisses, (CML)). La différenciation vasculaire des CSM peut être induite en culture statique en présence de facteurs de croissance. Par exemple, le facteur de croissance endothélial vasculaire (VEGF) est typiquement utilisé pour la différenciation endothéliale et le facteur de croissance transformant beta 1 (TGF beta1) pour la différenciation vers les CML. De plus, dans les vaisseaux natifs, un flux sanguin constant passe dans la lumière. Ce flux sanguin exerce différentes forces mécaniques sur les CE et les CML dans les vaisseaux. Pour cette raison, cette revue se concentre sur l'effet des forces mécaniques sur la différenciation vasculaire des CSM.

Dans la plupart des études analysées, le cisaillement combiné avec des facteurs de croissances semble avoir un effet synergique sur la différenciation. Nous avons ensuite discuté de l'éventuel mécanisme de la différenciation endothéliale induite par cisaillement. Il a été observé qu'avec la simulation par cisaillement, les CSM expriment le VEGF et en même temps diminuent l'expression de TGF-beta1, qui est le reflet d'une différenciation vers des CML. Ainsi, le cisaillement peut inhiber la différenciation en CML. Il est aussi connu que les CSM peuvent se différencier en ostéoblaste sous cisaillement. L'équilibre entre les CE et les ostéoblastes issus de CSM sous cisaillement dépend des paramètres du cisaillement, par exemple, la magnitude, les types et la durée du cisaillement.

Nous avons ensuite résumé les voies de signalisation pendant la différenciation endothéliale des CSM sous cisaillement. Le processus le plus important est la capacité de la cellule à sentir des stimuli mécaniques qui déclenchent la différenciation. Les composants cellulaires tels que les cils primaires, les canaux ioniques et les intégrines sont sensibles à la force due au cisaillement sur les cellules et transforment le signal mécanique en signal chimique pour l'activation des voies de signalisation. Les voies Raf–MEK–ERK et PI3K-Akt sont les deux principales voies impliquées dans la différenciation endothéliale induite par cisaillement.

Les CML qui se situent dans la média du vaisseau ne subissent pas de cisaillement, mais avec le flux sanguin sous forme de pulsation, elles se déforment par dilation et contraction répétitive. Ce type de mouvement génère une force mécanique de contrainte (cyclic strain en anglais). Il est montré dans diverses études que le *cyclic strain* peut jouer un rôle synergique dans la différenciation des CSM vers des CML. Cependant, il est plus souvent impliqué avec ou après un traitement par facteur de croissance, comme par exemple, par TGF-beta1.

Pour aboutir à un vaisseau issu de l'ingénierie tissulaire, il est important de maintenir le phénotype des cellules après différenciation jusqu'à l'implantation *in vivo*. Nous avons discuté dans cette partie de la revue, les avantages de la stimulation mécanique constante pour maintenir les CE et les CML différenciées *in vitro* jusqu'à l'implantation *in vivo*.

Finalement, en perspectives, il est nécessaire d'étudier le comportement des CSM sous stimulation mécanique dans un environnement 3D, qui simule la vraie condition *in vivo*. L'idéal serait de développer des bioréacteurs qui peuvent produire les deux types de forces mécaniques en même temps mais sur différentes couches de cellules, afin de fabriquer simultanément les CE comme intima et les CML comme média pour la construction d'un vaisseau artificiel.

© 2015. Published by The Company of Biologists Ltd | Journal of Cell Science (2015) 128, 2415-2422 doi:10.1242/jcs.167783

COMMENTARY

ARTICLE SERIES: STEM CELLS

The role of mechanical stimuli in the vascular differentiation of mesenchymal stem cells

Pan Dan[1,2], Émilie Velot[1], Véronique Decot[1,3] and Patrick Menu[1,*]

ABSTRACT

Mesenchymal stem cells (MSCs) are among the most promising and suitable stem cell types for vascular tissue engineering. Substantial effort has been made to differentiate MSCs towards vascular cell phenotypes, including endothelial cells and smooth muscle cells (SMCs). The microenvironment of vascular cells not only contains biochemical factors that influence differentiation, but also exerts hemodynamic forces, such as shear stress and cyclic strain. Recent evidence has shown that these forces can influence the differentiation of MSCs into endothelial cells or SMCs. In this Commentary, we present the main findings in the area with the aim of summarizing the mechanisms by which shear stress and cyclic strain induce MSC differentiation. We will also discuss the interactions between these mechanical cues and other components of the microenvironment, and highlight how these insights could be used to maintain differentiation.

KEY WORDS: Mesenchymal stem cells, Differentiation, Shear stress, Cyclic strain, Vascular tissue engineering

Introduction

Cardiovascular diseases, particularly clogging of the coronary artery, remain the biggest cause of mortality worldwide. Coronary artery bypass grafts (CABGs) are considered gold standard procedures for these diseases. Although the left internal mammary arteries and saphenous veins are still the preferential sources for CABGs, vascular tissue engineering has proven to be an attractive alternative. The engineering of small-diameter (<6 mm) vascular tissue has greatly advanced over the past two decades, with the majority of research efforts having been aimed at the generation of vascular grafts that mimic blood vessels.

Blood vessels typically comprise three main layers – the intima layer, which comprises endothelial cells; the media layer, which comprises smooth muscle cells (SMCs); and the outermost layer (adventitia), which is made up of fibroblasts and extracellular matrix (ECM) components. Endothelial cells are usually characterized by the expression of VE-cadherin, CD31 (also known as PECAM1) and vascular endothelial growth factor receptor 2 (VEGFR2, encoded by *KDR*), and by their capacity to take up acetylated low-density lipoproteins (ac-LDL), to form tubes in Matrigel® and to release nitric oxide. Smooth muscle cells, by contrast, are typified by the expression of contractile markers, such as smooth muscle α-actin (SMA, also known as ACTA2), calponin 1, SM22α (also known as TAGLN) and smooth muscle myosin heavy chain (SMMHC, also known as MYH11), and by the ability to synthesize ECM proteins (Owens, 1995). To be viable, the constructed graft needs to exhibit at least the following four properties – (i) a burst pressure superior to that of the saphenous veins; (ii) a long-term potency that resists the pressure of physiological circulation; (iii) avoidance of platelet adhesion that induces clot formation; and (iv) ease of engineering (L'Heureux et al., 2007). The first tissue-engineered blood vessel with these properties was constructed in 1998 and contained SMCs and endothelial cells that had both been isolated from human umbilical veins (L'Heureux et al., 1998). However, the use of mature vascular cells (i.e. those isolated from native blood vessels) is inherently limited because acquiring them demands an invasive procedure, they are typically available in insufficient quantities and they exhibit a low rate of proliferation (Shin'oka et al., 2001; Koike et al., 2004; L'Heureux et al., 2006). Thus, in order to advance vascular tissue engineering, stem cells have been intensively explored as alternative sources for both mature endothelial cells and SMCs (Ferreira et al., 2007). Among the various stem cell types that are suitable for application in vascular grafts, mesenchymal stem cells (MSCs) have been most extensively studied to date (Seifu et al., 2013). MSCs are found in different types of tissue of adult or perinatal origin, such as bone marrow, adipose tissue or Wharton's jelly from the umbilical cord (El Omar et al., 2014). Their high proliferation rate, multipotency and immunomodulatory properties make them a highly suitable candidate for vascular tissue engineering.

A number of factors are typically required to initiate vascular differentiation of stem cells *in vitro*. VEGF proteins are commonly used for differentiation into endothelial cells (Oswald et al., 2004), and transforming growth factor β1 (TGF-β1) or platelet-derived growth factor (PDGF) for differentiation into SMCs. In addition to these biochemical factors, the microenvironment of vascular cells exerts two main hemodynamic forces, shear stress and cyclic strain, which contribute to the differentiation process. Shear stress is generated by the blood passing through vessels, whereas cyclic strain is created by the pulsatile nature of blood flow, which produces a tensile stress that acts perpendicular to the vessel wall (Fig. 1). *In vitro*, both of these two mechanical cues can be replicated by different models, such as using a parallel-plate chamber for shear stress and a longitudinal stretch system for cyclic strain (see Box 1). MSCs are highly responsive to their mechanical environment, and different types of forces applied to the same MSC population result in divergent outcomes (Maul et al., 2011). Therefore, in this Commentary, we will summarize the available literature that describes a role for mechanical forces in the differentiation of MSCs into vascular cells and discuss different means to maintain differentiation.

The role of shear stress in the endothelial differentiation of MSCs

Endothelial cells regulate vascular tone and mural remodelling in a shear-dependent manner, which is commonly assumed to maintain

[1]UMR 7365 CNRS Université de Lorraine, Ingenierie Moleculaire et Physiopathologie Articulaire, Department of Cell and Tissue Engineering, Vectorization, Imaging, Biopôle de l'Université de Lorraine, Avenue de la forêt de Haye, C.S. 50184, Vandœuvre-lès-Nancy Cedex F-54505, France. [2]Department of Thoracic and Cardiovascular surgery, Zhongnan hospital of Wuhan University, Wuhan, 430071, China. [3]CHU de Nancy, Unité de Thérapie Cellulaire et Tissus, allée du Morvan, Vandœuvre-lès-Nancy F-54500, France.

*Author for correspondence (patrick.menu@univ-lorraine.fr)

Journal of Cell Science (2015) 128, 2415-2422 doi:10.1242/jcs.167783

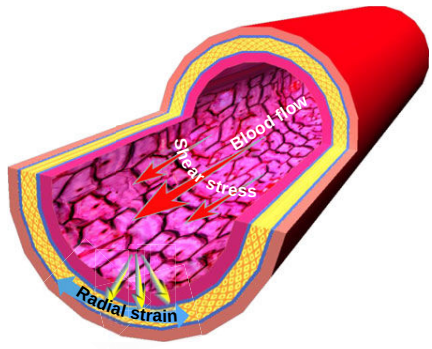

Fig. 1. Mechanical forces in native blood vessels. Endothelial cells are exposed to shear stress that is generated by blood flowing across the lumen surface. Because of the pulsatile nature of the hemodynamic stream, both endothelial cells and SMCs experience a cyclic tensile strain that is perpendicular to the vessel wall.

a constant level of wall shear stress across arteries. Recently published data suggest that the flow velocity experienced by endothelial cells varies in a species-dependent manner (Weinberg and Ross Ethier, 2007). In this section, we will summarize the main results published to date pertaining to the possibility of using mechanical stimulation to induce the differentiation of human and animal cells into endothelial cells.

The effect of shear stress on endothelial cells and MSCs

As pointed out earlier, the endothelium is in direct contact with blood and is therefore exposed to shear stress, which is in turn required for the development of new blood vessels both in embryos and in adults (le Noble et al., 2004; Folkman and Haudenschild, 1980). Blood flow in small-diameter arteries generates shear stresses that are within the range of 10–20 dyn/cm^2 in humans (Giddens et al., 1993). Such hemodynamic shear stress on endothelial cells is in fact important for the maintenance of the phenotype, orientation, metabolic activities and homeostasis of the vascular endothelium (Davies, 2009). Furthermore, blood flow exerts an anti-thrombotic effect in vessels by inducing the release of thrombomodulin by endothelial cells, which inactivates the pro-coagulant factor thrombin and activates the anticoagulant protein C (Yamawaki et al., 2005). As endothelial cells are an essential component of the vessel wall, much of the research has focused on obtaining endothelial cells *in vitro* after stem cell differentiation. Given the crucial role of shear stress in the differentiation of endothelial cells *in vivo*, it is believed that replicating shear stress in cell culture (*in vitro*) could be crucial for differentiating the stem cells towards the endothelial phenotype (Ahsan and Nerem, 2010; Yamamoto et al., 2005; Cheng et al., 2013).

The effect of shear stress on different types of MSCs has been studied previously. For example, bone-marrow-derived MSCs from a number of species are able to differentiate into endothelial-like cells when they are stimulated through physiological shear stress conditions (Engelmayr et al., 2006; Bai et al., 2010; Huang et al., 2010; Maul et al., 2011; Dong et al., 2009; Kim et al., 2011). Likewise, MSCs derived from human adipose tissue (hASCs) (Bassaneze et al., 2010; Zhang et al., 2011; Shojaei et al., 2013) and MSCs from other sources, such as amniotic fluid cells (Zhang et al., 2009) and human placenta (Wu et al., 2008), have also been shown to differentiate into endothelial-like cells under shear stress (see Table 1 for a summary).

Box 1. *In vitro* models of shear stress and cyclic strain for the differentiation of MSCs

The endothelium is exposed to both laminar and pulsatile shear stresses in blood vessels. In order to mimic the effect of flow on cultured MSCs, various types of device are typically used, including parallel-plate chambers, orbital shakers, and tubular and microfluidic devices. Parallel-plate chambers are constructed by sandwiching a silicone gasket between the plate chamber and a glass slide that is seeded with cells. A peristaltic pump then drives the medium through the chamber in order to generate a 2D laminar shear stress on the cells (Wang et al., 2005; Wu et al., 2008; Bai et al., 2010; Maul et al., 2011). Orbital shakers (or rotating disks) rotate the medium-coated disk so that the medium flows concentrically, thus generating laminar or turbulent shear stress over cells that are seeded onto the bottom of the disk (Fischer et al., 2009; Zhang et al., 2009; Bassaneze et al., 2010). Tubular shear stress systems perfuse medium through a tubular scaffold, the inner layer of which is seeded with MSCs (Kim et al., 2011; Dong et al., 2009; O'Cearbhaill et al., 2008). Microfluidic systems contain submillimeter-sized modules that are made out of gel, such as collagen, and filled with the cells of choice; these modules are then packed into a chamber with pillars to hold them in place, before the chamber is connected to a flow circuit to undergo fluid perfusion (Bruzewicz et al., 2008; Khan and Sefton, 2010; Khan et al., 2012).

To stretch MSCs, cells are usually seeded onto a flexible silicone membrane, which is elongated by negative suction to generate an equixial cyclic strain (Park et al., 2004; Gong and Niklason, 2008). Uniaxial cyclic strain can be generated by connecting one end of a membrane to a fixed frame while the other end is attached to a movable frame, thus producing a one-way motion (Park et al., 2004; Jang et al., 2011). Many of the bioreactors available today generate cyclic circumferential stretch together with axial stretch (reviewed by Huang and Niklason, 2014). (For more information, see Zhou and Niklason, 2012; Mironov et al., 2011).

Is shear stress sufficient for differentiation of MSCs?

In addition to shear stress, the physiological microenvironment of the vessels also plays a role in endothelial cell differentiation, particularly if it contains VEGF proteins. This effect has been shown in a study that compared the consequences of shear stress, treatment with VEGF-family members or a combination of both stimuli on rat MSCs (Bai et al., 2010). In that report, the two stimuli are shown to have a synergistic effect on endothelial cell differentiation. Furthermore, when VEGF was removed from the culture, and shear stress was continued for up to 48 h, loss of endothelial markers was observed, suggesting that de-differentiation had begun. By contrast, another study did not observe any endothelial cell markers on hASCs that had been treated with 10 dyn/cm^2 of shear stress alone, even after 96 h of stimulation (Bassaneze et al., 2010). The authors suggest that the failure to differentiate is caused by the lack of VEGFR2 expression in hASCs, which is essential to induce their differentiation into endothelial cells (Bassaneze et al., 2010).

A synergy between VEGF proteins and shear stress had already been shown in two studies (Wu et al., 2008; Fischer et al., 2009). When cells were cultured in endothelial cell growth supplement for 3 days under static conditions and subsequently exposed to shear stress of 12 dyn/cm^2 for at least 24 h, expression of CD31 and increased ac-LDL uptake were observed, as well as tube formation *in vitro*. Analogous results have been obtained by Zhang et al., who report that MSCs derived from human amniotic fluid and hASCs that have been cultivated in endothelial cell differentiation medium EGM™-2 for two weeks express von Willebrand factor (vWF) and CD31, and gain the ability to release endothelial nitric oxide synthase (eNOS, also known as NOS3) and to form tubes on Matrigel®. The subsequent application of shear stress further increases the expression of endothelial markers and enhanced functional characteristics (Zhang et al., 2009).

Journal of Cell Science

Journal of Cell Science (2015) 128, 2415-2422 doi:10.1242/jcs.167783

Table 1. Summary of the effects of shear stress on endothelial differentiation of MSCs

Mechanical force regime	Stem cell type	Stimulation	Effect of mechanical stimuli on the differentiation outcome	References
Shear stress alone on cells of animal origin	Murine MSC line C3H10T1/2	Pulsatile shear stress for 6, 12 and 24 h	Expression of endothelial cell markers, cell alignment, inhibition of SMC marker TGF-β	Wang et al., 2005, 2008
	Canine BMMSCs	3D pulsatile shear stress of 15 dyn/cm^2 for 4 days	Cell alignment, upregulation of endothelial cell markers and downregulation of SMC markers	Dong et al., 2009
	Rat BMMSCs	Pre-treatment with VEGF for 7 days, shear stress with or without pre-treatment	Expression of endothelial cell markers under shear stress, which is enhanced by pre-treatment; cell alignment is only observed under shear stress	Bai et al., 2010
	Rat BMMSCs	Laminar shear stress of 1 or 20 dyn/cm^2 up to 5 days	Cell alignment and expression of endothelial cell markers under high shear stress, downregulation of endothelial cell markers under low shear stress, downregulation of SMC markers under both conditions	Maul et al., 2011
Shear stress alone on human MSCs	Human ASCs	Shear stress of 10 dyn/cm^2 up to 96 h	Failure to induce expression of any endothelial cell marker, no cell alignment, increased synthesis of nitric oxide	Bassaneze et al., 2010
	Human BMMSCs	Shear stress of 2 or 20 dyn/cm^2 for 2 days and subsequent static culture for 5 days	Endothelial cell differentiation owing to high levels of shear stress	Yuan et al., 2013
Combination of shear stress and growth factors	Human placenta derived MSCs	Cells cultured in EGM™-2 subsequently subjected to 6 or 12 dyn/cm^2 shear stress	Cell alignment owing to a combination of stimuli, more substantial expression of endothelial cell markers and endothelial cell functionality under high shear stress	Wu et al., 2008
	Human ASCs	Pre-treatment with VEGF for 2 weeks and subsequent shear stress for 8 days	Cell alignment, ac-LDL uptake and expression of CD31	Fischer et al., 2009
	Human amniotic fluid derived MSCs/human ASCs	Pre-treatment with EGM™-2 medium for 2 weeks and shear stress for 48 h	Endothelial cell differentiation during pre-treatment, which was strengthened by shear stress application; shear-stress-mediated endothelial cell differentiation that is dependent on PI3K but not on MAPKs	Zhang et al., 2009
	Human BMMSCs	Low (2.5 dyn/cm^2) or high (10 dyn/cm^2) shear stress took place in EGM™-2	Low shear stress results in increased expression of endothelial cell markers, high shear stress leads to higher expression of SMC markers	Kim et al., 2011
Combination of shear stress and cyclic strain	Sheep BMMSCs	Cyclic flexure (1 Hz, 5%) and shear stress (1.105 dyn/cm^2) for up to 3 weeks	Expression of endothelial cell markers when both stimuli are combined	Engelmayr et al., 2006
	Human BMMSCs	Cyclic strain (1 Hz, 5%) and shear stress (10 dyn/cm^2) for 24 h	Cell alignment and morphology similar to that of endothelial cells, but with considerable expression of SMC markers	O'Cearbhaill et al., 2008
	Human ASCs	Combination of cyclic strain (1 Hz, 10%), shear stress (2.5 dyn/cm^2) and VEGF	Expression of endothelial cell markers	Shojaei et al., 2013

ac-LDL, acetylated low density lipoprotein; ASCs, adipose-derived MSCs; BMMSC, bone marrow mesenchymal stem cell; CD, cluster of differentiation; EGM™-2, endothelial growth medium; MAPK, mitogen-activated protein kinase; MSC, mesenchymal stem cell; PI3K, phosphatidylinositol 3-kinase; SMC, smooth muscle cell; TGF-β, transforming growth factor β; VEGF, vascular endothelial growth factor.

Taken together, these studies suggest that mechanical and biochemical influences synergize in order to increase endothelial cell functionality and the expression of endothelial cell markers.

How does shear stress affect endothelial differentiation of MSCs?

Inhibition of SMC differentiation

Although shear stress plays a role in endothelial cell differentiation, the underlying mechanism remains unclear. According to two independent studies, it appears that shear stress promotes endothelial differentiation, while downregulating differentiation towards a SMC phenotype (Wang et al., 2008; Dong et al., 2009). Specifically, the first study showed that murine MSCs subjected to a shear stress of 15 dyn/cm^2 express VEGF, but significantly decrease their expression of other growth factors – such as TGF-β1, as well as PDGF and its receptor – which are known to guide stem cells towards the SMC lineage (Wang et al., 2008). Similarly, Dong et al. have shown an increase in endothelial markers at both the mRNA and protein levels, whereas SMC markers, such as SMA and calponins, decrease after subjecting canine MSCs to a shear stress of 15 dyn/cm^2 over 2 days (Dong et al., 2009). Furthermore, the effect of shear stress on differentiation has been shown to vary depending on stress

Journal of Cell Science (2015) 128, 2415-2422 doi:10.1242/jcs.167783

intensity. For example, Kim et al. report that MSCs that have been exposed to low (2.5 dyn/cm^2) or high (10 dyn/cm^2) shear stress express endothelial markers, including CD31, vWF and VEGFR2. The expression of CD31 under low shear stress is considerably higher than that under high shear stress, whereas the expression of vWF and VEGFR2 is only slightly higher under low shear stress. Furthermore, MSCs that have been exposed to high shear stress show a significantly higher expression of SMC markers (myocardin, SMMHC and SM22α) (Kim et al., 2011). By contrast, other studies have suggested that shear stress increases the amount of TGF-β1 and of SMC markers (Park et al., 2007; Kobayashi et al., 2004). These apparent inconsistencies regarding the expression of TGF-β1 and SMC-specific markers could be attributable to the use of different types of stem cells, culture conditions or shear stress regimes.

Effects on the balance between osteoblastic and endothelial differentiation

The effects of mechanical forces on stem cell differentiation depends on the way the force is applied to cells (i.e. continuous stimulation or intermittent) and on its intensity; however, the fate of the stem cells might also be influenced by the stiffness of the substrate on which they are cultured. For example, two studies have reported that shear stress applied to stem cells leads to osteoblastic differentiation of MSCs (Lim et al., 2011; Yeatts et al., 2012). Furthermore, two studies by Kreke et al. have demonstrated that intermittent or low shear stress (below 3 dyn/cm^2) induces osteocalcin expression by bone marrow MSCs that have been cultured on fibronectin and enhances the expression of other bone proteins compared with that of cells cultured with osteogenic factors under static conditions (Kreke et al., 2005, 2008). McBride et al. have followed a similar approach and investigated shear-stress-mediated gene expression changes in the MSC line C3H/10T1/2 in order to determine the role of shear stress in osteogenesis (McBride et al., 2008). They find that exposure of cells to a continuous shear stress of either 0.2 dyn/cm^2 or 1 dyn/cm^2 for 30 or 60 min induces the upregulation of a number of ossification-related genes, including those encoding collagen type I, collagen type II, Runx2 and Sox9. In this experiment, the length of exposure to shear stress (30 or 60 min) was a stronger predictor of the genes that are upregulated than the intensity of the applied shear stress. By contrast, in an earlier study that exposed the same cell line to laminar shear stress (15 dyn/cm^2) for 6 or 12 h, shear-stress-mediated upregulation of endothelial instead of bone differentiation markers was observed (Wang et al., 2005).

Taken together, these results indicate that the intensity and duration of the shear stress employed affects the balance between osteogenic and endothelial differentiation and could thus lead to different outcomes depending on the regime used.

Effects of shear stress on mechanotransduction and associated signalling pathways

On the basis that shear stress alone can direct differentiation towards an endothelial cell phenotype, the underlying molecular mechanism has been explored. Mechanosensitive cell surface molecules, such as primary cilia, integrins, ion channels and focal adhesion proteins, are able to mediate cellular responses to various forces. The primary cilium, which is ubiquitous in mammals, is an immotile microtubule-based organelle that protrudes from the apical surface and is able to bend in response to flow (Praetorius and Spring, 2005; Satir et al., 2010). A model for primary-cilia-based mechanosensing has been described in which bending of the cell cilium by shear flow can activate ion channels embedded in the membrane (Janmey and McCulloch, 2007). More recently, a study has provided evidence that primary cilia are involved in the osteogenic differentiation of human bone marrow MSCs (hBMMSCs) (Hoey et al., 2012). Other studies have suggested that transmembrane proteins, including ion channels and integrins, could be activated directly by shear flow as well as cyclic strain because these mechanical forces induce changes to the membranes – including altering membrane tension, which activates ion channel conductance (Liu and Lee, 2014). Opening of these channels increases the cytoplasmic concentration of the associated ion, which then changes the membrane potential, or, alternatively, the ions themselves can act as second messengers (Wu et al., 1999). For example, it has been shown that Ca^{2+}-signalling pathways can be activated through the activation of the mitogen-activated protein kinase (MAPK) pathway, which controls osteogenic differentiation of MSCs (Barradas et al., 2013).

Integrins not only bind to many components of the ECM, such as collagen and laminin, but also to other proteins, such as VEGF-A or insulin-like growth factor binding proteins (IGFBP1 and IGFBP2) (Vlahakis et al., 2007). Integrins link the ECM to the cytoskeleton and so facilitate the formation of focal adhesions between the cell and the ECM (Hoffman et al., 2011). At focal adhesions, integrins can also translate physical forces into biological signals (Schwartz and Assoian, 2001). Specific interactions formed by the α and β subunits of integrins that are activated by shear stress trigger the focal adhesion kinase (FAK)–Src and the caveolin 1 (Cav1)–Fyn kinase pathways, thereby eliciting phosphorylation cascades of various downstream effectors and their interaction with each other through SH2- and SH3-domain-mediated interactions. The two pathways converge at the Raf–MEK–ERK axis in endothelial cells (Shyy and Chien, 2002). Cheng et al. have shown that the integrin–Ras–ERK pathway also has a role in endothelial cell differentiation. They report that exposure of endothelial progenitor cells (EPCs) to shear stress results in an increase in the endothelial maturation markers CD31 and vWF (Cheng et al., 2013). In this work, shear stress was also found to activate several mechanosensitive molecules, including integrin β1, Ras, ERK1/2, paxillin and FAK, which are all involved in cytoskeletal rearrangements, as well as in the differentiation into late EPCs (Cheng et al., 2013).

Other cell surface molecules, such as G-protein-coupled receptors (GPCRs) and the glycocalyx, also serve as sensors of shear stress (Ando and Yamamoto, 2009; Stolberg and McCloskey, 2009). Mechanical stress and/or ligand binding induces conformational changes in the GPCRs, which transduce a signal to the cytoplasmic tail. Guanosine triphosphate (GTP) can provoke further conformational changes of the receptor, leading to its association with Ras, which in turn activates phosphoinositide 3-kinase (PI3K)–Akt pathway. This pathway has been shown to regulate MSC survival, proliferation, migration and other cellular fates through crosstalk with the Wnt-signaling pathway (Huang et al., 2013). Furthermore, it has been shown that during endothelial cell differentiation of hASCs in response to shear stress, the acquisition of endothelial cell characteristics also depends on the PI3K–Akt pathway (Zhang et al., 2011). In this context, it is also worth mentioning that other protein kinases that are involved in cell growth and differentiation are recruited following mechanical stimulation of GPCRs, including p38-family MAPKs, ERK1/2, JNK-family kinases and YAP/TAZ (Kaneko et al., 2014). Other pathways may be involved downstream of these surface molecules as recently reviewed in (Shah et al., 2014).

Role of cyclic strain in the differentiation of MSCs into SMCs

SMCs are located in the middle layer of small-diameter arteries and play an important role in maintaining the elasticity and homeostasis of blood vessels. Their limited proliferative capacity and reduced

Journal of Cell Science (2015) 128, 2415-2422 doi:10.1242/jcs.167783

collagen production thus prevent the formation of neointima (scar tissue) and luminal narrowing (Paszkowiak and Dardik, 2003).

Biochemical factors such as TGF-β1 and PDGF have a well-established role in the differentiation of MSCs into SMCs. Successful SMC differentiation that is mediated by these growth factors is usually assessed by the expression of major SMC-specific proteins – including SMA, SM22α, calponin-family proteins, heavy caldesmon (h-caldesmon) and SMMHC – contraction in response to carbachol and KCl, and the production of ECM (Owens, 1995; Huang and Niklason, 2014). SMCs experience constant mechanical stimulation in blood vessels and undergo cyclic strain that results from pulsatile stresses from the systolic ejection of the heart. Under physiological conditions, the strain levels in blood vessels are in the range 5–30% at frequencies of 30–90 cycles per minute (0.5–1.5 Hz) (Huang and Li, 2008). This phenomenon has generated interest in recent years, and a number of studies have investigated the effect of cyclic strain on MSC differentiation into SMCs (summarized in Table 2).

Cyclic strain parameters for differentiation into SMCs

Cyclic strain is usually generated *in vitro* by the repetitive extension and constriction of the elastic substrates onto which cells have been seeded. Cyclic strain can be applied and investigated in both two- and three-dimensional (2D and 3D, respectively) systems, with elastic silicone membranes most commonly used as a scaffold for 2D models and tubular matrices for 3D models. In 2D stretch models, cyclic strain is divided into uniaxial and equiaxial strains. Uniaxial strain refers to the fluid force along only one axis, whereas equiaxial strain describes uniform strain in all directions. Park et al. have compared the efficacies of equiaxial and uniaxial strain in inducing differentiation of hBMMSCs into SMCs in a 2D model. Equiaxial strain decreases the expression of the SMC markers SMA and SM22α, whereas uniaxial strain transiently increases their expression after 1 day of treatment. Furthermore, hBMMSCs align perpendicularly to the uniaxial strain axis but not that of the equiaxial strain (Park et al., 2004). In fact, the majority of studies using 2D models have been performed with uniaxial cyclic strain and result in SMC-like cells (Hamilton et al., 2004; Kurpinski et al., 2009; Jang et al., 2011; Ghazanfari et al., 2009). 3D models that are designed to replicate the status of SMCs *in vivo* because the radial distension of the tubular grafts that is induced by blood flow pressure allow cells to experience an effective uniaxial cyclic stain, similar to that in their natural environment (Du et al., 2011; Zheng et al., 2012). However, unlike the perpendicular orientation that is observed in most 2D uniaxial cyclic strain experiments, SMCs in native vessels align themselves parallel to the principal direction of the strain. Furthermore, comparison between the effects of 2D uniaxial strain and 3D radial distension on SMC differentiation has shown that the latter results in a significantly lower level of expression of

Table 2. Summary of the effects of cyclic strain on differentiation of MSCs into SMCs

Mechanical force regime	Stem cell type	Stimulation	Effect of mechanical stimuli on the differentiation outcome	References
Cyclic strain alone	Rat BMMSCs	10%, 1 Hz uniaxial strain for 7 days	Cell alignment perpendicular to cyclic strain, expression of SMA and calponin	Hamilton et al., 2004
	Human BMMSCs	10%, 1 Hz uniaxial and equiaxial strain for 1–3 days	Cell alignment perpendicular to cyclic strain and transient increase of SMA, SM22α and collagen type I only under uniaxial cyclic strain; equiaxial strain results in downregulation of SMA and SM22α	Park et al., 2004
	Rat BMMSCs	10%, 1 Hz longitudinal strain for 6 days on 3D model	Cell alignment parallel to cyclic strain, expression of SMA and calponin, production of collagen	Nieponice et al., 2007
	Human BMMSCs	0–25%, 1–3 Hz uniaxial strain for 2–4 h	Cell alignment perpendicular to cyclic strain and SMA expression	Ghazanfari et al., 2009
	Human BMMSCs	2D 5%, 1 Hz uniaxial and 3D strain	Greater increase in expression of SMA and calponin proteins in 2D compared with that in a 3D model	O'Cearbhaill et al., 2010
Cyclic strain and chemical factors	Murine MSC line	10%, 1 Hz uniaxial strain with TGF-β1 for 6 days	Cell alignment in the direction of cyclic strain, increase in levels of SMA and SMMHC	Riha et al., 2007
	Human ASCs	10%, 1 Hz uniaxial strain with TGF-β1 for 7 days	Cell alignment in the direction of cyclic strain; cyclic strain alone decreases the expression of SMC markers, but combination of TGF-β1 and cyclic strain increases their levels	Lee et al., 2007
	Human ASCs	TGF-β1 and BMP-4 for 7 days, further cultivation on polyglycolic acid for 7 days, then 5% strain for 8 weeks	SMC differentiation is already induced by chemical factors alone; cyclic strain further enhances the expression of SMA and calponin, and the deposition of collagen	Wang et al., 2010
Cyclic strain and use of parallel microgrooves	Human BMMSCs	Pre-treatment (or not) with TGF-β1 for 24 h and subsequent 5%, 1 Hz uniaxial strain for 24 h, cells cultivated in parallel groove	Cell alignment parallel to the groove, expression of calponin, perpendicular cyclic strain does not change this alignment but reduces the levels of calponins	Kurpinski et al., 2006, 2009
	Rabbit MSCs	Microgroove and 3% and 10%, 0.26 Hz uniaxial strain for 3 days	Perpendicular cell arrangement on a flat surface with grooves acting as obstacles for this orientation, expression of SMA and h-caldesmon decreases with 3% strain but increases with 10% strain, maintenance of SMC marker expression on cells grown on grooved surface after cyclic strain has ceased	Jang et al., 2011

ASCs, adipose-derived MSCs; BMMSC, bone marrow mesenchymal stem cell; BMP-4, bone morphogenetic protein 4; h-caldesmon, heavy caldesmon; MSC, mesenchymal stem cell; SMA, smooth muscle actin; SMC, smooth muscle cell; SMMHC, smooth muscle myosin heavy chain; TGF-β1, transforming growth factor β1.

Journal of Cell Science (2015) 128, 2415-2422 doi:10.1242/jcs.167783

SMC-associated markers (O'Cearbhaill et al., 2010). Although 2D uniaxial strain induces a different response from that of the *in vivo* situation in terms of cell alignment, it is nevertheless more effective in mediating differentiation than cyclic strain applied in a 3D model. It is thus clear that additional 3D models need to be developed which are able to better replicate *in vivo* conditions and thus might be more effective in directing differentiation towards SMCs (Smith and Gerecht, 2014).

In the case of rat and human MSCs, cyclic strain alone has been shown to induce the expression of some but not all SMC markers, in particular markers of mature SMCs such as SMMHC (Nieponice et al., 2007; Hamilton et al., 2004; Ghazanfari et al., 2009; O'Cearbhaill et al., 2010). In order to increase differentiation efficiency, cyclic strain can be applied in combination with other factors, such as growth factors. For instance, it has been shown that in order to maintain the SMC phenotype induced by growth factors (e.g. TGF-β1, BMP-4), that is to avoid a loss of SMC-related markers, this stimulation needs to be followed by pulsatile strain (Wang et al., 2010). However, a different study has been successful in obtaining differentiation only by combining TGF-β1 and uniaxial strain, as these factors showed a positive synergistic effect (Kurpinski et al., 2009).

Based on the above studies, we can conclude that two methods can be used to ensure long-term (or stable) SMC differentiation – sequential stimulation (first by chemical then mechanical means) or synergistic stimulation (simultaneous chemical and mechanical stimulation).

A requirement for more accurate cyclic strain models for differentiation into SMCs

As a general rule, the duration of mechanical stimulation that is required to achieve differentiation into SMCs is longer than that for differentiation into endothelial cells. Cyclic strain should be applied for at least 3 days in order to mediate the expression of some SMC markers, such as SMA, but even this is insufficient for the expression of mature markers, such as SMMHC (Hamilton et al., 2004). Cyclic strain has also been used to induce other types of differentiation, such as differentiation into skeletal muscle cells (Haghighipour et al., 2012), neuron-like cells (Leong et al., 2012) and osteogenic lineages. It is worth noting that cyclic strain alone can evoke considerable expression of SMC markers, as well as upregulation of the osteoinductor bone morphogenic protein 2 (BMP-2) and the early matrix protein osteopontin (OPN) (Maul et al., 2011). In recent work, the role of cyclic strain intensity on MSC differentiation was investigated. It was shown that cells that are stretched at 0.1 Hz express higher levels of osteoblast-specific genetic and protein markers compared with cells that are stretched at 1 Hz, which express significantly higher levels of vascular-SMC-specific genetic and protein markers (Yao and Wong, 2015). These results also support the findings of an earlier study, in which cyclic strain of a low magnitude (0.26 Hz, 3%) mediated the differentiation of MSCs into osteogenic cells, whereas greater cyclic strain (0.26 Hz, 10%) favoured differentiation into SMCs (Jang et al., 2011).

Further research efforts are thus required to develop protocols that promote reliable cyclic-strain-induced differentiation of cells into SMCs that exhibit a contractile phenotype for use in vascular tissue engineering.

Maintaining endothelial cells and SMCs in their differentiated state

For the purpose of vascular tissue engineering, an ideal multilayer vessel would comprise an innermost layer of endothelial cells, a middle layer of SMCs and an outer layer comprising ECM and fibroblasts. The studies summarized above suggest that shear and cyclic stress can be used to differentiate MSCs into endothelial cells and SMCs, respectively. Questions remain, however, as to whether the differentiation that has been initiated *in vitro* can be maintained long term and how to avoid cellular dedifferentiation once the stimulation is terminated. One of the answers could be to maintain the tissue-engineered blood vessels (TEVs) under continuous stimulation with shear stress or cyclic strain. This can be achieved *in vitro* with the use of bioreactors or by grafting the vessel into a host organism *in vivo*, thereby exploiting the host's physiological environment to generate either shear stress by blood flow or cyclic strain by pulsatile stimulation.

In the area of bioreactors, Huang et al. have recently designed a bioreactor that can better simulate the physiological stresses acting on native arteries and that allows biaxial stretching during culture (Huang and Niklason, 2014; Huang et al., 2015). Biaxial stretching induces a greater wall thickness compared with stimulation with static or uniaxial stretch. Furthermore, this stimulation leads to the development of undulated collagen fibres and mature elastin in the ECM, which might contribute to the observed vascular compliance in the biaxial TEVs obtained with this bioreactor. These results suggest that this type of bioreactor could be used to optimize biomechanical conditioning of TEVs and, thus, could help to maintain cells in a differentiated state.

Regarding the *in vivo* implantation of vascular grafts to improve their patency after being engineered *in vitro*, interesting results have been obtained. For instance, Udelsman et al. have recently engineered a vessel by using a polymer that had been seeded with bone marrow mononuclear cells, which they then implanted into mice. After 7 months, they observed the development of a luminal endothelial cell layer, as well as a SMC-populated 'medial' layer that associated with components of ECM, including elastin and collagen type I and type III, suggesting that cells that have been biomechanically stimulated *in vivo* could differentiate into endothelial cells or SMCs (Udelsman et al., 2014). Zhao et al. have also shown that it is possible to maintain cell differentiation after implantation *in vivo*. These authors constructed a TEV by using endothelial cells and SMCs that had been differentiated from MSCs and seeded onto a decellularized ovine artery, which was subsequently interposed in the carotid arteries in an ovine host model. After 5 months, the analysis of the graft showed the existence of endothelium, smooth muscle, collagen and elastin, indicating that differentiation had been maintained over this period of time (Zhao et al., 2010).

Conclusion and perspectives

Shear stresses at physiological levels can differentiate MSCs into endothelial cells by inducing the expression of endothelial-cell-specific markers and endothelial-cell -specific functional properties. Cyclic strain, both in 2D and 3D models, can guide MSCs to differentiate into SMCs by inducing the expression of several SMC-associated markers. However, compared with shear stress-mediated endothelial cell differentiation, cyclic strain alone has only a relatively limited ability to induce SMC differentiation. It is clear that mechanical force can increase vascular differentiation in combination with biochemical factors, such as growth factors. Taken together, the studies described here suggest that the most effective device for generating high-functioning TEVs would be one that is capable of applying shear stress and cyclic strain on seeded MSC-derived endothelial cells and SMCs, in order to maintain their activity and differentiation state before use in tissue

engineering. However, much remains to be done to progress from 2D to 3D models and from *in vitro* to *in vivo* applications in order to be able to produce a mechanical-force-mediated tissue-engineered vessel for clinical use.

Acknowledgements
We thank Professor Kira Weissman for careful reading of the review.

Competing interests
The authors declare no competing or financial interests.

Funding
This study was supported by an overseas fellowship from the China scholarship council.

References

Ahsan, T. and Nerem, R. M. (2010). Fluid shear stress promotes an endothelial-like phenotype during the early differentiation of embryonic stem cells. *Tissue Eng. A* **16**, 3547-3553.
Ando, J. and Yamamoto, K. (2009). Vascular mechanobiology: endothelial cell responses to fluid shear stress. *Circ. J. Off. J. Jpn. Circ. Soc.* **73**, 1983-1992.
Bai, K., Huang, Y., Jia, X., Fan, Y. and Wang, W. (2010). Endothelium oriented differentiation of bone marrow mesenchymal stem cells under chemical and mechanical stimulations. *J. Biomech.* **43**, 1176-1181.
Barradas, A. M. C., Monticone, V., Hulsman, M., Danoux, C., Fernandes, H., Tahmasebi Birgani, Z., Barrère-de Groot, F., Yuan, H., Reinders, M., Habibovic, P. et al. (2013). Molecular mechanisms of biomaterial-driven osteogenic differentiation in human mesenchymal stromal cells. *Integr. Biol.* **5**, 920-931.
Bassaneze, V., Barauna, V. G., Lavini-Ramos, C., Kalil, J., Schettert, I. T., Miyakawa, A. A. and Krieger, J. E. (2010). Shear stress induces nitric oxide–mediated vascular endothelial growth factor production in human adipose tissue mesenchymal stem cells. *Stem Cells Dev.* **19**, 371-378.
Bruzewicz, D. A., McGuigan, A. P. and Whitesides, G. M. (2008). Fabrication of a modular tissue construct in a microfluidic chip. *Lab. Chip* **8**, 663-671.
Cheng, M., Guan, X., Li, H., Cui, X., Zhang, X., Li, X., Jing, X., Wu, H. and Avsar, E. (2013). Shear stress regulates late EPC differentiation via mechanosensitive molecule-mediated cytoskeletal rearrangement. *PLoS ONE* **8**, e67675.
Davies, P. F. (2009). Hemodynamic shear stress and the endothelium in cardiovascular pathophysiology. *Nat. Clin. Pract. Cardiovasc. Med.* **6**, 16-26.
Dong, J.-d., Gu, Y.-q., Li, C.-m., Wang, C.-r., Feng, Z.-g., Qiu, R.-x., Chen, B., Li, J.-x., Zhang, S.-w., Wang, Z.-g. et al. (2009). Response of mesenchymal stem cells to shear stress in tissue-engineered vascular grafts. *Acta Pharmacol. Sin.* **30**, 530-536.
Du, Y., Ghodousi, M., Qi, H., Haas, N., Xiao, W. and Khademhosseini, A. (2011). Sequential assembly of cell-laden hydrogel constructs to engineer vascular-like microchannels. *Biotechnol. Bioeng.* **108**, 1693-1703.
El Omar, R., Beroud, J., Stoltz, J.-F., Menu, P., Velot, E. and Decot, V. (2014). Umbilical cord mesenchymal stem cells: the new gold standard for mesenchymal stem cell-based therapies? *Tissue Eng. B Rev.* **20**, 523-544.
Engelmayr, G. C., Jr, Sales, V. L., Mayer, J. E., Jr and Sacks, M. S. (2006). Cyclic flexure and laminar flow synergistically accelerate mesenchymal stem cell-mediated engineered tissue formation: Implications for engineered heart valve tissues. *Biomaterials* **27**, 6083-6095.
Ferreira, L. S., Gerecht, S., Shieh, H. F., Watson, N., Rupnick, M. A., Dallabrida, S. M., Vunjak-Novakovic, G. and Langer, R. (2007). Vascular progenitor cells isolated from human embryonic stem cells give rise to endothelial and smooth muscle like cells and form vascular networks in vivo. *Circ. Res.* **101**, 286-294.
Fischer, L. J., McIlhenny, S., Tulenko, T., Golesorkhi, N., Zhang, P., Larson, R., Lombardi, J., Shapiro, I. and DiMuzio, P. J. (2009). Endothelial differentiation of adipose-derived stem cells: effects of endothelial cell growth supplement and shear force. *J. Surg. Res.* **152**, 157-166.
Folkman, J. and Haudenschild, C. (1980). Angiogenesis in vitro. *Nature* **288**, 551-556.
Ghazanfari, S., Tafazzoli-Shadpour, M. and Shokrgozar, M. A. (2009). Effects of cyclic stretch on proliferation of mesenchymal stem cells and their differentiation to smooth muscle cells. *Biochem. Biophys. Res. Commun.* **388**, 601-605.
Giddens, D. P., Zarins, C. K. and Glagov, S. (1993). The role of fluid mechanics in the localization and detection of atherosclerosis. *J. Biomech. Eng.* **115**, 588-594.
Gong, Z. and Niklason, L.E. (2008). Small-diameter human vessel wall engineered from bone marrow-derived mesenchymal stem cells (hMSCs). *FASEB J.* **22**, 1635-1648.
Haghighipour, N., Heidarian, S., Shokrgozar, M. A. and Amirizadeh, N. (2012). Differential effects of cyclic uniaxial stretch on human mesenchymal stem cell into skeletal muscle cell. *Cell Biol. Int.* **36**, 669-675.
Hamilton, D. W., Maul, T. M. and Vorp, D. A. (2004). Characterization of the response of bone marrow-derived progenitor cells to cyclic strain: implications for vascular tissue-engineering applications. *Tissue Eng.* **10**, 361-369.
Hoey, D. A., Tormey, S., Ramcharan, S., O'Brien, F. J. and Jacobs, C. R. (2012). Primary cilia-mediated mechanotransduction in human mesenchymal stem cells. *Stem Cells* **30**, 2561-2570.
Hoffman, B. D., Grashoff, C. and Schwartz, M. A. (2011). Dynamic molecular processes mediate cellular mechanotransduction. *Nature* **475**, 316-323.
Huang, N. F. and Li, S. (2008). Mesenchymal stem cells for vascular regeneration. *Regen. Med.* **3**, 877-892.
Huang, A. H. and Niklason, L. E. (2014). Engineering of arteries in vitro. *Cell. Mol. Life Sci.* **71**, 2103-2118.
Huang, Y., Jia, X., Bai, K., Gong, X. and Fan, Y. (2010). Effect of fluid shear stress on cardiomyogenic differentiation of rat bone marrow mesenchymal stem cells. *Arch. Med. Res.* **41**, 497-505.
Huang, F., Fang, Z.-f., Hu, X.-q., Tang, L., Zhou, S.-h. and Huang, J.-p. (2013). Overexpression of miR-126 promotes the differentiation of mesenchymal stem cells toward endothelial cells via activation of PI3K/Akt and MAPK/ERK pathways and release of paracrine factors. *Biol. Chem.* **394**, 1223-1233.
Huang, A. H., Lee, Y.-U., Calle, E. A., Boyle, M., Starcher, B. C., Humphrey, J. D. and Niklason, L. E. (2015). Design and use of a novel bioreactor for regeneration of biaxially stretched tissue-engineered vessels. *Tissue Eng. Part C Methods*. [Epub ahead of print] doi:10.1089/ten.tec.2014.0287.
Jang, J.-Y., Lee, S. W., Park, S. H., Shin, J. W., Mun, C., Kim, S.-H., Kim, D. H. and Shin, J.-W. (2011). Combined effects of surface morphology and mechanical straining magnitudes on the differentiation of mesenchymal stem cells without using biochemical reagents. *J. Biomed. Biotechnol.* **2011**, 860652.
Janmey, P. A. and McCulloch, C. A. (2007). Cell mechanics: integrating cell responses to mechanical stimuli. *Annu. Rev. Biomed. Eng.* **9**, 1-34.
Kaneko, K., Ito, M., Naoe, Y., Lacy-Hulbert, A. and Ikeda, K. (2014). Integrin αv in the mechanical response of osteoblast lineage cells. *Biochem. Biophys. Res. Commun.* **447**, 352-357.
Khan, O. F. and Sefton, M. V. (2010). Perfusion and characterization of an endothelial cell-seeded modular tissue engineered construct formed in a microfluidic remodeling chamber. *Biomaterials* **31**, 8254-8261.
Khan, O. F., Chamberlain, M. D. and Sefton, M. V. (2012). Toward an in vitro vasculature: differentiation of mesenchymal stromal cells within an endothelial cell-seeded modular construct in a microfluidic flow chamber. *Tissue Eng. A* **18**, 744-756.
Kim, D. H., Heo, S.-J., Kim, S.-H., Shin, J. W., Park, S. H. and Shin, J.-W. (2011). Shear stress magnitude is critical in regulating the differentiation of mesenchymal stem cells even with endothelial growth medium. *Biotechnol. Lett.* **33**, 2351-2359.
Kobayashi, N., Yasu, T., Ueba, H., Sata, M., Hashimoto, S., Kuroki, M., Saito, M. and Kawakami, M. (2004). Mechanical stress promotes the expression of smooth muscle-like properties in marrow stromal cells. *Exp. Hematol.* **32**, 1238-1245.
Koike, N., Fukumura, D., Gralla, O., Au, P., Schechner, J. S. and Jain, R. K. (2004). Tissue engineering: creation of long-lasting blood vessels. *Nature* **428**, 138-139.
Kreke, M. R., Huckle, W. R. and Goldstein, A. S. (2005). Fluid flow stimulates expression of osteopontin and bone sialoprotein by bone marrow stromal cells in a temporally dependent manner. *Bone* **36**, 1047-1055.
Kreke, M. R., Sharp, L. A., Woo Lee, Y. and Goldstein, A. S. (2008). Effect of intermittent shear stress on mechanotransductive signaling and osteoblastic differentiation of bone marrow stromal cells. *Tissue Eng. A* **14**, 529-537.
Kurpinski, K., Chu, J., Wang, D. and Li, S. (2009). Proteomic profiling of mesenchymal stem cell responses to mechanical strain and TGF-beta1. *Cell. Mol. Bioeng.* **2**, 606-614.
Kurpinski, K., Park, J., Thakar, R. G. and Li, S. (2006). Regulation of vascular smooth muscle cells and mesenchymal stem cells by mechanical strain. *Mol. Cell. Biomech.* **3**, 21-34.
le Noble, F., Moyon, D., Pardanaud, L., Yuan, L., Djonov, V., Matthijsen, R., Bréant, C., Fleury, V. and Eichmann, A. (2004). Flow regulates arterial-venous differentiation in the chick embryo yolk sac. *Development* **131**, 361-375.
Lee, W.-C.C., Maul, T. M., Vorp, D. A., Rubin, J. P. and Marra, K. G. (2007). Effects of uniaxial cyclic strain on adipose-derived stem cell morphology, proliferation, and differentiation. *Biomech. Model. Mechanobiol.* **6**, 265-273.
Leong, W. S., Wu, S. C., Pal, M., Tay, C. Y., Yu, H., Li, H. and Tan, L. P. (2012). Cyclic tensile loading regulates human mesenchymal stem cell differentiation into neuron-like phenotype. *J. Tissue Eng. Regen. Med.* **6** Suppl. 3, s68-s79.
L'heureux, N., Pâquet, S., Labbé, R., Germain, L. and Auger, F. A. (1998). A completely biological tissue-engineered human blood vessel. *FASEB J.* **12**, 47-56.
L'Heureux, N., Dusserre, N., Konig, G., Victor, B., Keire, P., Wight, T. N., Chronos, N. A. F., Kyles, A. E., Gregory, C. R., Hoyt, G. et al. (2006). Human tissue-engineered blood vessels for adult arterial revascularization. *Nat. Med.* **12**, 361-365.
L'Heureux, N., Dusserre, N., Marini, A., Garrido, S., de la Fuente, L. and McAllister, T. (2007). Technology Insight: the evolution of tissue-engineered vascular grafts—from research to clinical practice. *Nat. Clin. Pract. Cardiovasc. Med.* **4**, 389-395.

Lim, J. Y., Loiselle, A. E., Lee, J. S., Zhang, Y., Salvi, J. D. and Donahue, H. J. (2011). Optimizing the osteogenic potential of adult stem cells for skeletal regeneration. *J. Orthop. Res.* **29**, 1627-1633.

Liu, Y.-S. and Lee, O. K. (2014). In search of the pivot point of mechanotransduction: mechanosensing of stem cells. *Cell Transplant.* **23**, 1-11.

Maul, T. M., Chew, D. W., Nieponice, A., and Vorp, D. A. (2011). Mechanical stimuli differentially control stem cell behavior: morphology, proliferation, and differentiation. *Biomech. Model. Mechanobiol.* **10**, 939-953.

McBride, S. H., Falls, T. and Knothe Tate, M. L. (2008). Modulation of stem cell shape and fate B: mechanical modulation of cell shape and gene expression. *Tissue Eng. A* **14**, 1573-1580.

Mironov, V., Kasyanov, V. and Markwald, R. R. (2011). Organ printing: from bioprinter to organ biofabrication line. *Curr. Opin. Biotechnol.* **22**, 667-673.

Nieponice, A., Maul, T. M., Cumer, J. M., Soletti, L. and Vorp, D. A. (2007). Mechanical stimulation induces morphological and phenotypic changes in bone marrow-derived progenitor cells within a three-dimensional fibrin matrix. *J. Biomed. Mater. Res. A* **81A**, 523-530.

O'Cearbhaill, E. D., Punchard, M. A., Murphy, M., Barry, F. P., McHugh, P. E. and Barron, V. (2008). Response of mesenchymal stem cells to the biomechanical environment of the endothelium on a flexible tubular silicone substrate. *Biomaterials* **29**, 1610-1619.

O'Cearbhaill, E. D., Murphy, M., Barry, F., McHugh, P. E. and Barron, V. (2010). Behavior of human mesenchymal stem cells in fibrin-based vascular tissue engineering constructs. *Ann. Biomed. Eng.* **38**, 649-657.

Oswald, J., Boxberger, S., Jørgensen, B., Feldmann, S., Ehninger, G., Bornhäuser, M. and Werner, C. (2004). Mesenchymal stem cells can be differentiated into endothelial cells in vitro. *Stem Cells* **22**, 377-384.

Owens, G. K. (1995). Regulation of differentiation of vascular smooth muscle cells. *Physiol. Rev.* **75**, 487-517.

Park, J. S., Chu, J. S. F., Cheng, C., Chen, F., Chen, D. and Li, S. (2004). Differential effects of equiaxial and uniaxial strain on mesenchymal stem cells. *Biotechnol. Bioeng.* **88**, 359-368.

Park, J. S., Huang, N. F., Kurpinski, K. T., Patel, S., Hsu, S. and Li, S. (2007). Mechanobiology of mesenchymal stem cells and their use in cardiovascular repair. *Front. Biosci.* **12**, 5098-5116.

Paszkowiak, J. J. and Dardik, A. (2003). Arterial wall shear stress: observations from the bench to the bedside. *Vasc. Endovascular Surg.* **37**, 47-57.

Praetorius, H. A. and Spring, K. R. (2005). A physiological view of the primary cilium. *Annu. Rev. Physiol.* **67**, 515-529.

Riha, G. M., Wang, X., Wang, H., Chai, H., Mu, H., Lin, P. H., Lumsden, A. B., Yao, Q. and Chen, C. (2007). Cyclic strain induces vascular smooth muscle cell differentiation from murine embryonic mesenchymal progenitor cells. *Surgery* **141**, 394-402.

Satir, P., Pedersen, L. B. and Christensen, S. T. (2010). The primary cilium at a glance. *J. Cell Sci.* **123**, 499-503.

Schwartz, M. A. and Assoian, R. K. (2001). Integrins and cell proliferation: regulation of cyclin-dependent kinases via cytoplasmic signaling pathways. *J. Cell Sci.* **114**, 2553-2560.

Seifu, D. G., Purnama, A., Mequanint, K. and Mantovani, D. (2013). Small-diameter vascular tissue engineering. *Nat. Rev. Cardiol.* **10**, 410-421.

Shah, N., Morsi, Y. and Manasseh, R. (2014). From mechanical stimulation to biological pathways in the regulation of stem cell fate. *Cell Biochem. Funct.* **32**, 309-325.

Shin'oka, T., Imai, Y. and Ikada, Y. (2001). Transplantation of a tissue-engineered pulmonary artery. *N. Engl. J. Med.* **344**, 532-533.

Shojaei, S., Tafazzoli-Shahdpour, M., Shokrgozar, M. A. and Haghighipour, N. (2013). Effects of mechanical and chemical stimuli on differentiation of human adipose-derived stem cells into endothelial cells. *Int. J. Artif. Organs* **36**, 663-673.

Shyy, J. Y.-J. and Chien, S. (2002). Role of integrins in endothelial mechanosensing of shear stress. *Circ. Res.* **91**, 769-775.

Smith, Q. and Gerecht, S. (2014). Going with the flow: microfluidic platforms in vascular tissue engineering. *Curr. Opin. Chem. Eng.* **3**, 42-50.

Stolberg, S. and McCloskey, K. E. (2009). Can shear stress direct stem cell fate? *Biotechnol. Prog.* **25**, 10-19.

Udelsman, B. V., Khosravi, R., Miller, K. S., Dean, E. W., Bersi, M. R., Rocco, K., Yi, T., Humphrey, J. D. and Breuer, C. K. (2014). Characterization of evolving biomechanical properties of tissue engineered vascular grafts in the arterial circulation. *J. Biomech.* **47**, 2070-2079.

Vlahakis, N. E., Young, B. A., Atakilit, A., Hawkridge, A. E., Issaka, R. B., Boudreau, N. and Sheppard, D. (2007). Integrin alpha9beta1 directly binds to vascular endothelial growth factor (VEGF)-A and contributes to VEGF-A-induced angiogenesis. *J. Biol. Chem.* **282**, 15187-15196.

Wang, H., Riha, G. M., Yan, S., Li, M., Chai, H., Yang, H., Yao, Q., and Chen, C. (2005). Shear stress induces endothelial differentiation from a murine embryonic mesenchymal progenitor cell line. *Arterioscler. Thromb. Vasc. Biol.* **25**, 1817-1823.

Wang, H., Li, M., Lin, P. H., Yao, Q. and Chen, C. (2008). Fluid shear stress regulates the expression of TGF-beta1 and its signaling molecules in mouse embryo mesenchymal progenitor cells. *J. Surg. Res.* **150**, 266-270.

Wang, C., Cen, L., Yin, S., Liu, Q., Liu, W., Cao, Y. and Cui, L. (2010). A small diameter elastic blood vessel wall prepared under pulsatile conditions from polyglycolic acid mesh and smooth muscle cells differentiated from adipose-derived stem cells. *Biomaterials* **31**, 621-630.

Weinberg, P. D. and Ross Ethier, C. (2007). Twenty-fold difference in hemodynamic wall shear stress between murine and human aortas. *J. Biomech.* **40**, 1594-1598.

Wu, Z., Wong, K., Glogauer, M., Ellen, R. P. and McCulloch, C. A. G. (1999). Regulation of stretch-activated intracellular calcium transients by actin filaments. *Biochem. Biophys. Res. Commun.* **261**, 419-425.

Wu, C.-C., Chao, Y.-C., Chen, C.-N., Chien, S., Chen, Y.-C., Chien, C.-C., Chiu, J.-J. and Linju Yen, B. (2008). Synergism of biochemical and mechanical stimuli in the differentiation of human placenta-derived multipotent cells into endothelial cells. *J. Biomech.* **41**, 813-821.

Yamamoto, K., Sokabe, T., Watabe, T., Miyazono, K., Yamashita, J. K., Obi, S., Ohura, N., Matsushita, A., Kamiya, A. and Ando, J. (2005). Fluid shear stress induces differentiation of Flk-1-positive embryonic stem cells into vascular endothelial cells in vitro. *Am. J. Physiol. Heart Circ. Physiol.* **288**, H1915-H1924.

Yamawaki, H., Pan, S., Lee, R. T. and Berk, B. C. (2005). Fluid shear stress inhibits vascular inflammation by decreasing thioredoxin-interacting protein in endothelial cells. *J. Clin. Invest.* **115**, 733-738.

Yao, R. and Wong, J. Y. (2015). The effects of mechanical stimulation on controlling and maintaining marrow stromal cell differentiation into vascular smooth muscle cells. *J. Biomech. Eng.* **137**, 020907.

Yeatts, A. B., Geibel, E. M., Fears, F. F. and Fisher, J. P. (2012). Human mesenchymal stem cell position within scaffolds influences cell fate during dynamic culture. *Biotechnol. Bioeng.* **109**, 2381-2391.

Yuan, L., Sakamoto, N., Song, G. and Sato, M. (2013). High-level shear stress stimulates endothelial differentiation and VEGF secretion by human mesenchymal stem cells. *Cell. Mol. Bioeng.* **6**, 220-229.

Zhang, P., Baxter, J., Vinod, K., Tulenko, T. N. and Di Muzio, P. J. (2009). Endothelial differentiation of amniotic fluid–derived stem cells: synergism of biochemical and shear force stimuli. *Stem Cells Dev.* **18**, 1299-1308.

Zhang, P., Moudgill, N., Hager, E., Tarola, N., DiMatteo, C., McIlhenny, S., Tulenko, T. and DiMuzio, P. J. (2011). Endothelial differentiation of adipose-derived stem cells from elderly patients with cardiovascular disease. *Stem Cells Dev.* **20**, 977-988.

Zhao, Y., Zhang, S., Zhou, J., Wang, J., Zhen, M., Liu, Y., Chen, J. and Qi, Z. (2010). The development of a tissue-engineered artery using decellularized scaffold and autologous ovine mesenchymal stem cells. *Biomaterials* **31**, 296-307.

Zheng, W., Xie, Y., Zhang, W., Wang, D., Ma, W., Wang, Z. and Jiang, X. (2012). Fluid flow stress induced contraction and re-spread of mesenchymal stem cells: a microfluidic study. *Integr. Biol.* **4**, 1102-1111.

Zhou, J. and Niklason, L. E. (2012). Microfluidic artificial "vessels" for dynamic mechanical stimulation of mesenchymal stem cells. *Integr. Biol.* **4**, 1487.

2.2. Les biomatériaux

Les biomatériaux utilisés dans l'ITV se déclinent en deux parties : le substitut (scaffold) et la surface (coating), parfois, un seul biomatériau peut servir pour les deux fonctions.

- **Scaffold.** Le substitut a pour rôle de fournir une interface destinée à supporter l'accrochement cellulaire, et surtout, d'apporter des propriétés physiques, telles que la résistance à la pression sanguine, la perméabilité vasculaire, l'élasticité et la résistance aux manipulations chirurgicales. Ces substituts sont fabriqués soit à base de matériaux synthétiques[31], soit de polymères naturels[32], soit une combinaison des deux[33]. Les polymères synthétiques utilisés le plus couramment sont : i) les acides poly(glycoliques) (PGA), ii) les acides poly(lactiques) (PLA), les poly(L-lactiques) (PLLA) et leur copolymères, iii), les polyhydroxyalkanoates (PHA) et iv) et le polydioxanone (PDO). Cependant, le polyvinylidene fluoride (PVDF) est aussi étudié intensivement en association avec d'autres films dans l'ITV[34]. Les polymères naturels utilisés comme scaffold sont souvent ceux pouvant former un gel d'une certaine épaisseur, notamment le collagène et la gélatine[35]. Cependant, la dégradation rapide du scaffold issu de polymères naturels diminue la résistance du vaisseau, et il est difficile de contrôler cette dégradation. En effet, le premier vaisseau sanguin a été construit par Weinberg et Bell en 1986 en ensemençant les cellules sur un tube de gel de collagène, mais ce tube n'avait pas assez de propriétés physiques pour un usage clinique sans support synthétique[36]. Tous les scaffolds à base de Matrix extracellulaire MEC naturelles ont une résistance physique inférieure aux synthétiques. De plus, par rapport aux matériaux naturels, les propriétés mécaniques spécifiques, vitesse de dégradation, porosité et microstructure de polymères synthétiques peuvent être exactement adaptées. Le premier vaisseau sanguin fonctionnel a été construit en 1999 en utilisant l'acide polyglycolique[37].

  Au lieu de construire un nouveau tube, les vaisseaux dé-cellularisés ou dé-endothélialisés sont des candidats prêts à l'utilisation. En gardant les matrices majeures qui supportent la structure

du vaisseau, ce type de scaffold possède des propriétés plus similaires aux artères natives. De plus, sans cellules étrangères, ils n'entrainent pas de réaction immunitaire[38].

- **Coating.** Comme le scaffold dérivé de MEC naturelles ne possède pas de structure assez résistante, et que le scaffold dérivé de polymère synthétique manque de bioactivité, l'attention s'est portée par à modifier la surface du scaffold afin d'améliorer l'adhérence cellulaire. En effet, la composition biochimique, la topographie, la rigidité du coating sont susceptibles d'influencer l'adhésion, la prolifération et la différenciation cellulaire[30][39]. Comme il a été décrit dans la partie scaffold, deux origines de coating sont utilisables pour couvrir un scaffold : les polymères synthétiques et les naturels[40]. Les MEC naturelles sont étudiés intensivement depuis ces dernières années pour recouvrir le scaffold. Les MEC naturelless sont utilisés principalement pour mimer les conditions du tissu natif. A titre d'exemple, les CEs sont attachées naturellement sur une couche de MEC dans le vaisseau. Des polymères naturels tels que la fibrine, la fibronectine, le collagène, l'élastine, la soie, la kératine, le chitosan, l'alginate, l'amylose/amylopectine et l'acide hyaluronique ont été largement utilisés afin de mimer la MEC naturelle en ingénierie tissulaire[41][42][43]. D' autre part, les polymères synthétiques utilisés pour fabriquer un scaffold peuvent être aussi utilisés comme coating, mais plus souvent, ils sont utilisés incorporés avec des molécules bioactives, afin d'améliorer la performance cellulaire[44]. En adaptant les composants de la MEC, la liaison entre les différentes MEC, la rigidité de surface formée[45], et l'incorporation des facteurs de croissance ou de peptides adhésifs, ce type de coating a montré un effet bénéfique pour la performance cellulaire[46][47]. Généralement, le coating avec ces MEC est fait en déposant la solution d'ECM directement sur un substitut. Il est aussi possible de traiter le substitut pour le charger positivement ou négativement afin d'améliorer l'efficacité du recouvrement. Les films polyélectrolytes peuvent ainsi être utilisés pour cahrger le support.[48][49]. Ces films possèdant une certaine charge montrent une meilleure adhésion cellulaire en raison d'effet d'attraction statique. Les substituts

couverts de films de polyélectrolytes ont pu permettre d'obtenir de bons résultats résultats *in vitro* et *in vivo*[50].

2.3. Ensemencement cellulaire en 3D

Contrairement à l'ensemencement cellulaire en 2D qui dépose la suspension cellulaire directement sur un scaffold afin d'obtenir une couche uniforme, la technique d'ensemencement en 3D est relativement compliquée. L'efficacité d'ensemencement et l'uniformité de la distribution cellulaire tout le long du scaffold sont deux critères à prendre en compte. La méthode la plus simple et la plus largement utilisée est l'ensemencement passif. Il suffit d'injecter une suspension cellulaire directement dans la lumière d'un scaffold tubulaire[51]. En attendant le dépot des cellules pendant au moins 4 heures, les cellules tombent vers le bas de la lumière, celle-ci ne peut donc être être recouverte uniformément. A cause de cette limite, cette technique donne une efficacité d'ensemencement d'environ 10% à 25%[52]. Pour augmenter l'efficacité, la position du scaffold peut être modifiée régulièrement.

D'autres techniques dynamiques sont développées afin d'augmenter encore plus l'efficacité de recouvrement par les cellules. Des dispositifs qui permettent la rotation[53], l'aspiration[54], la perfusion[55], la centrifugation[56],etc. sont connuss pour avoir largement amélioré l' ensemencement. Le principe de ces techniques est d'éviter la chute des cellules à cause de la gravité vers un seul côté du scaffold et de permettre à toute la surface d'avoir la même opportunité d'être ensemencée par les cellules.

Lorsque les cellules sont attachées sur la lumière, une période de quelques jours à quelques semaines est nécessaire pour la maturation cellulaire[35] [57]. Pendant la maturation cellulaire *in vitro*, des nutriments et de l'oxygène sont fournis par le milieu de culture en échange passif. En raison du petit diamètre du greffon vasculaire, l'échange de nutriments et d'oxygène dans la lumière est limité. De plus, du fait de la consommation d'oxygène par lees cellules, la

concentration en oxygène dans le milieu varie, aboutissant à des conditions de culture hypoxique. Une faible pression d'oxygène (pO2) peut radicalement modifier le phénotype des cellule souches[58] vers un phénotype autre que vasculaire. Pour cela, divers efforts sont faits afin de cultiver les cellules dans des conditions stables en oxygène et en nutriments. Les vaisseaux issus de l'ingénierie peuvent être soumis à une culture dynamique en perfusant la lumière avec milieu de façon constante[59]. Cependant, la perfusion constante de milieu nécessite des systèmes spécifiques, une quantité énorme de milieu frais et le risque de décrocher les cellules ensemencées par le flux de milieu.

C'est pourquoi de nouvelles méthodes sont nécessaires pour régler le problème d'ensemencement cellulaire dans les vaisseaux de petit diamètre, ainsi que la maturation de ces vaisseaux.

OBJECTIFS DE TRAVAIL

Ce travail a été réalisé au sein de l'équipe Ingénierie Cellulaire et Tissulaire, Vectorisation du laboratoire Ingénierie Moléculaire et Physiopathologie Articulaire. L'objectif de l'équipe est de construire un greffon vasculaire à partir de cellules souches et de différents biomatériaux pour un usage clinique. Au niveau de la source cellulaire, l'équipe a étudié les performances des cellules endothéliales matures et des progéniteurs endothéliaux, la différenciation des cellules souches mésenchymateuses issues de la gelée de Wharton de cordon ombilical vers des cellules endothéliales (CEs) et des cellules musculaires lisses (CML). Au niveau des biomatériaux, l'équipe a réussi à cultiver ces cellules sur des films de polyélectrolytes et des greffons tubulaires (par exemple artère ombilicale ou alginate) couverts de films de polyélectrolytes.

A partir de ces bases de recherche, nous avons développé notre travail sur l'exploitation de différents aspects dans l'ingénierie vasculaire. Il se décompose en trois axes. Dans un premier temps, nous nous sommes intéressés à des biomatériaux synthétiques et naturels, en développant un scaffold à base de P(VDF-TrFE) fonctionnalisé par des nanoparticules de ZnO. Nous avons déterminé sa biocompatibilité *in vitro* avec des cellules souche mésenchymateuses et des cellules endothéliales matures. Ces scaffolds ont ensuite été implantés chez des rats en sous-cutané pour en évaluer la biocompatibilité et l'angiogenèse. Par ailleurs, nous avons imaginé utiliser la gelée de Wharton d'humain comme coating de surface dans le cadre de l'ingénierie vasculaire, et avons évalué ses caractéristiques et sa fonctionnalité. Enfin, nous avons mis au point une technique innovante pour résoudre un verrou dans l'ingénierie tissulaire vasculaire, à savoir la cellularisation de la surface luminale d'un vaisseau. Ce concept a été validé dans un modèle de remplacement carotidien chez lapin.

Enfin, une discussion et une conclusion globale sont données dans la dernière partie.

Partie II

Matériels, Méthodes, Résultats et discussion

Chapitre 1. Biomatériaux – Scaffold synthétique

Publication N°2 (reviewing dans Nano Research)

Résumé en français

Scaffold de poly (fluorure de vinylidène-trifluoroéthylène) et nanocomposite d'oxyde de zinc par électrofilage: valorisation des réactions d'oxydo-réduction et de l'effet piézo-électrique pour favoriser l'adhésion cellulaire et l'angiogenèse

Pan Dan[c#], Robin Augustine[a,b#], Alejandro Sosnik[b], Nandakumar Kalarikkal[a,d], Nguyen Tran[f], Brice Vincent[g], Sabu Thomas[a,e*], Patrick Menu[c], Didier Rouxel[g*]

Les deux auteurs ont également contribué à cet article

Le poly (fluorure de vinylidène-trifluoroéthylène) (P (VDF- TrFE)) est beaucoup apprécié dans le domaine des biomatériaux en raison de son effet piézo-électrique. Les matériaux piézo-électriques qui peuvent générer des signaux électriques en réponse à une contrainte mécanique peuvent être utilisés pour stimuler la prolifération cellulaire en ingénierie tissulaire. Les nanoparticules d'oxyde de zinc, incorporées dans les scaffolds, sont intéressantes en raison de leur capacité d'oxydo-réduction favorable sur le comportement cellulaire. Nous avons précédemment montré que l'incorporation de ZnO dans les scaffolds synthétiques pouvait favoriser l'adhérence, la migration et la prolifération des cellules aussi bien que l'angiogenèse.

Dans cette étude, les scaffolds d'ingénierie tissulaire à base de P (VDF-TrFE)/ZnO ont été fabriqués par la technique d'électrofilage. L'analyse SEM a montré les caractéristiques morphologiques de la matrice polymère. FTIR, XRD et DSC ont mis en évidence des changements dans les phases cristallines du copolymère à la suite de l'ajout de nanoparticules.

Le test de compatibilité avec du sang *in vitro* a montré peu ou pas d'insidences délétères, suggérant que ces scaffolds ne devraient pas provoquer de thrombose une fois utilisés comme substitut vasculaire.

Nous avons testé la biocompatibilité *in vitro* avec deux types de cellules qui sont les plus souvent étudiées, les cellules souches mésenchymateuses humaine (hCSM) et les cellules endothéliales issues des veines du cordon ombilical (HUVECs). Les résultats de viabilité des cellules et de toxicité du scaffold ont montré que lorsque moins de 4% de ZnO sont incorporés dans les scaffolds, aucune toxicité pour les CSM et les HUVECs n'est observée. De façon intéressante, l'incorporation de 2% de ZnO dans les scaffolds favorise significativement favorisé la prolifération de ces deux types de cellules. C'est donc ce protocole qui a été retenu pour la suite des études.

Pour évaluer leur comportement biologique, nous avons implanté en sous-cutané ces scaffolds en présence de ZnO et pré-ensemencés de hCSMs dans l'abdomen de rat. Trois semaines après implantation, les scaffolds sont récupérés et observés au microscope et en histologie. Aucune réponse immunologique significative n'a été observée avec les scaffolds contenant des nanocomposites et implantés dans les rats avec ou sans hCSMs. De façon inattendue, l'observation macroscopique a montré la présence de nombreux de petits néo-vaisseaux qui se développaient vers les scaffolds avec 2% de ZnO. Et ce phénomène est significativement plus important en présence de scaffolds pré-ensemencés de hCSMs. Par microscopie à fluorescence, nous avons observé que les hCSMs pré-ensemencées dans les scaffolds restaient adhérentes 3 semaines après leur implantation. Par analyse histologique, nous avons montré la présence de collagène dans les scaffolds à partir d'une semaine après l'implantation. De plus, l'angiogenèse commence à se développer à partir d'une semaine car on observe l'apparition de petits vaisseaux autour de scaffolds. Trois semaines après l'opération, les néo-vaisseaux ont commencé à pénétrer les scaffolds. Par cette approche histologique, nous avons montré que les

meilleurs résultats d'angiogenèse sont obtenus avec les scaffolds à 2% de ZnO et pré-ensemencés de hCSMs. En résumé, les résultats mettent en évidence un réel potentiel du scaffolds P(VDF-TrFE)/ZnO et suggèrent qu'ils puissent jouer un rôle intéressant dans l'élaboration de plates-formes nano-technologiques utilisables en ingénierie tissulaire.

Table of content data

Electrospun poly(vinylidene fluoride-trifluoroethylene)/zinc oxide nanocomposite tissue engineering scaffolds with enhanced cell adhesion and blood vessel formation

Robin Augustine[1,2*], Pan Dan[3] Alejandro Sosnik[1], Nandakumar Kalarikkal[2,4], Nguyen Tran[5], Brice Vincent[6], Sabu Thomas[2,7], Patrick Menu[3], Didier Rouxel[6]*

[1]Laboratory of Pharmaceutical Nanomaterials Science, Department of Materials Science and Engineering, Technion-Israel Institute of Technology, De-Jur Building, Technion City, 3200003 Haifa, Israel
[2]International and Inter University Centre for Nanoscience and Nanotechnology, Mahatma Gandhi University, Kottayam – 686 560, Kerala, India
[3]Ingénierie Moléculaire et Physiopathologie Articulaire, UMR 7365 CNRS - Université de Lorraine, Vandoeuvre-lès Nancy, F54500, France
[4]School of Pure and Applied Physics, Mahatma Gandhi University, Kottayam – 686 560, Kerala, India
[5]School of Surgery, Faculty of Medicine, Université de Lorraine, 54500 Vandoeuvre-lès-Nancy, France
[6]Institut Jean Lamour, UMR 7198 CNRS - Université de Lorraine, 54500 Vandoeuvre-lès-Nancy, France
[7]School of Chemical Sciences, Mahatma Gandhi University, Kottayam – 686 560, Kerala, India

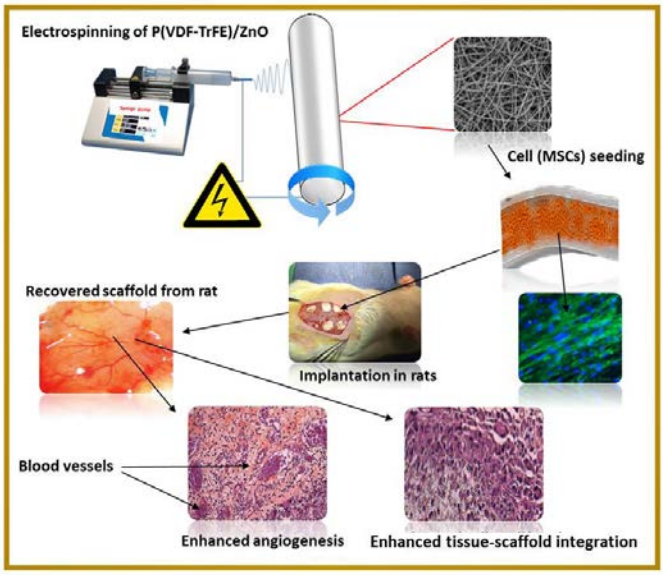

Poly(vinylidene fluoride-trifluoroethylene)/zinc oxide nanocomposite scaffolds were fabricated by electrospinning technique. Detailed characterization of the scaffolds showed that they are highly promising candidates for tissue engineering applications due the enhanced cell adhesion and vascularization potential.

Provide the authors' website if possible.

Robin Augustine, www.robinlab.in

Nano Res
DOI (automatically inserted by the publisher)
Research Article

Electrospun poly(vinylidene fluoride-trifluoroethylene)/zinc oxide nanocomposite tissue engineering scaffolds with enhanced cell adhesion and blood vessel formation

Robin Augustine[1,2,§] (✉), Pan Dan[3,§] Alejandro Sosnik[1], Nandakumar Kalarikkal[2,4], Nguyen Tran[5], Brice Vincent[6], Sabu Thomas[2,7], Patrick Menu[3], Didier Rouxel[6](✉)

[1]Laboratory of Pharmaceutical Nanomaterials Science, Department of Materials Science and Engineering, Technion-Israel Institute of Technology, De-Jur Building, Technion City, 3200003 Haifa, Israel

[2]International and Inter University Centre for Nanoscience and Nanotechnology, Mahatma Gandhi University, Kottayam – 686 560, Kerala, India

[3]Ingénierie Moléculaire et Physiopathologie Articulaire, UMR 7365 CNRS - Université de Lorraine, Vandoeuvre-lès Nancy, F54500, France

[4]School of Pure and Applied Physics, Mahatma Gandhi University, Kottayam – 686 560, Kerala, India

[5]School of Surgery, Faculty of Medicine, Université de Lorraine, 54500 Vandoeuvre-lès-Nancy, France

[6]Institut Jean Lamour, UMR 7198 CNRS - Université de Lorraine, 54500 Vandoeuvre-lès-Nancy, France

[7]School of Chemical Sciences, Mahatma Gandhi University, Kottayam – 686 560, Kerala, India

§ These authors contributed equally to this work.

Received: day month year / Revised: day month year / Accepted: day month year (automatically inserted by the publisher)
© Tsinghua University Press and Springer-Verlag Berlin Heidelberg 2011

ABSTRACT

Piezoelectric materials that can generate electrical signals in response to mechanical strain can be used to stimulate cell proliferation in tissue engineering. Poly(vinylidene fluoride-trifluoroethylene) (P(VDF- TrFE)) is a piezoelectric polymer widely used in biomaterial applications. Incorporation of ZnO nanoparticles into the P(VDF-TrFE) matrix could promote adhesion, migration and proliferation of cells as well as blood vessel formation (angiogenesis). In this study, a novel tissue engineering scaffold based on P(VDF-TrFE)/ZnO nanocomposites were fabricated by electrospinning technique and comprehensively characterized. SEM analysis shed light into the morphological features of the polymeric matrix and FTIR, XRD and DSC analyses revealed changes in the crystalline phases of the copolymer due to the addition of nanoparticles. Blood compatibility *in vitro*, biocompatibility and cytotoxicity studies showed no or minimal adverse effects and demonstrated that P(VDF-TrFE)/ZnO nanocomposite scaffolds were suitable for tissue engineering applications. Interestingly, when cultured on the nanocomposite scaffolds, mesenchymal stem cells (hMSCs) and human umbilical cord vein endothelial cells (HUVECs) showed higher cell viability, adhesion and proliferation. Nanocomposite scaffolds implanted into rat abdomen with or without hMSCs did not show significant immunological response. Very interestingly, nanocomposite scaffolds showed angiogenesis which in turn again higher for those which were pre-seeded with hMSCs. Overall, results highlight the potential of these novel P(VDF-TrFE)/ZnO nanocomposites as tissue engineering scaffolds which are biocompatible and can provide a favorable environment for the cell adhesion and angiogenesis which has great potential in tissue engineering.

KEYWORDS

Scaffolds, electrospinning, P(VDF- TrFE), ZnO, Angiogenesis, cell adhesion, stem cells

Address correspondence to Robin Augustine, robin@robinlab.in; Didier Rouxel, didier.rouxel@univ-lorraine.fr

1. Introduction

A wide range of polymeric materials has been used as tissue engineering scaffolds with many successful outcomes, but the search for an ideal scaffold material with multifunctional properties that can enhance cell adhesion, migration and proliferation is still on the way. Moreover, an active blood vessel network is necessary for the integration of the scaffold with the existing host tissue which is a most challenging task in the present scenario [1]. Though there are promising strategies to enhance angiogenesis such as incorporation of growth factors like vascular endothelial growth factor (VEGF) in scaffolds, their short half-lives make it less viable [2]. Sometimes, such approaches have resulted in transient efficacy with chronic inflammation, fibrosis and subsequent implant failure [3].

Previous studies demonstrated that electrical charges have a beneficial effect on cell adhesion, cell morphology and cell proliferation [4,5]. Piezoelectric scaffolds that can generate electric signals in response to pressure or vibration were used for various tissue engineering applications [6]. Poly[(vinylidenefluoride-co-trifluoroethylene] [P(VDF-TrFE)], a copolymer of poly(vinylidene fluoride) (PVDF) received special attention over other piezoelectric polymers because they could easily form the piezo active β phase without an additional process by adding small amounts of TrFE [7]. It have been reported to further undergo crystallization into four different crystalline phases (α, β, γ and δ) [8]. All the types, except the α phase, form polar phase. The spontaneous polarization of the γ and the δ phases leads to the formation of β phase and the α phase can be converted into the β phase by mechanical drawing or annealing under high pressure [9].

Electrospun tissue engineering scaffolds based on various biodegradable and non-biodegradable polymers have been extensively studied by many research groups [10]. The high electric potential and the stretching force applied during electrospinning process induce the polarization of P(VDF-TrFE) to form more β-phase crystals compared with the unprocessed powder [6]. Being a non-biodegradable polymer, P(VDF-TrFE) cannot be suggested for all kind of tissue engineering applications. However, previous studies invariably demonstrated that P(VDF-TrFE) is a good candidate for neural tissue engineering, [11][12] spinal cord regeneration [13] and skeletal muscle tissue engineering [14] Another recent study demonstrated the feasibility of electrospun P(VDF-TrFE) scaffold as a candidate biomaterial for the engineering of cardiovascular tissues utilizing stem cell-derived cardiovascular cells [15].

Zinc oxide (ZnO) nanoparticles has attracted a great deal of attention in recent years because of its multifunctional properties, especially the antibacterial activity that might be exploited in specific biomedical interventions to prevent biomaterials-associated infections [16]. ZnO nanostructures are also endowed with piezoelectric features [17] and reactive oxygen species (ROS) generation capacity[18] and thus find application in nanomedicine [19]. Our group previously reported that ZnO nanoparticles having 60 nm size can enhance animal cell proliferation under both *in vitro* and *in vivo* conditions [20][21]. Further, another study established that ZnO nanoparticles enhanced the expression of growth factors like fibroblast growth factor (FGF) and vascular endothelial growth factor (VEGF) which in turn promoted cell proliferation and angiogenesis [22] Even though there exist concerns regarding the toxicity of ZnO nanoparticles [23,24], their possible clinical application is under discussion [25].

Based on these insights from our previous studies and those reported by other researchers, we envisaged to exploit the simultaneous effect of the piezoelectric property of both P(VDF-TrFE) and ZnO nanoparticles along with the ROS mediated proliferative mechanism by ZnO nanoparticles towards the development of a tissue engineering scaffold material with high cell proliferation and angiogenesis. To the best of our knowledge, the use of electrospun P(VDF-TrFE) scaffolds containing ZnO nanoparticles as tissue engineering scaffold has not been reported yet. In this framework, the present

work investigated the production of this novel type of nanocomposite biomaterials and characterized the possible synergistic effect of both components on cell adhesion and angiogenesis.

2. Materials and Methods

2.1. Materials used

P(VDF-TrFE) (60:40 molar ratio, M_w ~ 500,000 g mol^{-1}) was obtained from Piezotech SAS, France. ZnO nanoparticles with average particle size of 60 nm (NanoGard®) (TEM image is given in **Fig. S-1** in the Electronic Supplementary Material (ESM)) were purchased from Alfa Aesar (UK). Acetone was obtained from Merck (India). Histopaque, polyethyleneimine (PEI), paraformaldehyde and (3-(4,5-dimethylthiazol-2-yl)-2,5-diphenyltetrazolium bromide) (MTT) were purchased from Sigma-Aldrich (USA). Lactate dehydrogenase (LDH) assay kit obtained from Roche (Switzerland). Phalloidin was purchased from Thermo Fisher Scientific (France). Minimum essential medium Eagle-alpha modification (α-MEM) (Lonza) was used for hMSCs culture and endothelial basic medium (Lonza) was used for human umbilical vein endothelial cells (HUVEC) culture. Both media were supplemented with 10% fetal bovine serum (FBS), 100 mg ml^{-1} Fungizone (Fisher), 100 IU ml^{-1} penicillin (Sigma-Aldrich) and 200 mM L-glutamine (Sigma-Aldrich). All the reagents used in this study were of analytical grade quality and used without further purification.

2.2. Electrospinning of P(VDF-TrFE)/ZnO nanocomposites

Scaffolds of P(VDF-TrFE)/ZnO nanocomposites were fabricated by electrospinning technique. The electrospinning apparatus was assembled by Holmarc (India) and consisted of a high-voltage power supply, a syringe pump and a 10 ml syringe attached with a 21G diameter needle. A steel rotating mandrel with a rotation speed of 1000 rpm was used as the collector. A 10-cm distance and an applied voltage of 18 kV were maintained between the needle and the collector. The solution flow rate was precisely maintained at 1.5 mL/h using the syringe pump. P(VDF-TrFE) solutions with different concentration of ZnO nanoparticles were prepared in acetone. For this, ZnO nanoparticles were accurately weighed and ultrasonicated for 15 min to properly disperse them. Then, a known quantity of P(VDF-TrFE) in the form of pellet was added to the above dispersion so that the final concentration of P(VDF-TrFE) was 14% w/v and the mixture stirred magnetically (12 h) until complete dissolution of the pellet. Finally, 10 ml of the prepared suspensions with different % w/w of ZnO nanoparticles with respect to the polymer (0%, 0.5%, 1%, 2% and 4% w/w hereafter referred as P(VDF-TrFE), P(VDF-TrFE)/ZnO-0.5, P(VDF-TrFE)/ZnO-1, P(VDF-TrFE)/ZnO-2, and P(VDF-TrFE)/ZnO-4 respectively) were electrospun for 6 h. After the completion of the process, the fibrous scaffold deposited on collector was carefully cut and removed using a sharp blade.

2.3. Scanning Electron Microscopy (SEM) and Energy-Dispersive X-ray spectroscopy (EDS)

The morphological features of the fabricated scaffolds were visualized by a Philips XL-30 FEG Scanning Electron Microscope at 5 kV (Netherlands). The neat P(VDF-TrFE) scaffolds as well as P(VDF-TrFE)/ZnO nanocomposite scaffolds were carefully sectioned with an approximate size of 3 x 3 mm using a sharp blade and mounted on SEM sample holders and subsequently coated with Pt. The average fiber diameter of each sample was measured using ImageJ software. Measurements were made at 100 random positions and the average of these measurements was used to determine the diameter of the fibers. Further, the presence of ZnO nanoparticles in the scaffolds was confirmed by EDS (EDAX, USA) attached to the Philips XL-30 FEG SEM.

2.4. Fourier Transform Infrared (FTIR) spectroscopy

FTIR spectra of neat P(VDF-TrFE) and P(VDF-TrFE)/ZnO nanocomposite scaffolds with

various contents of ZnO nanoparticles were obtained with a Perkin Elmer (USA), spectrum 400 FTIR spectrometer with PIKE Gladi ATR (USA) attachment and DTGS detector on a diamond crystal between 550–1500 cm^{-1} with 15 scans at 4 cm^{-1} resolution using Spectrum 400 software 62 (version 6.3).

2.5. X-Ray Diffraction (XRD)

X-Ray Diffraction (XRD) analysis was used to determine the crystallinity and presence of ZnO nanoparticles in P(VDF-TrFE)/ZnO nanocomposite scaffolds. XRD was recorded in the 2θ range of 20°–25° using a model D8-Advance of Bruker (Germany) with CuKα radiation of 8.04 keV and wavelength of 1.54 Å. The applied voltage was 40 kV and current was 25 mA.

2.6. Differential Scanning Calorimetry (DSC)

Calorimetric measurements were performed using TA Instruments Q200 differential scanning calorimeter (USA). Samples of approximately 5 mg were cut from the neat P(VDF-TrFE) and P(VDF-TrFE)/ZnO nanocomposite scaffolds and sealed in Al crucible pans having 30 µL capacity. All the runs were carried out under a dry nitrogen flow of 20 ml/min. Samples were heated from -80°C to 200°C at 10°C/min. Then, the samples were kept for 1 min at 200°C to erase the thermal history and cooled to -80°C. The melting temperature (T_m), the enthalpy of fusion (ΔH_f), the ferroelectric-to-paraelectric transition temperature (T_{F-P}) and the enthalpy change during ferroelectric-to-paraelectric transition (ΔH_{F-P}) were calculated from the heating ramp. The crystallization temperature (T_c), the paraelectric-to-ferroelectric transition temperature (T_{P-F}) and the enthalpy change during the paraelectric-to-ferroelectric transition (ΔH_{P-F}) were established from the cooling one.

2.7. Porosity measurement

Porosity of the fabricated membranes was measured using alcohol displacement method [26]. For this, P(VDF-TrFE) and nanocomposite scaffolds were immersed in 100% ethanol for 48 hours until it was saturated, and the percentage of porosity was calculated according to Eq. 1.

$$P = (W_2 - W_1)/\rho V_1 \quad X\ 100 \qquad (1)$$

where W_1 and W_2 are the weight of the scaffolds before and after immersing in ethanol respectively. V_1 is the volume of scaffold before immersing in ethanol and ρ is the density of ethanol. The experiment was repeated for three set of samples and the porosity was expressed as mean ± SD (n = 3).

2.8. Blood compatibility studies

Since the tissue engineering scaffolds are expected to come into direct contact with blood, the assessment of the hemocompatibility was of main interest. Two tests were performed, namely blood cells aggregation and hemolysis, according to the protocol reported elsewhere with minor modifications [27]. For this, human blood samples (approximately 10 mL) were collected from healthy volunteers in a tube containing 3.8% sodium citrate at 9:1 ratio (blood:anticoagulant) after the signing of a consent form. Normal saline and PEI were used as the negative and positive control of hemolysis, respectively. Both neat P(VDF-TrFE) and P(VDF-TrFE)/ZnO nanocomposite scaffolds were cut into 1 x 1 cm^2 size and sterilized by dipping in 70% alcohol for 20 min and UV irradiation for 20 min. The samples were incubated overnight in 1 mL of sterile PBS solution and these solutions were used for red blood cell (RBC) and white blood cell (WBC) aggregation, platelet activation and hemolysis tests.

(i) Blood cell aggregation study. To perform RBC aggregation studies, the blood was centrifuged at 700 rpm for 10 min to separate the RBCs from the blood plasma. This cell fraction was washed twice with saline and diluted with PBS (1:4). Then, 2 mL of this diluted RBCs were added to the PBS solution (in which the scaffolds were kept previously for overnight incubation) and then kept at 37°C for 20 min. The diluted RBCs were also incubated along with the negative and positive controls. To perform WBC compatibility study, cells were isolated from anticoagulated blood overlaid with histopaque by

centrifugation (15 min at 800 rpm). The collected WBCs were incubated with PBS solution in which the scaffolds were kept previously for overnight incubation, for 20 min at 37°C. Similar procedure was carried out for the incubation of WBCs with the positive and negative controls. After incubation, both RBCs and WBCs were isolated by centrifugation, resuspended in PBS and mounted on wet slides. Images were captured by optical microscope (Leica DMIRB, Germany).

(ii) Platelet aggregation. Platelets were isolated from anti-coagulated blood (1 mL) overlaid with histopaque (1 mL) in order to separate RBCs and WBCs as separate layers and were centrifuged for 15 min at 800 rpm at room temperature; platelets were separated as the topmost layer above the WBC fraction. The collected platelets were incubated with PBS solution in which the neat P(VDF-TrFE) and P(VDF-TrFE)/ZnO nanocomposite scaffolds were kept previously for overnight incubation, for 20 min at 37°C. A similar procedure was carried out for the incubation of platelets with the positive and negative controls. Images were captured by optical microscope (Leica DMIRB, Germany).

(iii) Hemolysis assay. Hemolysis assays were carried out on plain P(VDF-TrFE) and P(VDF-TrFE)/ZnO scaffolds. In brief, 100 µl of the separated blood was diluted with 800 µl of saline. To this diluted blood, 100 µl of each PBS solution in which the scaffolds were maintained previously for overnight incubation, was added. Here, normal saline was used as negative control (no hemolysis) and distilled water as positive control (complete hemolysis). The samples were incubated for 30 min at 37°C and centrifuged at 700 rpm for 5 min. The absorbance (OD) was measured at 541 nm using a UV–Vis spectrophotometer (Shimadzu double-beam spectrophotometer- Model 1700, Japan). The percentage of hemolysis (% Hemolysis) was calculated from Eq. 2.

$$\% \text{ Hemolysis} = [\text{OD of sample} - \text{OD of negative control}]/[\text{OD of positive control} - \text{OD of negative control}] \quad (2)$$

2.9. Cell compatibility and cell attachment

The cell compatibility and attachment was investigated with hMSCs and human umbilical cord vein endothelial cells (HUVECs). For this, fresh human umbilical cords were obtained after full-term births (cesarean section or normal vaginal delivery) with informed consent using the guidelines approved by the University Hospital Center of Nancy (France). hMSCs and HUVECs were isolated and amplified as previously reported [28]. hMSCs on passage 4 and HUVECs on passage 2 were seeded on neat P(VDF-TrFE) and P(VDF-TrFE)/ZnO nanocomposite scaffolds at 50,000 cells/cm^2 and cultured with appropriate medium for 24 h. To visualize cell attachment, samples were fixed with 4% paraformaldehyde for 15 min, permeabilized with 0.5% w/v Triton X-100 solution for 15 min and cell cytoskeletons were stained with phalloidin and nuclei were stained with DAPI. Then, the images were taken with a fluorescent microscope (Leica DMI 3000B, Germany). To assess cell compatibility of hMSCs and HUVECs on P(VDF-TrFE) or P(VDF-TrFE)/ZnO nanocomposite scaffolds, MTT and LDH assays were carried out according to the corresponding protocols provided by the manufacturer (n = 3).

2.10. In vivo implantation studies

In vivo implantation studies to determine the biocompatibility and biological performance of the nanocomposite scaffolds were carried out in Wistar rats. All the animal experiments were carried out after authorization of regional animal ethics committee in France (APAFIS#1123-2015070711576639V3). Based on the *in vitro* cell culture studies, P(VDF-TrFE), P(VDF-TrFE)/ZnO-1 and P(VDF-TrFE)/ZnO-2 were selected for animal studies. Before implantation, all the scaffolds were cut into 1 × 1 cm pieces and sterilized with 70% alcohol for 20 min and then with UV radiation for 20 min. One set of samples was seeded with hMSCs (50,000 cells/cm^2) and allowed to grow for 24 h prior to animal implantation. In order to track these cells, hMSCs were labeled with DiI

(D282, Invitrogen, France). A total of 6 rats (male, 231 ± 13 g) were used. Anesthesia was induced by inhalation of 4% isoflurane (Isovet, France) and maintained in 1.5% isoflurane. Scaffolds were implanted subcutaneously in the abdominal region. After 7 and 21 days of implantation, the implantation site was reopened and the scaffolds were visually inspected for immune reaction and angiogenesis. Scaffolds were then explanted for cell tracking and histological evaluation. Samples were cut into transverse and cross sections and stained with hematoxylin-eosin-saffron staining and Masson's trichrome staining. Stained sections were used to determine *in vivo* biocompatibility and formation of blood vessels. The stained sections were examined with a Leica DMI 3000B inverted light microscope.

2.11. Statistical analysis

Data are presented as mean ± standard deviation (S.D.). For fiber diameter, MTT and LDH evaluation, statistical significance was determined by ANOVA followed by t-test between each group, p-values less than 0.05 were defined as statistically significant.

3. Results

3.1. Morphology of scaffolds

In the present study, we aimed to develop a P(VDF-TrFE)/ZnO nanoparticles-based nanocomposite scaffold by means of an electrospinning technique. A schematic representation of the fabrication process is shown in **Scheme 1**.

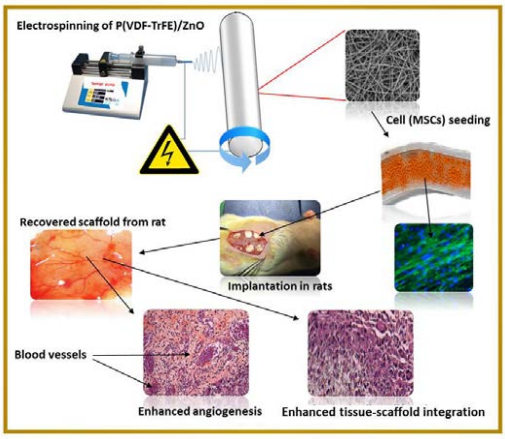

Scheme 1. Schematic representation of the production of electrospun P(VDF-TrFE)/ZnO nanocomposite scaffolds, the hMSC seeding and the implantation in rats (Figures are not to scale).

Representative morphological features of neat P(VDF- TrFE) and P(VDF- TrFE)/ZnO nanocomposite scaffolds are presented in **Fig. 1.** As expected, scaffolds were highly porous with randomly oriented fibers and good pore interconnectivity. In addition, both P(VDF-TrFE) and P(VDF-TrFE)/ZnO nanocomposite scaffolds displayed almost uniform fiber diameter. Higher magnification micrographs confirmed the presence of well-dispersed ZnO nanoparticles. When low ZnO nanoparticles load was used, the particles were mainly embedded and homogeneously dispersed in the P(VDF-TrFE) fiber **(Fig. 1E)**. Conversely, the increase of the ZnO content in the spinning solution resulted in the formation of nanoparticle agglomerates that protruded from the fiber and were visible on the surface **(Fig. 1F)**.

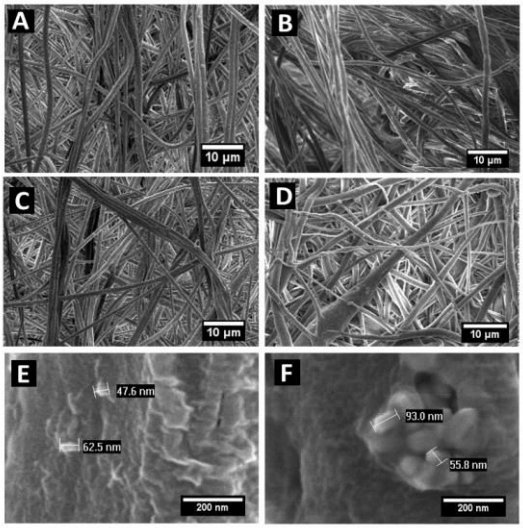

Figure 1 SEM micrographs showing the morphology of electrospun (A) P(VDF-TrFE), (B) P(VDF-TrFE)/ZnO-1, (C) P(VDF- TrFE)/ZnO-2 and (D) P(VDF- TrFE)/ZnO-4. E and F are the higher magnification images of B and D, respectively.

To further understand the impact of the incorporation of ZnO nanoparticles to the fibers, the diameter was measured (**Table 1**). In neat P(VDF-TrFE) scaffolds, fibers showed an average diameter of 1035 nm. In the case of P(VDF-TrFE)/ZnO nanocomposites, as the nanoparticle concentration increased, the fiber

diameter tended to vary. For example, in P(VDF-TrFE)/ZnO-1, the change was marginal without any statistical difference ($p = 0.68$). However, for P(VDF-TrFE)/ZnO-2, the diameter was significantly larger than the neat counterpart ($p = 0.0004$). Further increase in the ZnO nanoparticle content up to 4% w/w in the P(VDF-TrFE) scaffolds also led to an additional increase of the diameter ($p < 0.0001$ in both cases).

Table 1. Effect of ZnO nanoparticle concentration on the fiber diameter of P(VDF-TrFE) scaffolds.

Sample	Fiber average diameter ± S.D. (nm)
P(VDF-TrFE)	1035 ± 331
P(VDF-TrFE)/ZnO-1	1052 ± 275
P(VDF-TrFE)/ZnO-2	1185 ± 249
P(VDF-TrFE)/ZnO-4	1227 ± 301

3.2. EDS

EDS spectra of electrospun P(VDF-TrFE) scaffolds and its nanocomposite counterpart were used to confirm the presence of the ZnO nanoparticles in the polymer matrix (**Fig. 2**). Neat P(VDF-TrFE) scaffolds displayed sharp low-energy peaks that could be assigned to the elements carbon (Kα radiation with 0.277 keV) and fluorine (Kα radiation with 0.677 keV) (**Fig. 2A**). Similar results were reported elsewhere [29]. In the case of the nanocomposites, characteristic signals of Zn were observed at energy levels of 1.01 keV (Lα), 8.63 keV (Kα) and 9.5 keV (Kβ) (**Fig. 2B, C, D**).

These peaks were in full agreement with our previous results [20]. In addition, it is worth stressing that there was a remarkable increase in the intensity of the three characteristic peaks of Zn with the increase of the ZnO nanoparticle content. O and F showed characteristic kα emissions of 0.525 and 0.677 keV, respectively. Thus, it was practically impossible to discern the peaks corresponding to O from ZnO nanoparticles due to the overlapping high intensity F peaks belonging to P(VDF-TrFE).

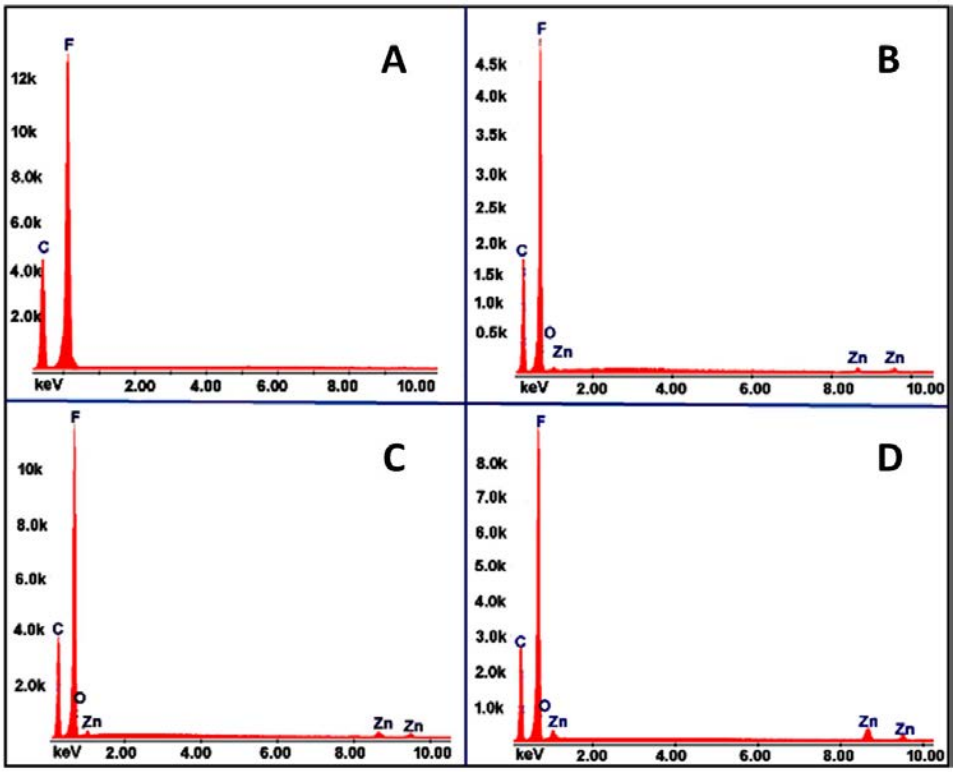

Figure 2 Representative EDS spectra of (A) electrospun P(VDF-TrFE), (B) P(VDF-TrFE)/ZnO-1, (C) P(VDF-TrFE)/ZnO-2, and (D) P(VDF-TrFE)/ZnO-4.

3.3. Crystalline phase analysis

(i) FTIR. FTIR spectra of electrospun neat P(VDF-TrFE) and P(VDF-TrFE)/ZnO nanocomposite scaffolds with growing concentrations of ZnO nanoparticles are shown in **Fig. 3A.** The 1283 cm^{-1} band was assigned to the symmetric CF_2 stretching vibration coupled to the backbone stretching and bending vibrations corresponding to *trans* isomer sequences that are four or more units long in the chain extended or β-phase structure [30][31]. The two bands near 845 cm^{-1} and the band at 1283 cm^{-1} band belonged to long sequences of at least three *trans* isomers [30]. This was assigned to a mixed mode of CH_2 rocking [32] and CF_2 asymmetric stretching vibration parallel to the chain axis [33]. Characteristic peaks at 1400, 1284 and 845 cm^{-1} corresponded to the electroactive β-phase, whereas a very weak and broad band at 975 cm^{-1} and an ill-defined peak around 613 cm^{-1} in neat P(VDF–TrFE) scaffolds were due to the non-polar α-phase [34,35]. It is worth noting that characteristic bands of α-phase at 1455, 1430, 1385, 1212, 1152, 976, 855 and 796 cm^{-1} were completely absent. The same was valid for the peak of γ-phase at 1232 cm^{-1}. Incorporation of ZnO nanoparticles did not result in any considerable shift in the characteristic IR bands. Since the analysis was conducted by ATR, semi-quantitative information regarding the relative amount of the different crystalline phases could be obtained (**Fig. 3B**). For this, the analysis focused on the spectrum region between 1500 and 1300 cm^{-1} and band at 1400 cm^{-1} which represents β-phase [35] was used to specifically compare the variation in intensity. In this context, the intensity of the band of β-phase at 1400 cm^{-1} increased due to the incorporation of ZnO nanoparticles, P(VDF-TrFE)/ZnO-2 showing the most substantial increase. Overall these findings stress the fundamental role of the production procedure in the microstructural properties of the polymer in the final product and the ability to fine tune them by incorporating solid nanoparticles that serve as nucleation and crystallization sites during the formation of the fibers.

(ii) XRD. Crystallinity in polymeric biomaterials determines physical, mechanical and biological properties. P(VDF-TrFE) is a semi-crystalline copolymer that consists of a ferroelectric crystalline β-phase embedded in an amorphous matrix, and the β-phase has quasi-hexagonal close-packing with orthorhombic mm^2 structure [36]. The X-ray diffraction patterns of electrospun P(VDF-TrFE)/ZnO nanocomposite scaffolds revealed that the main diffraction peak of the P(VDF-TrFE) and P(VDF-TrFE)/ZnO nanocomposite scaffolds was at $2\theta = 19.9^{\circ}$ (110) (**Fig. 3C**). This diffraction peak could be assigned to the (200) and (110) planes of the β-phase [37]. No other specific diffraction peaks corresponding to α, β or γ-phases were identified. Instead, a broad peak covering the 2θ region between 16° and 22° with a maximum at 19.9° was observed. When ZnO nanoparticles were incorporated, the corresponding diffraction peaks of ZnO nanoparticles were clearly apparent at 2θ values of 31.7^{o}, 34.3^{o}, 36.3^{o}, 47.3^{o}, 56.6^{o} and 63.8^{o} (**Fig. 3C**). Moreover, the greater the ZnO content, the more intense the signals.

(iii) DSC. To gain deeper insight into the thermal properties and the crystallization in the electrospun P(VDF-TrFE) scaffolds with and without ZnO nanoparticle, samples were analyzed by DSC. Two endothermic peaks were observed for all the fabricated scaffolds. The first peak around 67°C corresponded to the ferroelectric-to-paraelectric transition (T_{F-P}) of the copolymer and the second transition near 158°C was due to the melting of crystalline phases (T_m) in the polymer [38]. This broad endothermic peak during melting could be described as a superposition of the melting peaks for the lower-melting α phase and the higher melting β-phase (**Fig. S-2** in the ESM). Upon incorporation of ZnO nanoparticles into the fibers, the Tm and T_{F-P} did not show considerable variation (Table 2). In a similar way, during the cooling process, neat P(VDF-TrFE) and ZnO-loaded scaffolds exhibited exothermic peaks of T_c and T_{P-F} at approximately 141-143°C and 59-61°C, respectively. In P(VDF-TrFE)/ZnO scaffolds, there was no considerable variation in T_c or T_{P-F}. Interestingly, ΔH_c slightly decreased when low amounts of ZnO nanoparticles were incorporated to the scaffolds. Similarly, ΔH_{P-F} considerably increased with growing concentrations of ZnO nanoparticles up to 2% w/w ZnO. However, a further increase in ZnO content resulted in the decrease of ΔH_{P-F}.

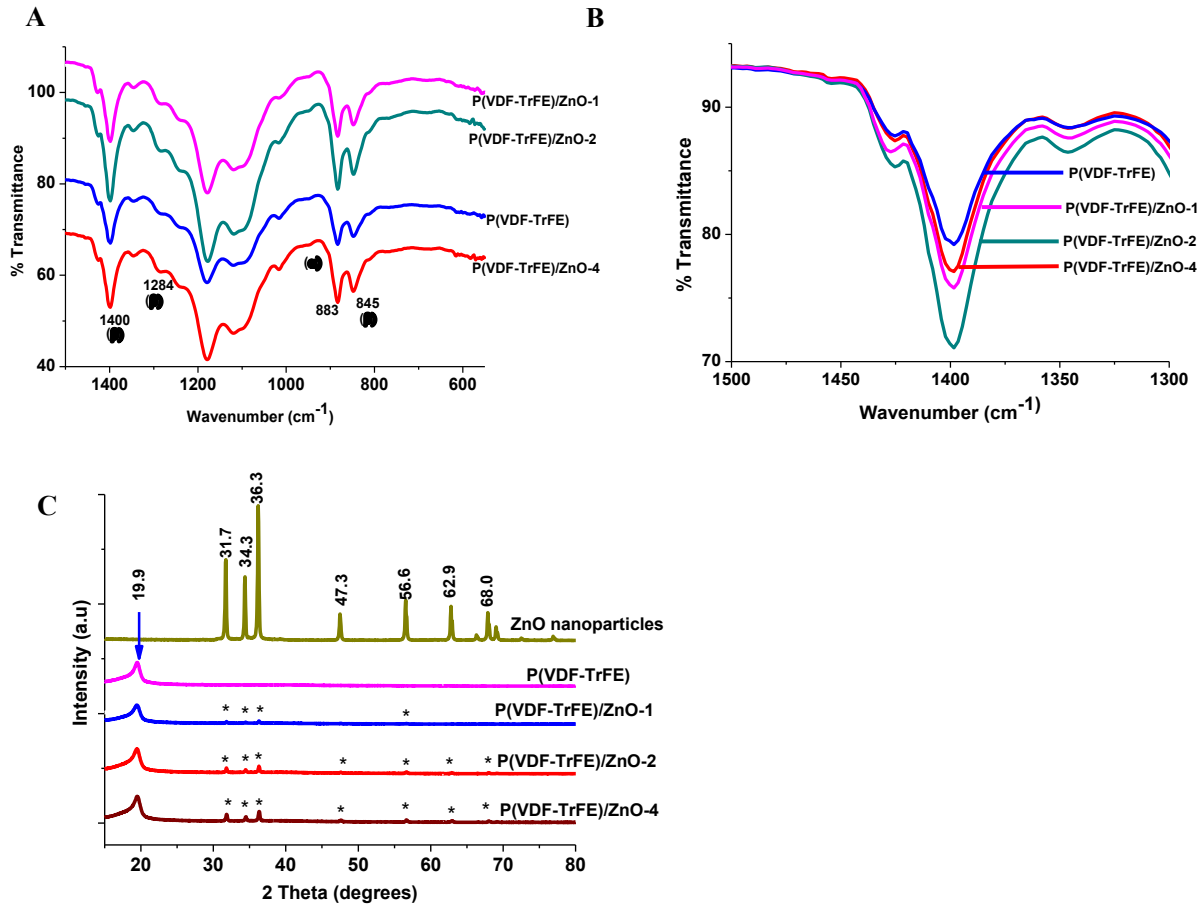

Figure 3 (A, B) FTIR spectra of (A) neat P(VDF-TrFE) and P(VDF-TrFE)/ZnO nanocomposite scaffolds with growing concentration of ZnO nanoparticles and (B) an enlarged view of the band at 1400 cm^{-1} which indicates the variation of relative intensity of β-phase in the nanocomposites. (C) XRD patterns of the scaffolds where (*) represents the diffraction patterns of ZnO nanoparticles in nanocomposite scaffolds.

Table 2. Effect ZnO nanoparticles on the thermal behavior of P(VDF-TrFE) scaffolds.

Samples	T_m (°C)	ΔH_f (J/g)	T_{F-P} (°C)	ΔH_{F-P} (J/g)	T_c (°C)	ΔH_c (J/g)	T_{P-F} (°C)	ΔH_{P-F} (J/g)
Neat P(VDF-TrFE)	158	25	67	10	143	27	61	9
P(VDF-TrFE)/ZnO-1	158	23	68	13	142	24	60	11
P(VDF-TrFE)/ZnO-2	159	23	68	12	141	24	59	12
P(VDF-TrFE)/ZnO-4	159	23	67	9	142	26	60	9

3.4. Porosity measurements

Porosity of the fabricated P(VDF-TrFE)/ZnO nanocomposite membranes was evaluated using alcohol displacement method and presented in **Table 3**. All the fabricated membranes showed porosity in the 88-92% range. There was no significant effect of nanofiller addition on the porosity of the scaffolds.

Table 3. Porosity of P(VDF-TrFE) membranes in percentage.

Sample	Porosity (%)
P(VDF-TrFE)	92.2 ± 1.5
P(VDF-TrFE)/ZnO-0.5	90.4 ± 1.8
P(VDF-TrFE)/ZnO-1	88.7 ± 2.2
P(VDF-TrFE)/ZnO-2	91.3 ± 2.1
P(VDF-TrFE)/ZnO-4	90.6 ± 1.2

3.5. Blood cell aggregation, platelet activation and hemolysis studies

Tissue engineering scaffolds are in direct contact with blood at the implantation site. Thus, the use of biomaterials that result in aggregation of blood cells is precluded. In this framework, the aggregation behavior of the blood cells (RBC, WBC and platelets) upon incubation with aqueous extracts of the pristine and modified scaffolds was studied (**Fig. 4**). No aggregation of blood cells was apparent as also observed with saline solution (negative control). In contrast, PEI (positive control) showed aggregation. Platelet activation is considered as the initial step of blood coagulation. Neat P(VDF-TrFE) scaffolds and nanocomposite scaffolds did not show any sign of platelet activation. In the case of the positive control, platelets aggregated and formed clumps of circular shape (**Fig. 4**)

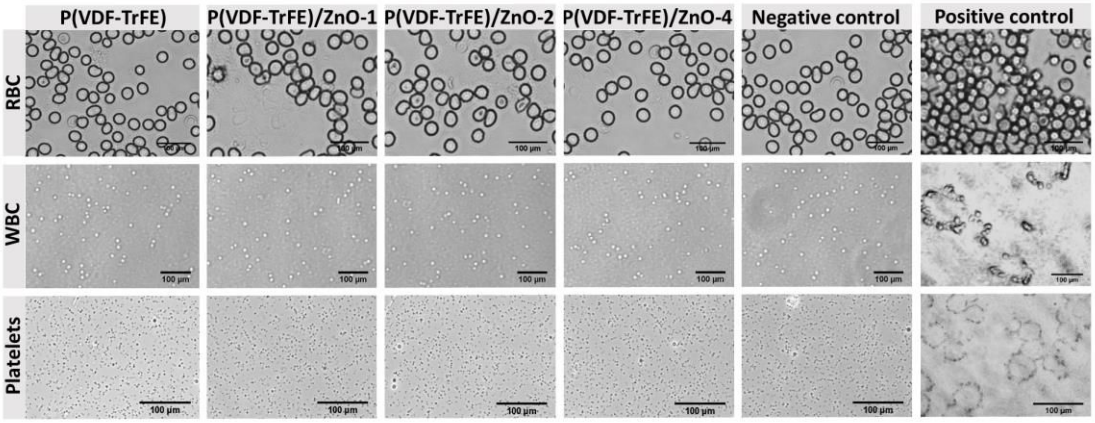

Figure 4. RBC, WBC and platelet aggregation upon contact with P(VDF-TrFE), P(VDF-TrFE)/ZnO-1, P(VDF-TrFE)/ZnO-2 and P(VDF-TrFE)/ZnO-4 extracts. PBS and PEI were included as negative and positive control.

Another important property to be tested to demonstrate blood compatibility of biomaterials is hemolysis. Hemocompatibilty has been calculated with respect to a negative control (Normal saline- assumed as 0% hemolytic) and a positive control (Double distilled water- assumed as 100% hemolytic). The hemolysis test results of the P(VDF- TrFE) scaffolds and P(VDF- TrFE)/ZnO nanocomposite scaffolds are shown in **Table 4.** All the tested samples showed comparable hemolysis without significant difference ($p>0.05$).

Table 4. Percentage of hemolysis due to P(VDF-TrFE) and P(VDF-TrFE)/ZnO nanocomposite scaffolds.

Sample	%Hemolysis ± S.D.
Neat P(VDF-TrFE)	0.3 ± 0.04
P(VDF-TrFE)/ZnO-0.5	0.2 ± 0.01
P(VDF-TrFE)/ZnO-1	0.3 ± 0.02
P(VDF-TrFE)/ZnO-2	0.3 ± 0.04
P(VDF-TrFE)/ZnO-4	0.3 ± 0.07
Negative control	0
Positive control	100

3.6. In vitro performance of the scaffolds

To further confirm the applicability of the developed scaffolds, cell viability, cytotoxicity and cell attachment studies were carried out using HUVECs and hMSCs. The viability of HUVECs grown in the presence of P(VDF-TrFE) was comparable with that grown on commercial cell culture plates (**Fig. 5A).** Very interestingly, HUVECS grown on P(VDF-TrFE)/ZnO-1 and P(VDF-TrFE)/ZnO-2 showed significantly higher viability than the control. In contrast, P(VDF-TrFE)/ZnO-4 was slightly cytotoxic. hMSCs showed a similar trend (**Fig. 5B**). Thus, viability values on controls, P(VDF-TrFE) and P(VDF-TrFE)/ZnO-1 were comparable. Similarly, hMSCs grown on P(VDF-TrFE)/ZnO-2 also showed higher viability than controls, P(VDF-TrFE)/ZnO-1 and P(VDF-TrFE)/ZnO-4. Finally, the viability of hMSCs was substantially smaller than controls in the presence of P(VDF-TrFE)/ZnO-4.

LDH assay was used as a complementary study to

reveal any possible cell membrane damage that could result in cell death at a later stage. Neat P(VDF-TrFE), P(VDF-TrFE)/ZnO-1 and P(VDF-TrFE)/ZnO-2 were almost nontoxic to both HUVECs and hMSCs (**Fig. 5C, D**). In contrast, P(VDF-TrFE)/ZnO-4 was cytotoxic on HUVECs but not on hMSCs.

To evaluate the ability of the scaffolds to allow endothelial cell adhesion which is a prerequisite of angiogenesis, HUVECs were seeded on P(VDF-TrFE) and nanocomposite scaffolds and then allowed to grow for 24 h. Previous reports indicated that the hMSCs can differentiate to endothelial cells [39]. **Fig. 5E** shows the cell adhesion of both cell types on P(VDF-TrFE) and P(VDF-TrFE)/ZnO nanocomposite scaffolds (additional micrographs of crystal violet stained cell seeded scaffolds are included in **Fig. S-3** in the ESM).

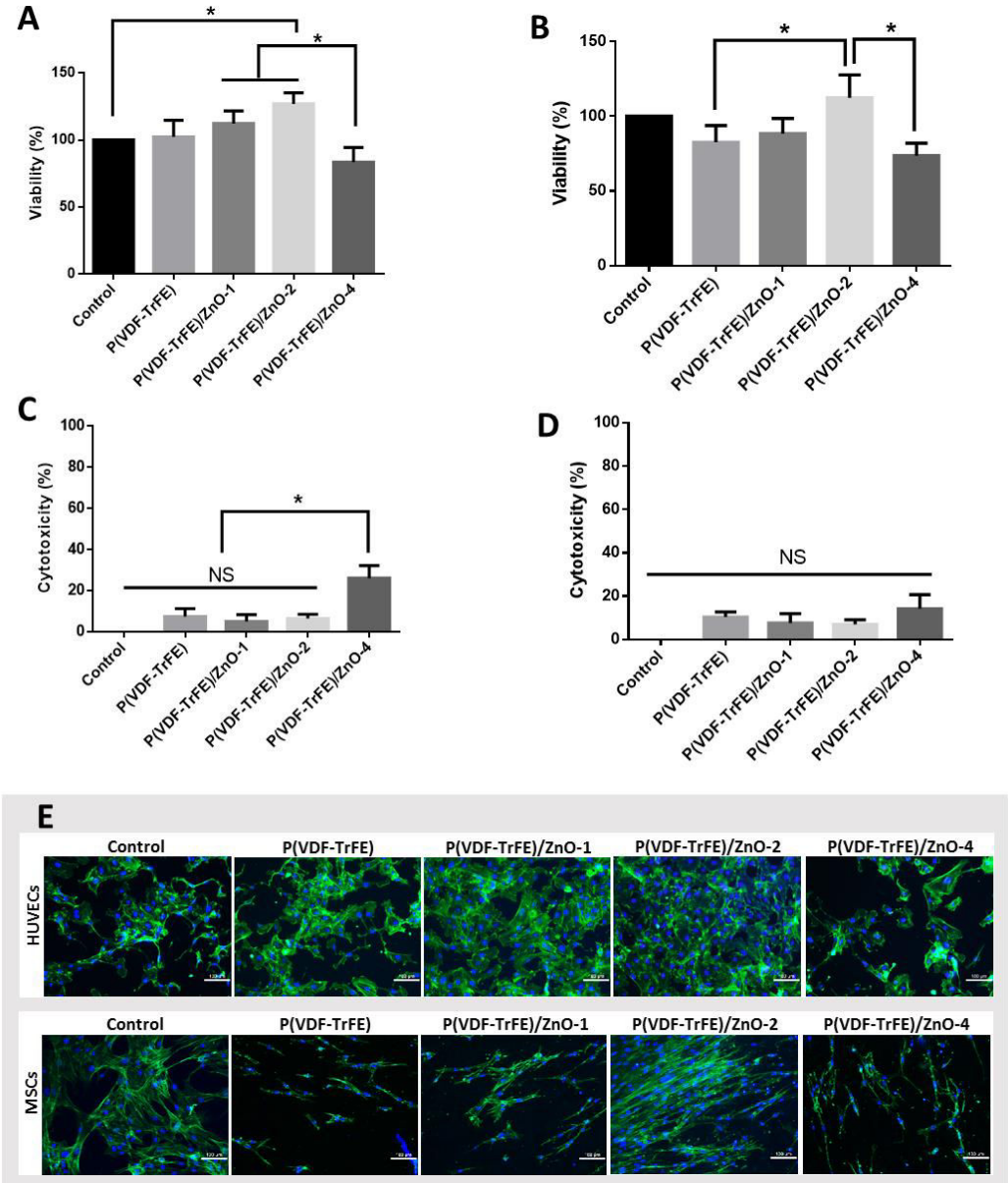

Figure 5 *In vitro* cell compatibility and cytotoxicity studies. (A, B) Cell viability of (A) HUVECs and (B) hMSCs on the scaffolds, as determined by MTT assay. (C, D) Cytotoxicity of (C) HUVECs and (D) hMSCs, as determined by LDH assay. Data are mean ± SD (n=3, * $p < 0.05$ indicate statistically significant differences using ANOVA and followed by a Tukey test between all groups). NS, no significance. Cell attachment of HUVECs and hMSCs (E) on the scaffolds after 24 hours of culture (50000 cells/cm^2 seeded).

HUVECs on neat P(VDF-TrFE) scaffolds showed similar proliferation and spread morphology as control plates. Unlike P(VDF-TrFE)/ZnO-4, cell adhesion and proliferation was much higher on P(VDF-TrFE)/ZnO-1 and P(VDF-TrFE)/ZnO-2. hMSCs grown on neat P(VDF-TrFE) scaffolds and P(VDF-TrFE)/ZnO-1 scaffolds presented slightly less cell adhesion and spreading than controls. However, P(VDF-TrFE)/ZnO-2 supported confluent growth of hMSCs with elongated morphology. As observed before, P(VDF-TrFE)/ZnO-4 led to a more considerable decrease in cell proliferation than the neat P(VDF- TrFE) and nanocomposite scaffolds with less content of ZnO nanoparticles.

3.7. In vivo angiogenesis in scaffolds

Based on the results of *in vitro* cell culture studies, P(VDF-TrFE), P(VDF-TrFE)/ZnO-1 and P(VDF-TrFE)/ZnO-2 scaffolds were selected for subcutaneous implantation studies to evaluate their *in vivo* performance (**Fig. S-4A in the ESM**). No visual inflammation or severe immunological response were observed at the implantation site for any of the implanted scaffolds after 7 and 21 days (**Fig. S-4B in the ESM**).

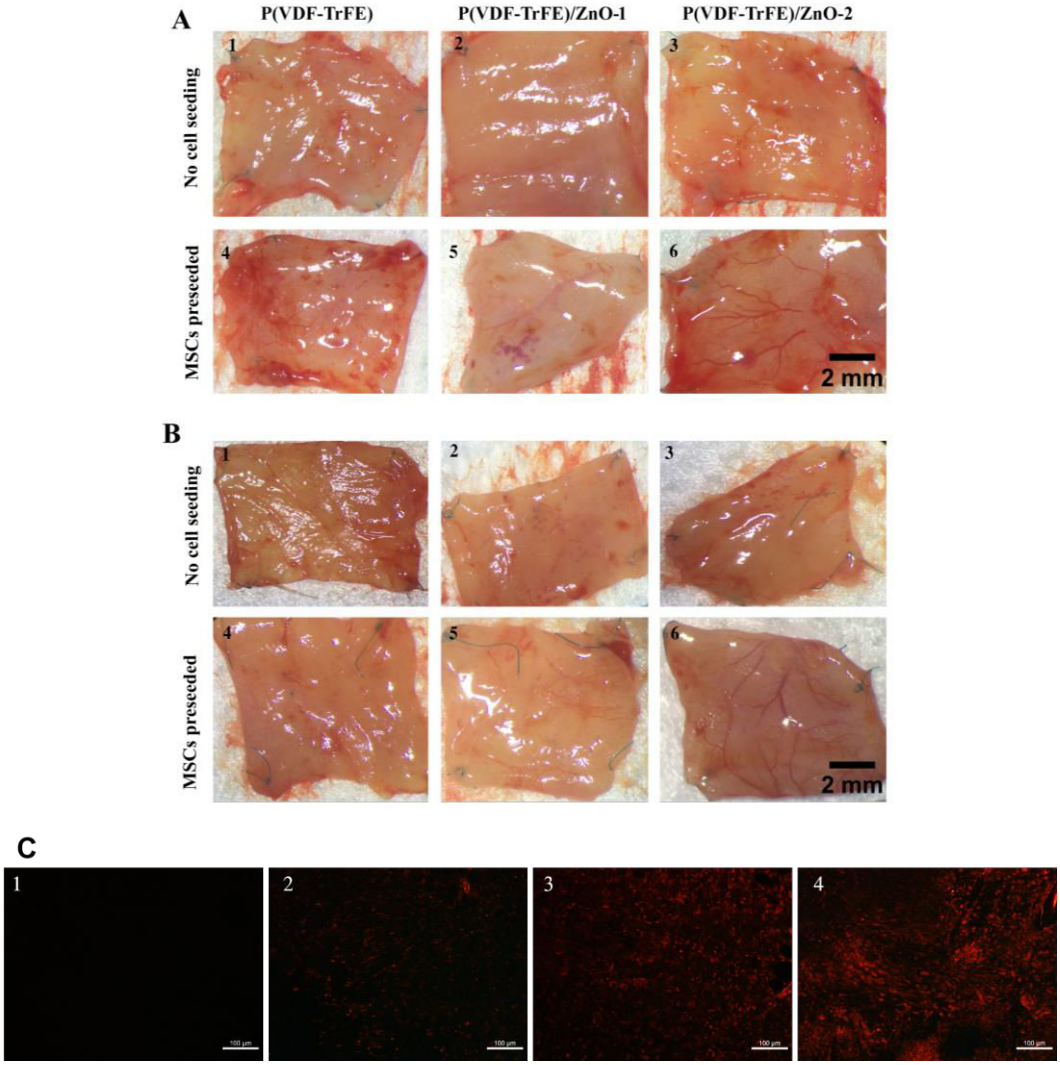

Figure 6 Observation on scaffolds after subcutaneous implantation. Macroscopic inspection of explanted samples at 7th day (A) and 21st day (B) after implantation. (C) Fluorescent cell tracking at 21st day after implantation. hMSCs were confirmed by pre-labeled DiI after eliminating the influence of autofluorescence of scaffolds and tissue. (C1) Scaffold without cells as control, (C2) P(VDF-TrFE), (C3) P(VDF-TrFE)/ZnO-1, (C4) P(VDF-TrFE)/ZnO-2.

Macroscopic observation clearly showed the formation of more blood vessels on the scaffolds containing ZnO nanoparticles. Highly branched vasculature was observed in the case of P(VDF-TrFE)/ZnO-2, pre-seeded with hMSCs (**Fig. 6A6, B6**). Tracking of fluorescently-labeled hMSCs confirmed their presence in the scaffolds even after 21 days of implantation (**Fig. 6C**). Histological evaluation of the cross section of scaffolds showed that 7 days after implantation, there were extensive networks of collagen fibers throughout the scaffold (**Fig. 7A**). Some inflammatory cells were found but there were no intergroup differences. After 7 days of implantation, neovascularization was observed in adjacent tissue around scaffold, number of newly formed blood vessels depended on percentage of ZnO nanoparticles and presence of hMSCs (**Fig. 7C**). After 21 days of implantation, the in-growth of blood vessels, especially on nanocomposite scaffolds pre-seeded with hMSCs, was noticed (**Fig. 7B**). Noteworthy to mention, throughout the period of study, the best angiogenic response was observed for P(VDF-TrFE)/ZnO-2 pre-seeded with hMSCs (**Fig. 7 C, D**). Transverse and cross sections of these scaffolds confirmed that the angiogenesis took place throughout the entire sample and not only on the surface (**Fig. S-5** and **Fig. S-6 in the ESM**).

4. Discussion

Synthetic biomaterials are being developed at a rapid pace for therapeutic applications and basic biological studies [40]. Their popularity is mostly due to easy manipulation and ability to tailor their properties for different tissue engineering applications, ability to mimic the natural extracellular matrix environment and thus, support cell growth (e.g., stem cells) and they can be produced at large industrial scale in a reproducible manner [41]. More recently, the design of synthetic biomaterials has shifted to incorporate molecular cues that control their interaction with the biological environment.

P(VDF-TrFE) has been recognized for its potential in tissue engineering for over a decade [42]. This P(VDF-TrFE) polymer and other nanocomposite incorporated copolymers are widely appreciated because of their piezoelectric properties and potential in tissue engineering [43,44]. Here, we reported on the synthesis of P(VDF-TrFE) scaffolds incorporated with ZnO nanoparticles by electrospinning.

Detailed morphological and spectroscopic characterizations confirmed the presence of ZnO nanoparticles in P(VDF-TrFE) fibers. Highly porous morphology of the fabricated scaffolds with randomly oriented fibers are highly promising for cell adhesion. A slight increase in fiber diameter due to the incorporation of growing concentrations of nanoparticles was observed. These results were in good agreement with our previous studies [20]. The possible reason for the increase in fiber diameter might be the increase in the viscosity of the spinning solution due to the presence of nanofiller agglomerates [45] that subsequently resulted in the increase in fiber diameter [46]. Lee and coworkers reported that electrospun P(VDF-TrFE) scaffolds with micron sized fibers are more effective for tissue engineering applications due to the higher cell growth [12]. All the scaffolds presented in this study also possessed micrometer sized fibers.

Once an engineered scaffold is implanted *in vivo*, a series of complex events will be initiated, including cell adhesion, migration, proliferation and scaffold-native tissue integration at the implantation site. It has been proposed that the electric potential that exists in the injured tissue could play a fundamental role in tissue repair [47]. Piezoelectric scaffolds can convert ambient mechanical energy into electric signals to enhance cell response [48]. FTIR analysis indicated relative amount of electro-active β-phase was higher in nanocomposite scaffolds than in the neat ones. XRD analysis further confirmed the presence of ZnO nanoparticles in the nanocomposite scaffolds owing to the more intense signals of ZnO with respect to nanoparticle loading. These results confirmed that ZnO nanoparticles were successfully incorporated into the polymer matrix during the electrospinning process without adversely affecting the formation of the piezoelectric β-phase.

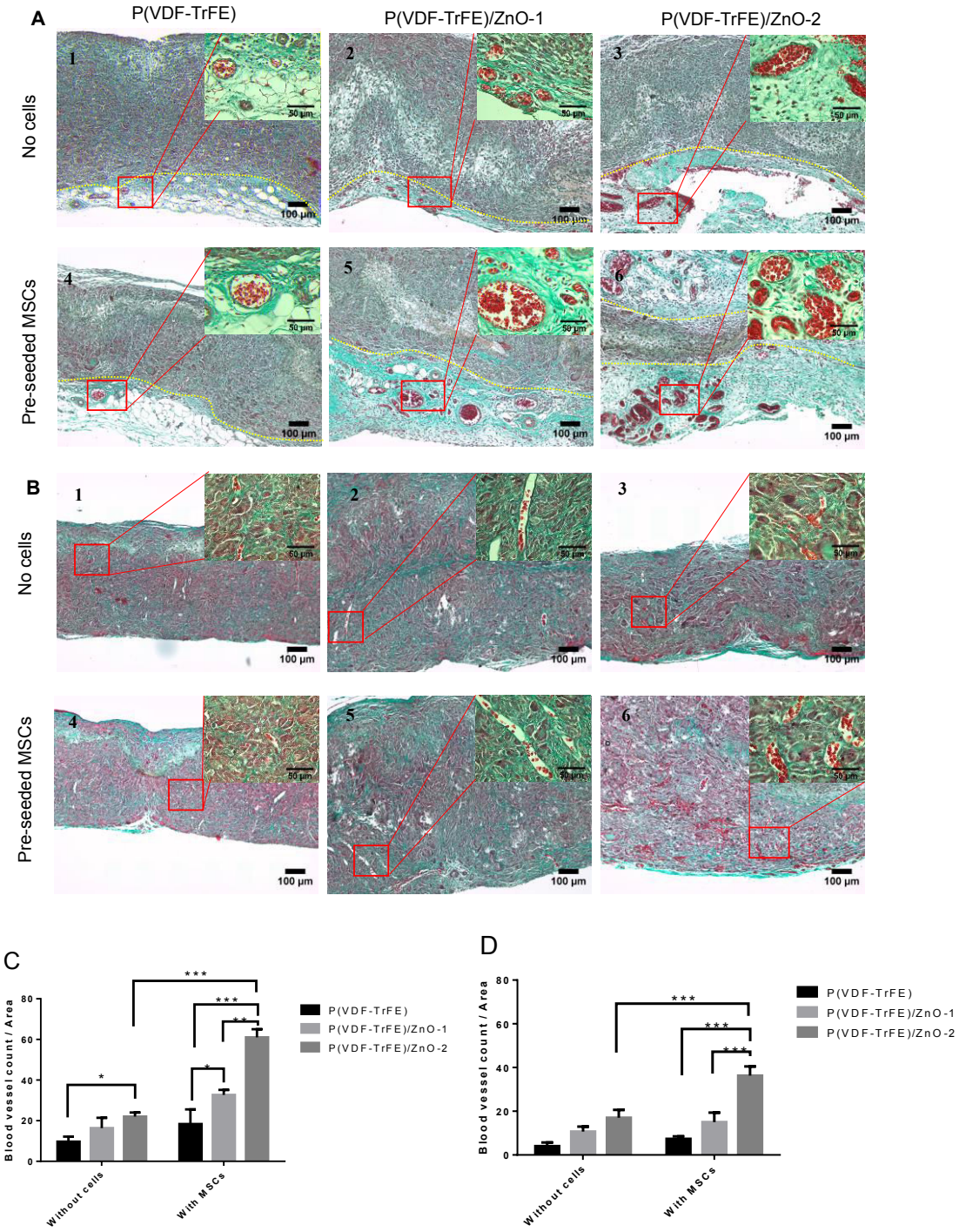

Figure 7 Histological analysis of scaffolds after implantation. Scaffolds were cross cut and stained with Masson trichrome. (A) 7th day after implantation, blood vessels were observed in connective tissue adjacent to scaffolds (distinguished by yellow dash lines). Collagen was found in all scaffolds (green). (B) Extensive angiogenesis was observed throughout the scaffolds after 21st day of implantation. Quantitative analysis of number of blood vessels in tissue adjacent to scaffolds after 7 days (C) and 21 days (D) of implantation. (n=3, 6 areas (1.3×1mm/area) of each cross section sample were randomly selected, blood vessels with diameter larger than 8μm were counted, ***$p < 0.001$).

DSC analysis demonstrated that incorporation of ZnO nanoparticles into the fibers did not affect the T_m and T_{F-P} owing to retention of the ferroelectric crystalline fraction or the lamellar thickness of the crystalline domains in the nanocomposite copolymer [37]. This demonstrated that lower percentage of ZnO nanoparticles in P(VDF-TrFE) resulted in relatively similar amount of crystalline phase in the polymer matrix. In the cooling process, neat P(VDF-TrFE) scaffolds exhibited T_c and T_{P-F} that are comparable with those reported in the literature [49]. The slight decrease in both T_c and T_{P-F} observed for the nanocomposites implies that the crystallization happened at lower temperatures than in neat P(VDF-TrFE). The ΔH_{F-P} endothermic peak can be weighted toward higher temperatures, which is an indication of the relative amount of the β phase to α phase in these samples [50]. This might further improve the performance of the scaffolds *in vivo*. For example, Guo *et al.* reported that electrospun polyurethane (PU)/PVDF piezoelectric composites (PU/PVDF) promote cell adhesion better than the pure PU counterpart [51]. We observed from the FTIR and DSC results that the incorporation of ZnO nanoparticles increased the crystalline β-phase [52]. These findings suggested that the enhancement in the electroactive phase in P(VDF-TrFE)/ZnO scaffolds could be one of the possible reasons for enhanced cell adhesion [53]. All the nanocomposite scaffolds irrespective of ZnO nanoparticle concentration have shown adequate porosity to facilitate cell migration, nutrient supply and blood vessel penetration [54].

Since P(VDF-TrFE) scaffolds could be eventually used in tissue engineering applications involving direct contact with blood, their compatibility with RBC and WBC was initially confirmed. In addition, in the case of platelets, they did not undergo aggregation with samples containing up to 4% w/w ZnO nanoparticles. Moreover, all the samples showed hemolysis levels <1%, the upper limit defined by ASTM (ASTM Standard, F756-08). From the overall results of blood cell aggregation and hemolysis tests, it can be concluded that P(VDF-TrFE)/ZnO nanocomposite scaffolds containing up to 4% w/w ZnO nanoparticles were compatible to all kind of studied blood cells and can be used for the fabrication of various tissue engineering scaffolds.

Studying the interaction of the scaffolds with cells *in vitro* was of interest to select the best prototypes towards the *in vivo* characterization. In this study, we demonstrated that the incorporation of 1-2% w/w of ZnO nanoparticles increased the attachment of both HUVECs and hMSCs. Apart from the effect of piezoelectric P(VDF-TrFE), ZnO nanoparticles are known to play a major role in cell adhesion and proliferation [55,56]. Conversely, P(VDF-TrFE)/ZnO-4 samples were slightly cytotoxic probably due to the damage of the cell membrane mediated by the nanofiller agglomerates that in these samples was more exposed at the nanofiber surface [22][57]. At the same time, it is important to mention that differences found in the cytotoxic concentration of ZnO nanoparticles reported in the literature might be due to the variation in the properties of nanoparticles (e.g., size, size distribution, shape, and purity) and the polymer matrix used. Previous studies have shown that the size and shape of ZnO nanoparticles could largely influence their cytotoxic effects [58,59]. Although a detailed study on the effect of size and morphology of ZnO nanoparticles on cell behavior of P(VDF-TrFE) fibers will be beyond the scope of this particular work, this needs to be further investigated in future studies.

Owing to the ability to form well cellularized scaffolds, P(VDF-TrFE)/ZnO could strengthen their function, and reduce failure after implantation [60]. Our study demonstrated that P(VDF-TrFE) incorporated with ZnO nanoparticles less than 4% w/w were not toxic to both HUVECs and hMSCs, both kinds of cells shown satisfactory viability on neat P(VDF-TrFE), P(VDF-TrFE)/ZnO-1 and P(VDF-TrFE)/ZnO-2, suggesting that these scaffolds could be utilized for the further development of various tissue engineered products.

Vascularization through a tissue engineering scaffold is considered as one of the most important events that determine the further success (or conversely the failure) of a tissue engineered construct. Our results demonstrated a higher blood vessel sprouting process in nanocomposite scaffolds. At early stage after implantation, blood vessels were found in adjacent tissue, while after 21 days of implantation,

blood vessels began to penetrate throughout the scaffold. Unlike the neat scaffolds where only very few blood vessels were formed even after 21 days of implantation, significantly more capillaries were observed in the case of P(VDF-TrFE)/ZnO nanocomposites ($p < 0.001$). ZnO nanoparticles can play crucial role to promote angiogenesis [61]. For instance, scaffolds seeded with hMSCs were reported to enhance angiogenesis, by secreting soluble angiogenic signaling molecules [62]. Thus, in parallel, hMSCs were also seeded on P(VDF-TrFE) or P(VDF-TrFE)/ZnO nanocomposites and allowed to grow for 24 h. Many circular groups of RBCs were also apparent in P(VDF-TrFE)/ZnO scaffolds can be considered as the hallmark of enhanced angiogenesis [22]. In the current study, P(VDF-TrFE)/ZnO scaffolds pre-seeded with hMSCs showed higher angiogenesis than unseeded ones. The beneficial effects from piezoelectric P(VDF-TrFE), ZnO nanoparticles and loaded hMSCs make the P(VDF-TrFE)/ZnO scaffolds very promising candidate in tissue engineering.

A schematic representation of the most likely mechanism behind the improved performance of P(VDF-TrFE)/ZnO scaffolds is given in **Scheme 2**. Electric potential generated by piezoelectric P(VDF-TrFE) scaffolds can enhance cell response [48]. Moreover, ZnO nanoparticles can generate reactive ROS like O_2^- and subsequently H_2O_2 [63]. This can enhance cell proliferation [20] and angiogenesis by the expression of growth factors like vascular endothelial growth factor (VEGF) and fibroblast growth factor (FGF) [22]. Though, further studies are required to give a conclusive remark regarding the mechanism of improved cell viability, cell adhesion, cell proliferation and angiogenesis, results strongly supported that both the piezoelectric property of P(VDF-TrFE) and the redox reaction taking place on the surface of ZnO nanoparticles play a major role.

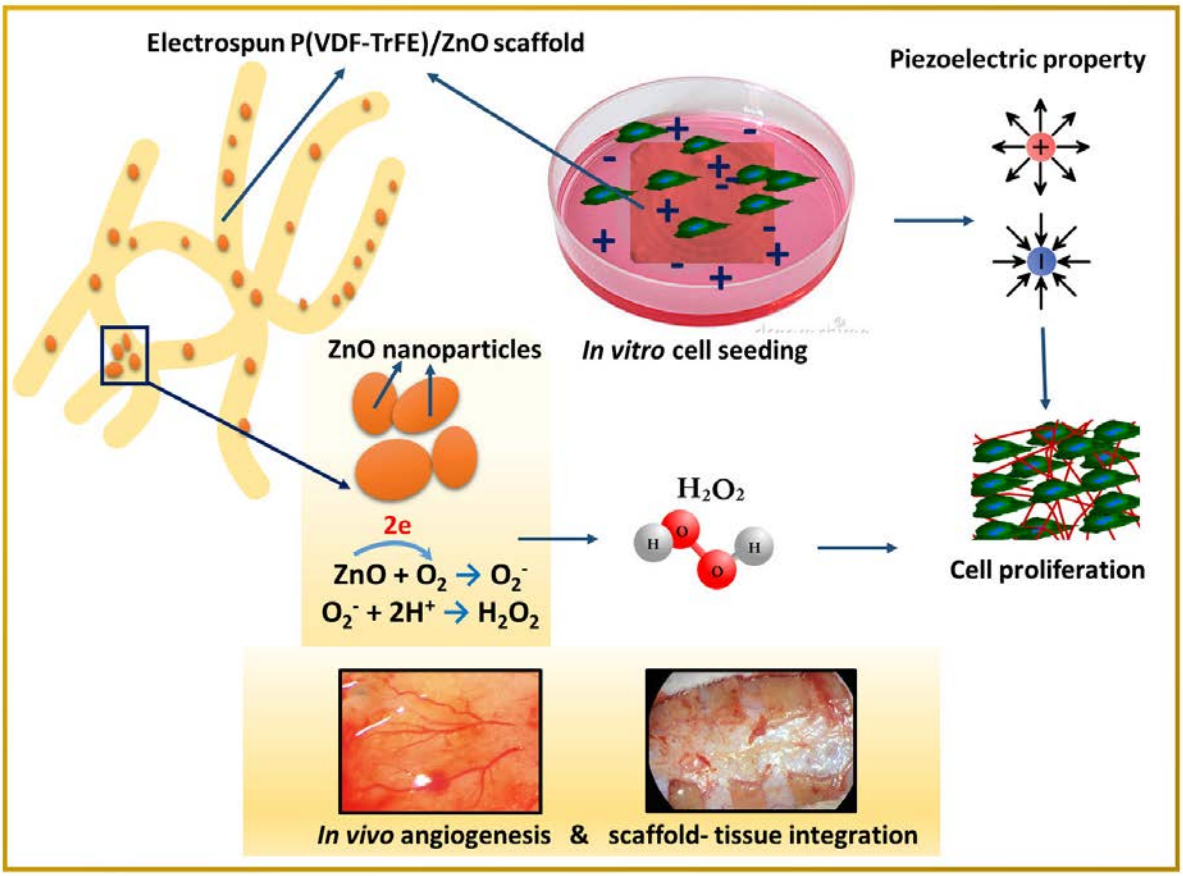

Scheme 2 Schematic illustration of the mechanism of cell proliferation on P(VDF-TrFE)/ZnO nanocomposite scaffolds. Both piezoelectric property of P(VDF-TrFE) and H_2O_2 molecules released due to ZnO nanoparticles will simultaneously enhance cell proliferation through the scaffolds.

5. Conclusion

Electrospun P(VDF-TrFE)/ZnO nanocomposite scaffolds with various concentrations of ZnO nanoparticles were fabricated and characterized. SEM, EDS and XRD analysis confirmed the successful incorporation of ZnO nanoparticles in the P(VDF-TrFE) fiber matrix. From the SEM micrographs, it was evident that at lower filler concentrations, ZnO nanoparticles were well dispersed in the P(VDF-TrFE) copolymer matrix. However, above 2% w/w, the agglomeration of ZnO nanoparticles in the polymer matrix was observed. Crystalline phase characterization indicated that the P(VDF-TrFE) in the scaffolds was mainly in the piezoelectric β-phase. All the scaffolds were highly blood compatible. *In vitro* cell culture studies using hMSCs and HUVECs showed that these scaffolds were cell compatible and supported cell adhesion in a more favorable way when the content of ZnO nanoparticles was 2% w/w. Finally, *in vivo* studies in rats confirmed the non-toxicity of the P(VD-TrFE)/ZnO scaffolds and their ability to promote angiogenesis. Moreover, the presence of ZnO nanoparticles in the scaffolds enhanced angiogenesis and favored more successful integration of the scaffold to the surrounding tissue, this being boosted by the pre-seeding of hMSCs. Collectively, this study suggests that P(VDF-TrFE) incorporated with low concentration of ZnO nanoparticles could be applied as a promising alternative in tissue engineering. However, concerns regarding systemic toxicity, fate of stem cells on the scaffold and long term patency of the scaffold should be addressed in detail before going to the clinical application of the developed material.

Acknowledgements

The authors gratefully acknowledge the financial support of Nancy-Brabois Institute of Technologies, Lorraine University, Nancy, France. The authors also acknowledge the Department of Biotechnology (DBT), Government of India, New Delhi, for the financial support through MSUB IPLSARE Program (BT/PR4800/INF/22/152/2012). RA thanks the Israel Council for Higher Education for postdoctoral fellowship. PD thanks the China scholarship council for overseas fellowship.

Electronic Supplementary Material: Supplementary material like TEM image of ZnO nanoparticle, DSC thermograms of scaffolds and more images of *in vitro* and *in vivo* studies are available in the online version of this article at http://dx.doi.org/10.1007/s12274-***-****-*

References

[1] Kuang, R.; Zhang, Z.; Jin, X.; Hu, J.; Shi, S.; Ni, L.; Ma, P. X.. Nanofibrous spongy microspheres for the delivery of hypoxia-primed human dental pulp stem cells to regenerate vascularized dental pulp. *Acta Biomater.* **2016**, 33, 225–234.

[2] Briquez, P. S.; Clegg, L. E.; Martino, M. M.; Gabhann, F. Mac.; Hubbell, J. A. Design principles for therapeutic angiogenic materials. *Nat. Rev. Mater.* **2016**, 1, 15006.

[3] Dondossola, E.; Holzapfel, B.; Alexander, S.; Filippini, S.; Hutmacher, D.; Friedl, P. Examination of the foreign body response to biomaterials by nonlinear intravital microscopy. *Nat. Biomed. Eng.*, in press, DOI: 10.1038/s41551-016-0007.

[4] McCaig, C. D.; Song, B.; Rajnicek, A. M. Electrical dimensions in cell science. *J. Cell Sci.* **2009**, 122, 4267–4276.

[5] McCaig, C. D.; Rajnicek, A. M.; Song, B.; Zhao, M. Controlling cell behavior electrically: current views and future potential. *Physiol. Rev.* **2005**, 85, 943–978.

[6] Weber, N.; Lee, Y. S.; Shanmugasundaram, S.; Jaffe, M.; Arinzeh, T. L. Characterization and in vitro cytocompatibility of piezoelectric electrospun scaffolds. *Acta Biomater*. **2010**, 6, 3550–3556.

[7] Hu, Z.; Tian, M.; Nysten, B.; Jonas, A. M. Regular arrays of highly ordered ferroelectric polymer nanostructures for non-volatile low-voltage memories. *Nat. Mater.* 2009, 8, 62–67.

[8] Huang, S., Yee, W. A.; Tjiu, W. C.; Liu, Y.; Kotaki, M.; Boey, Y. C. F.; Ma, J.; Liu, T.; Lu, X.. Electrospinning of polyvinylidene difluoride with carbon nanotubes: synergistic effects of extensional force and interfacial interaction on crystalline structures. *Langmuir ACS J. surfaces colloids* **2008**, 24, 13621–13626.

[9] Li, M.; Wondergem, H. J.; Spijkman, M. J.; Asadi, K.; Katsouras, I.; Blom, P. W. De Leeuw, D. M. Revisiting the δ-phase of poly(vinylidene fluoride) for solution-processed ferroelectric thin films. *Nat. Mater.* **2013**, 12, 433–438.

[10] Liu, Y.; Lu, J.; Li, H.; Wei, J; Li, X. Engineering blood vessels through micropatterned co-culture of vascular endothelial and smooth muscle cells on bilayered electrospun fibrous mats with pDNA inoculation. *Acta Biomater*. **2015**, 11, 114–125.

[11] Fine, E. G.; Valentini, R. F.; Bellamkonda, R.; Aebischer, P. Improved nerve regeneration through

piezoelectric vinylidenefluoride-trifluoroethylene copolymer guidance channels. *Biomaterials* **1991**, 12, 775–780.
[12] Lee, Y. S.; Collins, G.; Livingston Arinzeh T. Neurite extension of primary neurons on electrospun piezoelectric scaffolds. *Acta Biomater.* **2011**, 7, 3877–3886.
[13] Lee, Y. S.; Wu, S.; Arinzeh, T. L.; Bunge, M. B. Enhanced noradrenergic axon regeneration into schwann cell-filled PVDF-TrFE conduits after complete spinal cord transection. *Biotechnol. Bioeng*. **2016**, 9999, 1–13.
[14] Martins, P. M.; Ribeiro, S.; Ribeiro, C.; Sencadas, V.; Gomes, A. C.; Gama, F. M.; Lanceros-Méndez, S. Effect of poling state and morphology of piezoelectric poly(vinylidene fluoride) membranes for skeletal muscle tissue engineering. *RSC Adv.* **2013**, 3, 17938–17944.
[15] Hitscherich, P.; Wu, S.; Gordan, R.; Xie, L. H.; Arinzeh, T.; Lee, E. J. The effect of PVDF-TrFE scaffolds on stem cell derived cardiovascular cells. *Biotechnol. Bioeng.* **2016**, 113, 1577–1585.
[16] Zhu, P.; Weng, Z.; Li, X.; Liu, X.; Wu, S.; Yeung, K. W. K.; Wang, X.; Cui, Z.; Yang, X.; Chu, P. Biomedical Applications of Functionalized ZnO Nanomaterials: from Biosensors to Bioimaging. *Adv. Mater. Interfaces*, in press, DOI: 10.1002/admi.201500494.
[17] Liao, Q.; Zhang, Z.; Zhang, X.; Mohr, M.; Zhang, Y.; Fecht, H. J. Flexible piezoelectric nanogenerators based on a fiber/ZnO nanowires/paper hybrid structure for energy harvesting. *Nano Res*. **2014**, 7, 917–928.
[18] Kang, Z.; Yan, X.; Zhao, L.; Liao, Q.; Zhao, K.; Du, H.; Zhang, X.; Zhang, X.; Zhang, Y. Gold nanoparticle/ZnO nanorod hybrids for enhanced reactive oxygen species generation and photodynamic therapy. *Nano Res.* **2015**, 8, 1–11.
[19] Yan, Z.; Zhao, A.; Liu, X.; Ren, J.; Qu, X. A pH-switched mesoporous nanoreactor for synergetic therapy. *Nano Res*. **2016**, 1, 1–11.
[20] Augustine, R.; Malik, H. N.; Singhal, D. K.; Mukherjee, A.; Malakar, D.; Kalarikkal, N.; Thomas. S. Electrospun polycaprolactone/ZnO nanocomposite membranes as biomaterials with antibacterial and cell adhesion properties. *J. Polym. Res.* **2014**, 21, 347.
[21] Augustine, R.; Dominic, E. A.; Reju, I.; Kaimal. B.; Kalarikkal, N.; Thomas, S. Electrospun polycaprolactone membranes incorporated with ZnO nanoparticles as skin substitutes with enhanced fibroblast proliferation and wound healing. *RSC Adv.* **2014**, 4, 24777–24785.
[22] Augustine, R.; Dominic, E. A.; Reju, I.; Kaimal, B.; Kalarikkal, N.; Thomas, S. Investigation of angiogenesis and its mechanism using zinc oxide nanoparticle-loaded electrospun tissue engineering scaffolds. *RSC Adv.* **2014**, 4, 51528–51536.
[23] Sirelkhatim, A.; Mahmud, S.; Seeni, A.; Kaus, N. H. M.; Ann, L. C.; Bakhori, S. K. M.; Hasan, H.; Mohamad, D. Review on zinc oxide nanoparticles: Antibacterial activity and toxicity mechanism. *Nano-Micro Lett.* **2015**, 7, 219–242.
[24] Saptarshi, S. R.; Duschl, A.; Lopata, A. L. Biological reactivity of zinc oxide nanoparticles with mammalian test systems: an overview. *Nanomedicine (Lond)*. **2015**, 10, 2075–2092.
[25] Versiani, M. A.; Abi Rached-Junior, F. J.; Kishen, A.; Pécora J. D.; Silva-Sousa, Y. T.; de Sousa-Neto, M. D. Zinc Oxide Nanoparticles Enhance Physicochemical Characteristics of Grossman Sealer. *J. Endod.* **2016**, 42, 1804–1810.
[26] Liuyun, J.; Yubao, L.; Chengdong, X. Preparation and biological properties of a novel composite scaffold of nano-hydroxyapatite/chitosan/carboxymethyl cellulose for bone tissue engineering. *J. Biomed. Sci.* **2009**, 16, 65.
[27] Joshy, K. S.; Sharma, C. P.; Kalarikkal, N.; Sandeep, K.; Thomas, S.; Pothen, L. A. Evaluation of in-vitro cytotoxicity and cellular uptake efficiency of zidovudine-loaded solid lipid nanoparticles modified with Aloe Vera in glioma cells. *Mater. Sci. Eng. C* **2016**, 66, 40–50.
[28] El Omar, R.; Xiong, Y.; Dostert, G.; Louis, H.; Gentils, M.; Menu, P.; Stoltz, J.. F.; Velot, É.; Decot.; V. Immunomodulation of endothelial differentiated mesenchymal stromal cells: impact on T and NK cells. *Immunol. Cell Biol.* **2015**, 94, 342-356.
[29] Choi, Y. Y.; Yun, T. G.; Qaiser, N.; Paik, H.; Roh, H. S.; Hong, J.; Hong, S.; Han, S. M.; No, K. Vertically aligned P(VDF-TrFE) core-shell structures on flexible pillar arrays. *Sci. Rep*. **2015**, 5, 10728.
[30] Tashiro, K.; Takano, K.; Kobayashi, M.; Chatani, Y.; Tadokoro, H. Structural study on ferroelectric phase transition of vinylidene fluoride-trifluoroethylene random copolymers. *Polymer*. **1981**, 22, 1312–1314.
[31] Kim, K. J.; Kim, G. B.; Vanlencia, C. L.; Rabolt, J. F. Curie transition, ferroelectric crystal structure, and ferroelectricity of a VDF/TrFE(75/25) copolymer 1. The effect of the consecutive annealing in the ferroelectric state on curie transition and ferroelectric crystal structure. *J. Polym. Sci. Part B Polym. Phys.* **1994**, 32, 2435–2444.
[32] Tashiro, K.; Itoh, Y.; Kobayashi, M.; Tadokoro, H. Polarized Raman spectra and LO-TO splitting of poly(vinylidene fluoride) crystal form I. *Macromolecules* **1985**, 18, 2600–2606.
[33] Mattsson, B.; Ericson, H.; Torell, L. M.; Sundholm, F. Micro-Raman investigations of PVDF-based proton-conducting membranes. *J. Polym. Sci. Part A Polym. Chem.* **1999**, 37, 3317–3327.
[34] Yee, W. A.; Nguyen, A. C.; Lee, P. S.; Kotaki, M.; Liu, Y.; Tan, B. T.; Mhaisalkar, S. Lu, X. Stress-induced structural changes in electrospun polyvinylidene difluoride nanofibers collected using a modified rotating disk. *Polymer* **2008**, 49, 4196–4203.
[35] Mahdi, R. I.; Gan, W. C.; Abd Majid, W. H. Hot plate annealing at a low temperature of a thin ferroelectric P(VDF-TrFE) film with an improved crystalline structure for sensors and actuators. *Sensors* **2014**,14, 19115–19127.
[36] Xu, B.; Choi, J.; Borca, C. N.; Dowben, P. A.; Sorokin, A. V.; Palto, S. P.; Petukhova, N. N.; Yudin, S. G. Comparison of aluminum and sodium doped poly(vinylidene fluoride-trifluoroethylene) copolymers by x-ray photoemission spectroscopy. *Appl. Phys. Lett.* **2001**, 78, 448–450.
[37] Nguyen, V. S.; Rouxel, D.; Vincent, B.; Badie, L.; Dos Santos, F. D.; Lamouroux, E.; Fort, Y. Influence of

cluster size and surface functionalization of ZnO nanoparticles on the morphology, thermomechanical and piezoelectric properties of P(VDF-TrFE) nanocomposite films. *Appl. Surf. Sci.* **2013**, 279, 204–211.

[38] Bharti, V.; Xu, H. S.; Shanthi, G.; Zhang, Q. M.; Liang, K. Polarization and structural properties of high-energy electron irradiated poly(vinylidene fluoride-trifluoroethylene) copolymer films. *J. Appl. Phys*. **2000**, 87, 452–461.

[39] Oswald, J.; Boxberger, S.; Jørgensen, B.; Feldmann, S.; Ehninger, G.; Bornhäuser M.; Werner, C. Mesenchymal stem cells can be differentiated into endothelial cells in vitro. *Stem Cells* **2004**, 22, 377–384.

[40] Lutolf, M. P.; Hubbell, J. A. Synthetic biomaterials as instructive extracellular microenvironments for morphogenesis in tissue engineering. *Nat. Biotechnol*. **2005**, 23, 47–55.

[41] Place, E. S.; Evans, N. D.; Stevens, M. M. Complexity in biomaterials for tissue engineering. *Nat. Mater.* **2009**, 8, 457–470.

[42] Okoshi, T.; Chen, H.; Soldani, G.; Galletti, P. M.; Goddard, M. Microporous small diameter PVDF-TrFE vascular grafts fabricated by a spray phase inversion technique. *ASAIO Journal* **1992**, 38, M201-M206.

[43] Katsouras, I.; Asadi, K.; Li, M.; Van Driel, T. B.; Kjær, K. S.; Zhao, D.; Lenz, T.; Gu, Y.; Blom, P. W.; Damjanovic, D.; Nielsen, M. M. The negative piezoelectric effect of the ferroelectric polymer poly(vinylidene fluoride). *Nat. Mater.* **2016**, 15, 78–84.

[44] Zhang, X.; Zhang, C.; Lin, Y.; Hu, P.; Shen, Y.; Wang, K.; Meng, S.; Chai, Y.; Dai, X.; Liu, X.; Liu, Y. Nanocomposite Membranes Enhance Bone Regeneration Through Restoring Physiological Electric Microenvironment. *ACS Nano* **2016**, 10, 7279-7286.

[45] Zhang, D.; Karki, A. B.; Rutman, D.; Young, D. P.; Wang, A.; Cocke, D.; Ho, T. H.; Guo, Z. Electrospun polyacrylonitrile nanocomposite fibers reinforced with Fe3O4 nanoparticles: Fabrication and property analysis. *Polymer* **2009**, 50, 4189–4198.

[46] Baumgarten, P. K. Electrostatic spinning of acrylic microfibers. *J. Colloid Interface Sci*. **1971**, 36, 71–79.

[47] Huttenlocher, A.; Horwitz, A. R. Wound healing with electric potential. *N. Engl. J. Med*. **2007**, 356, 303–304.

[48] Hwang, G.T.; Byun, M.; Jeong, C. K.; Lee, K. J. Flexible Piezoelectric Thin-Film Energy Harvesters and Nanosensors for Biomedical Applications. *Adv. Healthc. Mater.* **2015**, 4, 646–658.

[49] Lonjon, A.; Laffont, L.; Demont, P.; Dantras, E.; Lacabanne, C. Structural and electrical properties of gold nanowires/P(VDF-TrFE) nanocomposites. *J. Phys. D. Appl. Phys.* **2010**, 43, 345401.

[50] Andrew, J. S.; Clarke, D. R. Effect of Electrospinning on the Ferroelectric Phase Content of Polyvinylidene Difluoride Fibers. *Langmuir* **2008**, 24, 670–672.

[51] Guo, H. F.; Li, Z. S.; Dong, S. W.; Chen, W. J.; Deng, L.; Wang, Y. F.; Ying, D. J. Piezoelectric PU/PVDF electrospun scaffolds for wound healing applications. *Colloids Surf. B. Biointerfaces* **2012**, 96, 29–36.

[52] Augustine, R.; Sarry, F.; Kalarikkal, N.; Thomas, S.; Badie, L.; Rouxel, D. Surface Acoustic Wave Device with Reduced Insertion Loss by Electrospinning P(VDF-TrFE)/ZnO Nanocomposites. *Nano-Micro Lett.* **2016**, 8, 282–290.

[53] Lee, Y.S.; Arinzeh, T. L. The influence of piezoelectric scaffolds on neural differentiation of human neural stem/progenitor cells. *Tissue Eng. Part A* **2012**, 18, 2063–2072.

[54] Li, W. J.; Laurencin, C. T.; Caterson, E. J.; Tuan, R. S.; Ko, F. K. Electrospun nanofibrous structure: A novel scaffold for tissue engineering. *J. Biomed. Mater. Res.* **2002**, 60, 613–621.

[55] Chhabra, H.; Deshpande, R.; Kanitkar, M.; Jaiswal, A.; Kale, V. P.; Bellare, J. R. A nano zinc oxide doped electrospun scaffold improves wound healing in a rodent model. *RSC Adv.* **2016**, 6, 1428–1439.

[56] Augustine, R.; Mathew A.; Sosnik A. Metal Oxide Nanoparticles as Versatile Therapeutic Agents Modulating Cell Signaling Pathways: Linking Nanotechnology with Molecular Medicine. *Appl. Mater. Today* 2017, in press.

[57] Paszek, E.; Czyz, J.; Woźnicka, O.; Jakubiak, D.; Wojnarowicz, J.; Łojkowski, W, et al. Zinc oxide nanoparticles impair the integrity of human umbilical vein endothelial cell monolayer in vitro. *J. Biomed. Nanotechnol.* **2012**, 8, 957–967.

[58] Hsiao I. L.; Huang, Y. J. Effects of various physicochemical characteristics on the toxicities of ZnO and TiO nanoparticles toward human lung epithelial cells. Sci. *Total Environ.* **2011**, 409, 1219–1228.

[59] Nair, S.; Sasidharan, A.; Divya Rani, V. V.; Menon, D.; Nair, S.; Manzoor, K, et al. Role of size scale of ZnO nanoparticles and microparticles on toxicity toward bacteria and osteoblast cancer cells. *J. Mater. Sci. Mater. Med.* **2009**, 20, 235–241.

[60] Mironov, V.; Kasyanov, V.; Markwald, R. R. Nanotechnology in vascular tissue engineering: from nanoscaffolding towards rapid vessel biofabrication. *Trends Biotechnol.* **2008**, 26, 338–244.

[61] Barui, A. K.; Veeriah, V.; Mukherjee, S.; Manna, J.; Patel, A. K.; Patra, S.; et al. Zinc oxide nanoflowers make new blood vessels. *Nanoscale* **2012**, 4, 7861–7869.

[62] Todeschi, M. R.; El Backly, R.; Capelli, C.; Daga, A.; Patrone, E.; Introna, M, et al. Transplanted Umbilical Cord Mesenchymal Stem Cells Modify the In Vivo Microenvironment Enhancing Angiogenesis and Leading to Bone Regeneration. *Stem Cells Dev.* **2015**, 24, 1570–1581.

[63] Hoffman, A. J.; Carraway, E. R.; Hoffmann, M. R. Photocatalytic Production of H_2O_2 and Organic Peroxides on Quantum-Sized Semiconductor Colloids. *Environ. Sci. Technol.* **1994**, 28, 776–785.

Electronic Supplementary Material

Electrospun poly(vinylidene fluoride-trifluoroethylene)/zinc oxide nanocomposite tissue engineering scaffolds with enhanced cell adhesion and blood vessel formation

Robin Augustine[1,2,§](✉), Pan Dan[3,§] Alejandro Sosnik[1], Nandakumar Kalarikkal[2,4], Nguyen Tran[5], Brice Vincent[6], Sabu Thomas[2,7], Patrick Menu[3], Didier Rouxel[6](✉)

[1]Laboratory of Pharmaceutical Nanomaterials Science, Department of Materials Science and Engineering, Technion-Israel Institute of Technology, De-Jur Building, Technion City, 3200003 Haifa, Israel

[2]International and Inter University Centre for Nanoscience and Nanotechnology, Mahatma Gandhi University, Kottayam – 686 560, Kerala, India

[3]Ingénierie Moléculaire et Physiopathologie Articulaire, UMR 7365 CNRS - Université de Lorraine, Vandoeuvre-lès Nancy, F54500, France

[4]School of Pure and Applied Physics, Mahatma Gandhi University, Kottayam – 686 560, Kerala, India

[5]School of Surgery, Faculty of Medicine, Université de Lorraine, 54500 Vandoeuvre-lès-Nancy, France

[6]Institut Jean Lamour, UMR 7198 CNRS - Université de Lorraine, 54500 Vandoeuvre-lès-Nancy, France

[7]School of Chemical Sciences, Mahatma Gandhi University, Kottayam – 686 560, Kerala, India

§ These authors contributed equally to this work.

Supporting information to DOI 10.1007/s12274-****-****-* (automatically inserted by the publisher)

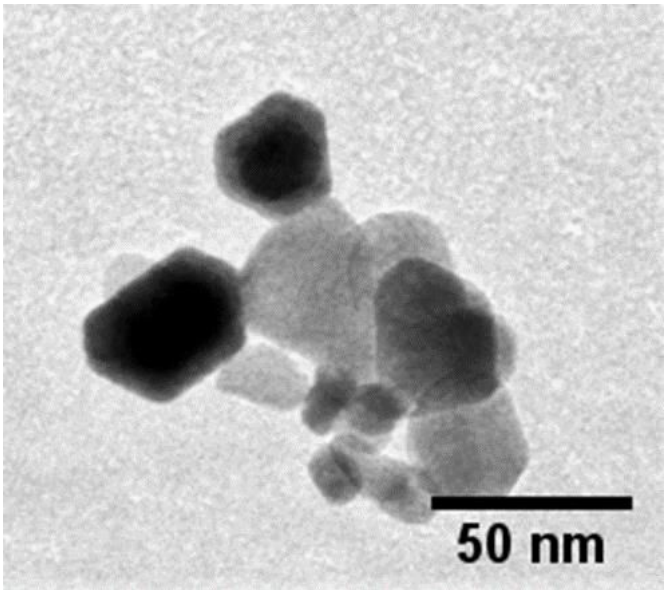

Fig. S-1 TEM (Philips CM 200) image of ZnO nanoparticles used in this study showing the morphological features and approximate size.

Address correspondence to Robin Augustine, robin@robinlab.in; Didier Rouxel, didier.rouxel@univ-lorraine.fr

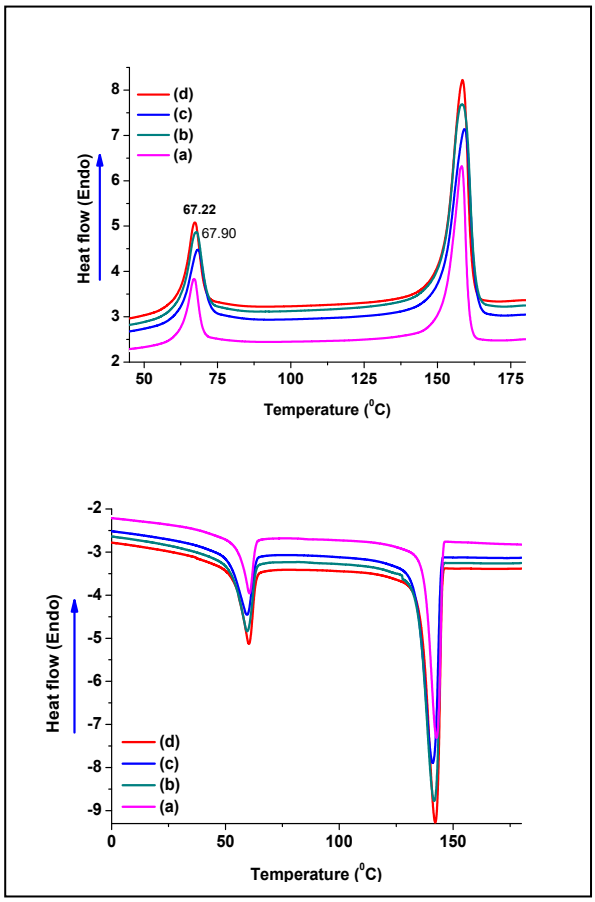

Fig. S-2 DSC thermograms of (a) P(VDF–TrFE), (b) P(VDF–TrFE)/ZnO-1, (c) P(VDF–TrFE)/ZnO-2, and (d) P(VDF–TrFE)/ZnO-4 during (A) heating and (B) cooling DSC scans.

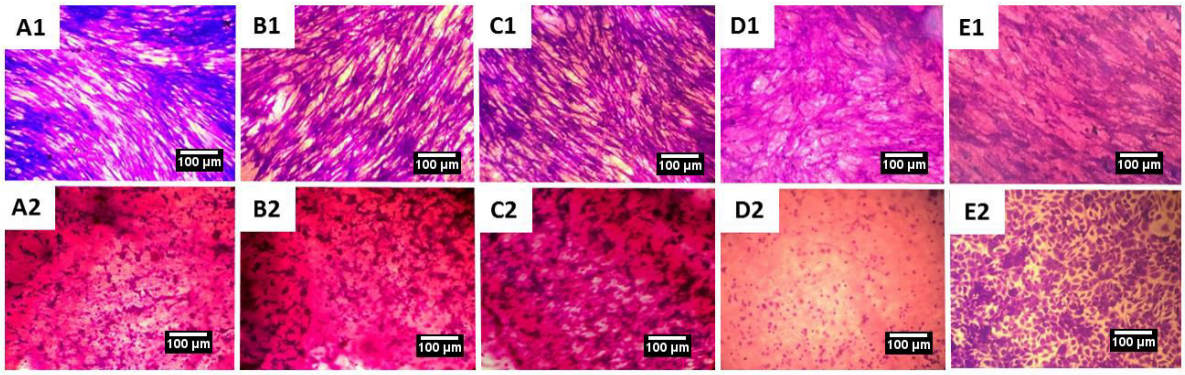

Fig. S-3 Attachment of MSCs (A1-E1) and HUVECs (A2-E2) on neat P(VDF-TrFE) (A1, A2), P(VDF-TrFE)/ZnO-1 (B1, B2), P(VDF- TrFE)/ZnO-2 (C1, C2) and P(VDF- TrFE)/ZnO-4 (D1, D2) after 24 h. (E1, E2) were MSCs and HUVECs grown on commercial cell culture plates as controls respectively. Cells were stained with crystal violet and observed under optical microscope.

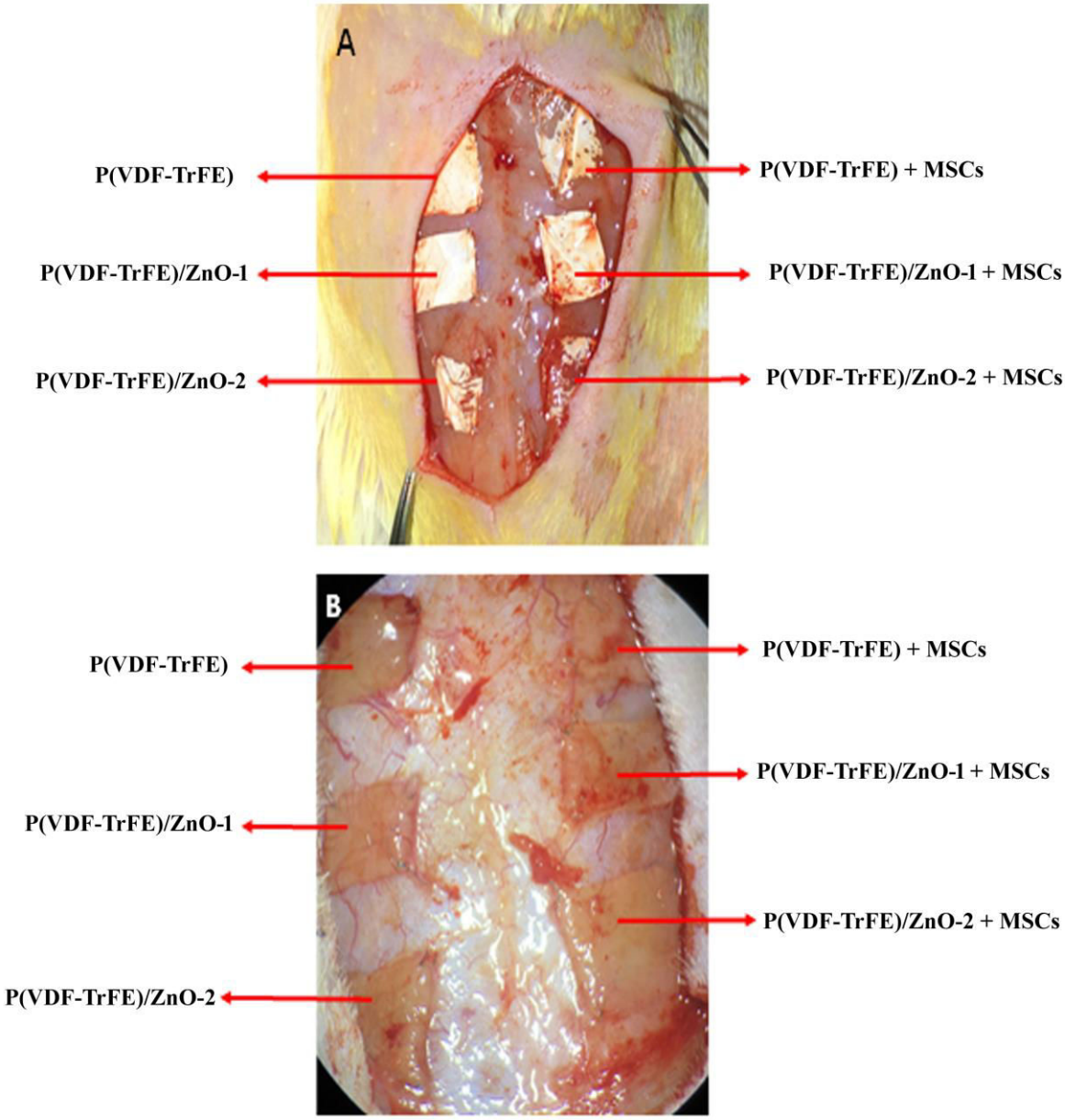

Fig. S-4 Subcutaneous implantation of scaffolds. (A) Photograph of scaffolds immediately after the subcutaneous implantation in the abdominal region of rats. Scaffolds were cut into 1 × 1 cm^2 size and attatched to rat tissue by fixing the four corner of scaffold with 7-0 sutures. (B) Photograph after 3 weeks of implantation, scaffolds were surrounded by connective tissue, with blood vessels developed toward the scaffolds. No visible sign of inflammation or immune rejection were observed.

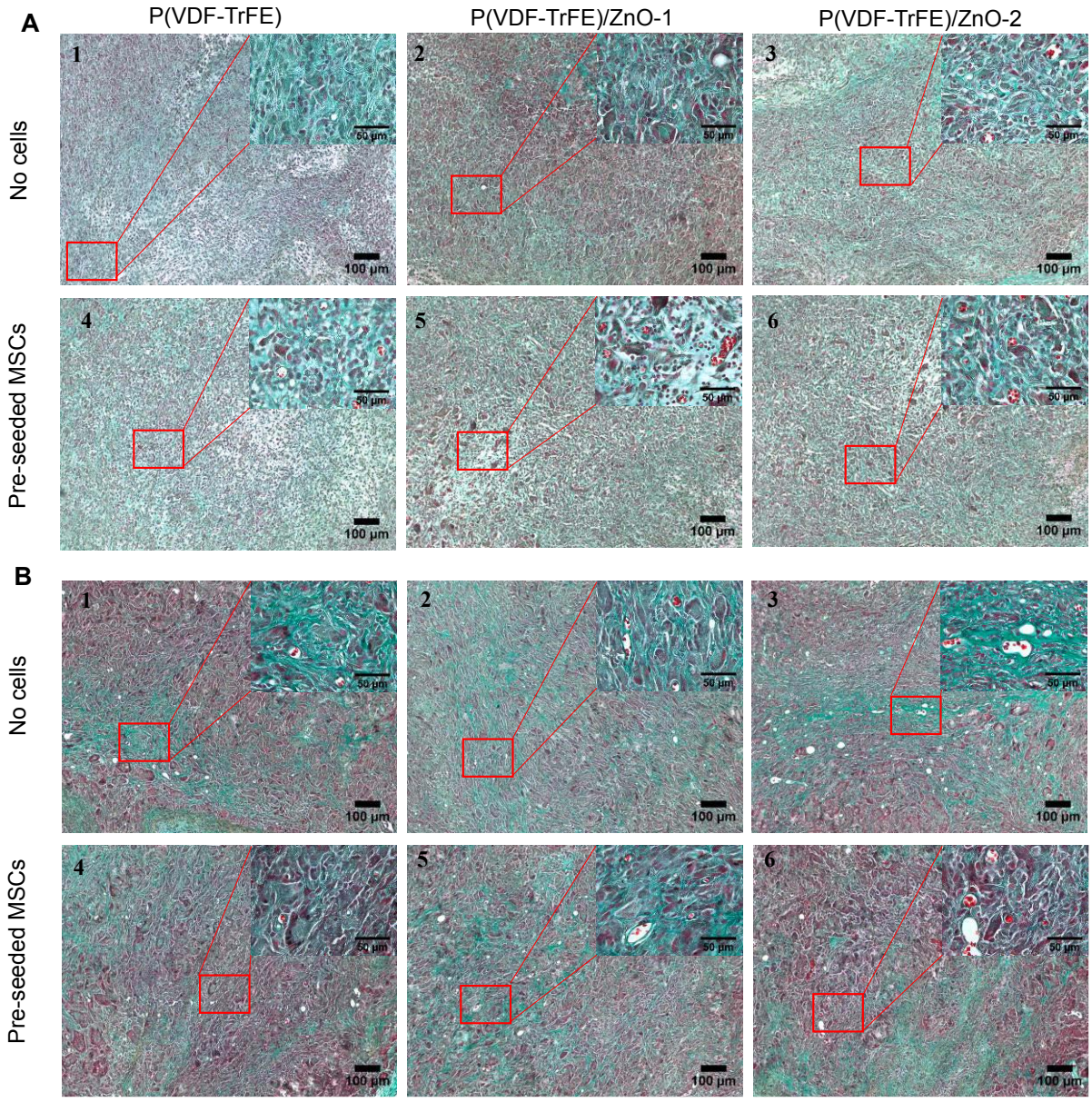

Fig. S-5 Transvers section of implanted scaffolds stained by Masson's trichrome. Collagen (green) can be found in all scaffolds as early as 7 days after implantation. Blood vessels with red blood cells (red) can be observed in all across the scaffolds, particularly in ZnO nanoparticles incorporated scaffolds. Pre-seeding of MSCs further enhanced angiogenesis in nanoparticle-containing scaffolds.

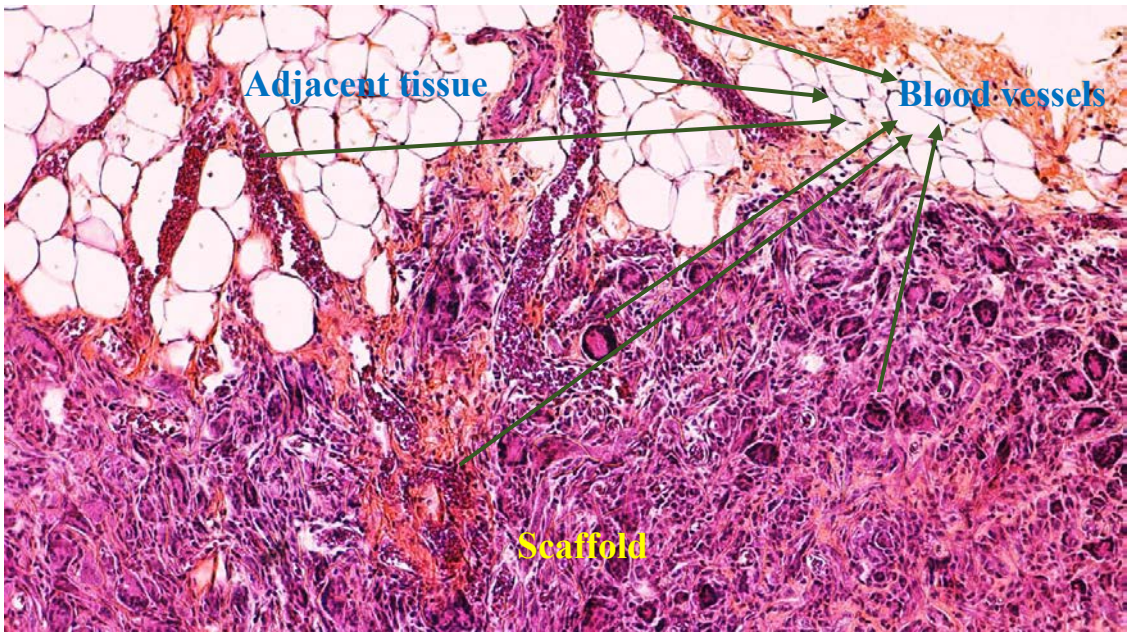

Fig. S-6 Cross sectional view showing the penetration of blood vessels through P(VDF-TrFE)/ZnO-2 with MSCs on day 21 after implantation. Scaffolds are stained with haematoxylin and eosin. Large number of blood vessels passing in through the scaffolds at various directions were clearly visible. Images are taken at 100X magnification.

***

Chapitre 2. Biomatériaux – coating naturel (1)

Publication N° 3

Résumé en français

Fabrication d'un nouveau revêtement en utilisant la matrice extracellulaire à partir de la gelée de Wharton humaine pour les applications d'ingénierie tissulaire

Pan Dan[a], Émilie Velot[a], Grégory Francius[b], Patrick Menu[a]* and Véronique Decot[a,c]

Dans la conception d'un biomatériau, il est important de distinguer *un substitut* (scaffold) et une surface (coating). Le coating est l'interface qui reste en contact direct avec les cellules. Ainsi, il est important de désigner un coating qui peut représenter l'environnement *in vivo*. L'un des buts essentiel dans l'ingénierie tissulaire est de développer une surface de revêtement naturel qui soit facile à manipuler, efficace pour l'adhésion cellulaire et entièrement biocompatible. La surface idéale serait dérivée de tissu humain, exempt d'agents pathogènes et dont le dépôt serait parfaitement contrôlable. Cependant, la source de tissus humains sains et facilement accessibles est limitée. Cet article présente une approche innovante pour fabriquer un revêtement de surfaces en utilisant une matrice extracellulaire naturelle (ECM) extraite de la gelée de Wharton (WJ) du cordon ombilical (appelée WJ-ECM).

Nous avons développé pour la première fois une technique d'isolation des ECM complètes issues de la gelée de Wharton. En digérant les tissus de la gelée de Wharton dans la trypsine pendant 24 h, puis en ajoutant du sérum de veau fœtal (SVF), nous avons obtenu une solution visqueuse dans laquelle se trouvent divers facteurs de croissance tels que le facteur de croissance vasculaire endothélial (VEGF), le facteur de croissance des fibroblastes 2 (FGF-2) et le facteur de croissance transformant-β1 (TGF-β1). Avec ces facteurs de croissances activés, cette solution peut être utilisée comme un complément pour la culture cellulaire. Nous avons

montré qu'avec le même pourcentage de SVF, un milieu supplémenté en WJ - ECM a favorarisé la prolifération des cellules souches mésenchymateuses.

Ensuite, nous avons réussi à fabriquer un coating *in vitro* avec cette solution sur des lamelles de verre chargées négativement. Nous avons montré par microscopie à force atomique (AFM), que le dépôt de WJ-ECM sur cette surface est homogène et que l'on avait la possibilité d'en contrôler l'épaisseur. En prenant le collagène commercial comme un contrôle positif, nous avons testé les propriétés physiques de ce coating, en particulier par le modèle de Young. *In vitro*, ce revêtement est approprié pour l'adhérence et la prolifération des cellules endothéliales matures et des cellules souches mésenchymateuses humaines. Une meilleure prolifération des cellules est observée sur le coating de WJ-ECM par rapport au collagène. En plus, les cellules souches mésenchymateuses cultivées sur ce nouveau coating sont capables de se différencier vers les cellules endothéliales en exprimant des marqueurs spécifiques endothéliaux tels que CD31, VE-Cadherin, VEGFR2 et Tie-2.

Comme les cellules endothéliales subissent un flux sanguin constant *in vivo*, il est important que les cellules ensemencées sur une surface restent adhérentes quelque soit le débit sanguin. Nous avons soumis à des contraintes de cisaillement physiologique les cellules à confluence cultivées sur WJ-ECM, sur du collagène, ou sur du verre. Après 12h de cisaillement, nous avons observé un plus grand nombre de cellules présentes sur la WJ-ECM par rapport à des surfaces conventionnelles telles que le collagène I. Nous avons donc cherché le mécanisme responsable de ce phénomène ; il est bien connu que les intégrines jouent un rôle majeur dans l'adhésion cellulaire à leur surface. Nous avons donc mesuré le niveau d'expression génétique des intégrines $\alpha 1$, $\alpha 2$ et $\beta 1$ qui sont les 3 intégrines souvent étudiées dans les CSMs et les cellules endothéliales. Nous avons montré qu'après cisaillement, l'expression des intégrines $\alpha 2$ et $\beta 1$ est augmentée par les CSMs et HUVECs cultivées sur WJ-ECM. Nous supposons donc que les intégrines $\alpha 2$ et $\beta 1$ sont impliquées dans la résistance des cellules aux flux. Par ailleurs, nous

avons aussi montré que l’expression d’un complexe de mécanosensors (CD31, VEGFR2 et VE-Cadherin) a augmenté dans les HUVECs soumises aux flux.

Nos données montrent clairement que la gelée de Wharton est un revêtement très prometteur pour la conception de surfaces biocompatibles humaines dans l'ingénierie tissulaire, ainsi que dans la médecine régénérative.

Acta Biomaterialia 48 (2017) 227–237

Contents lists available at ScienceDirect

Acta Biomaterialia

journal homepage: www.elsevier.com/locate/actabiomat

Full length article

Human-derived extracellular matrix from Wharton's jelly: An untapped substrate to build up a standardized and homogeneous coating for vascular engineering

Pan Dan [a], Émilie Velot [a], Grégory Francius [b], Patrick Menu [a,*], Véronique Decot [a,c]

[a] UMR 7365 CNRS, Ingénierie Moléculaire et Physiopathologie Articulaire Université de Lorraine, Vandœuvre-lès-Nancy Cedex 54505, France
[b] UMR 7564, Université de Lorraine, Laboratoire de Chimie Physique et Microbiologie pour l'Environnement, Villers-lès-Nancy 54600, France
[c] Unité de Thérapie Cellulaire et Tissulaire, CHRU de Nancy, Vandœuvre-lès-Nancy 54511, France

ARTICLE INFO

Article history:
Received 3 June 2016
Received in revised form 4 October 2016
Accepted 11 October 2016
Available online 18 October 2016

Keywords:
Biomimetic materials
Vascular tissue engineering
Wharton's jelly
ECM (extracellular matrix)
Coating

ABSTRACT

One of the outstanding goals in tissue engineering is to develop a natural coating surface which is easy to manipulate, effective for cell adhesion and fully biocompatible. The ideal surface would be derived from human tissue, perfectly controllable, and pathogen-free, thereby satisfying all of the standards of the health authorities. This paper reports an innovative approach to coating surfaces using a natural extracellular matrix (ECM) extracted from the Wharton's jelly (WJ) of the umbilical cord (referred to as WJ-ECM). We have shown by atomic force microscopy (AFM), that the deposition of WJ-ECM on surfaces is homogenous with a controllable thickness, and that this easily-prepared coating is appropriate for both the adhesion and proliferation of human mesenchymal stem cells and mature endothelial cells. Furthermore, under physiological shear stress conditions, a larger number of cells remained adhered to WJ-ECM than to a conventional coating such as collagen – a result supported by the higher expression of both integrins α2 and β1 in cells cultured on WJ-ECM. Our data clearly show that Wharton's jelly is a highly promising coating for the design of human biocompatible surfaces in tissue engineering as well as in regenerative medicine.

Statement of Significance

Discovery and design of biomaterial surface are a hot spot in the tissue engineering field. Natural matrix is preferred to mimic native cell microenvironment but its use is limited due to poor resource availability. Moreover, current studies often use single or several components of natural polymers, which is not the case in human body. This paper reports a natural extracellular matrix with full components derived from healthy human tissue: Wharton's jelly of umbilical cord. Reconstituting this matrix as a culture surface, our easily-prepared coating provides superior biocompatibility for stem and mature cells. Furthermore, we observed improved cell performance on this coating under both static and dynamic condition. This novel human derived ECM would be a promising choice for regenerative medicine.

© 2016 Acta Materialia Inc. Published by Elsevier Ltd. All rights reserved.

1. Introduction

The main goal of the tissue engineering triad is to create combinations of cells, scaffolds and environment (i.e. soluble mediators and/or mechanical stresses). For vascular tissue engineering, finding appropriate cells and scaffolds remain the two major challenges. Stem cells, and in particular, mesenchymal stem cells (MSCs), have emerged as the most promising source of suitable cells as a result of their good availability and ability to differentiate into vascular cells, as well as their immunosuppressive properties which are particularly interesting for allogeneic applications [1,2]. As to the scaffold, synthetic materials are most commonly used for engineered vascular grafts, but they are poor substrates for cells. Therefore, substantial effort has been made to develop new coatings, ranging from synthetic polymers to isolated natural extracellular matrix (ECM) to: (i) provide a solid base for cell anchorage to allow resistance to blood flow; (ii) favor endothelial differentiation of stem cells; and (iii) facilitate cell expansion to mimic the endothelial layer [3,4].

* Corresponding author.
E-mail address: patrick.menu@univ-lorraine.fr (P. Menu).

http://dx.doi.org/10.1016/j.actbio.2016.10.018
1742-7061/© 2016 Acta Materialia Inc. Published by Elsevier Ltd. All rights reserved.

Synthetic polymers have the advantage of being precisely tailored, and they can be combined with other biological interfaces, allowing for the construction of desired tissues [5]. However, those which have been studied to date have often exhibited poor biocompatibility and/or immunogenicity, limiting their clinical use. In the case of ECM, decades of extensive research on its structure and biological influence on cell behavior and fate have shown that its physical properties (elasticity, stiffness, resilience to the cellular environment, etc.), specific chemical signals exhibited by its peptide epitopes, and the nanoscale topography of microenvironmental adhesive sites, are all relevant to the design of biomimetic surfaces [6]. Nonetheless, current studies usually exploit one or several purified ECM components to construct surfaces [7], a practice which does not faithfully replicate the native ECM entire environment [8].

Complete ECM derived from human tissue could be an ideal source for natural matrices. In this context, tissues such as placenta and umbilical cord which are obtained from non-pathological medical procedures, could provide a good supply. For example, placenta has recently been treated using a chemical procedure (urea solubilization) to furnish a complex of ECM for tissue engineering [9]. Wharton's jelly of human umbilical cord contains various types of collagen and glycosaminoglycan, as well as growth factors and/or cytokines synthesized by mesenchymal stem cells, and thus may be viewed as a natural source for ECM-based coating [10]. Indeed, Hao et al. previously showed that mechanically-obtained ECM from Wharton's jelly can support MSC culture [11].

Here we describe a novel enzymatic method to isolate complete ECM from Wharton's jelly (this material will be referred to hereafter as WJ-ECM), which boasts many benefits relative to existing procedures. The most important advantages of our coating are its human tissue origins and a method of preparation that does not involve chemicals which are toxic to cells. To test our material, we prepared, characterized, and determined the *in vitro* response to WJ-ECM of MSCs and endothelial cells, which are currently the two most-used cell sources in vascular tissue engineering, under both static and dynamic conditions. Our data show that WJ-ECM-derived coating enhanced proliferation of both human MSCs (hMSCs) and human umbilical vein endothelial cells (HUVECs). This new surface also exhibits improved cell resistance to flow under shear stress, a phenomenon which is of particular interest in vascular tissue engineering. The role of integrins in the possible mechanism underlying cell retention under shear stress was also investigated.

2. Methods

2.1. Preparation of WJ-ECM coating

Fresh human umbilical cords were obtained after full-term births with informed consent using the guidelines approved by the Cell Therapy Unit of the University Hospital Center (CHRU) of Nancy (Authorization number: TCG/11/R/011). Briefly, whole umbilical cord was washed 3 times with Hank's balanced salt solution (HBSS) and cut into 5-cm explants, and Wharton's jelly was carefully isolated without taking umbilical cord membrane or vessels. The WJ of umbilical cord from 3 separate donors was then pooled prior to sample homogenization. The isolated WJ was further cut into 0.5-cm pieces using sterile surgical scissors. The WJ was then digested in trypsin (0.025%, Bioblock, 1158-0626, France) at 37 °C for 24 h with magnetic stirring (ratio of wet WJ/trypsin was 1 g: 5 ml), the stirred suspensions were centrifuged at 16,000*g* for 10 min, and the collected supernatants were filtered (100 μm filter). Fetal bovine serum (FBS) (Dutscher, S1900) was added into the solution (final concentration of 10%) to inhibit the trypsin reaction. The concentration of WJ (mg/ml) was calculated using lyophilized WJ tissues dissolved in final phosphate buffered saline (PBS). The obtained WJ-ECM solution was conserved at 4 °C for further use. To coat culture surfaces, the freshly-obtained or conserved WJ-ECM was deposited onto glass coverslips which had been carefully pre-treated with SDS-HCl [12]. The glass coverslips coated with WJ-ECM were incubated for 12 h at 37 °C, then washed twice with culture medium.

2.2. Characterization of the surface coating by AFM

Before each measurement, fresh samples were extensively rinsed with milli-Q water and then slowly and completely dried with nitrogen. AFM experiments were carried out using a MFP3D-BIO instrument (Asylum Research Technology, Atomic Force F&E GmbH, Mannheim, Germany). Silicon nitride cantilevers of conical shape were purchased from Olympus (OTR-400 PSA, Bruker-nano AXS, Palaiseau, France). The spring constants of the cantilevers measured using the thermal noise method were found to be 0.020–0.024 nN/nm. Experiments were performed both in air and in PBS buffer at room temperature. AFM images were recorded at room temperature (20 °C) in contact mode. The applied force between the tip and the surface was carefully monitored and minimized at approximately 0.2 nN for experiments performed in aqueous medium. All images were collected with a resolution of 512 × 512 pixels at a scan rate of 1 Hz. The nanoindentation method was used to quantify the mechanical properties. Young's modulus of the thin films was calculated from force vs. indentation curves. Mechanical properties were obtained by recording a grid map of 32-by-32 force curves at different locations on the thin deposits over the 10 μm × 10 μm surface area. The maximal loading force was 0.5 nN, the piezodrive was fixed to 1 μm and the approach rate was 1000 nm s^{-1}. The Young's modulus was estimated from the analysis of the approach curves according to the Sneddon model [13].

$$F = \frac{2E \cdot \mathrm{Tan}(\alpha)}{\pi(1-\nu^2)} R^{1/2}\delta^2 \cdot f_{\mathrm{BECC}}$$

where δ is the indentation depth, ν the Poisson coefficient, R the curvature radius of the AFM-tip apex and f_{BECC} is the Bottom Effect Cone Correction function that takes into account the presence of substrate stiffness [14]. All the force curves were analyzed by means of an automatic Matlab algorithm described elsewhere [15].

2.3. Biomolecular composition analysis

WJ-ECM solution (10 mg/ml) was analyzed using a human angiogenesis array kit (R&D systems, ARY007, France) according to the manufacturer's protocol, and the pixel density of detected spots was measured with Image J software.

2.4. Culture of hMSC and HUVEC cells

To isolate hMSCs from umbilical cord (UC), Wharton's jelly was sliced into 5-mm explants after removing the umbilical vessels and the umbilical outer layer membrane, and the slices were subsequently attached and cultured in minimum essential medium Eagle-alpha modification (α-MEM) (Lonza, BE12-169F) supplemented with 10% FBS, Fungizone® (100 mg/ml, Fisher, 11520496), penicillin (100 IU/ml, Sigma, P0781) and L-glutamine (200 mM, Sigma, G7513) on culture plates. The medium was changed every 3 days, and hMSC populations appeared as outgrowths from the UC fragments at day 6. After 15 days, the UC fragments were discarded, and the cells were passaged with trypsin and expanded until they reached sub-confluence. To isolate HUVECs,

full length UC was taken, the umbilical vein was washed carefully with HBSS to remove residual blood, an appropriate volume of trypsin was injected into the vein, the trypsin was harvested after 20 min of incubation at 37 °C, the suspension was centrifuged at 300*g* for 5 min, and finally, the pellet was suspended in endothelial basic medium (EBM™-2, Lonza) supplemented with 10% FBS, Fungizone® (100 mg/ml, Fisher, 11520496), penicillin (100 IU/ml, Sigma, P0781) and L-glutamine (200 mM, Sigma, G7513). Cells were cultivated on culture plates for 10 days until 90% confluence was reached.

2.5. Bioactivity of soluble factors in WJ-ECM

hMSCs at passage 4 were seeded onto 12-well plates at 3000 cells/cm^2. One milliliter of culture medium α-MEM supplemented with different percentages of WJ-ECM solution (2.5%, 10% and 40%, respectively) was added to different wells to observe its influence on cell proliferation. In order to ensure that the influence on cell proliferation was not due to FBS in the WJ-ECM solution but to active soluble factors in the solution, cells were seeded into different culture mediums with or without FBS. The various culture conditions were: hMSCs cultured ±10% FBS (the usual concentration in cell culture); WJ-ECM ± FBS, where (1) 40% of WJ-ECM solution (containing 10% of FBS) corresponds to 10% FBS in the cell culture medium and (2) 10% of WJ-ECM solution (containing 2.5% of FBS) which corresponds to 2.5% FBS in the cell culture medium. (Note, as the 10% WJ-ECM contains 2.5% FBS, we also evaluated a 2.5% FBS control). After 5 days of cell culture, cells were stained with Live/Dead assay (Sigma-Aldrich, 04511, France) and observed using a fluorescence microscope.

2.6. Cell viability and proliferation

The viability of both hMSCs and HUVECs on different surfaces was assessed by MTT (3-(4,5-dimethylthiazol-2-yl)-2,5-diphenylte trazolium bromide) assay. The MTT assays were carried out as per the manufacture's protocol (Sigma-Aldrich, M5655). Briefly, cells were seeded onto a 24-well plate containing cover slides coated with WJ-ECM at different viscosities; collagen (0.1 mg/ml) was used as a positive control, and cover slips alone as a negative control. Cells were seeded at a density of 5.10^3 cells/cm^2. After 1, 3 and 5 days of culture, medium was removed, 10% MTT in fresh medium was added, and the cells were incubated for 4 h. The MTT solution was then carefully removed after incubation, and 200 μl of DMSO per well were added to dissolve the produced formazan, followed by a further incubation for 5 min. 100 μl of solution from each well were transferred to a new 96-well plate, and the absorption at 570 nm read using an automated plate reader (Varioskan Flash, Thermo scientific, France).

2.7. Cell proliferation by DNA quantification

In parallel, at each time point, total DNA of each sample was collected and quantified using a Hoechst 33258 fluorescent dye assay (Invitrogen, H3569, France). Briefly, cells cultivated on different surfaces were washed twice with PBS and the cell pellet was harvested, after which the total DNA content was extracted with two freeze (liquid nitrogen)-thaw (37 °C) cycles. Fluorescence was measured with a microplate fluorescence reader (Varioskan Flash, Thermo scientific, France) using equal volumes of cell lysates and Hoechst 33258 dye solution (100 μg ml^{-1}). The number of viable cells per scaffold was calculated by extrapolation from a calibration curve that was generated as described in Rago et al. [16].

2.8. Endothelial differentiation of hMSCs

On passage 4, hMSCs were seeded at a density of 3000 cells/cm^2 onto glass coverslips coated with WJ-ECM or collagen or without coating. When cell confluence reached 40%, a commercial medium (EGM™-2) which is used for EC differentiation was added into the culture plates. hMSCs were cultivated in EGM™-2 for 14 days, with the medium being changed every 3 days. Protein and RNA were harvested for assessment of differentiation markers by Western-blot and quantitative real-time PCR, respectively.

2.9. Laminar shear stress assessment

To assess the cell adherence of both hMSCs and HUVECs under dynamic conditions, the cell nuclei were stained with Hoechst 33258 (Invitrogen, H3569) and the membrane with DiI (Invitrogen, D282), before being seeded onto coated glass coverslips. When the cell confluence reached 70%, the glass coverslips was assembled into a parallel-chamber flow system (Masterflex, USA). The shear stress that cells experienced was gradually increased to 20 dyn/cm^2, and applied for 12 h. After application of shear stress, the cells were fixed with 4% paraformaldehyde (Sigma-Aldrich, France), photos were taken by fluorescence microscopy (Leica DMI 3000B). 10 randomly chosen areas were investigated before and after shear stress, and the resulting images analyzed using the software Image J to count cell numbers [17]. Cells were then stained using crystal violet (Sigma-Aldrich, France) for large-scale images. For gene expression assessment, RNA was harvested directly after shear stress.

2.10. Quantitative real-time PCR

Total RNA from cell samples was isolated using the RNeasy Mini Kit (Qiagen). cDNA was synthesized from 100 ng total RNA using iScript Reverse Transcription Supermix (Bio-Rad). Quantitative Real-Time PCR (RT-PCR) was carried out using iQ™ SYBR® Green Supermix (Bio-Rad) and primers designed by us for human cluster of differentiation (CD)31, vascular endothelial (VE)-cadherin, vascular endothelial growth factor receptor 2 (VEGFR2), integrin α2, α3, and β1 and the ribosomal protein S29 (RP 29) with the use of the StepOnePlus™ device (Thermofisher, France). Cycling parameters were 3 min at 95 °C; 40 cycles of 30 s denaturation at 95 °C and 1 min of elongation at the annealing temperature (60 °C for CD31, VE-Cadherin, VEGFR2 and RP29, 54 °C for integrin α2, 56 °C for integrin α3 and 58 °C for integrin β1). Data were normalized using RP29 as a housekeeping gene. Analyses and fold differences were determined using the comparative CT method. Fold change was calculated from the △△CT values with the formula $2^{-\Delta\Delta CT}$ and data are reported relative to control values.

2.11. Statistical analysis

Results are presented as mean ± standard deviation. Statistical significance was determined by ANOVA followed by a *t*-test between each group; p-values less than 0.05 were considered as statistically significant.

3. Results

3.1. Extraction of WJ-ECM from Wharton's jelly

As an initial step, we compared chemical, mechanical and enzymatic procedures to extract the ECM from the WJ of the umbilical cord. These procedures included acetic acid, type II collagenase, PBS (mechanical) and trypsin-mediated methods. Acetic acid was

chosen as it was previously used to isolate and purify collagen I [18], one of the WJ-ECM components. When applied to the WJ, one week was required to achieve complete digestion of the ECM, and the procedure failed to produce enough ECM to coat glass substrates. Type II collagenase is commonly used for isolation of MSCs from the connective tissue of umbilical cord [19], but atomic force microscopy (AFM) analysis showed that this procedure was too aggressive for ECM extraction, as no collagen fibers could be detected after digestion. Similarly, analysis by AFM showed that Wharton's jelly stirred in PBS did not generate enough products to coat glass substrates. Taken together, these data demonstrated that acetic acid, type II collagenase, and PBS were unsuitable for obtaining an appropriate coating surface (Fig. S1).

We next investigated whether trypsin is able to digest WJ-ECM, as it is a common enzyme used in routine cell culture. Dissociated WJ tissue was digested in 0.025% trypsin at 37 °C for 24 h under magnetic stirring, the supernatant was collected after centrifugation, and FBS was added to stop the trypsin reaction. This method allowed us to obtain a viscous solution, with the viscosity between different batches remaining stable (Fig. 1a). Twenty-four hour-digestion and further centrifugation removed cells or other debris in the WJ-ECM (Fig. 1b, c). The complete WJ-ECM solution was lyophilized to obtain a dry powder, and the precise concentration of WJ-ECM in the solution was calculated according to this dry powder and original solution volume. The influence of FBS, trypsin and PBS in the mixed solution was also taken into account during the calculations.

Previous studies have demonstrated that WJ contains abundant growth factors, a beneficial feature as this would likely stimulate angiogenesis [20]. Therefore, following the enzymatic extraction procedure, the biomolecular composition of the WJ-ECM was determined using a human angiogenesis array (Fig. S2). Out of the 55 proteins that were screened for, 16 were detected in WJ-ECM (Figs. 1d, S2). These included several essential growth factors for vascular cell differentiation such as vascular endothelial growth factor (VEGF), fibroblast growth factor 2 (FGF-2) and transforming growth factor-β1 (TGF-β1). According to the results, there was little variability between healthy donors. When WJ-ECM solution was used as a cell culture supplement, increased hMSCs proliferation was observed (Fig. S3). This result indicated that the soluble factors in WJ-ECM remained active.

3.2. Fabrication of WJ-ECM derived coating

We tested the coating capacity of WJ-ECM on positively and negatively charged glass coverslips. Our obtained AFM images showed that WJ-ECM extract could not coat an electrically-neutral glass coverslip, but could produce a non-continuous thin layer on a positively-charged surface. On the other hand, WJ-ECM reliably formed a continuous coating on a negatively-charged surface (Figs. S4–S6).

To visualize the morphological features of the WJ-ECM coated surface, and in particular the thickness of the WJ-ECM-based coating, different concentrations of WJ-ECM solution were pipetted onto negatively-charged glass coverslips and incubated for 12 h at 37 °C before imaging by AFM. Depending on the concentration, WJ-ECM formed a homogeneous coating from 13 ± 5 nm to 74 ± 16 nm thick (Table 1 and Figs. S7–S12). At 5 mg/ml, a thickness of 45 ± 12 nm was obtained (Fig. 2a, b), similar to that produced by collagen (0.1 mg/ml) which was used as positive control (Fig. 2c, d). As the stiffness of the coated material has a significant effect on cell adhesion, proliferation and/or differentiation [21], the Young's modulus of the WJ-ECM was determined by the nanoindentation method using AFM. Mechanical measurements performed with AFM revealed an inverse correlation between the coating's Young modulus and its thickness. At the lowest concentration (1 mg/ml), the stiffness of the coating reached a maximal value of 1.34 ± 0.19 MPa (n = 1024). At 5 mg/ml, the stiffness was 1.18 ± 0.15 MPa (n = 1024), a value below that obtained for a collagen coating used as positive control (2.04 ± 0.17 MPa (n = 1024)) (Fig. 2e). Such an increase in stiffness is likely due to a decrease in the water content of the layer, as well as greater crystalline packing of WJ-ECM components during the adsorption process.

3.3. Static cell adhesion and proliferation

To examine the behavior of the cells seeded on this surface, the viability of the hMSCs and HUVECs was examined. Human MSCs showed a significantly higher mitochondrial activity when cultured on 5–8 mg/ml WJ-ECM than on glass coverslips alone (Fig. 3a). In the case of the HUVECs, no difference between WJ-ECM concentrations was observed. However, cellular mitochondrial activity was also significantly enhanced when compared to the activity of cells cultured on glass coverslips (Fig. 3b).

We next evaluated at different time points the adhesion and proliferation of HUVECs and hMSCs on WJ-ECM coating, when applied at a concentration of 5 mg/ml. Commercially available collagen I at 0.1 mg/ml and glass coverslips were used as positive and negative controls, respectively. Cells cultured on a collagen-coated surface showed a slightly higher viability than those cultured on coverslips at all 3 time points (day 1, day 2 and day 3 for hMSCs, day 1, day 3 and day 7 for HUVECs, taking into account their different proliferation rates), but this difference was not statistically significant. Interestingly, however, the WJ-ECM coated surface afforded a significantly higher mitochondrial activity, when measured at the third time point (Fig. 3c, d). Total DNA quantification was also performed to evaluate cell proliferation on different surfaces (glass, collagen and ECM coating). In agreement with the viability observation, the WJ-ECM-coated surface promoted cell proliferation both for hMSCs and HUVECs (Fig. 3e, f). The difference in proliferation rates became significant between the glass and ECM coatings at days 3 and 7 for hMSCs and HUVECs, respectively.

3.4. Differentiation of hMSCs to endothelial-like cells

Published studies, as well as our previous data, suggest that cell culture surface and medium can contribute to variations in the differentiation capacity of hMSCs [1,22]. As VEGF has been detected in the WJ-ECM, we thought to further investigate the endothelial differentiation potential of hMSCs. For this, we treated hMSCs expanded on WJ-ECM with Endothelial Growth Medium-2 (EGM™-2). Fourteen days after the induction of differentiation, Western-blot and RT-PCR revealed the expression of endothelial cell specific markers such as CD31, VEGFR2 and VE-Cadherin (Fig. 4a, b). These results confirmed that the functionalization of the cell culture surface is mandatory to induce differentiation of hMSCs, and show that the WJ-ECM coating is suitable for both the expansion and differentiation of hMSCs.

3.5. Cell retention under dynamic stimulation

Biomaterials in vascular tissue engineering must provide appropriate cell anchorage to resist physiological shear stress. To evaluate cell retention on WJ-ECM, we expanded MSCs and HUVECs onto 3 different surfaces (WJ-ECM coating, collagen and glass coverslips), then subjected them to 12 h of laminar shear stress at 20 dyn/cm^2. Crystal violet staining showed that more cells remained on WJ-ECM coating than the other two surfaces after shear stress (Fig. 5a). Cells from both sheared and static samples

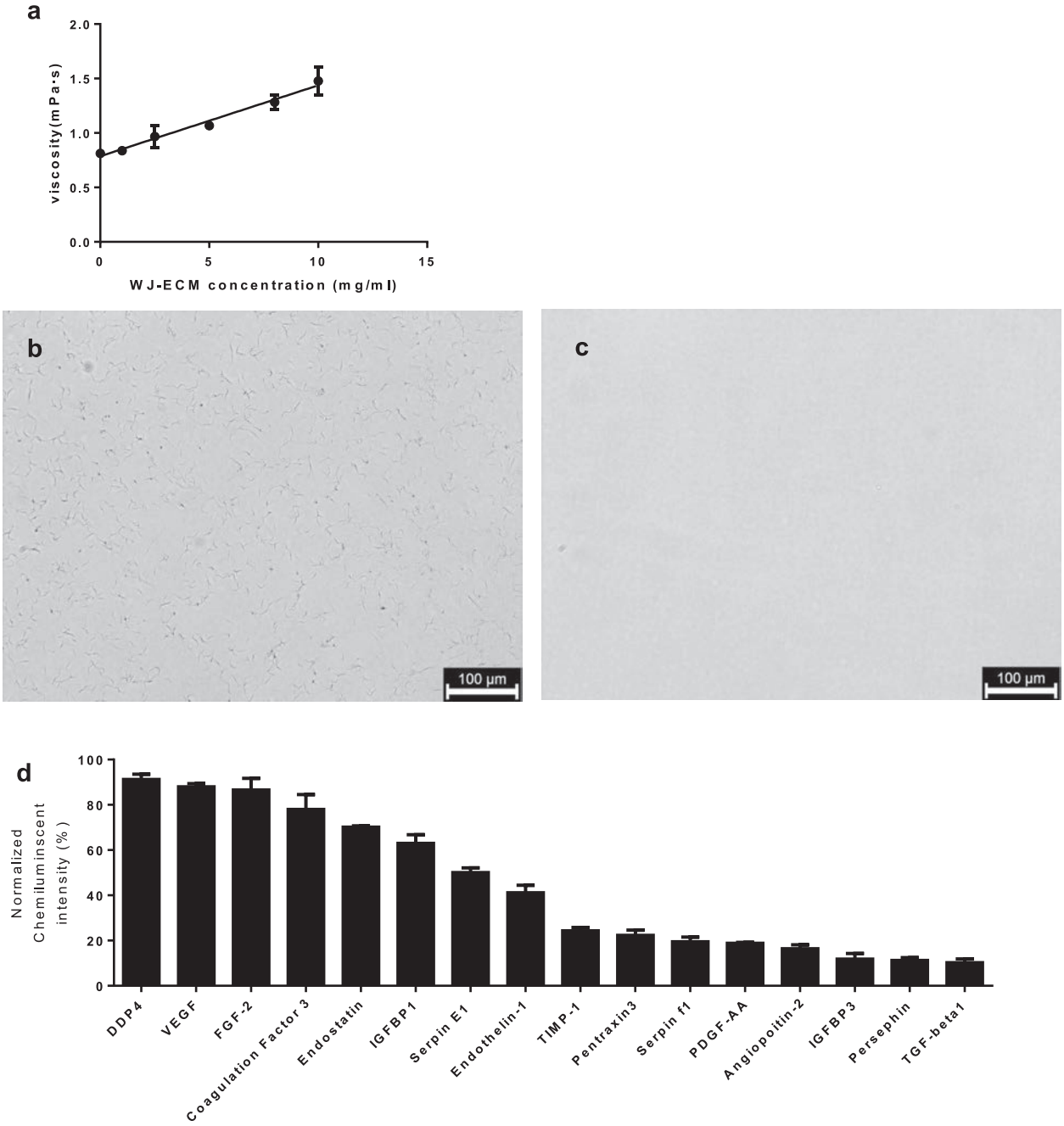

Fig. 1. Characterization of WJ-ECM solution. (a) The viscosity of WJ-ECM depended on its concentration. (b–c) Optical microscopic images showing the appearance of commercial collagen (0.1 mg/ml) (b) and WJ-ECM (5 mg/ml) (c) deposited on glass coverslips. (d) Cytokine analysis of WJ-ECM solution (10 mg/ml) was performed using a human angiogenesis array, and data were normalized on a scale ranging from negative control values (0%) to positive control values (100%). Data are representative of 3 independent batches, where each batch contained WJ tissue collected from 3 different healthy donors.

were also stained for membranes and nuclei (Fig. 5b), images of 10 randomly chosen fields on these coatings were taken using a fluorescence microscope, and the cells were then counted using Image J Software [17]. Notably, the WJ-ECM-coated surface maintained 92 ± 2% of MSCs after shear stress, whereas the collagen-coated surface and control glass coverslips retained 78 ± 3% and 74 ± 5% of MSCs, respectively (Fig. 5c). The retention of HUVECs on these different surfaces after 12 h of shear stress showed a similar pattern: the WJ-ECM coated surface retained 92 ± 3% of the HUVECs whereas 75 ± 11% and 74 ± 13% were retained on collagen and on glass coverslips, respectively (Fig. 5c). These results clearly suggest that WJ-ECM coating allows a better cell anchorage than commercially-available collagen I coating or glass, with the consequence that WJ-ECM may be a suitable coating to build up a continuous layer to mimic the endothelium during vascular tissue engineering.

Table 1
Concentration-dependent thickness and Young's modulus of WJ-ECM.

Surface coating solution (mg/ml)		Thickness of surface (nm)	Young's modulus (MPa)
Collagen	0.1	37 ± 15	2.04 ± 0.17
WJ-ECM solution	1	13 ± 5	1.34 ± 0.19
	2.5	34 ± 9	1.27 ± 0.12
	5	45 ± 12	1.18 ± 0.15
	7.5	61 ± 17	0.82 ± 0.10
	10	74 ± 16	0.61 ± 0.07

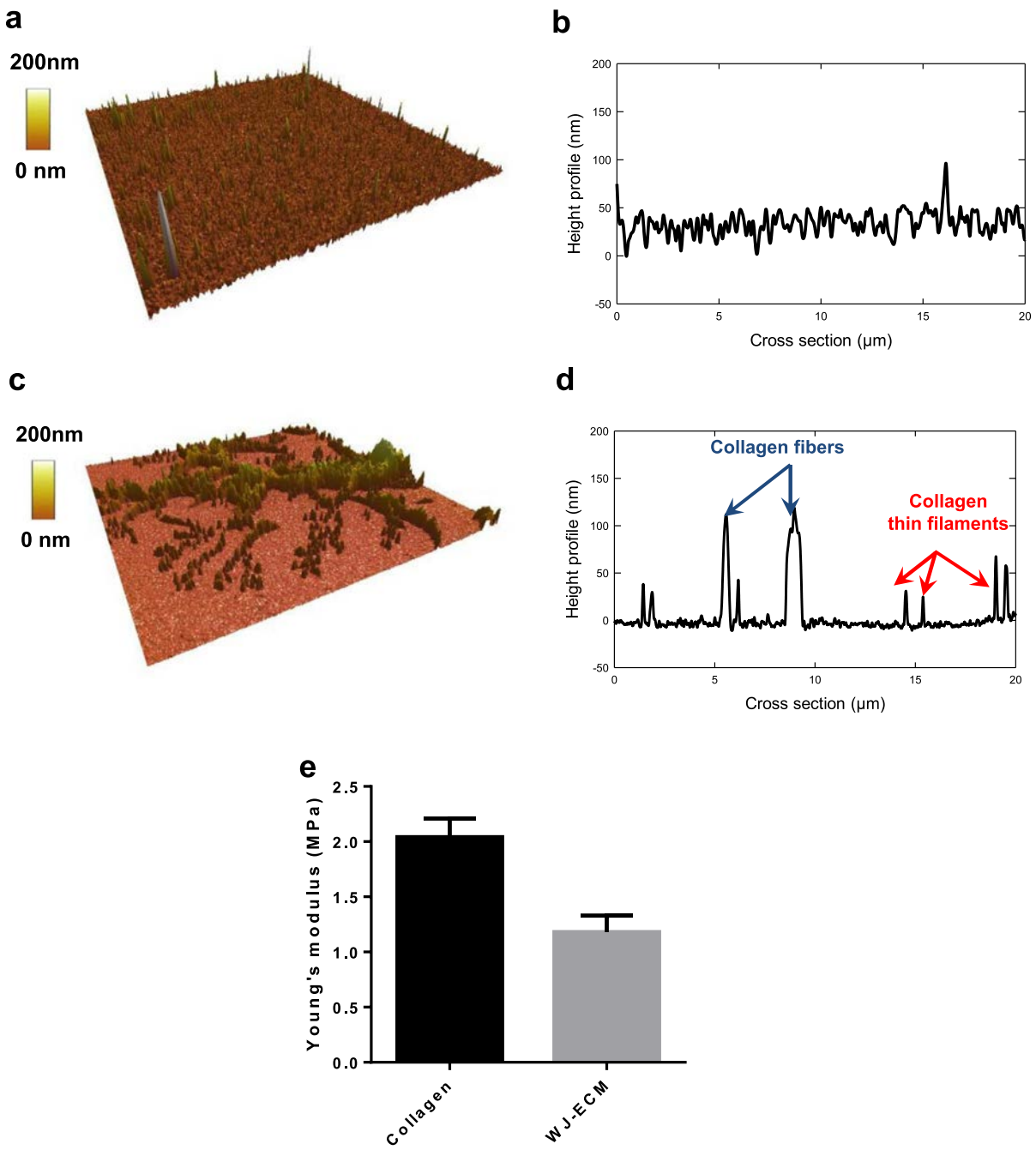

Fig. 2. Characterization of WJ-ECM derived coating. (a) Atomic force microscopy image of WJ-ECM at 5 mg/ml coated onto negatively-charged coverslips showing formation of a homogenous surface. (b) Cross-section of WJ-ECM coating, revealing a measured thickness of 45 ± 12 nm and an even distribution. (c) Commercial collagen (0.1 mg/ml) coating which served as a positive control. Collagen fibers are observed and they showed a random distribution. (d) The average thickness of the collagen coating was 37 ± 15 nm. (e) Young's modulus of collagen coating at 0.1 mg/ml and WJ-ECM coating at 5 mg/ml.

3.6. Gene expression responding to shear stress

Human MSCs and HUVECs are known to express a large range of integrin subunits [17,23,24]. Here we selected 3 representative integrins (integrins α2, α3 and β1) [25,26], to evaluate their expression in cells cultivated on different surfaces in the presence or absence of shear stress. Under static conditions, hMSCs expressed significantly higher levels of integrin α2 on the WJ-ECM surface than on glass coverslips or collagen (Fig. 6a). Furthermore, following 6 h of physiological shear stress, a significantly increased expression of integrins α2 and β1 on WJ-ECM was observed compared to the static condition on WJ-ECM (Fig. 6b). Under the same dynamic conditions, a slight decrease of α2 and β1 expression was observed in hMSCs cultured on collagen, and a significant increase of α2 expression was observed in hMSCs on glass. As for the HUVECs, higher β1 expression was observed on WJ-ECM relative to the other two surfaces under static condition (Fig. 6c). Under shear stress, a significant increase in expression of integrins α2 and β1 was observed in HUVECs cultured on WJ-ECM. On collagen, this increase was only significant for β1 (Fig. 6d). Thus overall, both hMSCs and HUVECs exhibited a significant increase in expression of integrins α2 and β1 due to shear stress on WJ-ECM relative to collagen. In the case of integrin α3 expression, no difference was detected under static culture conditions

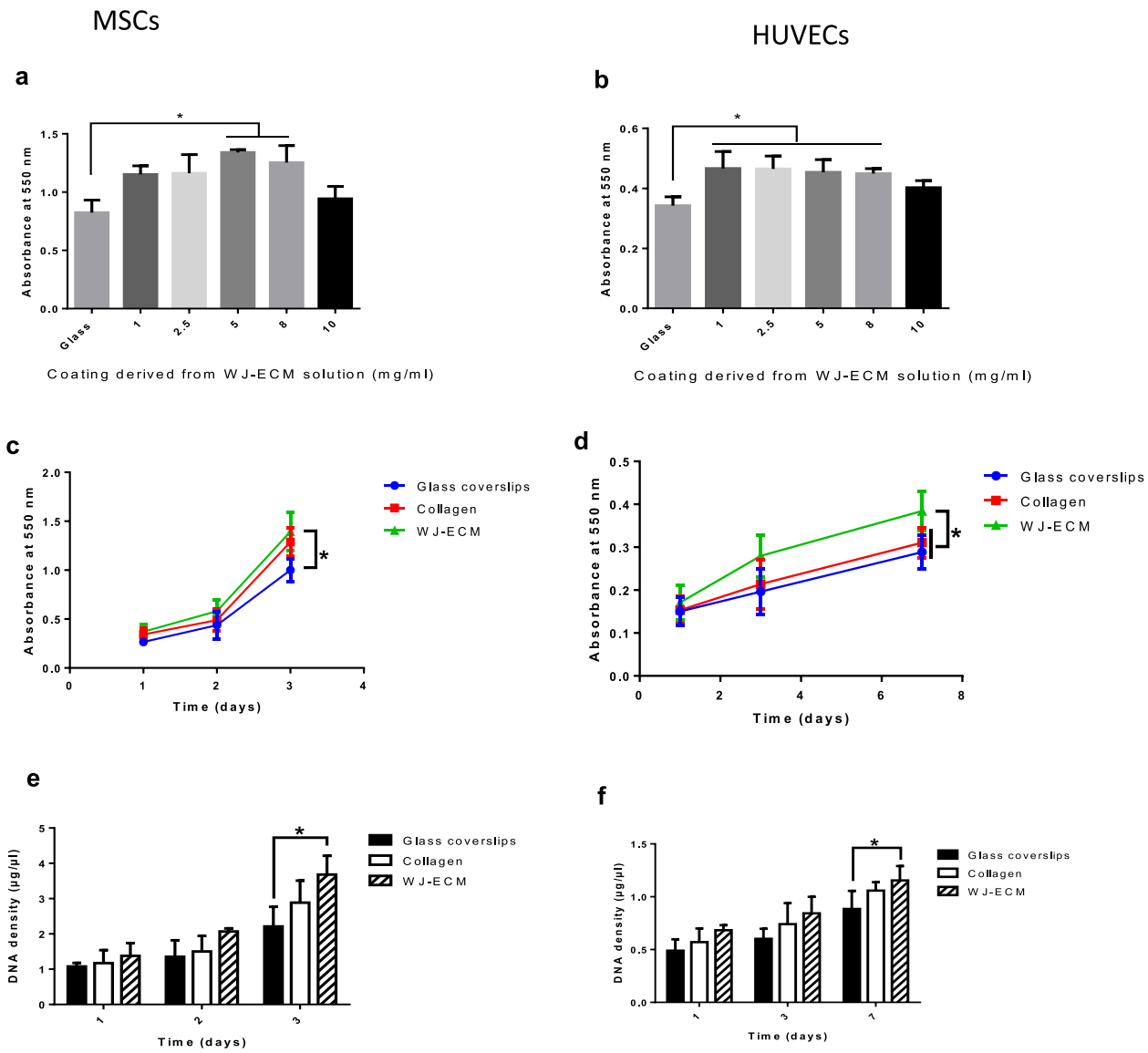

Fig. 3. Cell behavior on different surfaces. Cells were expanded on different coating surfaces formed from various concentrations of WJ-ECM. Cell adhesion was evaluated by MTT assay for mesenchymal stem cells (MSCs) after 72 h (a) and for endothelial cells (ECs) after 9 days (b). A single factor ANOVA test allowed rejection of the null hypothesis for all assays and a Tukey test between all groups was performed (SD, n = 4, $^{*}p < 0.05$). Cell proliferation of MSCs (c) and ECs (d) on glass coverslips, collagen (0.1 mg/ml) and WJ-ECM-coated slips (5 mg/ml) was measured at three time points by MTT assay. The DNA content of each sample was also measured at those time points for MSCs (e) and ECs (f) (SD, n = 4, $^{*}p < 0.05$ compared to glass coverslip surfaces). In all of the assays, the WJ-ECM coating at 5 mg/ml produced the best results in terms of both cell adhesion and proliferation.

irrespective of the surface employed. Furthermore a significant decrease in integrin α3 was observed after subjecting HUVECs cultured on all three surfaces to shear stress. Taken together, these results suggest that integrins α2 and β1 might be involved in helping cells cultured on WJ-ECM to resist shear stress.

In order to investigate the interaction between cells and WJ-ECM, we assessed the expression levels of mechanosensory complex of endothelia cells: CD31, VE-cadherin and VEGFR2 in HUVECs on this surface, and compared them with those obtained on collagen and glass coverslips under both static and dynamic conditions. Gratifyingly, higher levels of CD31, VE-cadherin and VEGFR2 were detected in HUVECs cultured on WJ-ECM than from cells cultured on collagen or glass coverslips (Fig. 6e).

Even more interestingly, dynamic conditions (20 dyn/cm^2 laminar shearing for 6 h), increased expression of these genes in cells cultured on collagen, but significantly decreased expression of these genes in cells culture on glass (Fig. 6f). Therefore, dynamic conditions enhance expression of the mechanosensory complex in cells grown on both collagen and WJ-ECM.

4. Discussion

Cardiovascular diseases, particularly atherosclerotic coronary artery diseases are still the leading cause of mortality the world over [27]. Tissue engineered vascular grafts which incorporate cells into a biodegradable scaffold, have emerged as a promising alternative for those patients who lack appropriate autologous graft candidates [28]. The main hurdle in small-diameter (<6 mm) vascular tissue engineering is the thrombogenicity of newly designed grafts. Studies aimed at resolving this challenge have to date focused on investigating cell sources and discovering new scaffold/coating that promote full cellularization. MSCs are now considered as the most promising source for vascular tissue engineering due to their excellent availability, ability to differenti-

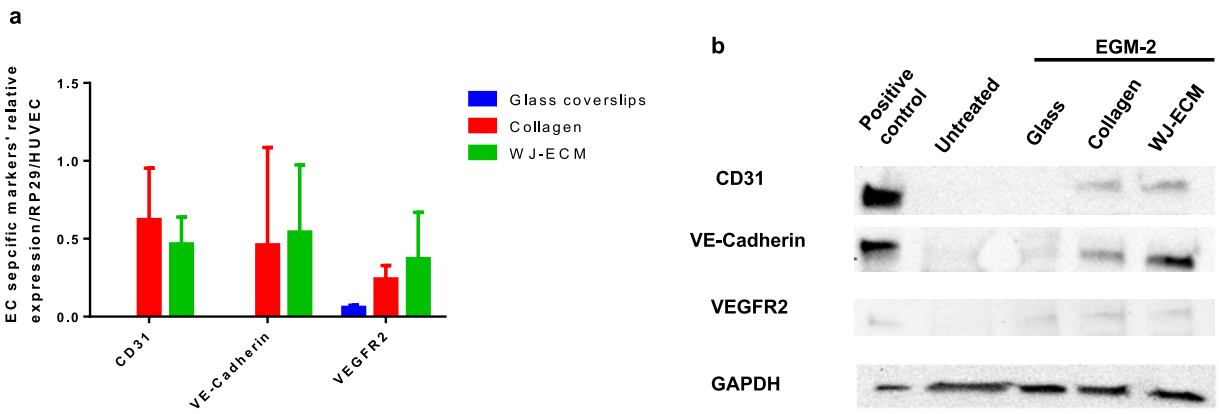

Fig. 4. Mesenchymal stem cells differentiate into an endothelial-like cell lineage. MSCs cultured on 3 different surfaces were treated with EGM™-2 for 14 days. (a) Endothelial specific gene expression was normalized to the house keeping gene RP29 and then normalized to positive HUVECs. (b) Expression of endothelial specific markers by Western-blot after EGM™-2 treatment. HUVECs were taken as a positive control, while untreated MSCs cultured on glass served as a negative control.

ate into smooth muscle cells and endothelial cells under appropriate stimulation, and their immunosuppressive properties [29,30]. On the other hand, mature endothelial cells are still the first choice for the purpose of mimicking the native environment [9]. Only grafts that are well cellularized or which can recruit circulating cells, can avoid long-term graft failure [31,32]. To this end, new synthetic and natural isolated scaffolds/coatings have been extensively studied. Unlike traditional approaches which isolate one or few components of tissue extracellular matrix, the full complement of ECM components is preferred in order to mimic the native cell environment. However, non-pathological human source is often limited. We describe in detail here a novel full ECM derived from healthy human Wharton's jelly (WJ-ECM).

The isolation of ECM from human tissue can be challenging in terms of restoring all of the functional components. Mechanical, chemical and enzymatic methods are most typically employed in ECM isolation. For example, ECM has been extracted from human placenta by chemical procedures and shown to contain various functional cytokines [9]. In this study, WJ tissue simply stirred in PBS failed to generate enough product to form a coating, while ECM derived from tissue dissolved in acetic acid was also unsatisfactory. Furthermore, this chemical treatment is a time-consuming procedure, and is typically used for collagen I isolation but not for obtaining full ECM. Here we choose to isolate complete ECM using enzymatic methods to simplify the isolation procedure, and more importantly, to maintain the ECM-containing tissue in a relatively physiological condition. We next compared collagenase II with trypsin, as both are routinely used in cell culture. Collagenase II generates a viscous solution, but which was unable to form a coating for *in vitro* cell culture, whereas trypsin readily yielded a viscous solution from human Wharton's jelly which was easily coated onto surfaces. Furthermore, abundant biological molecules such as VEGF, FGF-2, TGF-β1, endothelin-1, etc., which are considered important in vascular function, were detected in the solution [33]. As we used a semi-quantitative method to measure the growth factors and cytokines in the current study which allowed us to detect a large panel of factors, further quantitative assays and characterization of WJ-ECM will be required to fully characterize its composition in solution. These active growth factors and cytokines may allow WJ-ECM solution to be utilized in other applications, such as cell culture supplement and the formation of a gel for cell assays.

For studies *in vitro*, biomaterials are typically coated onto glass coverslips in order to obtain a surface with appropriate thickness. ECM proteins such as collagen and fibronectin can form a coating directly on glass coverslips and polystyrene-based culture surfaces [34], and even polyelectrolyte films exhibiting a certain charge can coat surfaces [12]. Inspired by this idea, we tested the influence of different surface charge on the coating efficiency. AFM results revealed that negatively-charged glass coverslips can facilitate WJ-ECM coating. Furthermore, compared to commercial collagen coating, WJ-ECM yielded a homogenous surface without collagen fibers. The thickness and stiffness of WJ-ECM coating depended on ECM concentration.

It has been previously shown that modified ECM coating can enhance cell adhesion and proliferation [35], probably due to several features such as its thickness and stiffness, and the incorporation of biological molecules [6]. In this study, the collagen-modified surface demonstrated higher cell adhesion and proliferation than the glass surface, but the WJ-ECM coating exhibited the highest cell attachment and proliferation with both hMSCs and HUVECs. Because the WJ-ECM is derived from human tissue, and the isolation procedure is completely physiological, WJ-ECM did not show any toxicity to cells. These features should make WJ-ECM a versatile tool in various type of tissue engineering to support cell cultures. Furthermore, WJ-ECM was capable of facilitating the differentiation of hMSCs into endothelial-like cells by expressing endothelial cell specific markers. This approach could allow the construction of a tissue engineered vessel using a single cell source [31].

In native blood vessels, the endothelium is exposed to stable shear stress that is generated by the flow of blood. Therefore, tissue engineered vascular grafts must support cell attachment under physiological shear stress. Surface components, and in particular, topography and stiffness, can influence cell attachment under dynamic condition [24]. A major limitation of current vascular tissue engineering is the low number of endothelial cells (ECs) or EC-replacing cells remaining after exposure to fluid shear stress representative of blood flow. Nonetheless, studies with modified substrates such as collagen coating have shown an amelioration in cell retention under shear stress conditions [36,37]. However, our results have shown that a collagen coating failed to improve cell resistance to laminar shear stress (although this behavior might be attributed to the use of a relatively lower concentration of collagen (0.1 mg/ml) relative to previous studies), whereas WJ-ECM significantly retained cells exposed to 6 h of shear stress. The underlying mechanism of the increased cell retention might be related to the stiffness of WJ-ECM surface, adhesive elements incorporated in the coating, and an interaction between cells, culture surface and shear stress [38]. Among the molecules involved in cell retention, integrins are a large family of transmembrane, heterodimeric cell-surface molecules, believed to be the principle

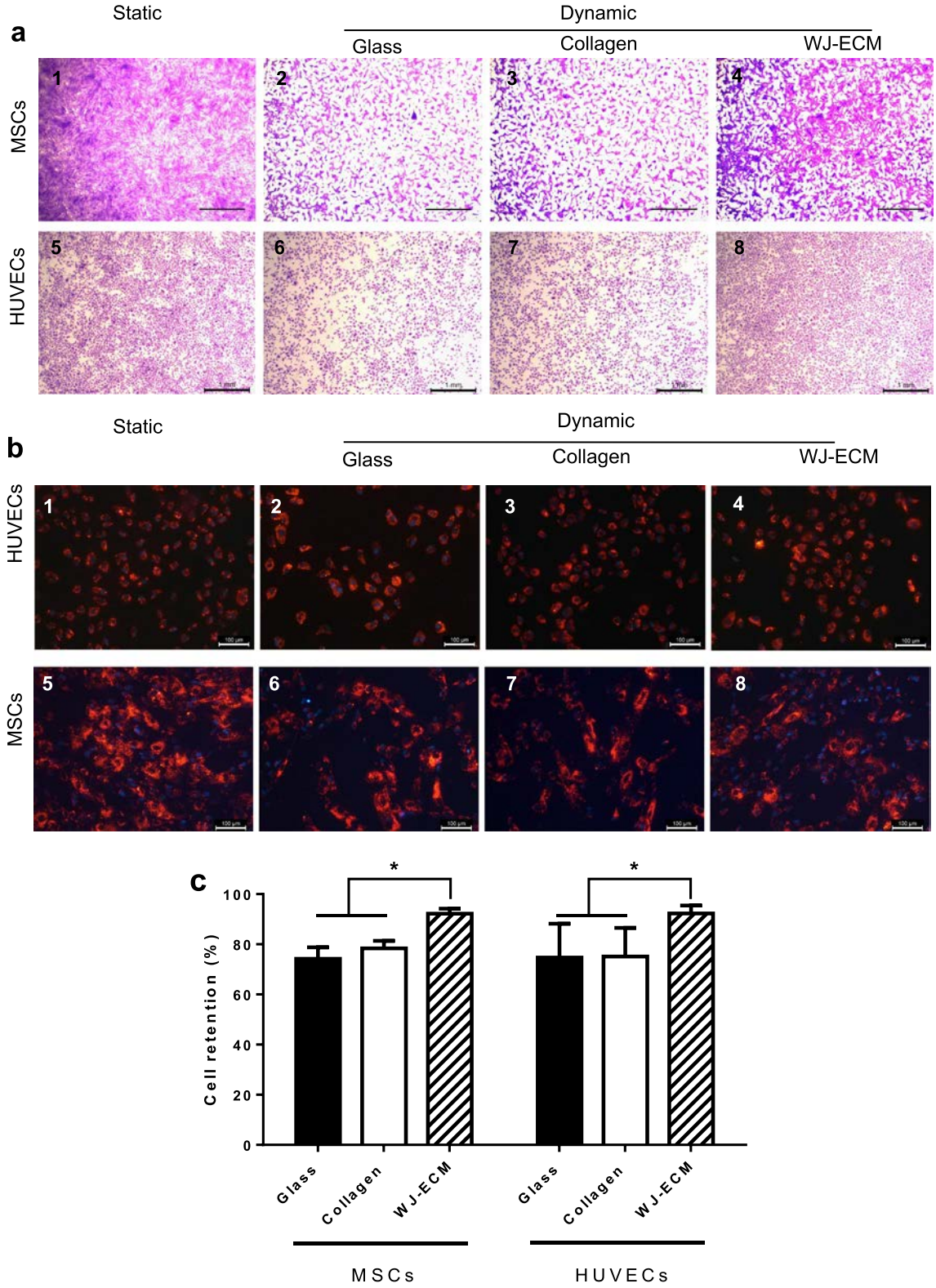

Fig. 5. Cell behavior under dynamic conditions. (a) and (b), Confluent cells cultured on 3 different surfaces (Static) were subjected to shear stress at 20 dyn/cm^2 for 12 h (Dynamic). (a) Cells were stained with crystal violet. Scale bar, 1 mm. (b) Fluorescence microscopy images in which the cell membrane was stained with DiI (red) and the nucleus was stained with Hoechst 33258 (blue). Scale bar, 100 μm. (c) Cell retention after 12 h of shear stress (n = 4. Statistical significance, indicated by (*), was determined with a one-way ANOVA followed by Tukey pairwise comparisons between all groups, $\alpha = 0.05$). Cell retention was calculated by counting cell numbers before and after shear stress. Cells were counted by Hoechst staining on 10 random areas (0.721 × 0.54 mm/area) on each culture surface. (For interpretation of the references to color in this figure legend, the reader is referred to the web version of this article.)

adhesion factors for cells to attach to their surfaces. They establish cell bonds with a range of ligands existing on ECM, and regulate cytoskeletal dynamics [23]. Integrins can thus be considered as important indicators of the interaction between cells, ECM and

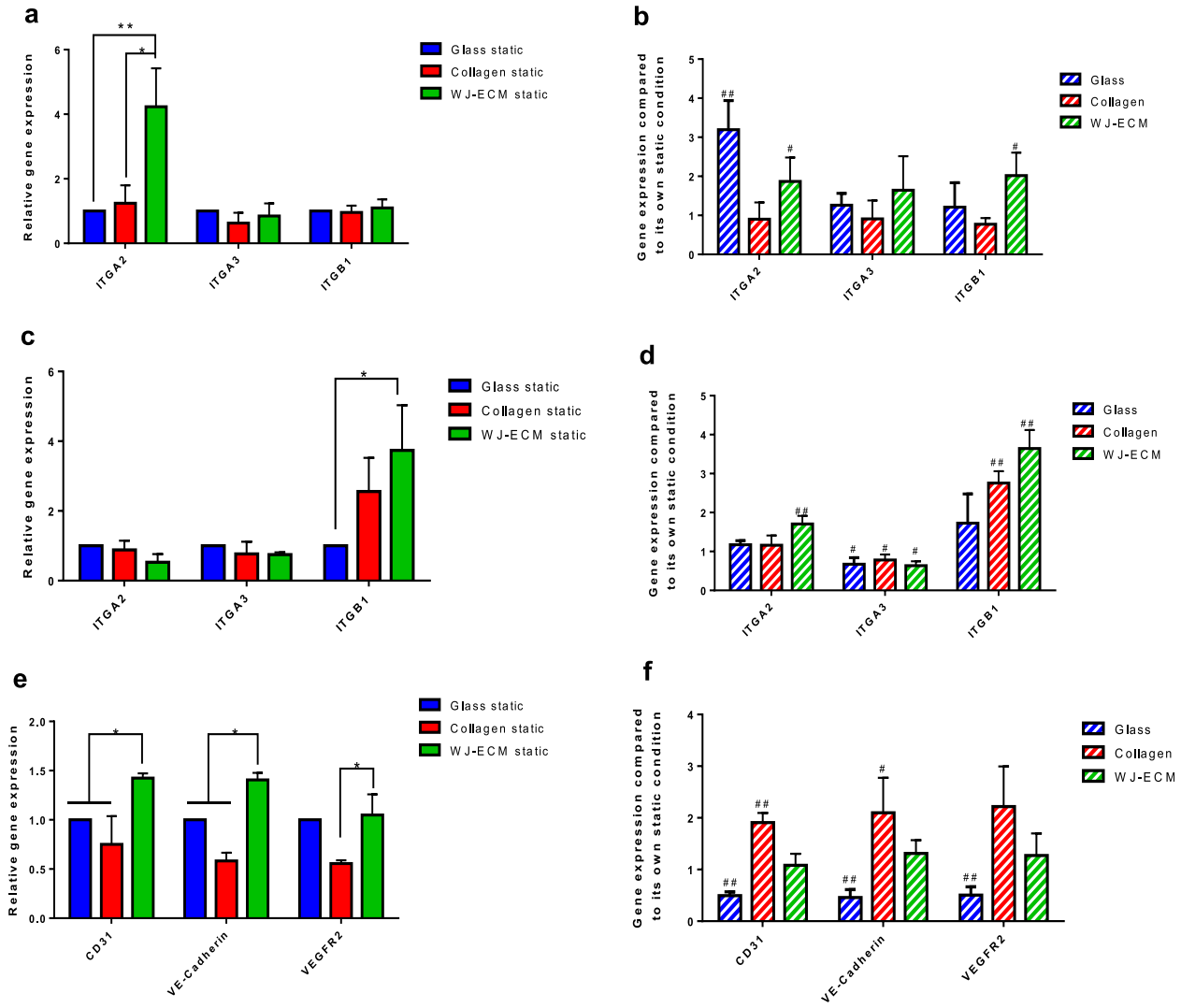

Fig. 6. Gene expression of MSCs and HUVECs cultured on different surfaces under static and dynamic conditions. Expression of integrins in hMSCs (a) and HUVECs (c) under static culture on glass coverslips, collagen and WJ-ECM. Expression levels are normalized to cells on glass coverslips (blue bars, $^{*}p < 0.05$, $^{**}p < 0.01$). Changes in integrin expression levels after 6 h of shear stress at 20 dyn/cm^2 for hMSCs (b) and HUVECs (d); expression levels were normalized to static conditions on glass coverslips, collagen and WJ-ECM, respectively. # indicates significant changes ($^{\#}p < 0.05$, $^{\#\#}p < 0.01$) compared to static expression levels. (e) Expression of mechanosensory complex proteins (CD31, VE-cadherin and VEGFR2) in HUVECs under static culture; mRNA levels are normalized to those in cells grown on glass coverslips (blue bars, $^{*}p < 0.05$). (f) Changes in the mechanosensory complex after 6 h exposure to shear stress at 20 dyn/cm^2; statistical analysis was performed as for integrins, where # indicates significant changes ($^{\#}p < 0.05$, $^{\#\#}p < 0.01$) compared to static expression levels. (For interpretation of the references to color in this figure legend, the reader is referred to the web version of this article.)

dynamic forces. It has been reported that integrins of ECs were responsible for cell retention under shear stress [25], as well as improved retention of MSCs with concomitant upregulation of integrins [39]. Our results show that both hMSCs and HUVECs exhibit a significant increase in expression of integrins α2 and β1 due to shear stress. On the other hand, once shear stress is applied to cells seeded on a defined support, the cells transmit a signal from their apical surface through the cytoskeleton to points of attachment, in order to foster cell-matrix adhesions [40]. It has been proposed that CD31, VE-cadherin and VEGFR2 serve as a mechanosensory complex for the attachment of ECs in response to shear stress [41]. Indeed, these three junctional adhesion molecules play crucial roles in cell-cell and cell-matrix attachment. In addition, cell culture on different surfaces has been reported to modify the expression level of EC functional markers [42]. Our results have revealed that the expression of the mechanosensory complex by ECs cultured on WJ-ECM coating was relatively high and was maintained with or without shear stress, which may explain the retention of the cells on the coating. On the other hand, HUVECs cultured on collagen under shear stress increased expression of mechanosensory complex, whereas expression of mechanosensory complex by cells grown on glass coverslips decreased significantly. Taken together, these results indicate that the WJ-ECM coating may find application in cell culture under both static and dynamic conditions.

5. Conclusion

In summary, we have demonstrated that our new, easily-prepared WJ-ECM coating is appropriate for both the adhesion and proliferation of the two cell types most commonly employed in vascular tissue engineering, human mesenchymal stem cells and mature endothelial cells. Furthermore, under conditions of physiological shear stress, a larger number of cells remained adherent to WJ-ECM than onto a conventional coating such as collagen – a result supported by a higher expression of both integrins

α2 and β1 in hMSCs and HUVECs cultured on WJ-ECM. Thus, overall, our data clearly show that Wharton's jelly derived-ECM is a highly promising coating for cell culture surfaces in tissue engineering and regenerative medicine.

Acknowledgements

The authors acknowledge the support of Dr. Jalal Bacharouche and the platform "Spectroscopy and Microscopy of Interfaces" (SMI, Jean Barriol Institute, Nancy) where AFM experiments were performed. We would like to thank the research federation FR3209 Bioingénierie Moléculaire, Cellulaire et Thérapeutique (Nancy, France) and China Scholarship Council (China). We would like to thank Miss Huiyi Zhang for her assistance with the preparation of WJ-ECM coating. We would also like to thank Prof. Kira J. Weissman for careful proof-reading of this manuscript.

Appendix A. Supplementary data

Supplementary data associated with this article can be found, in the online version, at http://dx.doi.org/10.1016/j.actbio.2016.10.018.

References

[1] R. El Omar, Y. Xiong, G. Dostert, H. Louis, M. Gentils, P. Menu, J.-F. Stoltz, É. Velot, V. Decot, Immunomodulation of endothelial differentiated mesenchymal stromal cells: impact on T and NK cells, Immunol. Cell Biol. 94 (2016) 342–356.
[2] J.A. Ankrum, J.F. Ong, J.M. Karp, Mesenchymal stem cells: immune evasive, not immune privileged, Nat. Biotechnol. 32 (2014) 252–260.
[3] F. Guilak, D.M. Cohen, B.T. Estes, J.M. Gimble, W. Liedtke, C.S. Chen, Control of stem cell fate by physical interactions with the extracellular matrix, Cell Stem Cell 5 (2009) 17–26.
[4] M.M. Stevens, J.H. George, Exploring and engineering the cell surface interface, Science 310 (2005) 1135–1138.
[5] J. Ringe, M. Sittinger, Regenerative medicine: selecting the right biological scaffold for tissue engineering, Nat. Rev. Rheumatol. 10 (2014) 388–389.
[6] K. von der Mark, J. Park, S. Bauer, P. Schmuki, Nanoscale engineering of biomimetic surfaces: cues from the extracellular matrix, Cell Tissue Res. 339 (2010) 131–153.
[7] B.M. Gillette, J.A. Jensen, M. Wang, J. Tchao, S.K. Sia, Dynamic hydrogels: switching of 3D microenvironments using two-component naturally derived extracellular matrices, Adv. Mater. 22 (2010) 686–691.
[8] E.S. Place, N.D. Evans, M.M. Stevens, Complexity in biomaterials for tissue engineering, Nat. Mater. 8 (2009) 457–470.
[9] M.C. Moore, V. Pandolfi, P.S. McFetridge, Novel human-derived extracellular matrix induces in vitro and in vivo vascularization and inhibits fibrosis, Biomaterials 49 (2015) 37–46.
[10] A. Can, S. Karahuseyinoglu, Concise review: human umbilical cord stroma with regard to the source of fetus-derived stem cells, Stem Cells 25 (2007) 2886–2895.
[11] H. Hao, G. Chen, J. Liu, D. Ti, Y. Zhao, S. Xu, X. Fu, W. Han, Culturing on Wharton's jelly extract delays mesenchymal stem cell senescence through p53 and p16INK4a/pRb pathways, PLoS One 8 (2013) e58314.
[12] N. Berthelemy, H. Kerdjoudj, C. Gaucher, P. Schaaf, J.-F. Stoltz, P. Lacolley, J.-C. Voegel, P. Menu, Polyelectrolyte films boost progenitor cell differentiation into endothelium-like monolayers, Adv. Mater. Deerfield Beach Fla. 20 (2008) 2674–2678.
[13] I.N. Sneddon, The relation between load and penetration in the axi-symmetric Boussinesq problem for a punch of arbitrary profile, Int. J. Eng. Sci. 3 (1965) 47–57.
[14] N. Gavara, R.S. Chadwick, Determination of the elastic moduli of thin samples and adherent cells using conical atomic force microscope tips, Nat. Nanotechnol. 7 (2012) 733–736.
[15] P. Polyakov, C. Soussen, J. Duan, J.F.L. Duval, D. Brie, G. Francius, Automated force volume image processing for biological samples, PLoS One 6 (2011) e18887.
[16] R. Rago, J. Mitchen, G. Wilding, DNA fluorometric assay in 96-well tissue culture plates using Hoechst 33258 after cell lysis by freezing in distilled water, Anal. Biochem. 191 (1990) 31–34.
[17] C.M. Frendl, S.M. Tucker, N.A. Khan, M.B. Esch, S. Kanduru, T.M. Cao, A.J. García, M.R. King, J.T. Butcher, Endothelial retention and phenotype on carbonized cardiovascular implant surfaces, Biomaterials 35 (2014) 7714–7723.
[18] N. Rajan, J. Habermehl, M.-F. Coté, C.J. Doillon, D. Mantovani, Preparation of ready-to-use, storable and reconstituted type I collagen from rat tail tendon for tissue engineering applications, Nat. Protoc. 1 (2006) 2753–2758.
[19] Y.-F. Han, R. Tao, T.-J. Sun, J.-K. Chai, G. Xu, J. Liu, Optimization of human umbilical cord mesenchymal stem cell isolation and culture methods, Cytotechnology 65 (2013) 819–827.
[20] K. Sobolewski, A. Małkowski, E. Bańkowski, S. Jaworski, Wharton's jelly as a reservoir of peptide growth factors, Placenta 26 (2005) 747–752.
[21] W.L. Murphy, T.C. McDevitt, A.J. Engler, Materials as stem cell regulators, Nat. Mater. 13 (2014) 547–557.
[22] K. Wingate, W. Bonani, Y. Tan, S.J. Bryant, W. Tan, Compressive elasticity of three-dimensional nanofiber matrix directs mesenchymal stem cell differentiation to vascular cells with endothelial or smooth muscle cell markers, Acta Biomater. 8 (2012) 1440–1449.
[23] T.D. Ross, B.G. Coon, S. Yun, N. Baeyens, K. Tanaka, M. Ouyang, M.A. Schwartz, Integrins in mechanotransduction, Curr. Opin. Cell Biol. 25 (2013) 613–618.
[24] D. Docheva, C. Popov, W. Mutschler, M. Schieker, Human mesenchymal stem cells in contact with their environment: surface characteristics and the integrin system, J. Cell Mol. Med. 11 (2007) 21–38.
[25] N.J. Turner, M.O. Murphy, C.M. Kielty, C.A. Shuttleworth, R.A. Black, M.J. Humphries, M.G. Walker, A.E. Canfield, Alpha2(VIII) collagen substrata enhance endothelial cell retention under acute shear stress flow via an alpha2beta1 integrin-dependent mechanism: an in vitro and in vivo study, Circulation 114 (2006) 820–829.
[26] K. Warstat, D. Meckbach, M. Weis-Klemm, A. Hack, G. Klein, P. de Zwart, W.K. Aicher, TGF-beta enhances the integrin alpha2beta1-mediated attachment of mesenchymal stem cells to type I collagen, Stem Cells Dev. 19 (2010) 645–656.
[27] D. Mozaffarian, E.J. Benjamin, A.S. Go, D.K. Arnett, M.J. Blaha, M. Cushman, S.R. Das, S. de Ferranti, J.-P. Després, H.J. Fullerton, V.J. Howard, M.D. Huffman, C.R. Isasi, M.C. Jiménez, S.E. Judd, B.M. Kissela, J.H. Lichtman, L.D. Lisabeth, S. Liu, R. H. Mackey, D.J. Magid, D.K. McGuire, E.R. Mohler, C.S. Moy, P. Muntner, M.E. Mussolino, K. Nasir, R.W. Neumar, G. Nichol, L. Palaniappan, D.K. Pandey, M.J. Reeves, C.J. Rodriguez, W. Rosamond, P.D. Sorlie, J. Stein, A. Towfighi, T.N. Turan, S.S. Virani, D. Woo, R.W. Yeh, M.B. Turner, American heart association statistics committee and stroke statistics subcommittee, heart disease and stroke statistics-2016 update: a report from the American heart association, Circulation 133 (2016) e38–e360.
[28] E. Benrashid, C.C. McCoy, L.M. Youngwirth, J. Kim, R.J. Manson, J.C. Otto, J.H. Lawson, Tissue engineered vascular grafts: origins, development, and current strategies for clinical application, Methods San Diego Calif. 99 (2016) 13–19.
[29] D.G. Seifu, A. Purnama, K. Mequanint, D. Mantovani, Small-diameter vascular tissue engineering, Nat. Rev. Cardiol. 10 (2013) 410–421.
[30] J.T. Krawiec, D.A. Vorp, Adult stem cell-based tissue engineered blood vessels: a review, Biomaterials 33 (2012) 3388–3400.
[31] Y. Zhao, S. Zhang, J. Zhou, J. Wang, M. Zhen, Y. Liu, J. Chen, Z. Qi, The development of a tissue-engineered artery using decellularized scaffold and autologous ovine mesenchymal stem cells, Biomaterials 31 (2010) 296–307.
[32] M.T. Koobatian, S. Row, R.J. Smith Jr., C. Koenigsknecht, S.T. Andreadis, D.D. Swartz, Successful endothelialization and remodeling of a cell-free small-diameter arterial graft in a large animal model, Biomaterials 76 (2016) 344–358.
[33] M.M. Martino, S. Brkic, E. Bovo, M. Burger, D.J. Schaefer, T. Wolff, L. Gürke, P.S. Briquez, H.M. Larsson, R. Gianni-Barrera, J.A. Hubbell, A. Banfi, Extracellular matrix and growth factor engineering for controlled angiogenesis in regenerative medicine, Front. Bioeng. Biotechnol. 3 (2015) 45.
[34] M.J. Sherratt, D.V. Bax, S.S. Chaudhry, N. Hodson, J.R. Lu, P. Saravanapavan, C.M. Kielty, Substrate chemistry influences the morphology and biological function of adsorbed extracellular matrix assemblies, Biomaterials 26 (2005) 7192–7206.
[35] D.N. Coakley, F.M. Shaikh, K. O'Sullivan, E.G. Kavanagh, P.A. Grace, S.R. Walsh, T.M. McGloughlin, Comparing the endothelialisation of extracellular matrix bioscaffolds with coated synthetic vascular graft materials, Int. J. Surg. Lond. Engl. 25 (2016) 31–37.
[36] A.D. Doyle, N. Carvajal, A. Jin, K. Matsumoto, K.M. Yamada, Local 3D matrix microenvironment regulates cell migration through spatiotemporal dynamics of contractility-dependent adhesions, Nat. Commun. 6 (2015) 8720.
[37] Y.-L. Han, Q. Xu, Z. Lu, J.-Y. Wang, Cell adhesion on zein films under shear stress field, Colloids Surf. B Biointerfaces 111 (2013) 479–485.
[38] X. Gong, H. Liu, X. Ding, M. Liu, X. Li, L. Zheng, X. Jia, G. Zhou, Y. Zou, J. Li, X. Huang, Y. Fan, Physiological pulsatile flow culture conditions to generate functional endothelium on a sulfated silk fibroin nanofibrous scaffold, Biomaterials 35 (2014) 4782–4791.
[39] S.E. McIlhenny, E.S. Hager, D.J. Grabo, C. DiMatteo, I.M. Shapiro, T.N. Tulenko, P. J. DiMuzio, Linear shear conditioning improves vascular graft retention of adipose-derived stem cells by upregulation of the alpha5beta1 integrin, Tissue Eng. Part A 16 (2010) 245–255.
[40] F.M. Watt, W.T.S. Huck, Role of the extracellular matrix in regulating stem cell fate, Nat. Rev. Mol. Cell Biol. 14 (2013) 467–473.
[41] E. Tzima, M. Irani-Tehrani, W.B. Kiosses, E. Dejana, D.A. Schultz, B. Engelhardt, G. Cao, H. DeLisser, M.A. Schwartz, A mechanosensory complex that mediates the endothelial cell response to fluid shear stress, Nature 437 (2005) 426–431.
[42] J. Chlupac, E. Filova, J. Havlikova, R. Matejka, T. Riedel, M. Houska, E. Brynda, E. Pamula, M. Rémy, R. Bareille, P. Fernandez, R. Daculsi, C. Bourget, L. Bacakova, L. Bordenave, The gene expression of human endothelial cells is modulated by subendothelial extracellular matrix proteins: short-term response to laminar shear stress, Tissue Eng. Part A 20 (2014) 2253–2264.

Supporting information

Human-derived extracellular matrix from Wharton's jelly: an untapped substrate to build up a standardized and homogeneous coating for vascular engineering

Pan Dan[a], Émilie Velot[a], Grégory Francius[b], Patrick Menu[a]* and Véronique Decot[a,c]

Supplementary Figures

S1

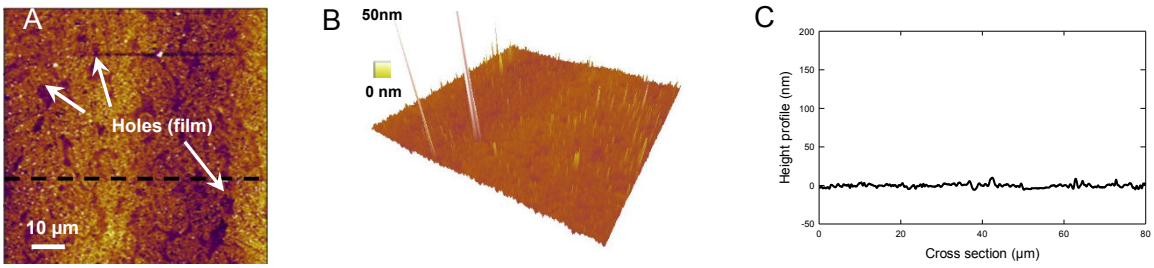

Supplemental Figure 1. WJ-ECM obtained using acetic acid. WJ-ECM was dissolved in acetic acid and coated on cover slips at a concentration of 5 mg/ml. The coating was then assessed by AFM, showing that little deposit was present, while the detected layer was thin and non-continuous. WJ-ECM dissolved in collagenase II or in PBS with magnetic stirring failed to generate any deposit that could be detected by AFM.

S2

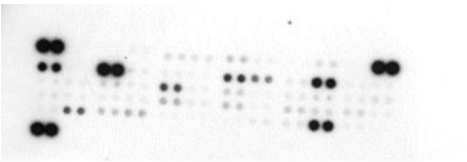

Supplemental Figure 2. Biomolecular composition of WJ-ECM solution. Cytokines were detected by human angiogenesis array, and the density of expressed cytokines was normalized to the positive controls situated on the left and right upper corners.

S3

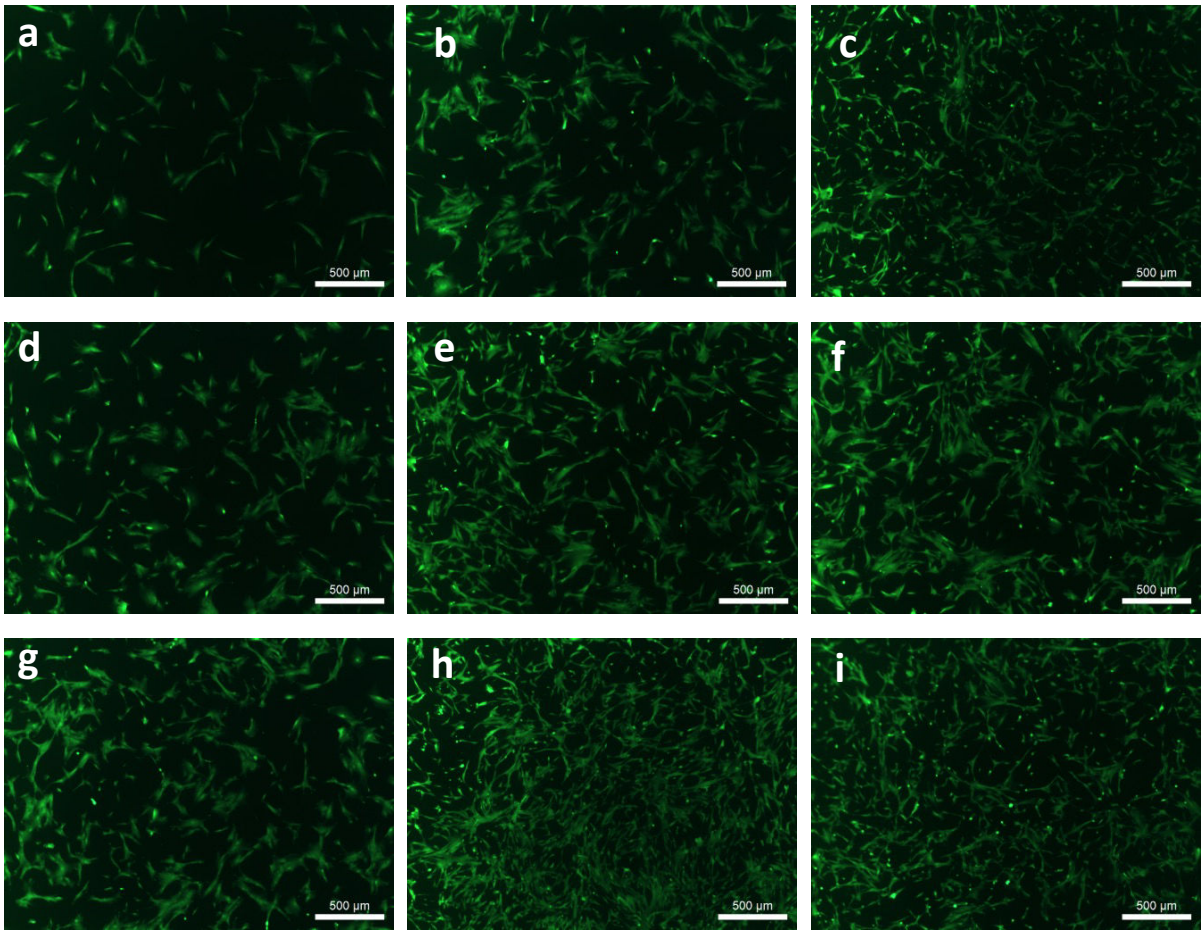

Supplemental Figure 3. Bioactivity of soluble factors in WJ-ECM solution. Cells were cultured in αMEM supplemented with different percentages of WJ-ECM solution for 5 days, before being labeled with live (green)/dead (red) staining (n=3). In order to ensure that the enhancement on proliferation was not due to FBS, each condition was compared to αMEM with the same percentage of FBS (a-c, 0% FBS; d-f, 2.5% FBS; g-i, 10% FBS). In culture medium without FBS (a), cells maintained a slow proliferation rate. When they were cultured in medium supplemented with 10% (b), 40% (c) of WJ-ECM without FBS, they showed a concentration-related enhancement of cell proliferation. FBS supplemented culture medium promoted cell proliferation (2.5% and 10% respectively, d and g), but WJ-ECM solution containing equal FBS further enhanced this proliferation (e-f, 10% WJ-ECM; h-i, 40% WJ-ECM). Moreover, freshly prepared WJ-ECM (e and h) or WJ-ECM conserved at -80°C (f and i) had a similar effect on cell proliferation. Scale bar, 500 µm.

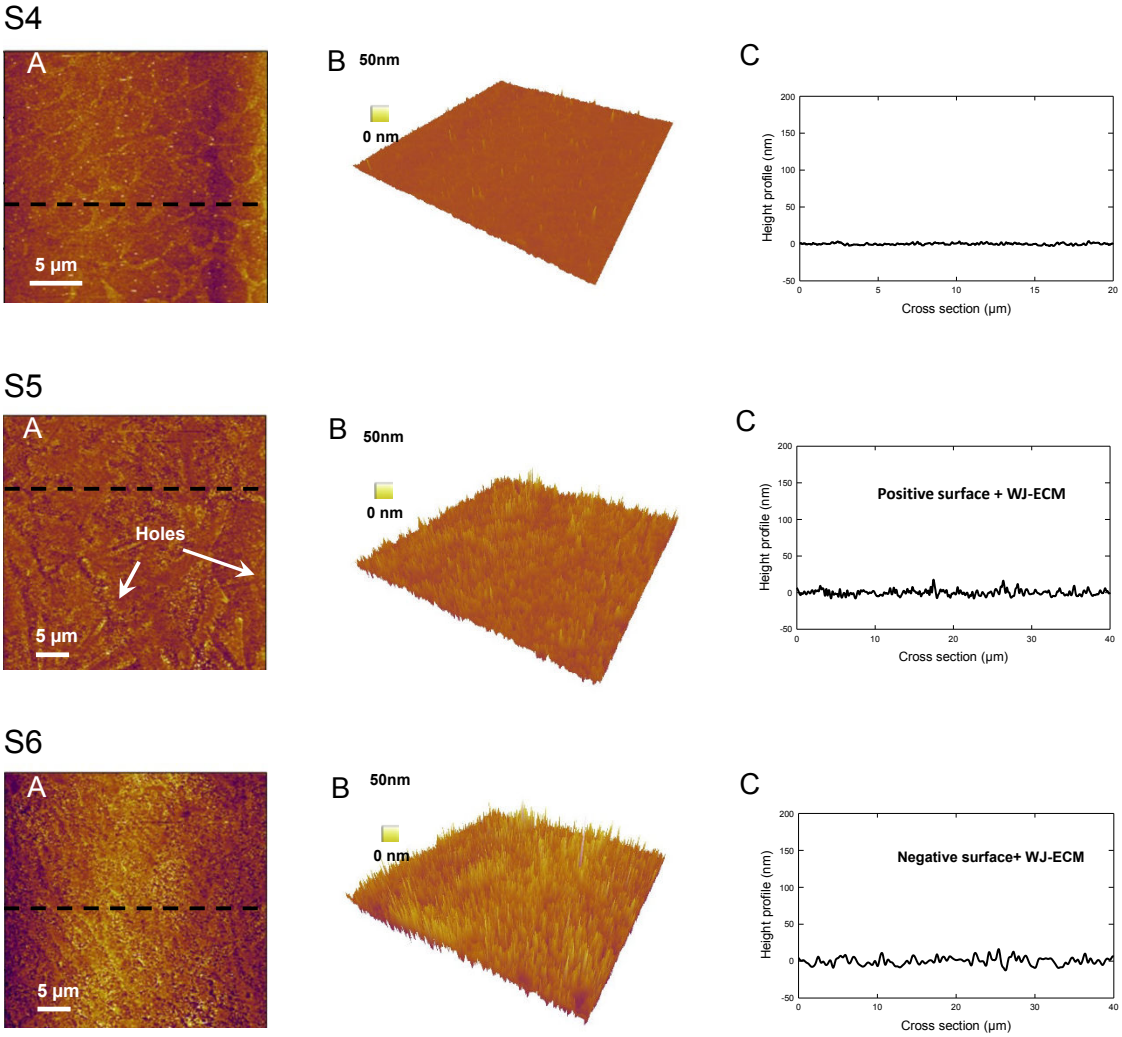

Supplemental Figure 4-6. Influence of scaffold charge on coating formation. (S4) WJ-ECM (5 mg/ml) generated from trypsin coated directly on glass coverslips failed to form a sufficient deposit. (S5) WJ-ECM coated onto a positively-charged scaffold formed a deposit, but the coating was not homogeneous and some holes were evident. (S6) WJ-ECM coated onto a negatively-charged scaffold formed a homogeneous coating with considerable thickness.

S7

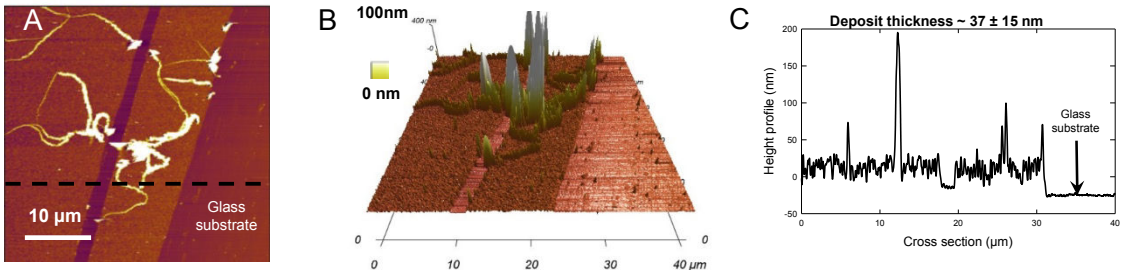

S8

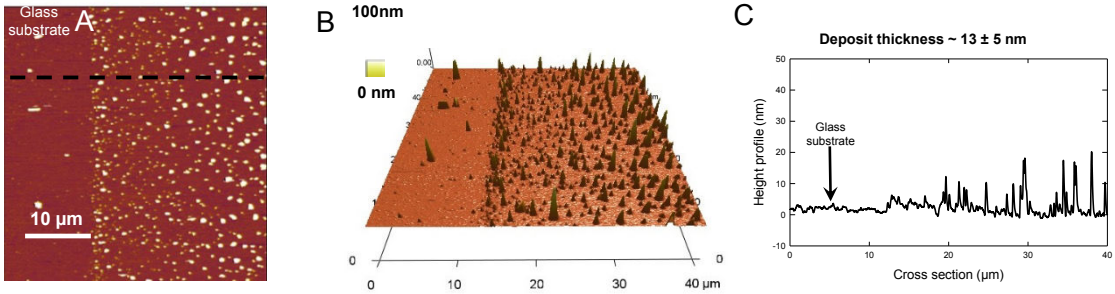

S9

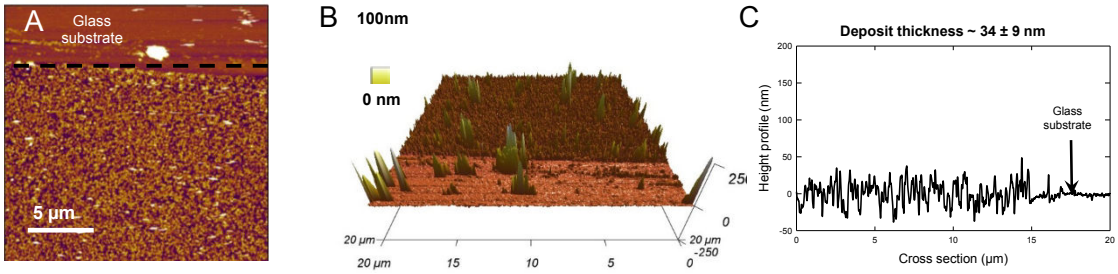

S10

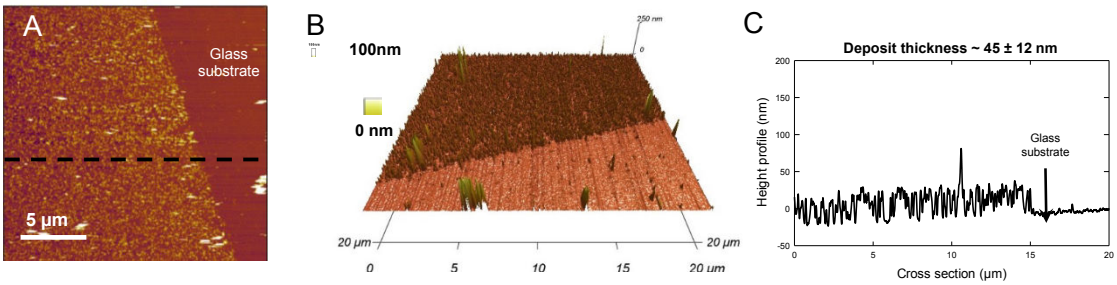

S11

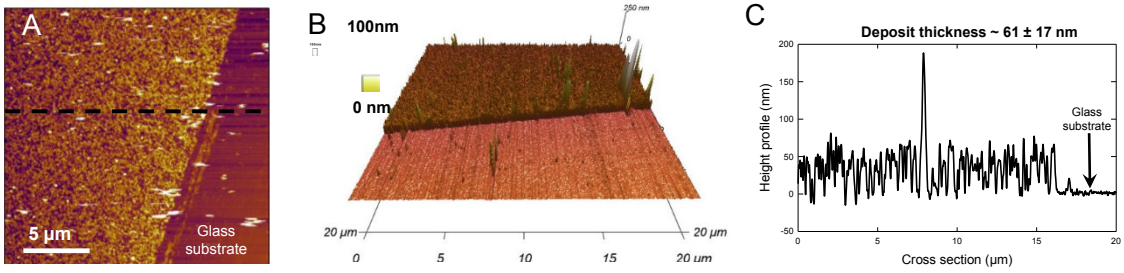

S12

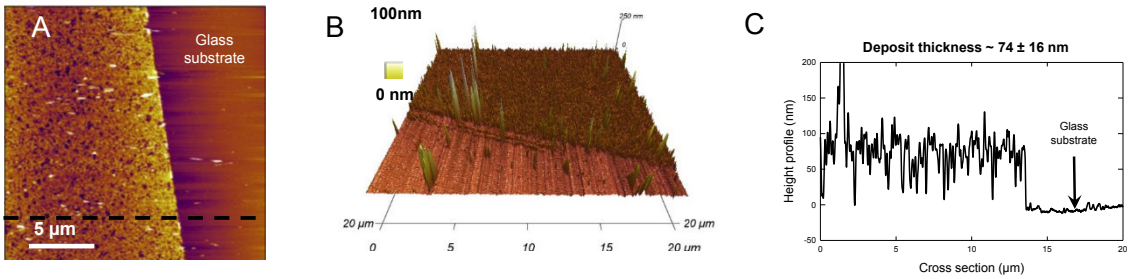

Supplemental Figure 7-12. Concentration dependent WJ-ECM coating. All the samples were partially scratched to show the coating and underlying glass coverslips. S7 shows the collagen control. WJ-ECM at concentrations ranging from 1 mg/ml to 10 mg/ml (1, 2.5, 5, 7.5, 10 mg/ml, respectively) formed coatings with thicknesses varying from 13 ± 5 nm to 74 ± 16 nm (S8-S12).

Chapitre 2 Biomatériaux – coating naturel (2)

Publication N° 4 (accepté *Bio-Med Mater Eng*)

Résumé en français

Matrice dérivée de cordon ombilical humain : un scaffold approprié pour l'application d'ingénierie tissulaire

Pan Dan[a], Émilie Velot[a], Benjamin Mesure[a], Guillaume Groshenry[a], Jalal Bacharouche[b], Véronique Decot[a,c] and Patrick Menu[a]*

L'un des objectifs dans le développement de nouveaux biomatériaux en médecine régénérative est de développer une matrice extracellulaire (ECM) multifonctionnelle proche d'un environnement natif pour les cellules. Pour ce faire, les polymères synthétiques et naturels ont été largement étudiés. Les polymères naturels attirent beaucoup d'attention parce qu'ils ont habituellement moins de risques de biocompatibilité. Le collagène et la fibronectine sont bien connus et appliqués dans diverses applications d'ingénierie tissulaire pour favoriser la culture cellulaire. Le collagène, la protéine la plus abondante chez les mammifères, peut être issu d'un tissu animal ou humain. Actuellement, le collagène commercial est plus souvent issu de la queue de rat ou du placenta humain. Avec le risque du rejet xénogénique, l'ECM d'origine animale ne constitue pas un potentiel clinique et renforce l'avantage de développer des produits dérivés de l'homme.

Cette étude vise à explorer la matrice dérivée de cordon ombilical humain (hUCM). Le cordon ombilical est connu pour contenir de très grande quantité de cytokines. Nous nous concentrons dans cette étude, sur les composants de la solution issue du cordon ombilical, et l'influence de sérum de veau fœtal (SVF) sur ces composants.

Après une digestion enzymatique, les tissus du cordon ombilical se présentent sous forme d'une solution visqueuse. Du SVF a été ajoutée dans la solution pour neutraliser la réaction enzymatique. Dans cette solution, divers facteurs de croissances sont retrouvés tels que VEGF, FGF-2, PDGF-AA et TGF-beta1. Par ailleurs, du collagène de type XVIII est aussi détecté par le kit angiogenesiss Assay. Le Western-blot a montré la présence du collagène I dans la solution. Par contre, en absence de SVF ajouté, aucun collagène n'est détecté, ce qui signifie le SVF est nécessaire pour neutraliser la digestion de trypsine.

Le cordon ombilical est surtout utilisé pour récupérer des cellules souches mésenchymateuses. Lorsqu'elle est utilisée comme source de matrice, la procédure d'isolement détruit les cellules dans le tissu et libère l'ADN cellulaire. Cet ADN résiduel peut induire une réponse immunitaire de l'hôte. Seuls les biomatériaux qui ne contiennent pas d'ADN résiduel peuvent avoir un potentiel de transfert clinique. Dans notre étude, la procédure se termine par l'addition de SVF pour inhiber la réaction de la trypsine. Il est connu que le SVF contient des nucléases stables à la chaleur qui permettent d'éliminer l'ADN résiduel. Cet avantage du SVF nous permet d'obtenir une hUCM sans ADN résiduel, qui suggère que la hUCM peut être utilisée en toute sécurité en médecine régénérative humaine.

Finalement, nous avons montré que la hUCM peut former un coating en 2D sur des lamelles et en 3D sur les artères ombilicales humaines. Le coating en 2D est capable de supporter l'adhésion de cellules souches mésenchymateuses et de cellules endothéliales matures.

Bio-Medical Materials and Engineering 00 (20xx) 1–6
DOI 10.3233/BME-171629
IOS Press

Human umbilical cord derived matrix: A scaffold suitable for tissue engineering application

Pan Dan [a], Émilie Velot [a], Benjamin Mesure [a], Guillaume Groshenry [a], Jalal Bacharouche [b], Véronique Decot [a,c] and Patrick Menu [a,*]

[a] *UMR 7365, Ingénierie Moléculaire et Physiopathologie Articulaire (IMoPA), CNRS–Université de Lorraine, Vandœuvre-lès-Nancy, 54505, France*

[b] *UMR 7564, Laboratoire de Chimie Physique et Microbiologie pour l'Environnement, Université de Lorraine, Villers-lès-Nancy, 54600, France*

[c] *Unité de Thérapie Cellulaire et Tissulaire, CHU de Nancy, Vandœuvre-lès-Nancy, 54500, France*

Received **TO BE UPDATED**
Accepted **TO BE UPDATED**

Abstract.
BACKGROUND: Human tissue derived natural extracellular matrix (ECM) has great potential in tissue engineering.
OBJECTIVE: We sought to isolate extracellular matrix derived from human umbilical cord and test its potential in tissue engineering.
METHODS: An enzymatic method was applied to isolate and solubilized complete human umbilical cord derived matrix (hUCM). The obtained solution was analyzed for growth factors, collagen and residual DNA contents, then used to coat 2D and 3D surfaces for cell culture application.
RESULTS: The hUCM was successfully isolated with trypsin digestion to acquire a solution containing various growth factors and collagen but no residual DNA. This hUCM solution can form a coating on 2D and 3D substrates suitable cell culture.
CONCLUSION: We developed a new matrix derived from human source that can be further used in tissue engineering.

Keywords: Human matrix, tissue engineering, growth factors, residual DNA, stem cells

1. Introduction

One of the focus to generate new biomaterials in regenerative medicine is the development of multi-functional extracellular matrix (ECM) that can mimic a natural environment for cells [1]. To do so, both synthetic and natural polymers have been widely investigated [2]. Natural polymers draw much attention because they usually have less concern about biocompatibility. Collagen and fibronectin are well known and applied in various tissue engineering applications to support cell culture. As the most abundant protein in mammals, collagen can be derived from animal or human tissue. Currently, commercial collagen

*Corresponding author: Patrick Menu, UMR 7365 CNRS–Université de Lorraine, Ingénierie Moléculaire et Physiopathologie Articulaire (IMoPA), 54505 Vandœuvre-lès-Nancy, France. E-mail: patrick.menu@univ-lorraine.fr; Tel.: +33 3 83 68 54 57; Fax: +33 3 83 68 54 09.

0959-2989/17/$35.00 © 2017 – IOS Press and the authors. All rights reserved

UNCORRECTED PROOF

is usually from rat-tail or human placenta [3,4]. With the concern of xenogeneic rejection, animal derived ECM has no clinical potential and this has led to develop human derived product. Human placenta can generate matrix containing numerous growth factors that have function in angiogenesis [5]. Platelet lysate is another promising source that can be used as clinical-grade supplement for cell expansion [6]. These achievements encourage the sighting of new human tissue sources for tissue engineering.

This study aims to explore human umbilical cord derived matrix (hUCM), which was known to contain huge amount of cytokines [7]. We used an enzymatic method to isolate and solubilized hUCM, characterized the obtained product and assessed its potential in tissue engineering.

2. Methods

2.1. Human umbilical cord derived matrix preparation

Human umbilical cords were collected at the delivery suite at regional maternity hospital of Nancy at the University of Lorraine in accordance with TCG/11/R/011 within 12 h of birth. The whole umbilical cord was cut into small pieces and the connective tissue was dissociated. Umbilical cord connective tissue (2–3 g, wet weight) was digested in 10 mL of trypsin (0.025%) at 37°C for 24 h with magnetic stirring. The stirred suspensions were centrifuged at 16,000g for 10 min. The collected supernatants were filtered (100 μm) and 5 mL of fetal bovine serum (FBS) was added to inhibit trypsin. PBS was added to have a 20 mL final solution. The obtained hUCM solution was conserved at 4°C for further use. The precise concentration of hUCM was calculated as follows: 10 mL of the prepared hUCM solution were lyophilized; 10 mL of solution containing 5 mL of trypsin, 2.5 mL of FBS and 2.5 mL of PBS were also lyophilized. The concentration of hUCM (mg/mL) was calculated by the dry powder weight of total hUCM minus the weight of lyophilized trypsin–FBS–PBS solution.

2.2. Characterization of the hUCM solution

The hUCM solution generated by trypsin digestion was characterized for its cytokine contents by an angiogenesis array kit (R&D systems, France) according to the manufacture's protocol. Detected spots were analyzed with Image J software for semi-quantitative measurement. Western-blot was performed to detect collagen I in the solution. Rat-tail collagen I was used as a positive control and the trypsin–FBS–PBS mixture as negative control.

In order to check whether the hUCM solution contains residual DNA after trypsin treatment, agarose gel electrophoresis (10%) was performed. The trypsin–FBS–PBS mixture was used as a control. We also assessed the influence of FBS on DNA stability by preparing hUCM solution without adding FBS.

2.3. Elaboration and characterization of the hUCM coating for cell culture

hUCM solution was used to form a coating for cell culture. For 2D coating, the solution was deposited on glass coverslips that were previously treated with SDS–HCl. The glass coverslips were incubated at 37°C for 1 h before being washed twice with PBS. For 3D coating, hUCM solution was injected into de-endothelialized umbilical artery and performed similarly to 2D coating. Atomic force microscopy was employed to evaluate the coating.

2D coating was used to assess its potential for cell culture. Human mesenchymal stem cells and human umbilical vein endothelial cells were isolated according to El Omar et al. [8] and cultured on hUCM

UNCORRECTED PROOF

coating for 5 days before being marked with phalloidine and DAPI for fluorescent microscopy observation as previously described [9].

3. Results

3.1. Characterization of human umbilical cord matrix

After 24 hours of magnetic stirring in presence of trypsin, hUCM was digested into a viscous solution (Fig. 1). The concentration of hUCM was then precisely calculated using a lyophilized solution. The influence of trypsin, FBS and PBS was also taken into account during calculation. A cytokine array focused on soluble factors revealed that the solution contained abundant growth factors and ECM proteins, including vascular endothelial growth factors (VEGF), fibroblast growth factors-2 (FGF-2), platelet derived growth factor-AA (PDGF-AA) and transforming growth factor-beta 1 and collagen XVIII (Fig. 2(a)). Collagen I was also detected by western blot in three independently prepared hUCM. We also observed that the neutralization of trypsin by FBS is mandatory, since collagen I was destroyed in absence of trypsin neutralization (Fig. 2(b)).

3.2. Residual DNA detection

The presence of residual human DNA was next determined. DNA was detected in samples without FBS, but residual DNA was destroyed when FBS was added. Thus, in all the three independently prepared full hUCM, no residual DNA was detected (Fig. 2(c)).

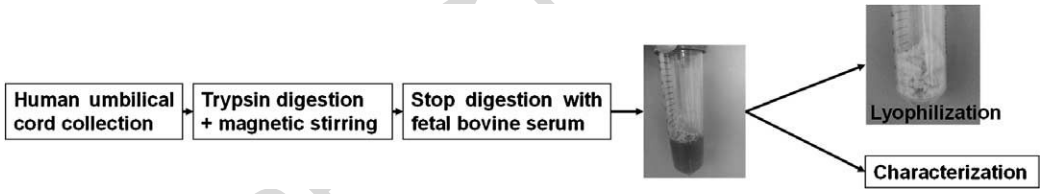

Fig. 1. Human umbilical cord matrix was obtained by trypsin digestion under magnetic stirring, followed by adding FBS. The solution was then lyophilized for precise concentration calculation or further biological characterization.

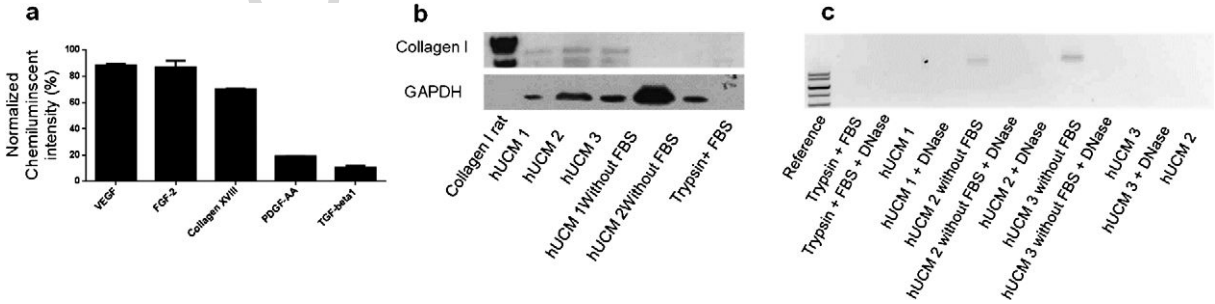

Fig. 2. Characterization of hUCM solution. (a) Biochemical analysis using human angiogenesis array demonstrated growth factors and collagen content. (b) Western-blot using collagen I antibody indicated that hUCM contained collagen I. (c) Residual DNA was determined by agarose gel electrophoresis. No residual DNA was detected in any of the three independently prepared hUCM.

ORIGINAL UNCORRECTED PROOF

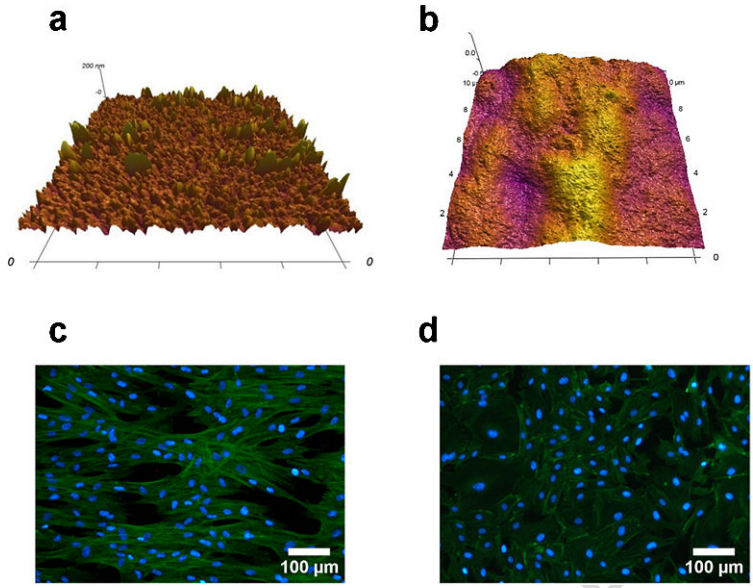

Fig. 3. A coating can be formed by hUCM on 2D substrate (a) and 3D substrate. The 2D coating can support cell adhesion of human mesenchymal stem cells (c) and human umbilical vein endothelial cells (d). (Colors are visible in the online version of the article.)

3.3. Cell culture coating derived from hUCM

On 2D glass coverslips, hUCM can form a coating which had a uniform distribution with thickness of 45 ± 12 nm. As assessed by AFM, hUCM can also coat 3D de-endothelialized umbilical artery (Fig. 3(a) and (b)).

Human mesenchymal stem cells and endothelial cells seeded on coated glass slides were showed to adhere as observed on fluorescent images indicating that the new coating is able to support cell adhesion and proliferation (Fig. 3(c) and (d)).

4. Discussion

The discovery of new human derived source for fabricating biomaterials remains a goal to reach in tissue engineering [10]. Besides placenta which is considered as an important and useful source for human derived extracellular matrix for tissue engineering, other sources of healthy human tissues are currently explored. This study reports an enzymatic method to isolate a complex matrix from human umbilical cord. This matrix derived from umbilical cord contained abundant growth factors, and extracellular protein such as collagen. These components clearly provide a suitable environment for stem cells and mature cells adherence and growth. Umbilical cord is considered as a niche for mesenchymal stem cells [11]. When used as a matrix source, the isolation procedure will destroy cells in the tissue and lead to the release of cell DNA. The residual human DNA may induce a host immune response. Only biomaterials which do not contain residual DNA may have a clinical transfer potential [12]. In our study, the procedure was ended by adding FBS to inhibit trypsin reaction. Interestingly, FBS was reported to contain heat-stable nucleases that can eliminate residual DNA [13]. This advantage of FBS allows us to obtain a hUCM without any residual DNA, which indicate the hUCM may be safely used in human

UNCORRECTED PROOF

regenerative medicine. However, we cannot exclude the risk of xenogeneic reaction due to presence of FBS, even if the percentage used was low. An alternative of FBS will be required to supply a full clinical grade hUCM.

5. Conclusion

Our results revealed an enzymatic method to obtain a complex matrix from human umbilical cord. The hUCM contained various growth factors and different types of collagen, which can provide a biomimetic environment for cell culture. No residual DNA was detected from the hUCM, which makes it a safe product for clinical transfer. The hUCM can easily form a coating on 2D and 3D substrates to support cell culture. This point makes hUCM a strong tool for tissue engineering.

Acknowledgements

We would like to thank the Research Federation 3209 BMCT (Nancy, France). Dan Pan is a PhD student supported by China scholarship council.

Conflict of interest

The authors have no conflict of interest to report.

References

[1] N. Huebsch and D.J. Mooney, Inspiration and application in the evolution of biomaterials, *Nature* **462** (2009), 426–432. doi:10.1038/nature08601.

[2] M.P. Lutolf and J.A. Hubbell, Synthetic biomaterials as instructive extracellular microenvironments for morphogenesis in tissue engineering, *Nat. Biotechnol.* **23** (2005), 47–55. doi:10.1038/nbt1055.

[3] N. Rajan, J. Habermehl, M.-F. Coté, C.J. Doillon and D. Mantovani, Preparation of ready-to-use, storable and reconstituted type I collagen from rat tail tendon for tissue engineering applications, *Nat. Protoc.* **1** (2006), 2753–2758. doi:10.1038/nprot.2006.430.

[4] P.S. Amenta, S. Gay, A. Vaheri and A. Martinez-Hernandez, The extracellular matrix is an integrated unit: Ultrastructural localization of collagen types I, III, IV, V, VI, fibronectin, and laminin in human term placenta, *Coll. Relat. Res.* **6** (1986), 125–152. doi:10.1016/S0174-173X(86)80021-8.

[5] M.C. Moore, V. Pandolfi and P.S. McFetridge, Novel human-derived extracellular matrix induces in vitro and in vivo vascularization and inhibits fibrosis, *Biomaterials* **49** (2015), 37–46. doi:10.1016/j.biomaterials.2015.01.022.

[6] G. Astori, E. Amati, F. Bambi, M. Bernardi, K. Chieregato, R. Schäfer, S. Sella and F. Rodeghiero, Platelet lysate as a substitute for animal serum for the ex-vivo expansion of mesenchymal stem/stromal cells: Present and future, *Stem Cell Res. Ther.* **7** (2016), 93.

[7] A. Can and S. Karahuseyinoglu, Concise review: Human umbilical cord stroma with regard to the source of fetus-derived stem cells, *Stem Cells* **25** (2007), 2886–2895. doi:10.1634/stemcells.2007-0417.

[8] R. El Omar, Y. Xiong, G. Dostert, H. Louis, M. Gentils, P. Menu, J.-F. Stoltz, É. Velot and V. Decot, Immunomodulation of endothelial differentiated mesenchymal stromal cells: Impact on T and NK cells, *Immunol. Cell Biol.* (2015).

[9] H. Rammal, J. Beroud, M. Gentils, P. Labrude, P. Menu, H. Kerdjoudj and E. Velot, Reversing charges or how to improve Wharton's jelly mesenchymal stem cells culture on polyelectrolyte multilayer films, *Biomed. Mater. Eng.* **23** (2013), 299–309.

[10] J. Ringe and M. Sittinger, Regenerative medicine: Selecting the right biological scaffold for tissue engineering, *Nat. Rev. Rheumatol.* **10** (2014), 388–389. doi:10.1038/nrrheum.2014.79.

UNCORRECTED PROOF

[11] Y. Yang, C. Melzer, V. Bucan, J. von der Ohe, A. Otte and R. Hass, Conditioned umbilical cord tissue provides a natural three-dimensional storage compartment as in vitro stem cell niche for human mesenchymal stroma/stem cells, ***Stem Cell Res. Ther.*** **7** (2016), 28.

[12] K. Sadtler, A. Singh, M.T. Wolf, X. Wang, D.M. Pardoll and J.H. Elisseeff, Design, clinical translation and immunological response of biomaterials in regenerative medicine, ***Nat. Rev. Mater.*** **1** (2016), 16040. doi:10.1038/natrevmats.2016.40.

[13] M. von Köckritz-Blickwede, O.A. Chow and V. Nizet, Fetal calf serum contains heat-stable nucleases that degrade neutrophil extracellular traps, ***Blood.*** **114** (2009), 5245–5246. doi:10.1182/blood-2009-08-240713.

UNCORRECTED PROOF

Discussion

En tenant compte des caractéristiques d'un greffon vasculaire, les CML, les CE et l'environnement de ces deux types de cellules revêtent un caractère essentiel pour notre étude. Cette thèse est surtout consacrée à l'étude des CE (microenvironnement des cellules et technique d'ensemencement) afin d'optimiser la perméabilité du greffon. Pour cela, nous avons abandonné le coating à base de film de polyélectrolytes qui n'est pas naturel et n'est pas approuvé par les autorités de Santé. Nos recherches se sont concentrées sur un milieu naturel composé d'une ECM issue d'une source humaine saine, produite en grande quantité et facilement récupérable. De plus, la méthode enzymatique pour la digestion présente plusieurs avantages essentiels: une procédure simple (trypsine+sérum), facile (protocole simple et connu, 24 heures), et sans danger (condition physiologique sans ajout d'élément chimique). Les ECM isolées de la gelée par cette méthode enzymatique conservent un complexe d'ECM et divers facteurs de croissance. Ces propriétés des WJ-ECM permettent leur utilisation comme biomatériaux mais également comme supplément de milieu de culture. Nous avons testé l'utilisation de ce coating en substrat 2D *in vitro*, et nous allons l'utiliser en 3D *in vivo* dans les chapitres suivants. Cependant, bien que nous ayons prouvé l'existence de deux types de collagène dans les WJ-ECM, et que la digestion par la trypsine détruit la liaison entre les protéines mais ne détruit pas les protéines elles-mêmes, une étude qualitative et quantitative s'avère nécessaire pour caractériser tous les types d'ECM dans la solution.

Chapitre 3. Nouvelle stratégie

Publication N° 4 (soumise à *JACC*)

Résumé en français

« Retourner la chaussette »: le fait d'inverser les surfaces d'un substitut artériel change tout dans l'ingénierie tissulaire vasculaire

Pan DAN[1, 4], Emilie VELOT[1], Nguyen TRAN[2], Dominique DUMAS[1], Véronique DECOT[1], 3 & Patrick MENU[1]

L'un des plus grands enjeux dans l'ingénierie tissulaire vasculaire de petit diamètre est d'obtenir une intima entièrement couverte de cellules, ce qui est essentiel pour la perméabilité *in vitro*. Les stratégies existantes dans l'ingénierie tissulaire vasculaire (procédés des feuillets cellularisés ou méthode du scaffold-guidé) consistent toutes à ré-endothélialiser l'intima par injection d'une suspension de cellules dans la lumière tubulaire. La maturation des tissus en bioréacteurs est coûteuse. Elle nécessite une régulation de l'apport en oxygène et du transfert des éléments nutritifs dans le milieu de culture. En outre, les greffons cliniquement pertinents doivent présenter une longueur supérieure à 10 cm. Pour une telle longueur, il est difficile d'obtenir une couche uniforme de cellules endothéliales couvrant toute la surface du scaffold. Pour cela, les greffons vasculaires de grande longueur sont habituellement fabriqués pour recruter les cellules endothéliales de l'hôte et non une pré-endothelialisation de l'intima. Dans cette publication, nous avons introduit une technologie qui consiste à retourner la lumière des substituts artériels avant leur ensemencement par des cellules, et testé leurs capacités à promouvoir l'adhésion et la performance des cellules *in vivo*.

La technique pourrait être comparée au retournement d'une chaussette. Elle est réalisée sur les artères ombilicales humaines ou des carotides de lapin. Un fil chirurgical de 4-0 deux fois plus long que l'artère est passé dans la lumière avec l'aide d'un cathéter. Un nœud est fait à

l'extrémité de l'artère avec un peu de tissu pris dans le nœud. Avec l'aide d'une pince, le fil est tiré de l'autre côté et permet ainsi de retourner l'artère. Par cette approche, l'intima se retrouve à l'extérieur, et l'adventice constitue alors la paroi de la lumière du vaisseau. Cette technique nous permet donc d'exposer toute la longueur de l'intima aux milieux de culture de façon homogène.

Pour dé-endothélialiser le greffon, nous avons trempé les artères retournées dans de la trypsine. Par microscope confocal et analyse histologique, nous avons confirmé l'absence de cellules endothéliales. Les artères sont ensuite trempées dans la solution d'ECM issue de la gelée de Wharton (WJ-ECM) pour former un coating favorisant l'adhésion cellulaire. L'histologie et la microscopie Coherent Anti-Strokes Raman Scattering (CARS) ont montré qu'un coating se forme autour des artères.

Les artères retournées et couvertes de WJ-ECM sont trempées dans une suspension contenant des cellules souches mésenchymateuses (CSMs) pré-marquées au DiI pour un ensemencement cellulaire soumise à une rotation. Les images mosaïques de fluorescence ont montré qu'un nombre plus important de cellules a adhéré à la surface de l'artère retournée avec une distribution uniforme qu'avec la technique traditionnelle qui consiste à injecter une suspension cellulaire dans la lumière. De plus, pendant la maturation des cellules ensemencées, le niveau de pression partiel d'oxygène reste stable sur toute la surface extérieure. Alors que dans les artères non retournées avec des cellules injectées dans la lumière, le niveau d'oxygène diminue progressivement, se traduisant par une hypoxie délétère au développement cellulaire, responsable de l'apoptose des cellules.

Les artères retournées et ensemencées avec des CSMs sont retournées à nouveau pour retrouver leur structure anatomique. Les artères re-endothélialisées sont soumises au flux pour un pré-conditionnement in vitro, préalable à une implantation chez l'animal. La perméabilité de ces artères est ensuite testée *in vivo* par le remplacement d'une carotide dans un modèle de lapin.

Une fois le greffon implanté, la perméabilité est suivie par échographie doppler. Trois semaines après l'opération, nous avons pu observer que les artères ensemencées de CSMs par injection sont totalement thrombosées, et les artères ensemencées de CSMs avec la technique de retournement restent perméables. L'analyse histologique n'a montré aucun signe de calcification sur les artères préalablement retournées. La microscopie confocal a montré que les CSMs pré-marquées au DiI restaient dans la lumière. De plus, elles expriment des marqueurs endothéliaux CD31 et vWF.

Article type: original investigations

Title: How, by an inside-out method, intraluminal endothelialization of vascular scaffolds could be improved

Short title: Inside-out method for endothelialized scaffolds

Pan DAN, MD, PhD, [a, b], Emilie VELOT, PhD, [a,c], Nguyen TRAN, PhD, [d], Anna KEARNEY-SCHWARTZ, MD, PhD, [e], Dominique DUMAS, PhD, [a], Veronique DECOT, PharmD, PhD, [a, f], Patrick MENU, [a,c*]

[a] UMR 7365 CNRS, Ingénierie Moléculaire et Physiopathologie Articulaire, Université de Lorraine, 54505, Vandœuvre-lès-Nancy, France
[b] Department of thoracic and cardiovascular surgery, Zhongnan Hospital of Wuhan University, 430071, China
[c] Faculté de Pharmacie, Université de Lorraine, 54000, Nancy, France
[d] Ecole de chirurgie, Faculté de Medecine, Université de Lorraine, 54505, Vandœuvre-lès-Nancy, France
[e] Inserm U1116, Risque cardiovasculaire, rigidité - fibrose et hypercoagulabilité, Université de Lorraine, 54 505 Vandœuvre-lès-Nancy, France
[f] Unité de Thérapie Cellulaire et Tissulaire, CHRU de Nancy, 54500, Vandœuvre-lès-Nancy, France

Acknowledgements
We would like to thank the research federation 3209 BMCT (Nancy, France) and China scholarship council. We further thank M. Naceur Charif and M. Guillaume Groshenry for their valuable assistance. We would also like to thank Dr. Hervé Kempf for careful proof-reading of this manuscript.

Corresponding author: Prof. Patrick Menu,
[a] UMR 7365 CNRS, Ingénierie Moléculaire et Physiopathologie Articulaire, Université de Lorraine, Vandœuvre-lès-Nancy Cedex, 54505, France
E-mail: patrick.menu@univ-lorraine.fr

Objective This study presents an innovative inside-out method to cellularize the lumen of small-diameter vascular grafts.

Background The small-diameter vascular graft intraluminal cellularization is a real technological hurdle in vascular tissue engineering related to the difficulty to obtain a homogeneous intima layer resistant to blood flow.

Methods Enzymatically de-endothelialized arteries were coated with Wharton's jelly-derived extracellular matrix, then reversed to expose the lumen to outside that could be easily cellularized with human mesenchymal stem cells. Appropriate cellularization was next evaluated by mosaic confocal microscopy and histology, before being reversed again to return to their anatomic structure and implanted into rabbits to replace the carotid. Their *in vivo* patency was evaluated by Doppler echography during three weeks after implantation. The cell behavior was assessed by histology and confocal microscopy.

Results The inside-out method allowed to obtain a homogeneous mesenchymal stem cell layer into the lumen of arteries. A mosaic confocal microscopy revealed a uniform cell coverage of the scaffold related to a constant level of PO_2 measurement within the artery. Three weeks post-implantation, all the arteries treated with the inside-out method remained patent. No blood circulation was detected in the control arteries. Cell tracking and immunofluorescent imaging showed a blood flow resistant intima layer formed by mesenchymal stromal cells on the lumen and that the MSC begun to differentiate into endothelial-like cells.

Conclusion Compared to endoluminal cellularization method, this straightforward and innovative biotechnology offers a substantial advantage for the vascular grafts cellularization.

Keywords: vascular grafts, natural scaffolds, intraluminal endothelialization, mesenchymal stem cells, Wharton's jelly

Abbreviations:

hWJ: human Wharton's jelly

ECM : extracellular matrix

hMSC: human mesenchymal stem cells

HUA: human umbilical artery

CARS: coherent anti-Strokes Raman scattering

UC: umbilical cord

PBS: phosphate-buffered saline

DAPI: 4',6-diamidino-2-phenylindole

DiI: 1,1'-Dioctadecyl-3,3,3',3'-Tetramethylindocarbocyanine Perchlorate ('DiI'; DiIC18(3))

Introduction

Approximately 0.4 million coronary bypass surgery were performed annually in the United States of America(1). Even though autologous arteries and veins are still the most common options, unavailability of autologous vessels makes sometimes a situation for surgeons, the search of alternative grafts for coronary bypass surgery has never stopped(2). Artificial vascular grafts of large-caliber (>6 mm) are being routinely used in cardiovascular surgery including aortic replacement and arterial bypass procedures(3). These synthetic grafts have shown impressive long-term patency rate, durability and safety. Meanwhile, synthetic small-diameter grafts for large-scale clinical use have not yet been developed due to thrombus formation and compliance mismatch of those synthetic materials(4). Over the last two decades, tissue engineered small-diameter vessels with combination of biomaterials and cells emerged as a promising alternative(5), (6).

Existing strategies of tissue engineered small-diameter vessels involve cell-sheet technology and scaffold-guided methods. Cell-sheet technology involves rolling different cell sheets to form a tubular conduit that contains cell layers similar to native vessels, this concept has shown interesting results by several cases studies and ongoing clinical trials. However, the preparation of self-assembled cell sheets is a labor-intensive and time-consuming (>12 weeks) procedure, which makes it difficult for wide clinical applications(7). Scaffold-guide method aims to create living vascular conduit by seeding cells to different kind of tubular biomaterials such as synthetic, natural or decellularized extracellular matrix (ECM)(2). Among these biomaterials, decellularized vascular scaffolds are considered ideal candidates to fulfill the vascular biomechanical properties(8). By modifying the surface of these decellularized vascular scaffolds, it is even possible to recruit host cells *in vivo* to make a neo-endothelium. This is a promising approach which simplify tissue engineering by avoiding cell manipulation, however, one major issues remains: even though it has been proved with success in several animal

models(9), (10), the ability of these biomaterials to recruit human cells once implanted in human body cannot be answered since the regenerative response depends largely on animal models. Therefore, pre-cellularization of the vascular graft is a more reliable approach to supply a functional conduit ready to be implanted. Unlike large-diameter grafts that do not need cellularization, endothelium is critical for small-diameter grafts to maintain their patency(11).

Indeed, one of the huge challenges in small-diameter vascular tissue engineering is to obtain an intima fully covered by an endothelial cell layer. Current strategies of vascular tissue engineering are all based on an intimal re-endothelialization by injection of a cell suspension into the luminal compartment of tubular grafts. For further tissue maturation, these strategies usually needed months-long periods or costly bioreactors responsible for multiple limitations such as poor oxygen supply(12) inside the vascular graft, difficulty of mass and nutrition transfer from culture media(7)(13). Moreover, to be clinically relevant, a vascular scaffold should be longer than 10 cm, making difficult to obtain a uniform intraluminal endothelial cell layer(14), (15). Herewith, we introduced a reverse technology based on flipping over the lumen of arterial scaffolds, exposing outside the luminal surface for an optimal cellularization.

The coating of the luminal surface played also a crucial point in the success of the graft cellularization, and especially should be able to retain cell undergoing shear stress. As we recently described a human natural coating surface, effective for cell adhesion and fully biocompatible(16), we aimed to combine this coating with this reverse technology to cellularize this scaffold.

Human Wharton's jelly mesenchymal stem cells (hWJ-MSCs), chosen for their good availability and ability to differentiate into vascular cells were used as candidate cells to re-create an intimal layer. Furthermore, their hypo-immunogenicity allows their use in an allogeneic context(17).

In this study, the reversed vascular de-endothelialized arteries were coated with Wharton's jelly

ECM and seeded with hWJ-MSCs, before being reversed again. The attachment and resistance of cells to the flow prior to *in vivo* implantation validated this innovative technological approach. Compared to the conventional intra-luminal seeding method, the inside out technology improved the cell coverage of the scaffold, enhanced cell resistance to the blood flow and maintain scaffold patency at least 3 weeks after implantation *into* rabbits.

Methods

Cell culture. Human mesenchymal stem cells (hMSCs) were isolated from the Wharton's jelly of the umbilical cord as previously described(17).

Fresh human umbilical cords were obtained with approval (TCG/11/R/011) from Regional Maternity Nancy University Hospital. Wharton's jelly extracellular matrix (WJ-ECM) was isolated as described elsewhere(16). WJ-ECM (5 mg/ml) was used to form a coating on de-endothelialized grafts after a 12 h of incubation at 37°C followed by two washes with phosphate-buffered saline (PBS). De-endothelialized arteries without any coating were taken as control. The presence of the coating on the luminal surface was confirmed by histological staining and coherent anti-Strokes Raman scattering (CARS).

CARS is a chemically selective label-free imaging technique to evaluate lipid accumulation in CH-stretching spectral region and use to detect coating. The experimental setup is based on CARS laser picoEmerald from APE which delivers synchronous two pulses which are overlapped in time and space and sent into a scanning microscope (SP8-CARS Leica). In the CARS operation mode, the anti-Stokes signal is filtered for lipids (2841 cm-1) and SHG for collagen and detected in the backward direction (CARS 2000/BP filter cube, CARS and SHG) with a Hybrid detector for the lowest noise and large dynamic range.

Images for a scan field of 132.41 um x 132.41 um (0.259 um/pixel), 8 bits in depth were obtained with for an water immersion 40 fold objective (1.1 NA, HC PL IRAPO CORR) at the

surface, 512x512 pixels, at 400 Hz for each experiment, and stored as 104 z-stack image sequences (step size of 40.38 um along the z-axis, 0,398 um/voxel). Simple image processing as three-dimensional (3D), rendering was performed using the LAF AF version 2.7 software package (Leica).

De-endothelialization Grafts were treated with trypsin (0.025%, Bioblock, 1158-0626, France) at 37°C for 30 min to remove the endothelial cell layer. De-endothelialization was confirmed by confocal microscopy using endothelial specific markers CD31 and vWF.

Reverse technique for arterial scaffolds. Umbilical cord arteries of 12 cm or greater in length were isolated and preserved at -80°C(9). Rabbit carotid arteries were isolated from New Zealand White rabbits at a length of 4 to 5 cm. Preserved umbilical cord arteries and rabbit carotid arteries were washed twice with PBS. A 4-0 surgical suture of length that was twice longer than the arteries was passed through artery lumen with a catheter guide, one end of the artery was tied with a suture from the outside to fix arterial tissue in the suture knot. With a surgical forceps, the knotted end of the artery was pulled to make it pass through the lumen in order to reverse it. The knot was made in the middle of the suture to be maintained in the versed lumen for further reversing. Once reversed, the artery was soaked successively in three different solutions: one for de-endothelialization, one for scaffold coating and another with suspended cells for cell seeding.

Cellularization. Reversed arteries were soaked into a 15 ml conical tube containing 0.7×10^6 cells. Once cells were seeded, arteries were further rotated for 12 h to favor homogenization of cell adhesion. Arteries were then kept in static culture for cell maturation.

Before *in vivo* implantation, the cellularized artery was reversed once again with the suture previously left in the artery.

A commonly used technique to treat tubular graft was employed as a control technique. Control grafts were filled with trypsin by injection. After de-endothelialization, arteries were coated and

cellularized with hMSCs suspension containing 0.7×10^6 cells/ml injected into the lumen.

***In vitro* PO_2 detection within the lumen of arteries.** Arteries were cultured in cell culture medium (α-MEM supplemented with 10% FBS) in an incubator at 37°C. PO_2 in the middle and at one extremity (2 cm away from the borders) of 12 cm arteries was recorded every 12 h with an oximeter (Licox, France). The PO_2 was examined in 3 conditions for 5 days. Two situations in natural condition, where the oxygen detection probe was inserted in the de-endothelialized graft lumen, coated with WJ-ECM artery and seeded with hMSCs by injection. One situation in reversed condition, where the oxygen detection probe was attached to the external surface of an artery coated with WJ-ECM and seeded with hMSCs exposed to culture medium; then the reversed artery was re-reversed after 3 days and PO_2 in the lumen side was followed for another 6 days. Cell culture medium was changed every 3 days.

***In vitro* cell performance on differently treated scaffolds.** LIVE/DEAD® Cell Viability Assay (Sigma-Aldrich, 04511, France) was performed to evaluate the potential cell injury induced by the different techniques to coat scaffolds. Grafts seeded with hMSCs by injection or reverse technique were cultured for 5 days before undergoing to *in vitro* shear stress (20 dyn/cm^2) for 6 h. Grafts were washed twice with PBS and treated with LIVE/DEAD® Assay. Cells were observed by fluorescent microscopy (Leica DMI 3000B).

To show the homogenous repartition of cells on the luminal surface, cells labeled with DiI (Invitrogen, D282) were seeded into arteries and cultured for 5 days. Grafts were then fixed with 4% paraformaldehyde (Sigma-Aldrich, France). Grafts were next cut open longitudinally and observed by fluorescent microscopy to take large-scale mosaic images. Images of whole arteries that have been taken sequentially were reconstructed to demonstrate cell distribution along the entire grafts. Cell coverage density and uniformity of distribution were analyzed using Image J by examining the luminal surface stained with DAPI and DiI.

Pre-conditioning of cell-seeded grafts and cell retention under shear stress. Arteries with

cells on the luminal side were pre-conditioned *in vitro* with cell culture medium flow passing through the lumen. The fluid flow was generated by a peristaltic pump and the magnitude of flow was progressively increased to 20 dyn/cm^2 and lasted for 6 h(18). Cells were labeled with DiI for membrane and DRAQ5^{TM} (Abcam, 108410) for nuclei and observed by fluorescent microscopy before and after shear stress to assess cell resistance. Grafts prepared for animal experiments were all pre-conditioned for 6 h on the day before surgery.

Rabbit carotid artery replacement surgery. Animal experiments were carried out with guidelines for animal experiments established by the Ministry of National education, Higher education and Research in France (Project number: APAFIS#1123-2015070711576639v3). The protocol was approved by regional ethic committee (Permit number: C545475). New Zealand White rabbits (male, average weight 3 to 3.5 kg) were used for common carotid replacement surgery(9). Anesthesia was induced and maintained with isoflurane inhalation. After systemic heparin perfusion, the common carotid artery was isolated and clamped on the proximal and distal end. Four to five centimeters of carotid artery were excised. Grafts were implanted with end-to-end anastomose after resection of carotid artery. Rabbits received the antibiotic enrofloxacine (5 mg/kg) subcutaneously once post-operatively. For analgesia, buprenorphine (0.3 mg/kg) was administrated intravenously at the beginning and the end of surgery. Acetylsalicylic acid (20 mg/day) was given orally until sacrifice. The patency of implanted artery was monitored by Doppler echography every 3 days. After 3 weeks of implantation, animals were anesthetized as described above and grafts were removed for further examination. Animals were then euthanized with intravenous administration of pentobarbital sodium (1 ml/kg).

Histology and immunofluorescent examination of grafts. *In vitro* treated arteries, explanted grafts and native carotid arteries were fixed in 4% paraformaldehyde solution. For histological evaluation, samples were dehydrated in a series of graded ethanol solutions, following xylene

substitutes and then embedded in paraffin. Paraffin embedded tissue sections of 5 µm were stained with hematoxylin/eosin (HE), Masson's trichrome or von Kossa, to assess respectively cell distribution, vessel wall remodeling and presence of mineralization. Three weeks after implantation, endothelial differentiation of stem cells that were seeded before implantation was examined by immunofluorescent imaging. Arteries were opened longitudinally, allowing to access the luminal cells. Samples were incubated in 5% bovine serum albumin (BSA) in PBS for 1 h at room temperature before staining with primary antibodies including CD31 (Dako), von Willebrand factor (vWF) (Dako) and vascular endothelial-cadherin (Cell Signaling), diluted in 5% BSA-PBS. After an overnight incubation at 4°C, corresponding secondary antibodies were used at a dilution of 1: 200 for 1 h at room temperature. All samples were imaged using a Leica SP5 confocal microscope.

Statistical analysis

Results are presented as mean ± standard deviation. Statistical significance was determined by ANOVA followed by a t-test between each group; $p < 0.05$ were considered as statistically significant.

Results and discussion

The luminal surface endothelialization of a tissue engineered graft is the grail to ensure the vascular patency. Different approaches have been developed during the last years to reinforce the anti-thrombogenic property of the graft (for more details, see review(19)). However, the spontaneous endothelialization is limited in human, contrary to results obtains in animals, without understanding the reasons for this difference. It is hence important to propose to surgeons, small diameter natural vascular graft already endothelialized. Now the cellularization of the vascular inner surface with functional endothelial cells is really impossible, because weak cell behavior. This work proposes an original approach, never been described, based on a

reverse technic that allows exposing the vascular luminal surface to the outside. By this way, it becomes easier to obtain a homogenous cells seeding.

An important source of human small diameter arteries could be valorized from umbilical cords. These human de-endothelialized arteries were used as vascular matrix. To avoid graft rejection, these arteries were cellularized with mesenchymal stem cells.

To validate the soundness of the reverse technic efficacy, and to make sure that cells were suitably seeded on the luminal surface, functional and able to resist to physiological shear stress, the grafts were implanted in the animal. The choice of rabbit, the bypass procedure and the extensive arterial injury (arteriotomy and anastomosis) were previously set(9). The use of non immunodeficient rabbits which increase human cellularized graft reject risks represents another challenge for xenograft evaluations. The carotid has been chosen, as it is relative close to umbilical artery diameter and the implantation site easy to access for the blood flow follows. Although some designed conditions increased the failure probability, they are closed to real surgical situations.

Setting of the reverse technique. The human umbilical arteries of 10 cm length were easily reversed (Fig. 1A and Online Video 1). This technique thus makes the luminal surface on the outside of the vessel and the adventitia inside of the vessel (Fig. 1B-D). Once reversed, the luminal surface is homogenous exposed to solution for treatment.

De-endothelialization and surface modification of reversed arteries. Reversed arteries were then soaked in trypsin solution for complete de-endothelialization because of full contact with the enzyme. The de-endothelialization was confirmed by histological analysis and the absence of detection of CD31 and vWF by confocal microscopy (Online Fig. 1).

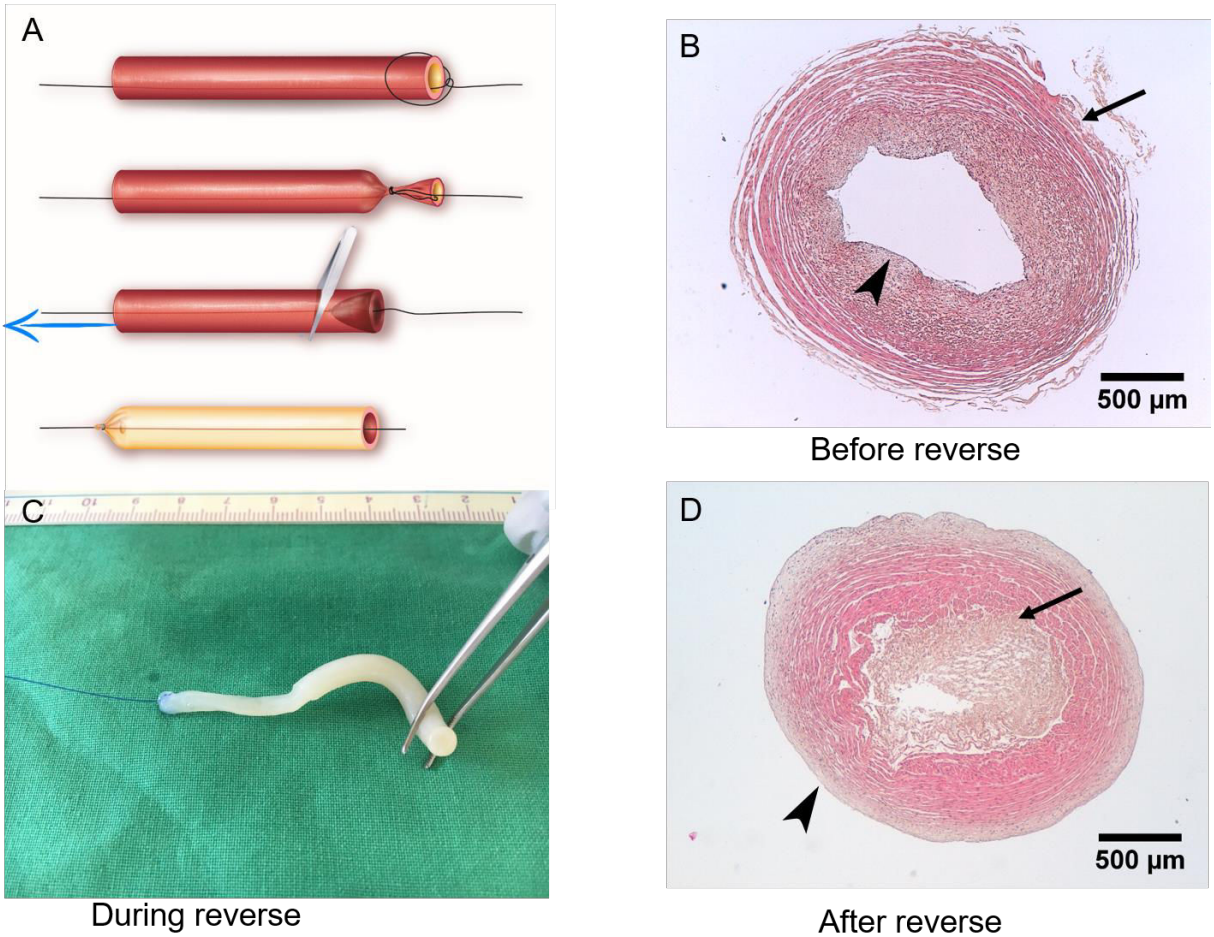

Figure 1. Inside-out technique to reverse arterial scaffolds. (A) Schematic diagram showing the reverse technique. A surgical suture was passed through the lumen and tied at one end of the artery, then the artery was pulled from the other end to turn the inside on the outside. (B) Histological section before reversing arteries showing the original structure of an artery with intima inside (arrowhead) and adventitia outside (arrow). (C) Picture showing the vessel during the reverse technique. (D) Histological section of an artery after reversal, the intima (arrowhead) was turned into the outside and the adventitia (arrow) was turned into the inside.

To improve cell adherence, de-endothelialized scaffolds were then soaked in complex extracellular matrix of Wharton's jelly (WJ-ECM) to form a coating. The choice of this coating has been guided by a recent study showing the superiority of this approach(16). The presence of WJ-ECM coating was observed by coherent anti-Strokes Raman scattering (CARS) microscopy (Fig. 2A) and confirmed by histological analysis showing a uniform layer on the de-endothelialized scaffold with a thickness of 17.20 ± 2.47 µm (Fig. 2B).

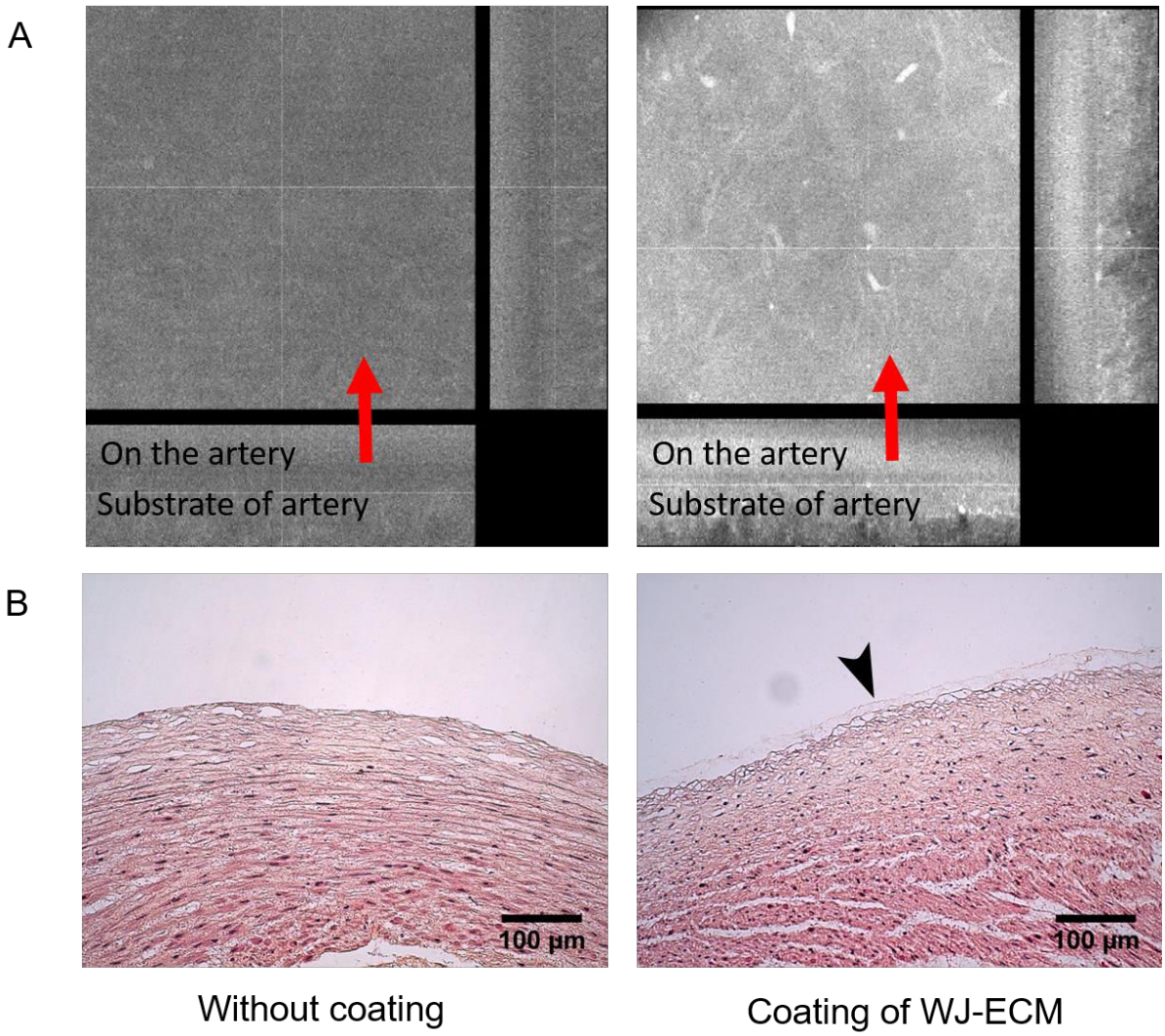

Figure 2. Wharton's jelly extracellular matrix (WJ-ECM) coating on reversed umbilical arteries. (A) Detection of a lipid layer on de-endothelialized umbilical arteries after soaking in WJ-ECM solution for 12 h by coherent anti-Strokes Raman scattering microscopy. (B) Representative histologic section showing a uniform layer of 17.2 ± 2.47 μm on reversed and de-endothelialized arteries.

Pre-endothelialization on reversed arteries with hMSCs. Once coated with WJ-ECM, arteries were seeded with hMSCs. To evaluate cell circumferential attachment, histological analyses of cross sections were performed, showing a full coverage of cells on WJ-ECM coated scaffolds (Fig. 3A). The large-scale mosaic images showed that, even on un-coated arteries, the reverse technique significantly ameliorated cell attachment throughout the surface of the 10 cm

length (Fig. 3B) than the control. By injecting cells into the lumen, a uniform cell distribution was barely achieved (43.2 ± 10.8% of coverage on uncoated scaffolds and 47.5 ± 16.9% on WJ-ECM coated scaffolds), whereas the cell coverage was significantly increased on reversed arteries (73.4 ± 4.9% on uncoated scaffolds and 79.9 ± 6.8 % on WJ-ECM coated scaffolds, respectively; Fig. 3C, n=3). All current endothelialization methods in vascular tissue engineering use injection of cell suspension into the lumen with further rotation. However, the limit of injection relate to the difficulty of achieving a uniform cell layer, because cells in suspension in the small vascular cavity can hardly move to distribute homogenously with rotation(20). Moreover too long period of rotation would lead to cell death because oxygen was progressively consumed in the sealed lumen. In the reverse artery situation, the cells were soaked in a large volume of medium for 12 h of rotation, with a constant oxygen level, leading to a better cell distribution.

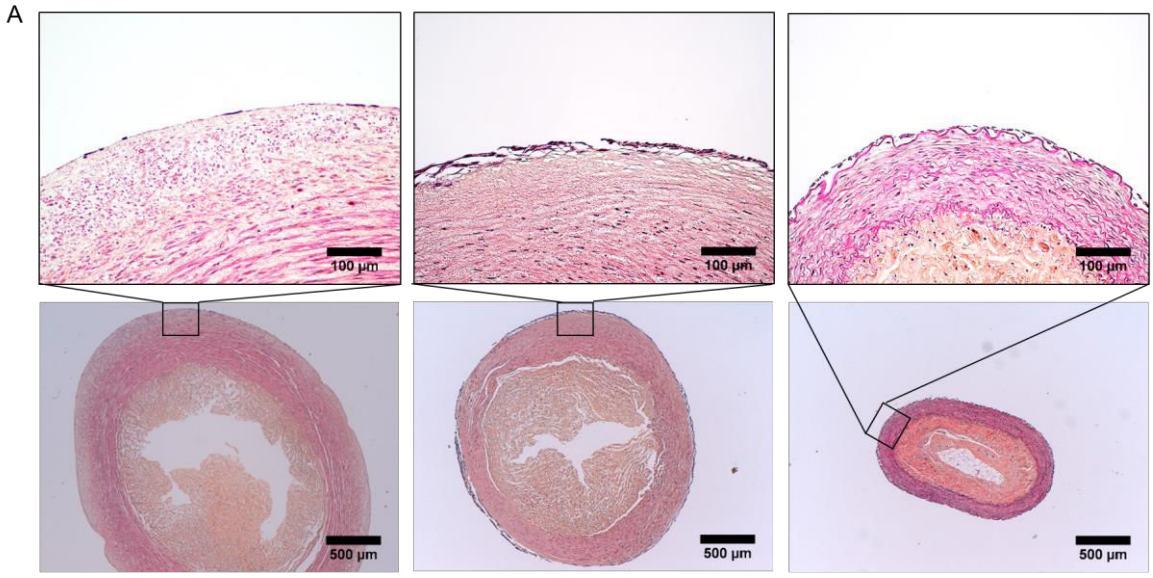

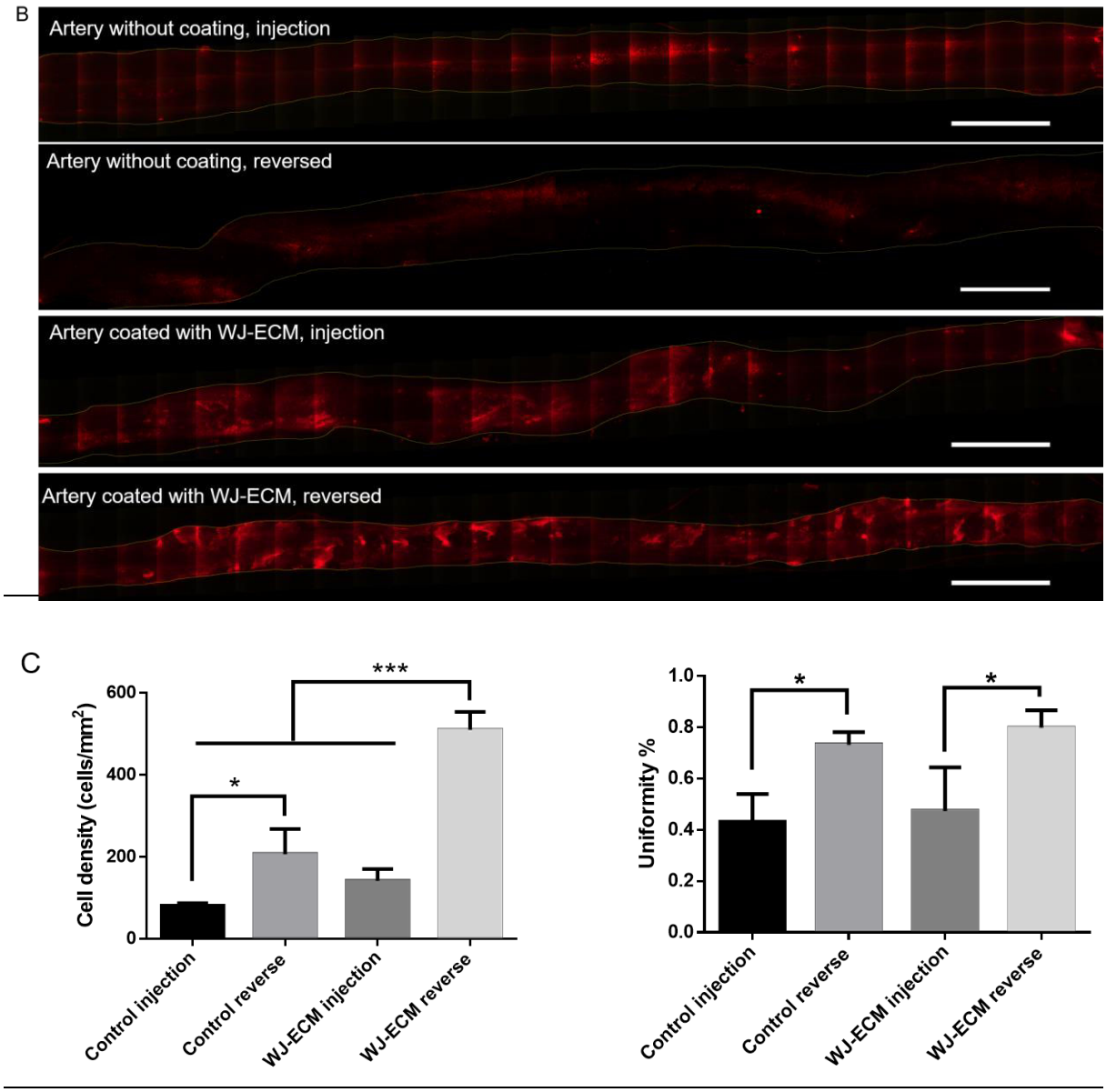

Figure 3. Evaluation of cell attachment after seeding on differently treated arteries. Histological analysis showing a full circumferential attachment on both human umbilical arteries and rabbit carotids coated with Wharton's jelly extracellular matrix (WJ-ECM). (B) Large-scale mosaic images of cell distribution in arteries. Arteries were opened longitudinally and DiI-labeled human mesenchymal stem cells (hMSCs) observed under fluorescent microscopy. Artery outlines were marked in yellow. Scale bar, 1 cm. (C) Quantitative analysis of cell density and uniformity of cell distribution in arteries (n = 3), * indicate p<0,05, *** indicate p<0,001. Results are presented as mean +/- SD.

Increased cell attachment and coverage is related to a better access to oxygen supply. Once

cell attachment was achieved, arteries were cultured *in vitro* for 5 days. As a better endothelialization was observed on reversed scaffolds, we hypothesized that this may be due to a better access to both oxygen and nutrition supplies for cells seeded on the outer surface. To confirm this hypothesis, the local partial pressure of oxygen (PO_2) was examined in reversed scaffolds compared to conventional scaffolds seeded or not with cells (Fig. 4). In the arteries devoid of living cells, PO_2 in the lumen remained stable for 5 days (148.4 ± 0.9 mmHg). When measured in arteries with cells growing in the lumen, PO_2 decreased within cell culture due to oxygen consumption and poor oxygen exchange with the culture medium (from 122.2 ± 0.8 mmHg to 37.3 ± 2.2 mmHg at border and from 114.6 ± 4.1 mmHg to 33.1 ± 2.6 mmHg in the middle; $p<0.05$). Regarding reversed arteries with cells cultured in direct contact with the culture medium, PO_2 persisted at a relatively higher level during several days of culture (165.1 ± 3.1 mmHg). As expected, when these arteries were then reversed back to put the seeded cells in the lumen, PO_2 gradually decreased after 2 days to a low level (66.9 ± 13.5 mmHg at border and 60.2 ± 9.6 mmHg in the middle) (Fig. 4). Most studies in vascular tissue engineering build-up very short length vessels, even though these studies provide a large amount of promising alternatives(8), (21), (22), (23). Yet clinically applicable vessels for coronary bypass grafts should be longer than 10 cm. But long vascular graft studies are all cell-free, based on an autologous host cell recruitment(10), (15), (24). The hurdle of creating great length small diameter graft with pre-endothelialization is the limited oxygen supply in the lumen to support cell viability for a long period. The oxygen exchange for short vascular grafts would be relatively easy to achieve without *in vitro* perfusion. Whereas for a long length, a constant medium flow needed for long period, could generate a risk of pulling out the un-sealed cells. Here we showed the reversed arteries can expose all cells on the luminal surface to the same high level of oxygen and medium nutrition for *in vitro* culture. In this study, once the cellularized arteries were reversed again, the intra-luminal PO_2 started to decrease, but the cells

were already confluent and the graft was sheared before being implanted.

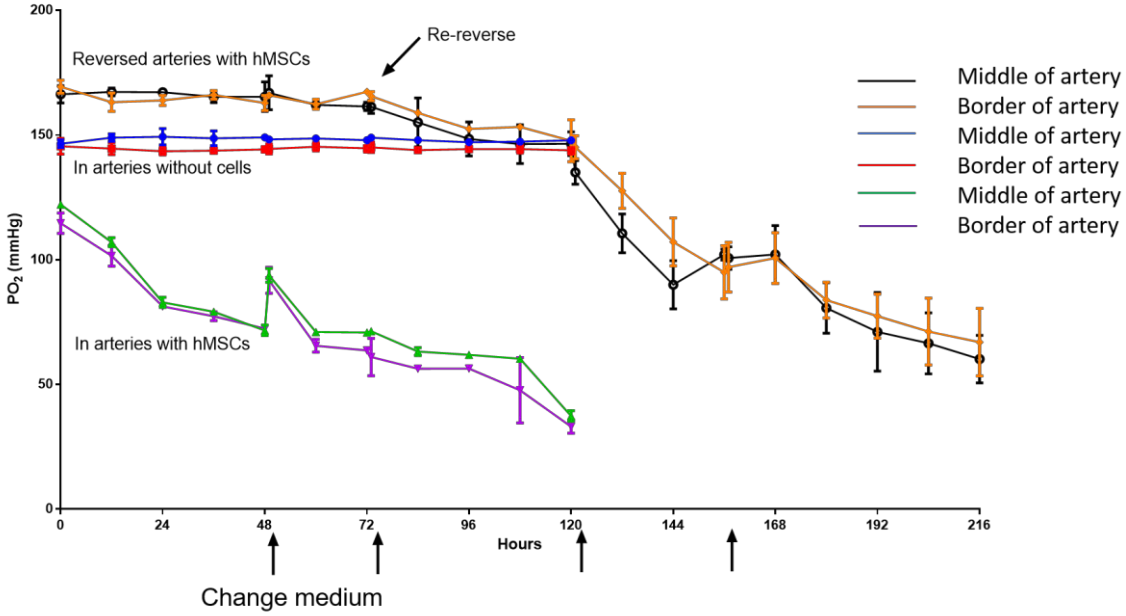

Figure 4. Detection of oxygen pressure (PO_2) in natural or reversed arteries seeded or not with human mesenchymal stem cells (hMSCs). The PO_2 in the lumen stayed stable in arteries without living cells (blue line for the PO_2 measured at the border and red line the one measured at the middle of the arteries). The PO_2 decreased progressively in arteries with living cells grown in the lumen (green line for border and crystal line for middle). On reversed arteries, oxygen remains stable at a higher level till being reversed, then oxygen decreased progressively to a similar level of the one with cells cultured in the lumen (orange line for the border and black line for the middle). Each condition was measured in 3 independent experiments (n = 3).

Cells grown on reversed scaffold show better resistance to a mechanical stress. As the reverse technique produced better results for cell attachment and oxygen supply than cell intra-luminal injection, the following studies focus on coated and non-coated re-endothelialized reversed arteries. The viability and resistance of intraluminal cells were assessed after *in vitro* 6 hours of physiological shear stress (20 dyn/cm^2) for pre-conditioning(18). Cell resistance was enhanced on WJ-ECM coated arteries compared to un-coated arteries as observed by histological analysis (Fig. 5 A and B). This result was confirmed by the detection of DiI labeled MSCs after shear stress. The use of the LIVE/DEAD® Assay showed that the remaining cells

were viable (Fig. 5C).

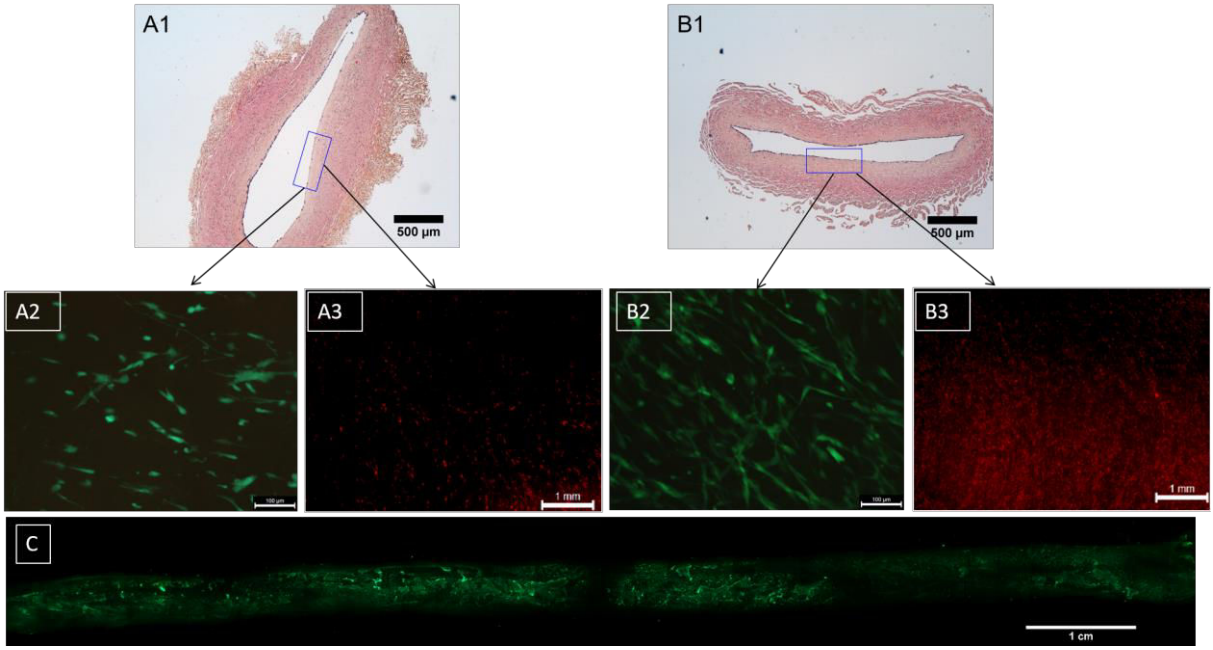

Figure 5. Evaluation of cell retention after shear stress on either uncoated reversed arteries (A) or Wharton's jelly extracellular matrix (WJ-ECM) coated reversed arteries (B). (A1) and (B1) Histological analysis after hematoxylin / eosin staining showing a thin intima layer formed on the lumen surface. (A2) and (B2) Cell coverage evaluated by the detection of DiI labelled human mesenchymal stem cells (hMSCs) after shear stress on coated or uncoated arteries. (A3) and (B3) Evaluation of cell viability on coated or uncoated arteries using LIVE/DEAD® Assay after shear stress. (C) Living hMSCs covering all the artery length detected by confocal mosaic microscopy.

The cellularized reversed scaffold shows a better *in vivo* patency. Two origins of vessels were chosen to assess their *in vivo* patency after intima formation: one autologous (rabbit carotid) and another of human origin (human umbilical cord artery) implanted in a rabbit carotid replacement model, these vessels were reversed, de-endothelialized, coated, cellularized with hMSCs, re-reversed and underwent shear stress. The confocal microscopy showed a full coverage of hMSCs on the luminal surface (Fig. 6A) before implantation. A blood flow was observed in the artery immediately after implantation, and 3 weeks after, just before euthanasia (Fig. 6B and C). The patency was verified by Doppler echography showing a blood flow at the

implantation site (Fig. 6D, E and Online Video 2). At the end of the experiment, both rabbit carotids and human UC arteries treated by the reverse technique remained patent (Table 1). No sign of inflammation or rejection was observed on the grafts (Fig. 6C). The explanted grafts did not show any adhering blood cells on the vascular wall (Fig. 6F). On the other hand, human UC arteries that have been re-endothelialized by injecting cell suspension were all thrombosed one week post-implantation.

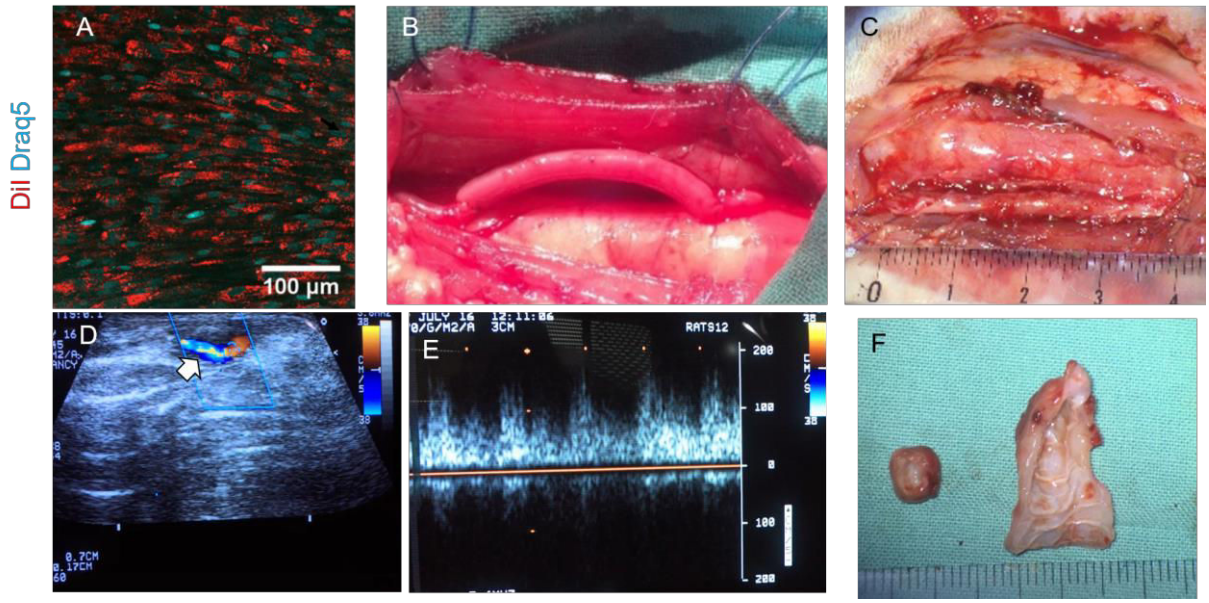

Figure 6. (A) DiI / DRAQ5™ labelled human mesenchymal stem cells (hMSCs) on coated arteries pre-conditioned by shear stress before implantation into rabbits. (B) and (C) Blood flow observed in the artery immediately after implantation, and 3 weeks after, just before euthanasia. (D) and (E) Doppler echography showing blood flow at the implantation site. (F) Explanted grafts cut longitudinally to show the absence of thrombus 3 weeks after implantation.

Table 1: Patency of implanted grafts at the end of experiment (3 weeks)

Protocol to cellularize grafts	Patency
Injection (umbilical arteries) + WJ-ECM + hMSCs	0/5
Reverse technique (umbilical arteries) + WJ-ECM + hMSCs	5/5
Reverse technique (rabbit carotids) + WJ-ECM+ hMSCs	3/3

Histological analyses were performed to further characterize explanted grafts (Fig. 7). H&E and Masson's trichrome stainings showed the presence of a thrombus in injection-mediated arteries whereas in reversed arteries, the lumen remained intact with a complete endothelium. Von Kossa staining showed calcification within the thrombus, whereas in the patent grafts, no calcification was observed in the vessel wall.

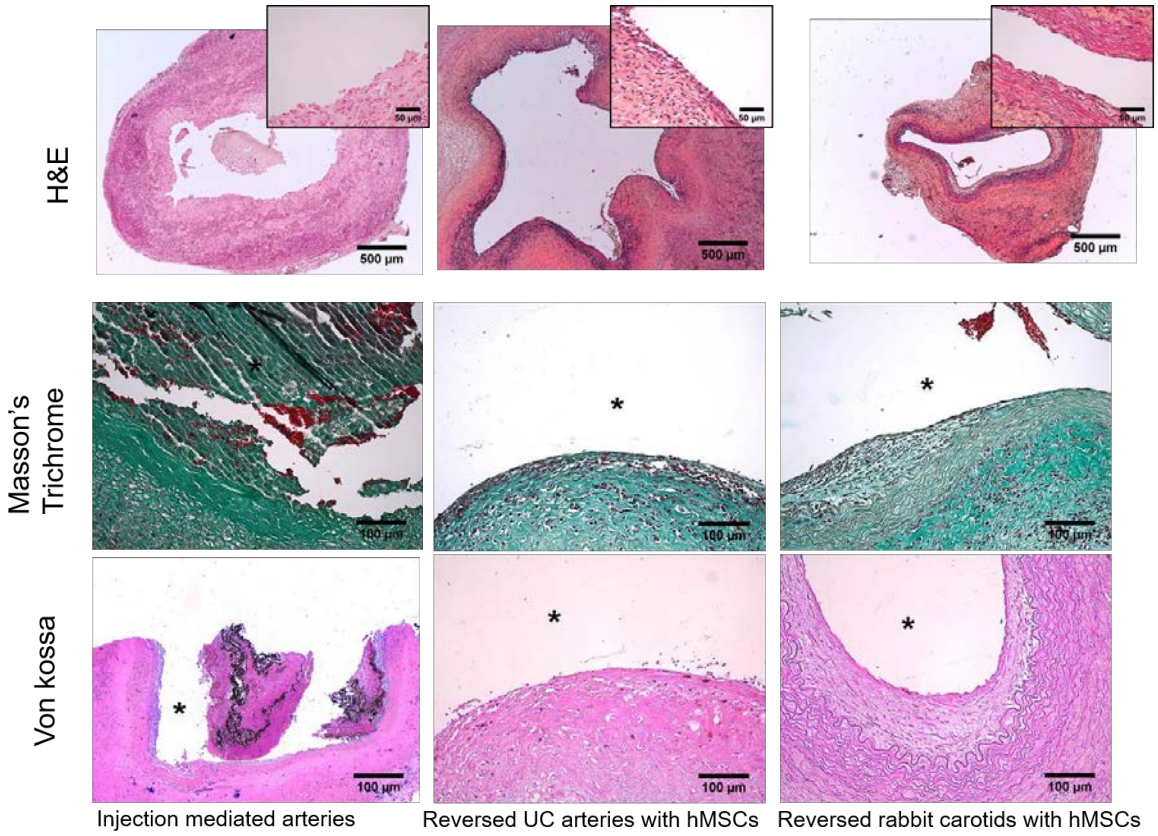

Figure 7. Histological analyses performed to further characterize explanted grafts. (A) and (B) Visualization of a thrombus in the lumen of cell injected arteries by hematoxylin / eosin and Masson's trichrome stainings. No thrombus was detected in cellularized reversed arteries either coated or not. (C) Von Kossa staining showing calcification within the thrombus, whereas in the patent grafts, no calcification was observed in the vessel wall.

We next analyzed if DiI labelled human WJ-MSCs were still present 3 weeks after being implanted into the animal model (Fig. 8). We noticed that, i) in spite of the flow, coated cells formed a homogenous luminal layer, ii) the hMSCs exhibited an endothelial-like phenotype confirmed by the expression of endothelial specific markers CD31 and vWF.

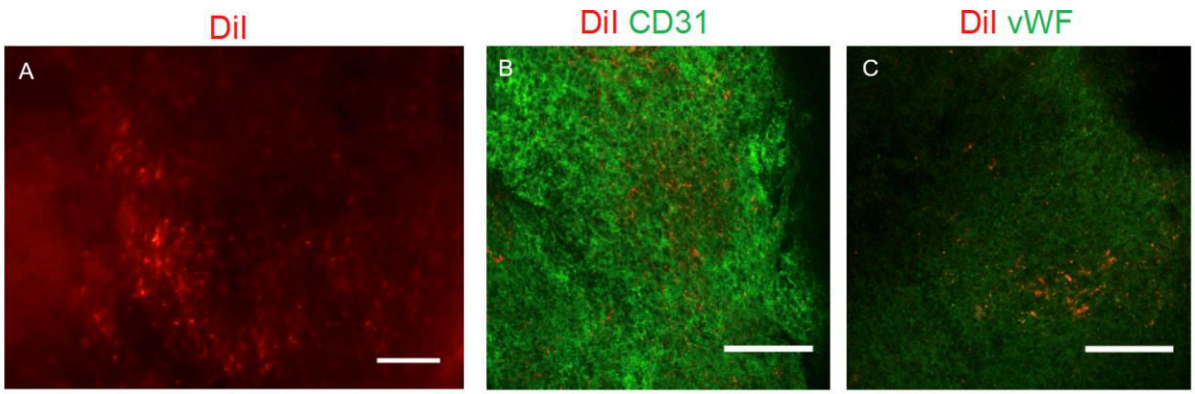

Figure 8. (A) Detection of DiI labelled human mesenchymal stem cells (hMSCs) (red) 3 weeks after being implanted into the animal model. (B) Expression of endothelial markers CD31 (green) and (C) von Willebrand factor (green) detected on the intima layer of the cellularized reversed arteries.

All these results present a major step forward for endothelialization research in the vascular field and suggested that the reverse-mediated procedure allows cells to adhere, proliferate and differentiate *in vivo*.

Conclusions

Obtaining a functional intimal layer remains a challenge in vascular tissue engineering. In this study, we described an innovative reverse technique, which allows optimal cellularization for intima formation. Our results showed that this technique is useful for more than 10 cm vascular scaffold and that once cellularized, the scaffold remains patent at least 3 weeks after being implanted in a rabbit carotid replacement model. Moreover, the pre-seeded hMSCs were still present after these 3 weeks of implantation and start their differentiation towards an endothelial-like phenotype. Taken together, all these results showed that the reverse technique is applicable to tissue-engineered small diameter vascular grafts and may be combined with different surface modification. Once flipped inside-out, the intima surface is entirely exposed to allow a full de-endothelialization or decellularization, a controlled surface modification, a homogeneous cell seeding, etc. which finally restores reliably a cellularized intima surface. As such, these

available engineered vessels could be next stored in liquid nitrogen to be part of a vessel bank. This straightforward technology could also be applied to other vascular sources such as saphenous vein or synthetic vascular grafts.

COMPETING FINANCIAL INTERESTS

The authors declare no competing financial interests.

Perspectives:

Competency in medical knowledge: Finding an appropriate method for effective cellularization is mandatory to prevent small-caliber graft failure, maintain patency and contractility following in vivo implantation. To achieve this goal, the inside-out method proposed in this work shows a clear advantage upon intra-luminal injection method.

Translational outlook 1: The vascular graft obtained with this method present a homogenous intima layer, confirming cell adherence. These cells underwent shear stress before implantation in an animal model. Doppler echography confirms the patency of the cellularized graft. After 3 weeks, the implanted vascular graft showed the absence of thrombus and the presence of a viable homogenous seeded cell layer.

Translational outlook 2: The aim of this work is to propose to surgeons a pre-cellularized vascular graft based on widely available human umbilical artery scaffold coated with allogeneic cells with low rejection risk, i.e., human mesenchymal stem cells. In the future, these grafts could be used to be a part of a cellularized vascular graft tissue bank.

The cellularization of the luminal surface by this method allows the following significant improves: biomimicking vascular designs and/or relatively long production times (typically several months).

References

1. Mozaffarian D, Benjamin EJ, Go AS, et al. Heart Disease and Stroke Statistics-2016 Update: A Report From the American Heart Association. Circulation 2016;133:e38–e360.

2. Seifu DG, Purnama A, Mequanint K, Mantovani D. Small-diameter vascular tissue engineering. Nat. Rev. Cardiol. 2013;10:410–421.

3. Ravi S, Chaikof EL. Biomaterials for vascular tissue engineering. Regen. Med. 2010;5:107.

4. Sugiura T, Tara S, Nakayama H, et al. Novel Bioresorbable Vascular Graft With Sponge-Type Scaffold as a Small-Diameter Arterial Graft. Ann. Thorac. Surg. 2016;102:720–727.

5. L'heureux N, Pâquet S, Labbé R, Germain L, Auger FA. A completely biological tissue-engineered human blood vessel. FASEB J. 1998;12:47–56.

6. L'Heureux N, Dusserre N, Konig G, et al. Human tissue-engineered blood vessels for adult arterial revascularization. Nat. Med. 2006;12:361–365.

7. Huang AH, Niklason LE. Engineering of arteries in vitro. Cell. Mol. Life Sci. CMLS 2014;71:2103–2118.

8. Quint C, Kondo Y, Manson RJ, Lawson JH, Dardik A, Niklason LE. Decellularized tissue-engineered blood vessel as an arterial conduit. Proc. Natl. Acad. Sci. 2011;108:9214–9219.

9. Kerdjoudj H, Berthelemy N, Rinckenbach S, et al. Small Vessel Replacement by Human Umbilical Arteries With Polyelectrolyte Film-Treated ArteriesIn Vivo Behavior. J. Am. Coll. Cardiol. 2008;52:1589–1597.

10. Koobatian MT, Row S, Smith Jr RJ, Koenigsknecht C, Andreadis ST, Swartz DD. Successful endothelialization and remodeling of a cell-free small-diameter arterial graft in a large animal model. Biomaterials 2016;76:344–358.

11. Cahill PA, Redmond EM. Vascular endothelium - Gatekeeper of vessel health. Atherosclerosis 2016;248:97–109.

12. Wion D, Christen T, Barbier EL, Coles JA. PO2 Matters in Stem Cell Culture. Cell Stem Cell 2009;5:242–243.

13. Dahan N, Sarig U, Bronshtein T, et al. Dynamic Autologous Reendothelialization of Small-Caliber Arterial Extracellular Matrix: A Preclinical Large Animal Study. Tissue Eng. Part A 2017;23:69–79.

14. Mohebbi-Kalhori D, Rukhlova M, Ajji A, Bureau M, Moreno MJ. A novel automated cell-seeding device for tissue engineering of tubular scaffolds: design and functional validation. J. Tissue Eng. Regen. Med. 2012;6:710–720.

15. Mahara A, Somekawa S, Kobayashi N, et al. Tissue-engineered acellular small diameter long-bypass grafts with neointima-inducing activity. Biomaterials 2015;58:54–62.

16. Dan P, Velot É, Francius G, Menu P, Decot V. Human-derived extracellular matrix from Wharton's jelly: An untapped substrate to build up a standardized and homogeneous coating

for vascular engineering. Acta Biomater. 2016.

17. El Omar R, Xiong Y, Dostert G, et al. Immunomodulation of endothelial differentiated mesenchymal stromal cells: impact on T and NK cells. Immunol. Cell Biol. 2015.

18. Inoguchi H, Tanaka T, Maehara Y, Matsuda T. The effect of gradually graded shear stress on the morphological integrity of a huvec-seeded compliant small-diameter vascular graft. Biomaterials 2007;28:486–495.

19. Krawiec JT, Vorp DA. Adult stem cell-based tissue engineered blood vessels: A review. Biomaterials 2012;33:3388–3400.

20. Fercana G, Bowser D, Portilla M, et al. Platform Technologies for Decellularization, Tunic-Specific Cell Seeding, and In Vitro Conditioning of Extended Length, Small Diameter Vascular Grafts. Tissue Eng. Part C Methods 2014;20:1016–1027.

21. De Valence S, Tille J-C, Mugnai D, et al. Long term performance of polycaprolactone vascular grafts in a rat abdominal aorta replacement model. Biomaterials 2012;33:38–47.

22. Ahmed M, Hamilton G, Seifalian AM. The performance of a small-calibre graft for vascular reconstructions in a senescent sheep model. Biomaterials 2014;35:9033–9040.

23. McAllister TN, Maruszewski M, Garrido SA, et al. Effectiveness of haemodialysis access with an autologous tissue-engineered vascular graft: a multicentre cohort study. Lancet Lond. Engl. 2009;373:1440–1446.

24. Fukunishi T, Best CA, Sugiura T, et al. Tissue-Engineered Small Diameter Arterial Vascular Grafts from Cell-Free Nanofiber PCL/Chitosan Scaffolds in a Sheep Model. PloS One 2016;11:e0158555.

Online video 1:

Reverse technique with human umbilical artery: A 4-0 surgical suture of length that was twice longer than the arteries was passed through artery lumen with a catheter guide, one end of the artery was tied with a suture from the outside to fix arterial tissue in the suture knot. With a surgical forceps, the knotted end of the artery was pulled to make it pass through the lumen in order to reverse it. The knot was made in the middle of the suture to be maintained in the versed lumen for further reversing. The reversed artery was now ready for treatment and be endothelialized with hMSCs. Once cellularized, the artery can be easily re-reversed with the residual suture.

Online Video 2: Echography on implanted grafts.

This video demonstrated the patency of implanted grafts (reversed arteries with coating of WJ-ECM and hMSCs). 3 weeks after implantation, compared to control side (native rabbit carotid, no operated), blood flow can be observed in the implanted side.

Chapitre 4. Expérimentation animale

Travail en cours de rédaction

Nous avons montré dans le chapitre précèdent que la technique de retournement est compatible pour deux types d'artères (artères ombilicales et carotides du lapin) avec le coating de WJ-ECM. Ce chapitre envisage de compléter l'idée de retournement avec un autre coating et une stratégie évoluée sur le modèle d'animal.

1. Coating conventionnel, coating naturel et coating natif

Compte tenu du fait que le collagène a été étudié en 2D comme un contrôle positif dans le chapitre 2, nous avons aussi étudié son rôle en comparaison avec la WJ-ECM sur un substitut 3D. De plus, la WJ-ECM est issue de la gelée qui se trouve dans le cordon ombilical autour des vaisseaux. Aussi, les artères isolées sont toujours recouvertes d'une couche de gelée (**Fig. 1**). Nous avons donc eu l'idée d'utiliser la gelée native (WJ natif) autour des artères comme support des cellules. Il suffit alors d'ensemencer les cellules directement à l'extérieur des artères ombilicales et de les retourner une seule fois juste avant de les pré-conditionner et implanter *in vivo.*

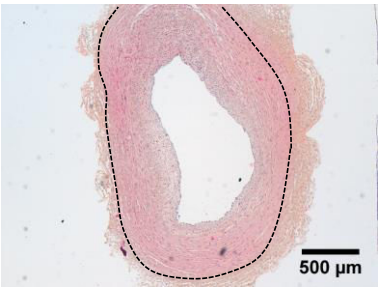

Fig. 1 La gelée native autour de l'artère ombilicale. Une couche de gelée (brune) distinguée par une ligne de pointillés est à l'extérieur de l'artère.

Pour cela, nous avons ensemencé les CSM sur 4 différentes surfaces d'artères: surface dé-endothélialisée comme contrôle négatif, collagène comme contrôle positif, coating de WJ-ECM

et coating natif directement sur l'extérieur. Toutes les 3 surfaces (collagène, WJ-ECM, et WJ natif) sont favorables pour l'adhésion des CSM. Et ces trois surfaces ont joué un rôle positif dans la résistance des cellules au flux **(Fig. 2)**. Il a été montré que le substitut vasculaire recouvert de collagène ou autre ECM peut renforcer la résistance cellulaire au flux[1], [2], nos résultats ici ont aussi prouvé que plus de cellules cultivées sur collagène sont restées après 6 heures de cisaillement par rapport à contrôle. De plus, le substitut couvert de WJ-ECM en 2D a montré un meilleur effet sur la résistance cellulaire (chapitre 2). Ici, la surface de WJ-ECM en 3D, ainsi que la WJ-natif ont montré un effet encore supérieur à celui du collagène. Ces résultats nous permettent donc de conclure que les artères couvertes de WJ-ECM ou de WJ-natif peuvent conduire à des greffons vasculaires entièrement cellularisés.

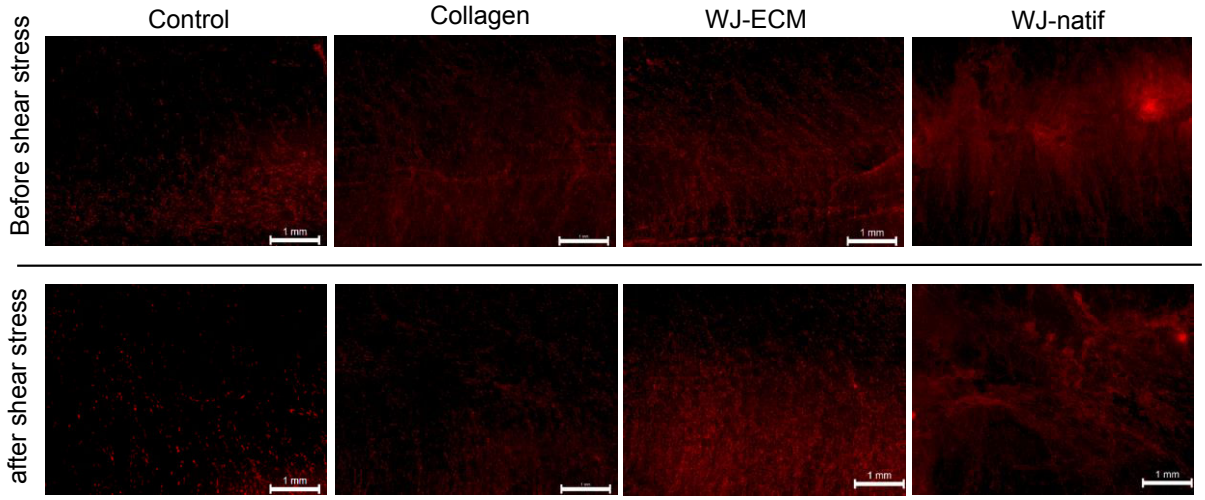

Fig. 2 Comportement cellulaire en statique et dynamique sur 4 différentes surfaces. Les cellules marquées de DiI sont ensemencées à l'extérieur des artères (artère retournée pour contrôle, collagène et WJ-ECM). Après 5 jours de culture en statique, les artères sont retournées de nouveau pour retrouver les cellules dans la lumière afin de les soumettre à la culture dynamique pendant 6 heures. Images prises au microscope fluorescent (Leica, France)

2. Différentiation endothéliale des CSM sur le coating en 3D

Nous avons montré dans le chapitre 2 que les CSM cultivées sur la WJ-ECM peuvent se différencier vers des CE sous les stimulations d'un ensemble de facteurs de croissance (EGM-2™). Cependant, la différenciation vasculaire des cellules en 3D est plus difficile à atteindre en

raison l'insuffisance de facteurs de croissance fournis aux cellules situées au centre d'un substitut tubulaire[3], [4]. Nous avons essayé de différencier les CSM cultivées en 3D dans les artères ombilicales couvertes de WJ-ECM. Les CSM sont ensemencées à la densité de 3000 cellules/cm^2, soit sur des artères retournées, soit par injection dans la lumière. 30 jours après culture dans EGM-2^{TM,} les artères sont évaluées par microscopie confocale en testant l'expression des marqueurs endothéliaux (CD31 et VE-Cadherin). Il est montré dans la **Fig. 3** que les CSM ensemencées sur des artères retournées ont exprimé des marqueurs endothéliaux plus forts que celles ensemencées par injection. Nous supposons que pendant 30 jours de culture, les cellules cultivées à l'extérieur des vaisseaux ont acquis plus d' éléments pour la différenciation, où les cellules dans la lumière n'ont pas reçu suffisamment de facteurs de croissance pour la différenciation endothéliale.

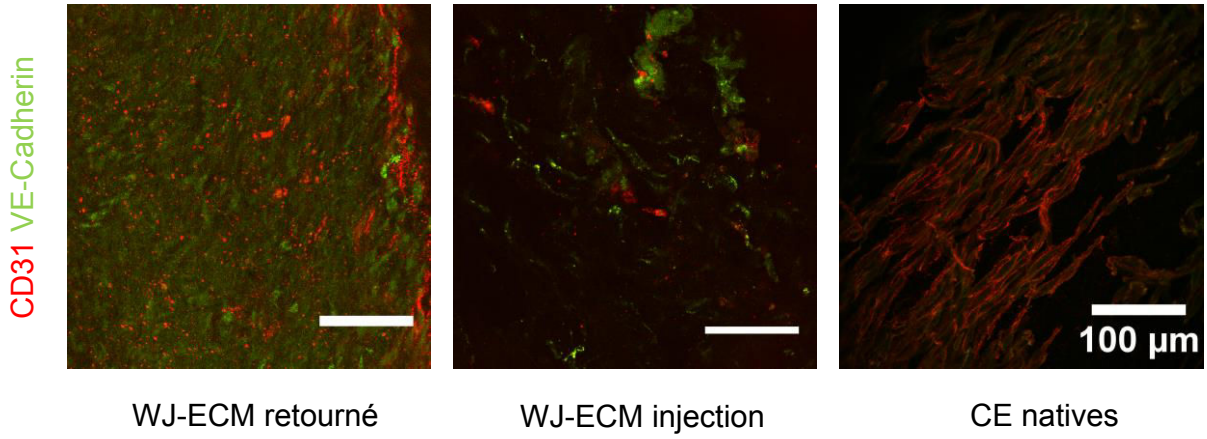

Fig.3 Différenciation endothéliale des CSM sur WJ-ECM en 3D. Plus de CSM cultivées sur l'extérieur des artères retournées ont exprimé des marqueurs endothéliaux que celles cultivées dans la lumière.

3. **Expérimentation animale**

Pour valider n'importe quel concept dans l'ingénierie vasculaire, il faut tester la perméabilité du greffon dans un modèle animal. Il est connu qu'un remplacement artériel au niveau de la carotide chez le lapin est un modèle optimal au niveau des petits animaux. Pour l'ingénierie

vasculaire, les lapins ressemblent aux humains au niveau du mécanisme de la thrombogénicité, la perméabilité et l'endothélialisation[5]. Nous avons donc choisi de valider notre coating de WJ-ECM et la technique de retournement chez le lapin. Dans de précédents travaux de notre équipe, le remplacement artériel a été effectué par anastomose termino-latérale[6]. Ce type d'opération conduit à un angle au niveau des deux sites d'anastomose qui change les patterns hémodynamiques[7]. Dans ce travail, nous avons effectué un remplacement de façon termino-terminale au niveau de la carotide du lapin, ce type d'anastomose peut éviter la turbulence une fois la circulation sanguine rétablie.

Dans un premier temps, nous avons validé la faisabilité de ce modèle avec une carotide de lapin autologue. La réussite de ce modèle a été confirmée par la perméabilité du greffon 3 semaines après opération (**Fig. 4**).

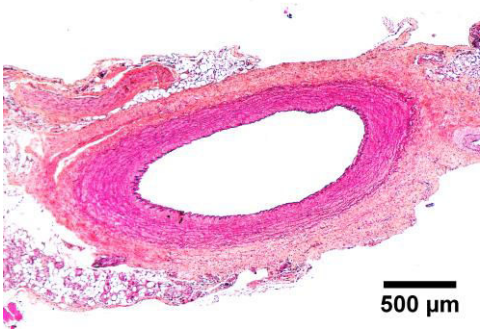

Fig. 4 Analyse histologique d'un greffon autologue. Une carotide a été explantée et tout de suite réimplantée dans le même lapin. 3 semaines après l'opération, le lapin a été euthanasié et le greffon a été examiné pour sa perméabilité. Coloration : HES.

Dans un deuxième temps, nous avons effectué des remplacements artériels avec ce modèle chez 27 lapins pour différents groupes de greffons. Les résultats ont montré des perméabilités différentes dans le **Tableau 1**

Tableau 1. La perméabilité des greffons 3 semaines après l'opération.

Type de greffon	Perméabilité
AO retournée + WJ-ECM sans cellules	0/3
AO avec WJ native comme l'intima sans cellules	0/3
AO injectée de WJ-ECM et injectée de CSM	0/5
AO retournée + collagène + CSM	3/3
AO retournée + WJ-ECM + CSM	5/5
AO avec WJ native + CSM	5/5
Carotide lapin retournée + WJ-ECM + CSM	3/3

La perméabilité du greffon a été suivie par l'écho-doppler tous les 3 jours après opération jusqu'à 3 semaines (**Fig. 5**). L'analyse histologique a confirmé la perméabilité en montrant une lumière nette sans thrombose (**Fig.6**).

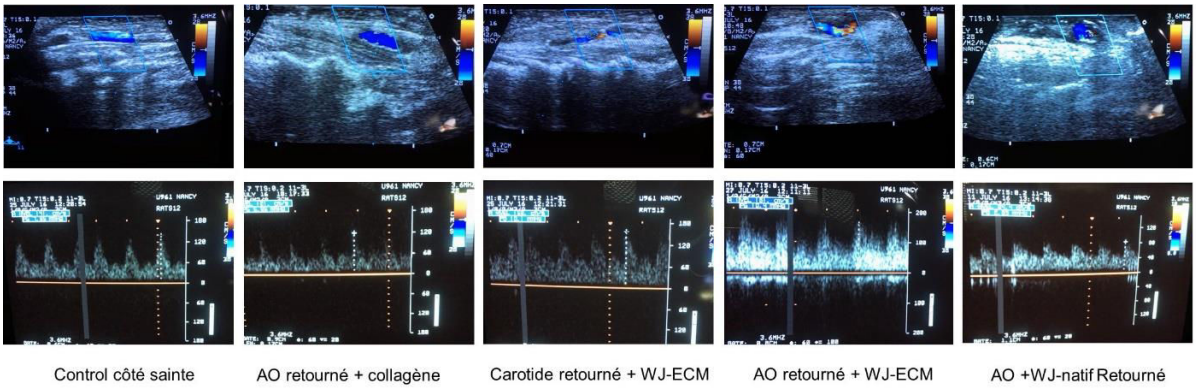

Fig. 5. Échographie des greffons perméables 3 semaines après opération. La perméabilité est confirmée par la circulation sanguine dans les greffons (bleu). La vitesse et la pression sanguine n'ont pas montré de différence par rapport au contrôle (côté non opéré).

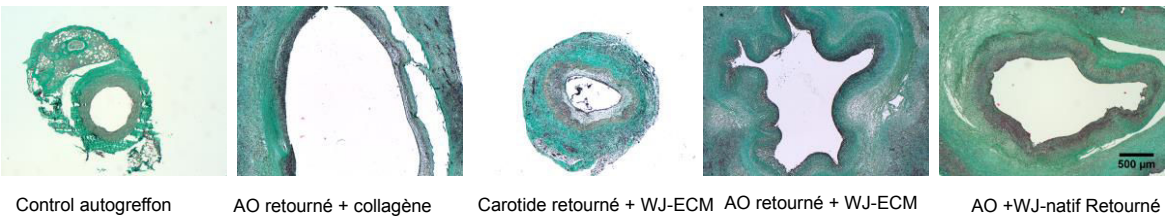

Fig. 6. Histologie des greffons 3 semaines après opération. Coloration: Masson's trichrome.

L'ensemble de ces résultats, ainsi que les résultats des chapitres précédents montrent que la solution WJ-ECM est une alternative avec grand potentiel dans l'ITV. Le coating à base de WJ-ECM peut améliorer l'adhésion, la prolifération, la différenciation et la résistance des CSM en substrat 2D et 3D. Cependant, le coating seul n'a pas montré d'amélioration pour la perméabilité sur les artères ombilicales, cela indique que les artères recouvertes de coating n'ont pas réussi de recruter les cellules circulantes de lapin. Les artères retournées pour mettre la gelée de Wharton dans la lumière comme un coating natif n'ont plus réussi à recruter les cellules de l'hôte pour l'endothélialisation. Mahara *et al.* ont montré un greffon vasculaire avec des modifications de la lumière et ils ont réussi de re-endothélialiser par recrutement *in vivo*[8]. En effet, les modifications de la lumière sont souvent effectuées par incorporation des éléments adhésifs pour les cellules et aussi les médicaments anti-thrombotiques (héparine par exemple)[6], [9]. Dans notre travail, les artères recouvertes de différents coating (collagène, WJ-ECM, WJ-natif) ont renforcé l'efficacité d'endothélialisation avec les CSM *in vitro* qui ensuite a amené une totale perméabilité *in vivo*.

La technique de retournement a été utilisée dans ce chapitre pour 3 différents coating. Mise à part la WJ-ECM qui été présentée dans le chapitre précédent, la technique est compatible avec le collagène et la WJ-natif. Par conséquent, nous pouvons envisager que cette technique pourra être appliquée dans d'autres coating (naturel ou synthétique) dans l'ITV. Grâce aux caractéristiques des artères ombilicales, nous avons ensemencé les CSM directement sur l'extérieur de l'artère, et un seul retournement a été suffisant pour retrouver les CSM dans la

lumière pour *une* implantation *in vivo*. Grace à cette stratégie on peut envisager de développer une banque tissulaire avec les artères ombilicales richement entourées de WJ-natif. Ces artères peuvent être conservées au moment de la naissance afin d'être disponibles pour chacun si nécessaire. Cependant, des études plus approfondies sont nécessaires pour caractériser les comportements cellulaires (adhésion, prolifération, alignement et différenciation) sur la WJ-natif. Et la technique de conserver WJ-natif avec une épaisseur désirée est aussi importante afin de contrôler cette surface. En conclusion, la technique de retournement donne la possibilité d'utiliser divers coatings dans l'ITV, et surtout d'utiliser la WJ-natif comme un coating naturel dans l'ITV.

Références :

[1] N.J. Turner, M.O. Murphy, C.M. Kielty, C.A. Shuttleworth, R.A. Black, M.J. Humphries, M.G. Walker, A.E. Canfield, Alpha2(VIII) collagen substrata enhance endothelial cell retention under acute shear stress flow via an alpha2beta1 integrin-dependent mechanism: an in vitro and in vivo study, Circulation. 114 (2006) 820–829. doi:10.1161/CIRCULATIONAHA.106.635292.

[2] J. Chlupáč, E. Filová, T. Riedel, M. Houska, E. Brynda, M. Remy-Zolghadri, R. Bareille, P. Fernandez, R. Daculsi, C. Bourget, L. Bordenave, L. Bačáková, Attachment of human endothelial cells to polyester vascular grafts: pre-coating with adhesive protein assemblies and resistance to short-term shear stress, Physiol. Res. Acad. Sci. Bohemoslov. 63 (2014) 167–177.

[3] G. Chen, Y. Lv, P. Guo, C. Lin, X. Zhang, L. Yang, Z. Xu, Matrix mechanics and fluid shear stress control stem cells fate in three dimensional microenvironment, Curr. Stem Cell Res. Ther. 8 (2013) 313–323.

[4] E.D. O'Cearbhaill, M. Murphy, F. Barry, P.E. McHugh, V. Barron, Behavior of human mesenchymal stem cells in fibrin-based vascular tissue engineering constructs, Ann. Biomed. Eng. 38 (2010) 649–657. doi:10.1007/s10439-010-9912-x.

[5] D.D. Swartz, S.T. Andreadis, Animal models for vascular tissue-engineering, Curr. Opin. Biotechnol. 24 (2013) 916–925. doi:10.1016/j.copbio.2013.05.005.

[6] H. Kerdjoudj, N. Berthelemy, S. Rinckenbach, A. Kearney-Schwartz, K. Montagne, P. Schaaf, P. Lacolley, J.-F. Stoltz, J.-C. Voegel, P. Menu, Small Vessel Replacement by Human Umbilical Arteries With Polyelectrolyte Film-Treated ArteriesIn Vivo Behavior, J. Am. Coll. Cardiol. 52 (2008) 1589–1597. doi:10.1016/j.jacc.2008.08.009.

[7] S.S. White, C.K. Zarins, D.P. Giddens, H. Bassiouny, F. Loth, S.A. Jones, S. Glagov, Hemodynamic Patterns in Two Models of End-to-Side Vascular Graft Anastomoses: Effects of Pulsatility, Flow Division, Reynolds Number, and Hood Length, J. Biomech. Eng. 115 (1993) 104–111. doi:10.1115/1.2895456.

[8] A. Mahara, S. Somekawa, N. Kobayashi, Y. Hirano, Y. Kimura, T. Fujisato, T. Yamaoka, Tissue-engineered acellular small diameter long-bypass grafts with neointima-inducing activity, Biomaterials. 58 (2015) 54–62. doi:10.1016/j.biomaterials.2015.04.031.

[9] M.T. Koobatian, S. Row, R.J. Smith Jr, C. Koenigsknecht, S.T. Andreadis, D.D. Swartz, Successful endothelialization and remodeling of a cell-free small-diameter arterial graft in a large animal model, Biomaterials. 76 (2016) 344–358. doi:10.1016/j.biomaterials.2015.10.020.

DISCUSSION - CONCLUSION

Dans l'ingénierie tissulaire vasculaire, plusieurs éléments essentiels sont à prendre en considération pour réussir à construire un greffon qui se rapproche le plus possible d'un vaisseau natif aussi bien au niveau des propriétés physiques et que des propriétés biologiques. Le but de cette discussion est de passer en revue différents aspects qui peuvent influencer les propriétés d'un tel scaffold : de la nature des biomatériaux aux cellules utilisées, de la culture statique au comportement dynamique, de la culture *in vitro* à l'implantation chez l'animal, des phénomènes cellulaires aux mécanismes moléculaires, etc. Sur la base de ce que nous avons découvert sur les biomatériaux, les cellules, les techniques de culture cellulaire, les comportements des greffons *in vivo*, … nous essayons de donner nos points de vue et d'apporter de nouveaux éléments dans le domaine de l'ingénierie vasculaire.

Les cellules sont un des éléments les plus importants dans la construction d'un greffon artificiel, elles permettent au greffon de devenir vivant[65]. Aussi, pour les cellulariser, plusieurs défis doivent être relevés : la source de cellules, le maintien du phénotype cellulaire *in vitro* jusqu'à *in vivo*[66]. A ce jour, il est communément reconnu que les cellules souches, notamment les CSMs constituent la source la plus favorable en raison de leur capacité de se différencier vers des lignées vasculaires sous stimulations appropriées[28], et de leurs propriétés immunomodulatrices qui évitent le rejet *in vivo*[67]. Nous avons prouvé dans cette thèse que les CSMs issues de la gelée de Wharton du cordon ombilical peuvent, dans certaines conditions, exprimer les marqueurs endothéliaux ; cette différenciation a été obtenue en condition de 2D et 3D. Cependant, nous voulons souligner que, globalement, la différenciation vasculaire des cellules souches nécessite des jours voire des semaines[32][68]. De plus, il est important de maintenir le phénotype vasculaire après différenciation, en culture sur du long-terme et au cours des passages. Par exemple, les CML issues de la différenciation, doivent exprimer les marqueurs des CML et en même temps maintenir leurs fonctions contractiles[69]; de même, les CEs doivent exprimer les marqueurs endothéliaux et libérer les molécules telles que eNos et

Ac-LDL[70]. Dans ce travail, nous avons proposé une technique pour réduire le temps de différenciation et maintenir le phénotype basée sur une combinaison de stimulations induites par des facteurs de croissance et des forces mécaniques telles que la contrainte de cisaillement et l'étirement (stretch) cyclique. Cette technique se rapproche des conditions réelles dans les vaisseaux natifs où les cellules sont sous constantes stimulations mécaniques et alimentées par du sang contenant des facteurs de croissance[71]. Il est prouvé que pendant la différenciation *in vitro*, les facteurs de croissance permettent aux cellules d'exprimer les marqueurs vasculaires, et la stimulation mécanique révèle leurs fonctionnalités vasculaires[72].

Dans un vaisseau natif, les CEs bordent la lumière et adhèrent sur une couche d'ECM appelée la limitante élastique interne ; les CML du média sont enchassées dans une ECM contenant beaucoup de collagène et d'élastine. Ces ECM fonctionnent comme un scaffold qui maintient la forme et l'élasticité du vaisseau, supporte les cellules et interagit avec elles. C'est pour respecter cette architecture que de nombreuses études sont consacrées à la recherche de nouveaux biomatériaux qui puissent assurer ces fonctions. En général, les biomatériaux se déclinent en deux types selon la source : synthétique ou naturel et selon leur fonction : scaffold et/ou coating[28].

Ce travail de thèse présente plusieurs facettes puisqu'il a permis de mettre au point un scaffold synthétique, un coating naturel et une matrice issue d'artère dé-endothélialisée et recouverte d'un coating naturel. Au niveau du scaffold, il existe trois sources différentes : un polymère synthétique (PCL, P(VDF)), un polymère naturel (collagène, fibronectine) et des artères dé-cellularisées[46]. Chaque source a montré des avantages et inconvénients.

Les scaffolds synthétiques sont souvent fabriqués avec des polymères qui, de par leur disponibilité, facilitent leur industrialisation, avec l'avantage de proposer un produit adaptable synthétisé en grande quantité[36]. Ils peuvent être fabriqués en fonction des propriétés désirées,

telles que leur épaisseur, le diamètre du tube, la résistance à la pression sanguine, la perméabilité trans-murale, la micro ou nano géométrie qui favorise les comportements cellulaires, etc[38][73]. Nous avons participé, avec des équipes indienne (International and Inter University Centre for Nanoscience and Nanotechnology, Mahatma Gandhi University), israélienne (Laboratory of Pharmaceutical Nanomaterials Science, Department of Materials Science and Engineering, Technion-Israel Institute of Technology) et de l'Institut Jean Lamour (IJL, Université de Lorraine), au développement d'un scaffold à base de P(VDF-TrFE), dont le potentiel dans l'ingénierie vasculaire est reconnu depuis1992 [74]. Ce type de scaffold bénéficie d'un effet piézo-électrique, capable de transformer des stimulations mécaniques en signaux électriques. Et il a été montré que la potentiel électrique joue un rôle important dans la guérison des blessures [75]. Cette propriété donc favorise l'adhésion et la prolifération des cellules. Des nanoparticules de ZnO ont été incorporées pour la première fois dans le polymère, ce qui fonctionnalise ce scaffold. Certaines stratégies dans le développement des nouveaux biomatériaux s'orientent vers la combinaison de polymères synthétiques dotés de certaines propriétés (ici piézo-électrique) avec d'autres matériaux, par exemple des polymères naturels (collagène, fibronectine, etc.) pour améliorer la biocompatibilité du scaffold et favoriser l'adhésion cellulaire[76][77]. Dans notre étude, les micro- ou nano- particules de ZnO (mais d'autres particules tels les peptides adhésifs, les facteurs de croissance ou des médicaments peuvent être utilisées) interviennent dans la régulation des interactions entre les cellules et le scaffold [78][79]. Une fois les micro- ou nano- particules incorporées dans un scaffold synthétique, il est important d'en contrôler la libération[80]. Pour vérifier la biocompatibilité, les scaffolds sont généralement testés avec les cellules *in vitro* et un modèle animal *in vivo*. Dans ce travail, nous avons montré que les CSM et CE matures mises en culture *in vitro,* adhéraient au scaffold synthétique, suggérant une compatibilité biologique. Avant d'envisager de l'utiliser dans différents domaines d'ingénierie tissulaire, il faut s'assurer que le scaffold

l'est aussi *in vivo*. Nous avons développé un modèle animal dans lequel les polymères fonctionnalisés sont implantés en sous-cutané. Nous avons montré non seulement qu'ils ne provoquaient pas de rejet par les animaux, mais qu'une angiogenèse se développait pour vasculariser le scaffold. Nous avons donc montré dans cette partie de l'étude que le scaffold P(VDF-TrFE)/ZnO-2% cellularisé avec des CSM est biocompatible aussi bien *in vitro* que *in vivo*. Cependant, le scaffold a été étudié sous forme de membrane mais pas sous celle d'un tuyau dont les caractéristiques (déformabilités, résistance à la pression, compliance, …) devront être vérifiées. De plus, des tests *in vivo* devront être réalisés pour attester de ses capacités d'assurer les fonctions d'un greffon artériel. Par conséquent, des études complémentaires approfondies sont nécessaires pour répondre au cahier des charges de l'ingénierie vasculaire, en fabriquant un scaffold tubulaire capable d'assurer la perméabilité sanguine lors d'un remplacement artériel.

Les polymères naturels constituent une deuxième voie pour fabriquer un scaffold. D'une façon globale, les scaffolds sont composés d'ECM qui peuvent être fabriqués avec des polymères naturels parmi lesquels le collagène est le plus souvent étudiée[81]. Ce type de scaffold ne présente normalement pas de risque de biocompatibilité, mais il est difficile, lors de leur construction sous forme tubulaire, d'en contrôler l'épaisseur et la longueur. Cependant les scaffolds à base d'ECM naturelle ont souvent de moins bonnes propriétés physiques que les synthétiques, mais ont l'avantage de se rapprocher de l'environnement des cellules en réel. Les polymères naturels utilisés pour fabriquer un scaffold vasculaire ne sont pas sous forme solide mais dissous en solution. Lors de leur fabrication, l'orientation des ECM est difficile à contrôler. Certains auteurs ont montré que la méchanotransduction modifie l'orientation, et l'interaction des cellules et du scaffold peut induire un remodelage sur le scaffold [82]. En outre, le microenvironnement dans les tissus natifs comprend divers types d'ECM avec des pourcentages

différents pour chacune d'elles. La mise au point de scaffold à base d'ECM naturelles doit s'orienter vers la recherche des différents ECM avec l'optimisation de leur pourcentage[73].

Le troisième type de scaffold se décline sous la forme de matrice dé-cellularisée obtenue à, partir de la décellularisation d'un vaisseau (artère ou veine)[62]. Ce scaffold tubulaire est dé-cellularisé par des traitements chimiques qui détruisent toutes les cellules du vaisseau traité, puis d'un traitement par la nucléase qui élimine les ADN et ARN résiduels[83]. L'avantage de ce genre de scaffolds est de respecter l'ECM avec ses propriétés physiques peu réduites, et de ne plus contenir de cellule susceptible de provoquer des réactions immunogènes. Par ailleurs, leur source pourrait être abondante, en particulier issue d'animaux. Depuis plus de dix ans, notre équipe utilise les artères ombilicales comme scaffold, ces artères sont largement disponibles et surtout ils adhèrent parfaitement aux critères de petit diamètre destinés à l'usage clinique. De plus, il est possible d'obtenir des artères ombilicales d'une longueur supérieure à 30 cm (par exemple, pour le pontage du cœur, un greffon plus que 10 cm est nécessaire selon la distance entre l'aorte et le point pathologique de la coronaire), avec un diamètre stable tout au long de l'artère et sans ramification. Grâce à ces caractéristiques, les artères ombilicales constituent un parfait candidat pour fabriquer des greffons destinés à l'usage clinique[84]. Cependant, les artères ombilicales se présentent souvent en spirales dans les cordons, de ce fait, une attention particulière doit être prêtée pendant le traitement pour obtenir un greffon vasculaire rectiligne. Des études précédentes de notre équipe ont étudié plus particulièrement l'intima et la perméabilité du greffon *in vivo* [55]. Par rapport à la dé-cellularisation, cette approche est beaucoup plus simple (30 min dans la trypsine au lieu de 3 jours de traitement dans différentes solutions chimiques) et la dé-endothélialisation conserve la média donc ne change pas les propriétés physiques du greffon. Nous avons montré aussi dans cette étude que la média contenant des CML du cordon n'avait pas provoqué de réaction immunogène délétère (aucune réaction inflammatoire n'est observée chez l'animal). Par ailleurs, nous avons aussi

montré qu'il était possible de dé-cellulariser la totalité de l'artère ombilicale (résultats non publiés) pour s'affranchir de toute réaction immunogène.

Les scaffolds sont destinés à fournir un substitut qui nécessite le recouvrement de sa surface luminale en contact direct avec les cellules sanguines. Donc il est aussi très important dans l'ingénierie tissulaire de développer des coatings appropriés[85]. Les polymères synthétiques ainsi que naturels sont tous intensivement étudiés dans cette optique. Cependant, les polymères naturels sont préférés pour mieux mimer les conditions natives[86]. Le collagène, la fibrine, l'élastine sont souvent utilisés pour modifier les surfaces d'un scaffold afin d'en améliorer le comportement cellulaire. Néanmoins, l'environnement des cellules ne se résume pas qu'à une seule composant d'ECM mais à un complexe de diverses ECM. Ainsi, des efforts doivent être faits pour rechercher de nouvelles sources d'ECM complexes et aussi le développement de techniques qui respectent toutes les ECM au cours de leur isolement[87]. Dans ce travail, nous avons exploité la possibilité d'isoler un complexe d'ECM à partir de la gelée de Wharton (WJ-ECM). La gelée de Wharton est typiquement utilisée pour isoler des CSM, puisqu'elle est une niche de cellules souches, riche en diverses ECM et en facteurs de croissance[88]. Nous avons montré qu'avec une digestion enzymatique, il était possible d'obtenir un complexe d'ECM contenant du collagène de type I et de type XVIII, ainsi que plusieurs facteurs de croissance actifs. Il existe différentes méthodes pour isoler les ECM issues de tissu animal ou humain. Une attention particulière doit être prêtée pour choisir la méthode appropriée afin d'atteindre les objectifs suivants : isoler le plus d'ECM possible (quantité et types), conserver les facteurs de croissance actifs, ne pas ajouter de composant étranger ou toxique, et éliminer les cellules ou débris cellulaires ainsi que les acides nucléiques. Notre méthode de digestion enzymatique et la neutralisation par du SVF favorisent la conservation les facteurs de croissance. De plus, l'ajout de SVF facilite l'élimination des acides nucléiques qui pourraient être sources de réactions immunogènes[89]. Le deuxième avantage de la gelée de Wharton est de l'utiliser en

tant que coating, permettant de recouvrir la surface luminale des vaisseaux tout en contrôlant son dépôt. D'après nos expériences, le succès de sa formation dépend des conditions expérimentales. En 2D sur lame de verre, il est nécessaire que la surface soit chargée négativement (par traitement chimique) pour favoriser l'adhésion cellulaire, alors qu'en 3D sur des artères ombilicales et des carotides de lapin, la solution de WJ-ECM peut former un coating directement sans prétraitement. Ensuite, nous avons montré que le coating de WJ-ECM avait significativement amélioré les comportements des cellules cultivées. Nous avons également comparé les qualités de gelée à celles du collagène, un coating classique et conventionnel[41]. Les meilleures performances de la gelée sont sans doute dues au complexe ECM qui s'approche plus de l'ECM native. Diverses ECM peuvent fournir différents ligands favorisant l'interaction spécifique avec les cellules, et la présence de facteurs de croissance renforce l'adhésion, la prolifération, la différenciation et la résistance des cellules face aux flux.

La dernière partie de la thèse développe une technique favorisant l'endothélialisation des substituts artériels. Selon notre point de vue, cette technique de retournement lève un verrou et apporte une plus-value en ingénierie vasculaire. L'objectif ultime est de fournir des vaisseaux cellularisés capables de répondre aux besoins en pontage aorto-coronaire. Pour ce faire, les vaisseaux artificiels doivent d'abord posséder une longueur de plus que 10 cm. La fabrication des vaisseaux suffisamment longs, avec 3 couches cellulaire, en particulier avec la cellularisation convenable de l'intima est difficile en raison de l'approvisionnement en oxygène et en nutriments *in vitro*[90]. C'est pour cette raison, que les études existantes proposent souvent des vaisseaux artificiels d'une longueur d'environ 5 cm, inutilisables en clinique[84][78]. Par ailleurs, il existe des greffons plus longs que 10 cm, à base d'artères dé-cellularisés, dont la surface luminale est modifiée *in vitro* (peptide adhésifs, héparine, etc.) pour que les greffons puissent recruter les cellules circulantes une fois implantés *in vivo*[27]. Une couche des cellules endothéliales a été retrouvée dans ces greffons après implantation dans différents modèles

animaux[91]. Cependant, comme il a été prouvé chez l'homme qu'il était difficile de recruter les cellules de l'hôte, cette approche semble difficilement applicable[92]. La meilleure stratégie reste alors d'endothélialiser l'intima avant l'implantation. La difficulté réside dans la cellularisation de l'intima d'un greffon de plus de 10cm de long. L'adhésion uniforme et homogène des cellules sur toute la surface est impérative, et la maturation des cellules ensemencées est difficile. La technique que nous avons mise au point consiste en un simple retournement pour mettre l'intima à l'extérieur. Ainsi, toute la surface extérieure se trouve accessible pour la dé-endothélialisation, le coating, l'ensemencement et la maturation cellulaire. Par rapport aux bioréacteurs qui perfusent les milieux dans la lumière, cette technique est beaucoup plus simple, applicable en toute sécurité sanitaire et ne coute presque rien. De plus, les substituts traités ainsi sont perméables une fois implantés pour un remplacement artériel chez le lapin. Ce résultat démontre que la technique de retournement n'endommage pas l'artère pendant la manipulation. Par ailleurs, cette technique a été testée sur deux différents substituts artériels : artères ombilicale et carotide. Elle pourrait s'appliquer à d'autres substituts artériels ou synthétiques. Par conséquent, cette technique de retournement a prouvé un concept de mieux cultiver un greffon vasculaire *in vitro* pour l'usage *in vivo*, et cette technique pourra servir comme une procédure de façon routinière dans l'ingénierie vasculaire.

Les résultats de ce travail de thèse ouvrent de très larges perspectives dans le domaine de l'ingénierie tissulaire vasculaire. Même si le développement du scaffold fonctionnalisé demande des études complémentaires, la valorisation de la gelée de Wharton parait une avancée intéressante et semble répondre aux exigences cliniques. Ce nouveau coating a été conjugué à la cellularisation de la surface luminale d'un vaisseau et l'ensemble a donné des résultats prometteurs, puisque cette construction favorise la résistance cellulaire au flux sanguin et la perméabilité. Sans oublier de mentionner l'utilisation de cellules mésenchymateuses qui semblent se différencier en CEs. L'étape qui devrait suivre est l'essai sur d'autres mammifères.

Par la suite, on peut imaginer une première application clinique pour mettre en place un shunt vasculaire pour l'hémodialyse, puis pour remplacer une coronaire.

Références

(En plus de celles proposées dans les articles)

[1] D. Mozaffarian, E.J. Benjamin, A.S. Go, D.K. Arnett, M.J. Blaha, M. Cushman, S.R. Das, S. de Ferranti, J.-P. Després, H.J. Fullerton, V.J. Howard, M.D. Huffman, C.R. Isasi, M.C. Jiménez, S.E. Judd, B.M. Kissela, J.H. Lichtman, L.D. Lisabeth, S. Liu, R.H. Mackey, D.J. Magid, D.K. McGuire, E.R. Mohler, C.S. Moy, P. Muntner, M.E. Mussolino, K. Nasir, R.W. Neumar, G. Nichol, L. Palaniappan, D.K. Pandey, M.J. Reeves, C.J. Rodriguez, W. Rosamond, P.D. Sorlie, J. Stein, A. Towfighi, T.N. Turan, S.S. Virani, D. Woo, R.W. Yeh, M.B. Turner, American Heart Association Statistics Committee and Stroke Statistics Subcommittee, Heart Disease and Stroke Statistics-2016 Update: A Report From the American Heart Association, Circulation. 133 (2016) e38–e360. doi:10.1161/CIR.0000000000000350.

[2] G.A. Roth, M.H. Forouzanfar, A.E. Moran, R. Barber, G. Nguyen, V.L. Feigin, M. Naghavi, G.A. Mensah, C.J.L. Murray, Demographic and Epidemiologic Drivers of Global Cardiovascular Mortality, N. Engl. J. Med. 372 (2015) 1333–1341. doi:10.1056/NEJMoa1406656.

[3] A. Carrel, VIII. On the Experimental Surgery of the Thoracic Aorta and Heart, Ann. Surg. 52 (1910) 83–95.

[4] F. Sellke, P.J. Del Nido, Sabiston and Spencer Surgery of the Chest, 9th Edition, in: Sabiston Spencer Surg. Chest 9th Ed., n.d.

[5] M. Nichols, N. Townsend, P. Scarborough, M. Rayner, Cardiovascular disease in Europe 2014: epidemiological update, Eur. Heart J. 35 (2014) 2950–2959. doi:10.1093/eurheartj/ehu299.

[6] S. Yusuf, D. Wood, J. Ralston, K.S. Reddy, The World Heart Federation's vision for worldwide cardiovascular disease prevention, The Lancet. 386 (2015) 399–402. doi:10.1016/S0140-6736(15)60265-3.

[7] H.C. Stary, Natural History and Histological Classification of Atherosclerotic Lesions An Update, Arterioscler. Thromb. Vasc. Biol. 20 (2000) 1177–1178. doi:10.1161/01.ATV.20.5.1177.

[8] S. Glagov, E. Weisenberg, C.K. Zarins, R. Stankunavicius, G.J. Kolettis, Compensatory Enlargement of Human Atherosclerotic Coronary Arteries, N. Engl. J. Med. 316 (1987) 1371–1375. doi:10.1056/NEJM198705283162204.

[9] A.R. Grüntzig, Å. Senning, W.E. Siegenthaler, Nonoperative Dilatation of Coronary-Artery Stenosis, N. Engl. J. Med. 301 (1979) 61–68. doi:10.1056/NEJM197907123010201.

[10] G.N. Levine, E.R. Bates, J.C. Blankenship, S.R. Bailey, J.A. Bittl, B. Cercek, C.E. Chambers, S.G. Ellis, R.A. Guyton, S.M. Hollenberg, U.N. Khot, R.A. Lange, L. Mauri, R. Mehran, I.D. Moussa, D. Mukherjee, B.K. Nallamothu, H.H. Ting, 2011 ACCF/AHA/SCAI Guideline for Percutaneous Coronary Intervention: a report of the American College of Cardiology Foundation/American Heart Association Task Force on Practice Guidelines and the Society for Cardiovascular Angiography and Interventions, Circulation. 124 (2011) e574–651. doi:10.1161/CIR.0b013e31823ba622.

[11] B.R. Shah, L.A. McCoy, J.J. Federspiel, D. Mudrick, P.A. Cowper, F.A. Masoudi, B.L. Lytle, C.L. Green, P.S. Douglas, Use of Stress Testing and Diagnostic Catheterization After Coronary StentingAssociation of Site-Level Patterns With Patient Characteristics and Outcomes in 247,052 Medicare Beneficiaries, J. Am. Coll. Cardiol. 62 (2013) 439–446. doi:10.1016/j.jacc.2013.02.093.

[12] E. Kedhi, K.S. Joesoef, E. McFadden, J. Wassing, C. van Mieghem, D. Goedhart, P.C. Smits, Second-generation everolimus-eluting and paclitaxel-eluting stents in real-life practice (COMPARE): a randomised trial, Lancet Lond. Engl. 375 (2010) 201–209. doi:10.1016/S0140-6736(09)62127-9.

[13] T. Palmerini, G. Biondi-Zoccai, D. Della Riva, A. Mariani, P. Genereux, A. Branzi, G.W. Stone, Stent thrombosis with drug-eluting stents: is the paradigm shifting?, J. Am. Coll. Cardiol. 62 (2013) 1915–1921. doi:10.1016/j.jacc.2013.08.725.

[14] L. Qi-Hua, Z. Qi, Z. Yu, L. Xiao-Long, J. Hai-Gang, Y. Jian-Feng, S. Yi, Long-term effect of second-generation drug-eluting stents for coronary artery disease, everolimus-eluting versus zotarolimus-eluting stents: a meta-analysis, Coron. Artery Dis. 26 (2015) 259–265. doi:10.1097/MCA.0000000000000222.

[15] P.W. Serruys, M.-C. Morice, A.P. Kappetein, A. Colombo, D.R. Holmes, M.J. Mack, E. Ståhle, T.E. Feldman, M. van den Brand, E.J. Bass, N. Van Dyck, K. Leadley, K.D. Dawkins, F.W. Mohr, SYNTAX Investigators, Percutaneous coronary intervention versus coronary-artery bypass grafting for severe coronary artery disease, N. Engl. J. Med. 360 (2009) 961–972. doi:10.1056/NEJMoa0804626.

[16] M.E. Farkouh, M. Domanski, L.A. Sleeper, F.S. Siami, G. Dangas, M. Mack, M. Yang, D.J. Cohen, Y. Rosenberg, S.D. Solomon, A.S. Desai, B.J. Gersh, E.A. Magnuson, A. Lansky, R. Boineau, J. Weinberger, K. Ramanathan, J.E. Sousa, J. Rankin, B. Bhargava, J. Buse, W. Hueb, C.R. Smith, V. Muratov, S. Bansilal, S. King, M. Bertrand, V. Fuster, FREEDOM Trial Investigators, Strategies for multivessel revascularization in patients with diabetes, N. Engl. J. Med. 367 (2012) 2375–2384. doi:10.1056/NEJMoa1211585.

[17] A. Kapur, R.J. Hall, I.S. Malik, A.C. Qureshi, J. Butts, M. de Belder, A. Baumbach, G. Angelini, A. de Belder, K.G. Oldroyd, M. Flather, M. Roughton, P. Nihoyannopoulos, J.P. Bagger, K. Morgan, K.J. Beatt, Randomized comparison of percutaneous coronary intervention with coronary artery bypass grafting in diabetic patients. 1-year results of the CARDia (Coronary Artery Revascularization in Diabetes) trial, J. Am. Coll. Cardiol. 55 (2010) 432–440. doi:10.1016/j.jacc.2009.10.014.

[18] A.P. Kappetein, T.E. Feldman, M.J. Mack, M.-C. Morice, D.R. Holmes, E. Ståhle, K.D. Dawkins, F.W. Mohr, P.W. Serruys, A. Colombo, Comparison of coronary bypass surgery with drug-eluting stenting for the treatment of left main and/or three-vessel disease: 3-year follow-up of the SYNTAX trial, Eur. Heart J. 32 (2011) 2125–2134. doi:10.1093/eurheartj/ehr213.

[19] F.D. Loop, B.W. Lytle, D.M. Cosgrove, R.W. Stewart, M. Goormastic, G.W. Williams, L.A. Golding, C.C. Gill, P.C. Taylor, W.C. Sheldon, Influence of the internal-mammary-artery graft on 10-year survival and other cardiac events, N. Engl. J. Med. 314 (1986) 1–6. doi:10.1056/NEJM198601023140101.

[20] N.D. Desai, E.A. Cohen, C.D. Naylor, S.E. Fremes, Radial Artery Patency Study Investigators, A randomized comparison of radial-artery and saphenous-vein coronary bypass grafts, N. Engl. J. Med. 351 (2004) 2302–2309. doi:10.1056/NEJMoa040982.

[21] S. Goldman, G.K. Sethi, W. Holman, H. Thai, E. McFalls, H.B. Ward, R.F. Kelly, B. Rhenman, G.H. Tobler, F.G. Bakaeen, J. Huh, E. Soltero, M. Moursi, M. Haime, M. Crittenden, V. Kasirajan, M. Ratliff, S. Pett, A. Irimpen, W. Gunnar, D. Thomas, S. Fremes, T. Moritz, D. Reda, L. Harrison, T.H. Wagner, Y. Wang, L. Planting, M. Miller, Y. Rodriguez, E. Juneman, D. Morrison,

M.K. Pierce, S. Kreamer, M.-C. Shih, K. Lee, Radial artery grafts vs saphenous vein grafts in coronary artery bypass surgery: a randomized trial, JAMA. 305 (2011) 167–174. doi:10.1001/jama.2010.1976.

[22] H. Hirose, A. Amano, S. Takanashi, A. Takahashi, Coronary artery bypass grafting using the gastroepiploic artery in 1,000 patients, Ann. Thorac. Surg. 73 (2002) 1371–1379.

[23] Y. Gao, F. Liu, L. Zhang, X. Su, J.Y. Liu, Y. Li, Acellular blood vessels combined human hair follicle mesenchymal stem cells for engineering of functional arterial grafts, Ann. Biomed. Eng. 42 (2014) 2177–2189. doi:10.1007/s10439-014-1061-1.

[24] N. L'Heureux, N. Dusserre, G. Konig, B. Victor, P. Keire, T.N. Wight, N.A.F. Chronos, A.E. Kyles, C.R. Gregory, G. Hoyt, R.C. Robbins, T.N. McAllister, Human tissue-engineered blood vessels for adult arterial revascularization, Nat. Med. 12 (2006) 361–365. doi:10.1038/nm1364.

[25] C. Michiels, Endothelial cell functions, J. Cell. Physiol. 196 (2003) 430–443. doi:10.1002/jcp.10333.

[26] J.S. Pober, W.C. Sessa, Evolving functions of endothelial cells in inflammation, Nat. Rev. Immunol. 7 (2007) 803–815. doi:10.1038/nri2171.

[27] M.T. Koobatian, S. Row, R.J. Smith Jr, C. Koenigsknecht, S.T. Andreadis, D.D. Swartz, Successful endothelialization and remodeling of a cell-free small-diameter arterial graft in a large animal model, Biomaterials. 76 (2016) 344–358. doi:10.1016/j.biomaterials.2015.10.020.

[28] D.G. Seifu, A. Purnama, K. Mequanint, D. Mantovani, Small-diameter vascular tissue engineering, Nat. Rev. Cardiol. 10 (2013) 410–421. doi:10.1038/nrcardio.2013.77.

[29] H. Rammal, C. Harmouch, J.-J. Lataillade, D. Laurent-Maquin, P. Labrude, P. Menu, H. Kerdjoudj, Stem cells: a promising source for vascular regenerative medicine, Stem Cells Dev. 23 (2014) 2931–2949. doi:10.1089/scd.2014.0132.

[30] R. El Omar, J. Beroud, J.-F. Stoltz, P. Menu, E. Velot, V. Decot, Umbilical Cord Mesenchymal Stem Cells: The New Gold Standard for Mesenchymal Stem Cell-Based Therapies?, Tissue Eng. Part B Rev. (2014). doi:10.1089/ten.TEB.2013.0664.

[31] L.J. Fischer, S. McIlhenny, T. Tulenko, N. Golesorkhi, P. Zhang, R. Larson, J. Lombardi, I. Shapiro, P.J. DiMuzio, Endothelial differentiation of adipose-derived stem cells: effects of endothelial cell growth supplement and shear force, J. Surg. Res. 152 (2009) 157–166. doi:10.1016/j.jss.2008.06.029.

[32] M.-Y. Chen, P.-C. Lie, Z.-L. Li, X. Wei, Endothelial differentiation of Wharton's jelly-derived mesenchymal stem cells in comparison with bone marrow-derived mesenchymal stem cells, Exp. Hematol. 37 (2009) 629–640. doi:10.1016/j.exphem.2009.02.003.

[33] T. Ahsan, R.M. Nerem, Fluid shear stress promotes an endothelial-like phenotype during the early differentiation of embryonic stem cells, Tissue Eng. Part A. 16 (2010) 3547–3553. doi:10.1089/ten.TEA.2010.0014.

[34] G. Chen, Y. Lv, P. Guo, C. Lin, X. Zhang, L. Yang, Z. Xu, Matrix mechanics and fluid shear stress control stem cells fate in three dimensional microenvironment, Curr. Stem Cell Res. Ther. 8 (2013) 313–323.

[35] W.L. Murphy, T.C. McDevitt, A.J. Engler, Materials as stem cell regulators, Nat. Mater. 13 (2014) 547–557. doi:10.1038/nmat3937.

[36] M.P. Lutolf, J.A. Hubbell, Synthetic biomaterials as instructive extracellular microenvironments for morphogenesis in tissue engineering, Nat. Biotechnol. 23 (2005) 47–55. doi:10.1038/nbt1055.

[37] J. Ringe, M. Sittinger, Regenerative medicine: Selecting the right biological scaffold for tissue engineering, Nat. Rev. Rheumatol. 10 (2014) 388–389. doi:10.1038/nrrheum.2014.79.

[38] S.J. Lee, J. Liu, S.H. Oh, S. Soker, A. Atala, J.J. Yoo, Development of a composite vascular scaffolding system that withstands physiological vascular conditions, Biomaterials. 29 (2008) 2891–2898. doi:10.1016/j.biomaterials.2008.03.032.

[39] F. Ahmed, N.K. Dutta, A. Zannettino, K. Vandyke, N.R. Choudhury, Engineering interaction between bone marrow derived endothelial cells and electrospun surfaces for artificial vascular graft applications, Biomacromolecules. 15 (2014) 1276–1287. doi:10.1021/bm401825c.

[40] D.D. Swartz, J.A. Russell, S.T. Andreadis, Engineering of fibrin-based functional and implantable small-diameter blood vessels, Am. J. Physiol. Heart Circ. Physiol. 288 (2005) H1451–1460. doi:10.1152/ajpheart.00479.2004.

[41] C.B. Weinberg, E. Bell, A blood vessel model constructed from collagen and cultured vascular cells, Science. 231 (1986) 397–400.

[42] L.E. Niklason, J. Gao, W.M. Abbott, K.K. Hirschi, S. Houser, R. Marini, R. Langer, Functional arteries grown in vitro, Science. 284 (1999) 489–493.

[43] S.S. Silva, J.F. Mano, R.L. Reis, Potential applications of natural origin polymer-based systems in soft tissue regeneration, Crit. Rev. Biotechnol. 30 (2010) 200–221. doi:10.3109/07388551.2010.505561.

[44] Y. Zhao, S. Zhang, J. Zhou, J. Wang, M. Zhen, Y. Liu, J. Chen, Z. Qi, The development of a tissue-engineered artery using decellularized scaffold and autologous ovine mesenchymal stem cells, Biomaterials. 31 (2010) 296–307. doi:10.1016/j.biomaterials.2009.09.049.

[45] M.P. Lutolf, P.M. Gilbert, H.M. Blau, Designing materials to direct stem-cell fate, Nature. 462 (2009) 433–441. doi:10.1038/nature08602.

[46] R.A. Pérez, J.-E. Won, J.C. Knowles, H.-W. Kim, Naturally and synthetic smart composite biomaterials for tissue regeneration, Adv. Drug Deliv. Rev. 65 (2013) 471–496. doi:10.1016/j.addr.2012.03.009.

[47] S. Gomes, I.B. Leonor, J.F. Mano, R.L. Reis, D.L. Kaplan, Natural and Genetically Engineered Proteins for Tissue Engineering, Prog. Polym. Sci. 37 (2012) 1–17. doi:10.1016/j.progpolymsci.2011.07.003.

[48] J.F. Mano, G.A. Silva, H.S. Azevedo, P.B. Malafaya, R.A. Sousa, S.S. Silva, L.F. Boesel, J.M. Oliveira, T.C. Santos, A.P. Marques, N.M. Neves, R.L. Reis, Natural origin biodegradable systems in tissue engineering and regenerative medicine: present status and some moving trends, J. R. Soc. Interface R. Soc. 4 (2007) 999–1030. doi:10.1098/rsif.2007.0220.

[49] P. Chandra, S.J. Lee, Synthetic Extracellular Microenvironment for Modulating Stem Cell Behaviors, Biomark. Insights. 10 (2015) 105–116. doi:10.4137/BMI.S20057.

[50] D.E. Discher, P. Janmey, Y. Wang, Tissue Cells Feel and Respond to the Stiffness of Their Substrate, Science. 310 (2005) 1139–1143. doi:10.1126/science.1116995.

[51] W. Liu, K. Merrett, M. Griffith, P. Fagerholm, S. Dravida, B. Heyne, J.C. Scaiano, M.A. Watsky, N. Shinozaki, N. Lagali, R. Munger, F. Li, Recombinant human collagen for tissue engineered corneal substitutes, Biomaterials. 29 (2008) 1147–1158. doi:10.1016/j.biomaterials.2007.11.011.

[52] F. Guilak, D.M. Cohen, B.T. Estes, J.M. Gimble, W. Liedtke, C.S. Chen, Control of Stem Cell Fate by Physical Interactions with the Extracellular Matrix, Cell Stem Cell. 5 (2009) 17–26. doi:10.1016/j.stem.2009.06.016.

[53] N. Berthelemy, H. Kerdjoudj, C. Gaucher, P. Schaaf, J.-F. Stoltz, P. Lacolley, J.-C. Voegel, P. Menu, Polyelectrolyte Films Boost Progenitor Cell Differentiation into Endothelium-like Monolayers, Adv. Mater. Deerfield Beach Fla. 20 (2008) 2674–2678. doi:10.1002/adma.200702418.

[54] T. Boudou, T. Crouzier, K. Ren, G. Blin, C. Picart, Multiple functionalities of polyelectrolyte multilayer films: new biomedical applications, Adv. Mater. Deerfield Beach Fla. 22 (2010) 441–467. doi:10.1002/adma.200901327.

[55] H. Kerdjoudj, N. Berthelemy, S. Rinckenbach, A. Kearney-Schwartz, K. Montagne, P. Schaaf, P. Lacolley, J.-F. Stoltz, J.-C. Voegel, P. Menu, Small Vessel Replacement by Human Umbilical Arteries With Polyelectrolyte Film-Treated ArteriesIn Vivo Behavior, J. Am. Coll. Cardiol. 52 (2008) 1589–1597. doi:10.1016/j.jacc.2008.08.009.

[56] A.J. Melchiorri, L.G. Bracaglia, L. Kimerer, N. Hibino, J.P. Fisher, In Vitro Endothelialization of Biodegradable Vascular Grafts via Endothelial Progenitor Cell Seeding and Maturation in a Tubular Perfusion System Bioreactor, Tissue Eng. Part C Methods. (2016). doi:10.1089/ten.TEC.2015.0562.

[57] G.A. Villalona, B. Udelsman, D.R. Duncan, E. McGillicuddy, R.F. Sawh-Martinez, N. Hibino, C. Painter, T. Mirensky, B. Erickson, T. Shinoka, C.K. Breuer, Cell-Seeding Techniques in Vascular Tissue Engineering, Tissue Eng. Part B Rev. 16 (2010) 341–350. doi:10.1089/ten.teb.2009.0527.

[58] C.C. Anamelechi, E.C. Clermont, M.T. Novak, W.M. Reichert, Dynamic seeding of perfusing human umbilical vein endothelial cells (HUVECs) onto dual-function cell adhesion ligands: Arg-Gly-Asp (RGD)-streptavidin and biotinylated fibronectin, Langmuir ACS J. Surf. Colloids. 25 (2009) 5725–5730. doi:10.1021/la803963r.

[59] L.A. Solchaga, E. Tognana, K. Penick, H. Baskaran, V.M. Goldberg, A.I. Caplan, J.F. Welter, A Rapid Seeding Technique for the Assembly of Large Cell/Scaffold Composite Constructs, Tissue Eng. 12 (2006) 1851–1863. doi:10.1089/ten.2006.12.1851.

[60] T. Kitagawa, T. Yamaoka, R. Iwase, A. Murakami, Three-dimensional cell seeding and growth in radial-flow perfusion bioreactor for in vitro tissue reconstruction, Biotechnol. Bioeng. 93 (2006) 947–954. doi:10.1002/bit.20797.

[61] W.T. Godbey, B.S. Stacey Hindy, M.E. Sherman, A. Atala, A novel use of centrifugal force for cell seeding into porous scaffolds, Biomaterials. 25 (2004) 2799–2805. doi:10.1016/j.biomaterials.2003.09.056.

[62] C. Quint, Y. Kondo, R.J. Manson, J.H. Lawson, A. Dardik, L.E. Niklason, Decellularized tissue-engineered blood vessel as an arterial conduit, Proc. Natl. Acad. Sci. 108 (2011) 9214–9219. doi:10.1073/pnas.1019506108.

[63] D. Wion, T. Christen, E.L. Barbier, J.A. Coles, PO2 Matters in Stem Cell Culture, Cell Stem Cell. 5 (2009) 242–243. doi:10.1016/j.stem.2009.08.009.

[64] S. Hsu, I. Tsai, D. Lin, D.C. Chen, The effect of dynamic culture conditions on endothelial cell seeding and retention on small diameter polyurethane vascular grafts, Med. Eng. Phys. 27 (2005) 267–272. doi:10.1016/j.medengphy.2004.10.008.

[65] G. Shen, H.C. Tsung, C.F. Wu, X.Y. Liu, X. Wang, W. Liu, L. Cui, Y.L. Cao, Tissue engineering of blood vessels with endothelial cells differentiated from mouse embryonic stem cells, Cell Res. 13 (2003) 335–341. doi:10.1038/sj.cr.7290178.

[66] H. Kurobe, M.W. Maxfield, C.K. Breuer, T. Shinoka, Concise Review: Tissue-Engineered Vascular Grafts for Cardiac Surgery: Past, Present, and Future, Stem Cells Transl. Med. 1 (2012) 566–571. doi:10.5966/sctm.2012-0044.

[67] J.A. Ankrum, J.F. Ong, J.M. Karp, Mesenchymal stem cells: immune evasive, not immune privileged, Nat. Biotechnol. (2014). doi:10.1038/nbt.2816.

[68] R.J. Galas Jr, J.C. Liu, Vascular endothelial growth factor does not accelerate endothelial differentiation of human mesenchymal stem cells, J. Cell. Physiol. 229 (2014) 90–96. doi:10.1002/jcp.24421.

[69] M.B. Chan-Park, J.Y. Shen, Y. Cao, Y. Xiong, Y. Liu, S. Rayatpisheh, G.C.-W. Kang, H.P. Greisler, Biomimetic control of vascular smooth muscle cell morphology and phenotype for functional tissue-engineered small-diameter blood vessels, J. Biomed. Mater. Res. A. 88 (2009) 1104–1121. doi:10.1002/jbm.a.32318.

[70] N. Koike, D. Fukumura, O. Gralla, P. Au, J.S. Schechner, R.K. Jain, Tissue engineering: creation of long-lasting blood vessels, Nature. 428 (2004) 138–139. doi:10.1038/428138a.

[71] P. Dan, É. Velot, V. Decot, P. Menu, The role of mechanical stimuli in the vascular differentiation of mesenchymal stem cells, J. Cell Sci. 128 (2015) 2415–2422. doi:10.1242/jcs.167783.

[72] C. Wang, L. Cen, S. Yin, Q. Liu, W. Liu, Y. Cao, L. Cui, A small diameter elastic blood vessel wall prepared under pulsatile conditions from polyglycolic acid mesh and smooth muscle cells differentiated from adipose-derived stem cells, Biomaterials. 31 (2010) 621–630. doi:10.1016/j.biomaterials.2009.09.086.

[73] E.S. Place, N.D. Evans, M.M. Stevens, Complexity in biomaterials for tissue engineering, Nat. Mater. 8 (2009) 457–470. doi:10.1038/nmat2441.

[74] T. Okoshi, H. Chen, G. Soldani, P.M. Galletti, M. Goddard, Microporous small diameter PVDF-TrFE vascular grafts fabricated by a spray phase inversion technique, ASAIO J. Am. Soc. Artif. Intern. Organs 1992. 38 (1992) M201–206.

[75] A. Huttenlocher, A.R. Horwitz, Wound healing with electric potential, N. Engl. J. Med. 356 (2007) 303–304. doi:10.1056/NEJMcibr066496.

[76] D.N. Coakley, F.M. Shaikh, K. O'Sullivan, E.G. Kavanagh, P.A. Grace, S.R. Walsh, T.M. McGloughlin, Comparing the endothelialisation of extracellular matrix bioscaffolds with coated synthetic vascular graft materials, Int. J. Surg. Lond. Engl. 25 (2016) 31–37. doi:10.1016/j.ijsu.2015.11.008.

[77] H. Kobayashi, D. Terada, Y. Yokoyama, D.W. Moon, Y. Yasuda, H. Koyama, T. Takato, Vascular-inducing poly(glycolic acid)-collagen nanocomposite-fiber scaffold, J. Biomed. Nanotechnol. 9 (2013) 1318–1326.

[78] W.S. Choi, Y.K. Joung, Y. Lee, J.W. Bae, H.K. Park, Y.H. Park, J.-C. Park, K.D. Park, Enhanced Patency and Endothelialization of Small-Caliber Vascular Grafts Fabricated by Coimmobilization of Heparin and Cell-Adhesive Peptides, ACS Appl. Mater. Interfaces. 8 (2016) 4336–4346. doi:10.1021/acsami.5b12052.

[79] X. Yao, R. Peng, J. Ding, Cell-material interactions revealed via material techniques of surface patterning, Adv. Mater. Deerfield Beach Fla. 25 (2013) 5257–5286. doi:10.1002/adma.201301762.

[80] W. Gong, D. Lei, S. Li, P. Huang, Q. Qi, Y. Sun, Y. Zhang, Z. Wang, Z. You, X. Ye, Q. Zhao, Hybrid small-diameter vascular grafts: Anti-expansion effect of electrospun poly ε-caprolactone on heparin-coated decellularized matrices, Biomaterials. 76 (2016) 359–370. doi:10.1016/j.biomaterials.2015.10.066.

[81] J.M. Aamodt, D.W. Grainger, Extracellular matrix-based biomaterial scaffolds and the host response, Biomaterials. 86 (2016) 68–82. doi:10.1016/j.biomaterials.2016.02.003.

[82] L. Amadori, N. Rajan, S. Vesentini, D. Mantovani, Atomic Force and Confocal Microscopic Studies of Collagen-Cell-Based Scaffolds for Vascular Tissue Engineering, Adv. Mater. Res. 15-17 (2007) 83–88. doi:10.4028/www.scientific.net/AMR.15-17.83.

[83] P.M. Crapo, T.W. Gilbert, S.F. Badylak, An overview of tissue and whole organ decellularization processes, Biomaterials. 32 (2011) 3233–3243. doi:10.1016/j.biomaterials.2011.01.057.

[84] L. Gui, A. Muto, S.A. Chan, C.K. Breuer, L.E. Niklason, Development of Decellularized Human Umbilical Arteries as Small-Diameter Vascular Grafts, Tissue Eng. Part A. 15 (2009) 2665–2676. doi:10.1089/ten.tea.2008.0526.

[85] J. Chlupáč, E. Filová, T. Riedel, M. Houska, E. Brynda, M. Remy-Zolghadri, R. Bareille, P. Fernandez, R. Daculsi, C. Bourget, L. Bordenave, L. Bačáková, Attachment of human endothelial cells to polyester vascular grafts: pre-coating with adhesive protein assemblies and resistance to short-term shear stress, Physiol. Res. Acad. Sci. Bohemoslov. 63 (2014) 167–177.

[86] M.M. Stevens, J.H. George, Exploring and engineering the cell surface interface, Science. 310 (2005) 1135–1138. doi:10.1126/science.1106587.

[87] N. Huebsch, D.J. Mooney, Inspiration and application in the evolution of biomaterials, Nature. 462 (2009) 426–432. doi:10.1038/nature08601.

[88] A. Can, S. Karahuseyinoglu, Concise Review: Human Umbilical Cord Stroma with Regard to the Source of Fetus-Derived Stem Cells, STEM CELLS. 25 (2007) 2886–2895. doi:10.1634/stemcells.2007-0417.

[89] M. von Köckritz-Blickwede, O.A. Chow, V. Nizet, Fetal calf serum contains heat-stable nucleases that degrade neutrophil extracellular traps, Blood. 114 (2009) 5245–5246. doi:10.1182/blood-2009-08-240713.

[90] G. Fercana, D. Bowser, M. Portilla, E.M. Langan, C.G. Carsten, D.L. Cull, L.N. Sierad, D.T. Simionescu, Platform Technologies for Decellularization, Tunic-Specific Cell Seeding, and In Vitro Conditioning of Extended Length, Small Diameter Vascular Grafts, Tissue Eng. Part C Methods. 20 (2014) 1016–1027. doi:10.1089/ten.tec.2014.0047.

[91] A. Mahara, S. Somekawa, N. Kobayashi, Y. Hirano, Y. Kimura, T. Fujisato, T. Yamaoka, Tissue-engineered acellular small diameter long-bypass grafts with neointima-inducing activity, Biomaterials. 58 (2015) 54–62. doi:10.1016/j.biomaterials.2015.04.031.

[92] R.Y. Kannan, H.J. Salacinski, P.E. Butler, G. Hamilton, A.M. Seifalian, Current status of prosthetic bypass grafts: A review, J. Biomed. Mater. Res. B Appl. Biomater. 74B (2005) 570–581. doi:10.1002/jbm.b.30247.

Résumé

L'ingénierie tissulaire vasculaire se focalise sur le développement d'un substitut cellularisé, qui présente des caractéristiques biologiques et mécaniques similaires à celles d'un vaisseau natif. Aussi, l'enjeu repose sur le choix de la source cellulaire, des biomatériaux utilisés pour la construction des scaffolds et du coating, mais également sur la technique utilisée pour les combiner entre eux. Ce travail a exploité trois aspects différents dans l'ingénierie vasculaire. (1) la fabrication d'un substitut synthétique à base de poly (fluorure de vinylidène-trifluoroéthylène) (P(VDF-TrFE) fonctionnalisé par des nanoparticules d'oxyde de zinc. Nous avons testé ses propriétés physiques et montré que ce substitut est biocompatible avec les cellules souches mésenchymateuses (CSM) et les cellules endothéliales matures. Les scaffolds P(VDF-TrFE)/ZnO-2% cellularisés avec des CSM et implantés chez des rats en sous-cutané, n'ont entrainé ni rejet ni inflammation. De plus, une angiogenèse précosse a été observée en raison d'un effet synergétique entre scaffold fonctionnalisé et cellules. (2) Nous avons, pour la première fois, isolé un complexe d'une matrice extracellulaire à partir de la gelée de Wharton du cordon ombilical humain (ECM-GW). La technique d'isolement mise au point est simple et respecte les caractéristiques physiologiques. Diverses formes ECM et de facteurs de croissance ont été retrouvés ce qui ouvre des perspectives intéressantes. Utilisé comme coating sur un substrat 2D et 3D, nous avons montré que l'ECM-GW favorisait significativement l'adhésion, la prolifération, et la différenciation cellulaire *in vitro*. (3) Nous avons mis au point une technique de retournement d'un vaisseau artériel qui expose l'intima vers l'extérieur, la rendant plus accessible. Cette technique a largement facilité et amélioré l'ensemencement et la maturation des cellules intra-luminales. Implantés en remplacement artériel chez les lapins, ces greffons cellularisés issus de cette technique présentent une perméabilité supérieure à 3 semaines. L'ensemble de ces travaux contribue à proposer de nouvelles perspectives prometteuses pour l'avenir de l'ingénierie vasculaire.

Mots clés: Ingénierie vasculaire, biomatériaux, scaffold, coating, stimulation mécanique, cellules souches mésenchymateuses, polymère synthétique et naturel, technique de retournement.

Abstract

The ultimate goal of vascular tissue engineering is to create a cellularized graft, which has similar mechanical and biological properties to native vessels. However, cell source, biomaterials used for scaffolds construction or coating, and also the technique for combining the two remain the biggest challenges. This work investigated the three different aspects in vascular engineering. (1) We fabricated a synthetic substitute based on poly(vinylidene fluoride-trifluoroethylene) (P (VDF-TrFE) incorporated with zinc oxide nanoparticles. We tested the physical properties and we also showed that this substitute is fully biocompatible with mesenchymal stem cells (MSC) and mature endothelial cells. The P (VDF-TrFE)/ZnO-2% scaffolds pre-seeded with MSCs were implanted in rats at subcutaneous level, no rejection or inflammation was observed. Furthermore, best angiogenesis was observed in the scaffolds due to a synergistic effect of cells and scaffolds. (2) We isolated a complex ECM from Wharton's jelly of human umbilical cord (WJ-ECM) for the first time with an enzymatic method. The technique of isolation was simple and keeps the product in a physiological condition. Various ECM and growth factors were found in this solution. We succeed in fabricating a coating with this solution on 2D and 3D substrate that significantly favored *in vitro* cell adhesion, proliferation and differentiation. (3) We have invented a technique that reverse the intima of an arterial substitute outside. This technique has greatly facilitated and improved seeding and maturation of cells on the intima. Cellularized grafts with this technique remained patent for 3 weeks in an arterial replacement model in rabbits. All these works give us new options for a better future in vascular engineering.

Key words: Vascular tissue engineering, biomaterials, scaffolds, coating, mechanical stimulation, mesenchymal stem cells, synthetic and natural polymers, reverse technique.